

# MULTIPHYSICS STUDY OF MICROWAVE IRRADIATION FOR ROCK PRE-CONDITIONING AND BREAKAGE



Khashayar Teimoori

DEPARTMENT OF MINING AND MATERIALS ENGINEERING  
MCGILL UNIVERSITY, MONTREAL, CANADA

December 2020

A THESIS SUBMITTED TO MCGILL UNIVERSITY IN PARTIAL FULFILMENT OF THE  
REQUIREMENTS FOR THE DEGREE OF DOCTOR OF PHILOSOPHY IN MINING AND  
MATERIALS ENGINEERING

© KHASHAYAR TEIMOORI 2020

*This thesis is dedicated to*

*My parents, Mahmoud Teimoori and Dr. Akram Salimi, for their unconditional love, support,  
and inspiration in teaching me honesty, integrity, and hard work,*

*and*

*My lovely wife, Dr. Maryam Noori, who has been a constant and patient source of support and  
encouragement.*

# Abstract

Today, mining and civil engineering companies are accelerating toward faster production rates and seeking alternative technologies that can provide more efficient and continuous rock breakage systems. To this end, many studies have suggested several alternatives over the past two decades. From the literature review part of the present work, it can be concluded that an optimal combination of both mechanical methods and novel application of microwaves is now the potential candidate for pre-conditioning of rocks prior to their breakage by mechanical tools. This application has been shown to be an innovative process for reducing rocks' overall strength, because microwaves can rapidly and selectively heat rocks and generate and propagate intergranular fractures at their grain boundaries. However, a thorough understanding of the two types of microwaves, single-mode and multi-mode, which has yet to be determined, is essential for an efficient selection between the two types to obtain optimal pre-conditioning. The aim of the present dissertation is to obtain a clear indication of the impact of both single-mode and multi-mode microwave irradiation on rocks by using a multiphysics approach, pointing to two different systematic heating and pre-conditioning effects: surface and volumetric. The following two research stages were developed and fulfilled in the present dissertation.

In the first stage, rectangular specimens of basalt were first exposed to electromagnetic waves (microwaves) in a high-power (up to 15 kW) single-mode microwave cavity system at various operating parameters, including power level, exposure time, and distance of the rock from waveguide horn antenna. Then, the following three research phases were designed and implemented to analyze the experimental data: (1) surface temperature analysis by thermal imaging, (2) surface microcrack quantitative analysis by Scanning Electron Microscopy, and (3) volumetric microcrack qualitative analysis by micro-Computed Tomography. The obtained data of surface temperature and microcracks in the irradiated specimens demonstrated that basalt was susceptible to low microwave powers ( $< 10$  kW); longer microwave exposures resulted in more and denser microcracks. In addition, regardless of microwave power level and exposure time, high- and low-concentrated electromagnetic fields were provided by single-mode microwave irradiation within the cavity space, which emphasize the importance of the distance of rock from the horn antenna as the primary factor that significantly influences the form, distribution, and intensity of surface temperature on a rock under irradiation. Thus, the results suggest that maximum heating

and pre-conditioning of rocks in the single-mode microwave irradiation system can only be achieved by placing the rock in high density zones of the electromagnetic waves and close to their wavelengths.

In the second stage, the effects of multi-mode microwave irradiation on cylindrical samples of four rock types: basalt, granite, and two types of kimberlite, were investigated and analyzed. Cylindrical core samples at two different sizes, standard BTS and UCS, were prepared for irradiation tests in a multi-mode microwave system at various microwave exposure times and power levels. The results of microwave tests were evaluated by data obtained from thermal images. To present a better picture of how microwave energy is converted into heat within a rock sample, the study implemented the method of calorimetry for measurement of the absorbed heat (energy) in the irradiated rocks; energy analyses were then conducted. The size of the samples was found to have a great impact on the absorption of the heat in all four rock types. In addition, a numerical model of the multi-mode microwave irradiation system with a novel strategy for simulation of a rotational stirrer fan was developed, analyzed, and validated against the experimental data. The validated numerical model was then employed to study the effects of variation in the dielectric properties of rocks on their power dissipation. It was found that the higher the input dielectric constant and loss factor, the greater the average dissipated power in the rock sample. The validated numerical models of this thesis yield a powerful tool that can be applied to other rock types as well, provided that their thermal, electrical, and physical material properties are known.



## Résumé

Aujourd'hui, les compagnies de génie minier et civil se dirigent vers des taux de productions de plus en plus rapides tout en recherchant des technologies alternatives permettant une rupture systémique des roches plus efficace et en continue. Jusqu'à maintenant, plusieurs études suggèrent différentes alternatives depuis les deux dernières décennies. Après une révision de la partie critique du présent travail, nous pouvons conclure que la combinaison d'une méthode mécanique et de la nouvelle méthode d'application de micro-ondes est un candidat potentiel pour le chauffage et pré-conditionnement des roches précédant leurs ruptures grâce aux outils mécaniques. Cette application a pu démontrer le processus comme étant innovatif par réduction de la résistance global de la roche car les micro-ondes peuvent rapidement et sélectivement chauffer le roc ainsi que générer et propager des fractures intergranulaires sur les joints de grains. Cependant, une compréhension des deux types de micro-ondes (mode-mono et mode-multi), qui reste à être approfondie, est essentielle pour une sélection efficace entre les deux types pour un chauffage et pré-conditionnement optimal. L'objectif de la présente dissertation est d'atteindre une indication claire de l'impact de l'irradiation des modes mono et multi de micro-ondes sur les roches en utilisant une approche multiphysique pointant sur deux effets systémiques de chauffage et pré-conditionnement : effet surfacique et effet volumétrique. Les deux étapes de recherche suivantes furent développées et réalisées dans la présente dissertation.

Lors de la première étape, des spécimens rectangulaires de basalte furent premièrement exposé à des ondes électro-magnétiques (micro-ondes) d'une forte puissance (jusqu'à 15 kW) de mode-mono dans la cavité de l'appareil micro-onde tout en faisant varier les paramètres de fonctionnement qui incluent: le niveau de puissance, le temps d'exposition, la distance entre le roc et le cornet de l'antenne à micro-ondes. Par après, les trois phases de recherche suivantes furent conçues et implémentées afin d'analyser les données expérimentales suivantes : (1) analyse thermique de surface par imagerie thermique, (2) analyse quantitative de microfissures par Microscopie Électronique à Balayage, et (3) visualisation volumétrique des microfissures par Micro-Tomodensitométrie. Les résultats obtenus de la température de surface et des microfissures des spécimens irradiés démontrent que le basalte est sensible aux micro-ondes de faible puissance (< 10 kW); une exposition de longue durée produit une grande quantité de microfissures et de plus grande densité. De plus, indépendamment du niveau de puissance des micro-ondes et du temps

d'exposition, des champs électromagnétiques de haut et bas niveau furent produit par une irradiation de micro-ondes en mode-mono dans la cavité de l'appareil, mettant l'emphase sur l'importance entre la distance du roc et celle du cornet de l'antenne du micro-onde comme le premier facteur qui influence la forme, la distribution et l'intensité de la température de surface sur le roc irradié. Donc, les résultats suggèrent que le chauffage maximal et le pré-conditionnement du roc avec le mode mono de l'appareil d'irradiation de micro-ondes peuvent seulement être obtenus en plaçant le roc dans une zone d'ondes électromagnétiques de haute densité et proche de leurs longueurs d'ondes.

Lors de la deuxième, les effets du mode-multiple d'irradiation du micro-onde sur des échantillons de quatre types de roches de forme cylindrique: basalte, granite et deux types de kimberlite furent étudiés et analysés. Des échantillons des roches de différentes grandeurs, BTS standard et UCS, furent préparés pour les tests d'irradiation en mode-multi de l'appareil à des temps d'exposition et niveaux de puissance variés. Les résultats des tests à l'aide de l'appareil micro-ondes furent évalués grâce aux données recueillis par imagerie thermique. Afin de donner une meilleure représentation sur comment l'énergie des micro-ondes est convertie en chaleur à l'intérieur des échantillons de roches, la présente étude implémenta la méthode calorimétrique dans le but de mesurer la chaleur absorbée (énergie) par les roches irradiées; une analyse énergétique fut conduite par la suite. La taille des échantillons démontra avoir un grand impact sur l'absorption de la chaleur pour les quatre types de roches. En addition, un modèle numérique du mode-multi d'irradiation de l'appareil micro-ondes avec une nouvelle stratégie simulant une hélice mélangeuse rotative fut développée, analysée puis validée par rapport aux données expérimentales. Le modèle numérique validé fut ensuite utilisé afin d'étudier les effets de la variation des propriétés diélectriques des roches sur leur dissipation d'énergie. Il fut trouvé que plus l'apport de la constante diélectrique et de son facteur de perte est élevé, plus l'énergie moyenne dans le roc est dissipée. Les modèles numériques validés de cette thèse apportent un puissant outil pouvant être appliqué aux autres types de roches, pourvu que leurs propriétés matérielles thermiques, électriques et physique soient connus.

# Acknowledgments

Many thanks to Professor Ferri P. Hassani and Professor Agus P. Sasmito for their kind support and for giving direction to my thoughts during this work by their great supervision. Especially, Professor Ferri Hassani—without whom this project would not have been realized—was the main source of encouragement and support: financial, technical, and moral. I would also like to express my appreciation to Professor Ali Ghoreishi-Madiseh from the University of British Columbia for his great discussion and guidance. I am grateful to all members of the EMERG lab and Mine Multiphysics research group at Mining and Materials Engineering Department, McGill University, for sharing their knowledge and friendship.

During the journey towards the completion of my Ph.D. thesis, I have been overwhelmed by the tremendous support and help from Dr. Richard Cooper whom I would like to express my sincere gratitude. A special thank goes to Professor Mainul Hasan who has always inspired me through his great discussion and provided me with strong support and encouragement. I personally learnt a lot from him because he is an honest source of encouragement and inspiration in the department. Another special thanks should also go to Professor Alessandro Navarra who was the other source of encouragement and inspiration. I wish to express my special appreciation to Professor Ali M. Sadegh from the City University of New York who has been a good role model to me and the main source of encouragement and moral support throughout my graduate studies. My Appreciation is extended to Professor Hojatollah Vali for all his encouragement, and all my friends, especially Dr. M. Hadi Amini, Dr. Ali Behfarnia, Dr. Hooman Rahmani, Dr. Golshan Fahimi, Dr. Hamid Rajebi, and Mr. John Forster for their friendship and academic advices.

I would like to express my gratitude to De Beers Canada, Inc. (De Beers group) for providing the rock samples used in this research thesis. Without the rock samples it would not have been possible to complete this research successfully. In addition, fulfillment of this doctoral thesis could not have been achieved without the following main sources of funding: De Beers Canada and the McGill Engineering Doctoral Awards (MEDA) award, which made my Ph.D. work easier.

Finally, the completion of this work was not possible without the great support of my beautiful family. I greatly thank my mother and father for installing in me the values of honesty, integrity, hard work, and education. Most of all, Maryam, my love, whom I thank for her encouragement and all the sacrifices she has made for me.

## **Contribution to Original Knowledge**

The present thesis takes into account all the previous efforts and aims to study the effects of both single-mode and multi-mode microwave irradiation on various rock types with several experimental tests and by different rock characterization methods. In addition, the current thesis presents a novel numerical model of the multi-mode microwave irradiation system with a rotational stirrer fan, which is also validated against the experimental data from calorimetric measurements. The validated numerical model is used to accurately predict the effects of multi-mode microwave irradiation with different operating parameters, such as power level and exposure time, on rocks with different dielectric properties. The numerical modeling approach is the initial step to gain more in-depth information into phenomena occurring inside rocks and/or minerals under microwave irradiation. This is a novel contribution that can be employed for future investigations on the microwave-assisted pre-conditioning and breakage of rocks and minerals without costly experiments. It can also be a promising tool for the optimization (improving heating and pre-conditioning capacity) and investigations on the effectiveness of microwave cavity designs for maximum impact and, finally, successful future implementation of large-scale microwave-assisted rock breakage systems.

In short, this thesis presents:

- 1- How the technology of microwave irradiation can be applied to rocks and/or minerals for their breakage and/or processing with an efficient approach;
- 2- All major influencing microwave parameters of both single-mode and multi-mode microwave cavities in a microwave-assisted pre-conditioning and breakage of rocks;
- 3- A clearer indication of the impact of microwave pre-conditioning to lower the strength of hard rocks to facilitate the use of continuous mechanical breakage (excavation) systems, especially in deep underground and space mining;
- 4- A novel strategy for the development of a multi-mode microwave irradiation system using the finite element method;
- 5- Different scenarios for utilizing the microwave technology at various capacities for investigating the effectiveness and energy-saving potential of multi-mode microwave cavities for future industrial applications of rock pre-conditioning and breakage.

## Statement of Originality

I, hereby, certify that all of the work within this thesis is the original work of the author. Any published (or unpublished) ideas and/or methods from the work of others are fully acknowledged in the text, and a full list of references is given in the bibliography.

Khashayar Teimoori



*Khashayar Teimoori*

December 2020

# Table of Contents

<b>Dedication</b> .....	<b>ii</b>
<b>Abstract</b> .....	<b>iii</b>
<b>Résumé</b> .....	<b>v</b>
<b>Acknowledgments</b> .....	<b>vii</b>
<b>Contribution to Original Knowledge</b> .....	<b>viii</b>
<b>Statement of Originality</b> .....	<b>ix</b>
<b>Table of Contents</b> .....	<b>x</b>
<b>List of Figures</b> .....	<b>xiv</b>
<b>List of Tables</b> .....	<b>xxii</b>
<b>Nomenclature</b> .....	<b>xxiv</b>
<b>List of Abbreviation</b> .....	<b>xxvi</b>
<b>Chapter 1 Introduction</b>	<b>1</b>
1.1 Background and motivation .....	1
1.2 Research objectives.....	4
1.2.1 Fundamental research .....	6
1.2.2 Applied research.....	6
1.3 Thesis outline .....	7
<b>Chapter 2 Literature review</b>	<b>10</b>
2.1 History of rock breakage techniques .....	11
2.1.1 Conventional and novel rock breakage methods.....	11
2.1.2 Evolution of microwave applications in rock mechanics and rock engineering..	15
2.2 Review of recent research on microwave irradiation of rocks and minerals .....	19
2.2.1 Experimental studies.....	19
2.2.2 Modeling and simulation literatures .....	40
2.2.3 Technical and economic analyses .....	46
2.3 Research gaps and outlook.....	49
<b>Chapter 3 Fundamental principles of microwaves for heating and pre-conditioning of rocks</b>	<b>51</b>
3.1 Electromagnetic wave theory .....	52
3.1.1 Introduction to Maxwell’s equations.....	52
3.1.2 Electromagnetic waves in materials .....	53

3.1.3	Electromagnetic spectrum, safety, and compliance .....	54
3.2	Mechanisms of microwave heating of materials .....	55
3.2.1	Polarization in linear dielectrics .....	56
3.2.1.1	Orientational (dipolar) polarization .....	57
3.2.1.2	Ionic (conduction) polarization.....	58
3.2.1.3	Interfacial polarization.....	59
3.2.2	Definition of relative permittivity of materials .....	59
3.2.3	Definition of relative permeability materials .....	60
3.2.4	Definition of electrical conductivity and resistivity of materials .....	60
3.2.5	Calculation of penetration depth .....	62
3.2.6	Energy in electromagnetic waves.....	64
3.2.7	Coupling of electromagnetics theory and heat transfer in materials.....	65
3.3	Influencing parameters in rock heating and pre-conditioning by microwaves.....	65
3.3.1	Electrical and thermal properties of rocks.....	66
3.3.1.1	Factors affecting rocks' dielectric properties.....	66
3.3.1.2	Factors affecting rocks' electrical conductivity and resistivity .....	69
3.3.1.3	Variations of rocks' thermal conductivity and specific heat capacity .....	71
3.3.2	Mineralogy and physio-mechanical characteristics of rocks .....	73
3.3.3	Microwave system characteristics.....	73
3.3.3.1	Multi-mode microwave cavities with stirrer fans .....	74
3.3.3.2	Single-mode microwave cavities with horn antennas.....	75
3.4	Summary and conclusions .....	76

**Chapter 4 Rock-microwave system characterization methods and procedures 77**

4.1	Rock samples utilized .....	78
4.2	Measurement methods for rocks' material properties .....	80
4.2.1	Measurement methods of dielectric properties .....	80
4.2.1.1	Coaxial probe method.....	80
4.2.1.2	Resonant cavity (cavity perturbation) method.....	82
4.2.1.3	Parallel plate method.....	83
4.2.1.4	Transmission line method.....	84
4.2.1.5	Free space method.....	84

4.2.1.6	Analysis of the methods and variations of the measured dielectric properties of selected rocks.....	85
4.2.2	Measurement of electrical conductivity of selected rocks .....	89
4.2.3	Measurement of thermal properties of selected rocks .....	90
4.3	Instrumental methods utilized.....	91
4.3.1	Method of thermal imaging for temperature data acquisition.....	91
4.3.2	Method of calorimetry for thermal energy (absorbed heat) measurement.....	93
4.3.3	Method of Scanning Electron Microscopy for rock surface characterization.....	94
4.3.4	Method of micro-Computed Tomography for rock volumetric characterization.....	95

**Chapter 5 Multiphysics study of single-mode microwave irradiation effects on rock pre-conditioning and breakage 97**

5.1	Introduction.....	98
5.1.1	Experiments of single-mode microwave irradiation on basalt specimens .....	99
5.1.2	Microwave system setup and research procedures.....	100
5.2	Phase I: Thermal image analysis from surface temperature measurement.....	103
5.2.1	Methodology and procedures .....	103
5.2.2	Results and discussion.....	105
5.2.2.1	Effect of distance from microwave horn antenna .....	110
5.2.2.2	Effect of microwave power level.....	114
5.2.2.3	Effect of microwave exposure time: an energy effectiveness analysis of single-mode microwave irradiation .....	116
5.3	Phase II: SEM image analysis from surface microcrack quantification.....	118
5.3.1	Methodology and procedures .....	118
5.3.2	Results of SEM images and discussion.....	120
5.4	Phase III: Volumetric microcrack visualization from micro-CT scan.....	124
5.5	Conclusions.....	128

**Chapter 6 Multiphysics study of multi-mode microwave irradiation effects on rock pre-conditioning and breakage 129**

6.1	Introduction.....	130
6.2	Experimental tests of multi-mode microwave irradiation .....	132
6.2.1	Experimental conditions and procedures .....	132



6.2.2	Calculation of microwave ramp-up time.....	133
6.2.3	Results and discussion.....	135
6.2.3.1	Thermal analysis from surface temperature measurements.....	136
6.2.3.2	Heat (energy) analysis from calorimetric measurements.....	143
6.2.3.3	Effect of microwave ramp-up time.....	145
6.3	Numerical modeling of multi-mode microwave irradiation.....	147
6.3.1	Novel model of multi-mode microwave system with rotating stirrer fan.....	148
6.3.2	Mathematical modeling.....	150
6.3.2.1	Electromagnetic physics (Maxwell's theory).....	151
6.3.2.2	Thermal physics (heat transfer theory).....	151
6.3.2.3	Initial and boundary conditions.....	153
6.3.3	Numerical methodology.....	154
6.3.3.1	COMSOL multiphysics.....	154
6.3.3.2	Finite element method.....	155
6.3.3.3	Mesh independence study.....	156
6.3.3.4	Novel simulation strategy for rotation of the stirrer fan.....	157
6.3.4	Results and discussion.....	160
6.3.4.1	Model validation.....	160
6.3.4.2	Analysis of dielectric property variations.....	162
6.4	Conclusions.....	167
<b>Chapter 7</b>	<b>Concluding remarks</b>	<b>168</b>
7.1	Summary and conclusions.....	168
7.2	Outlook and recommendations for future research.....	171
<b>BIBLIOGRAPHY</b>		<b>172</b>
<b>APPENDIX A</b>		<b>188</b>
A.1	Supplementary data from Chapter 6.....	188

# List of Figures

## Chapter One

Figure 1.1: A conceptual illustration of microwave-assisted rock pre-conditioning system prior to breakage by a disc cutter.....	3
Figure 1.2: Flowchart of the theses research objectives .....	7

## Chapter Two

Figure 2.1: Conceptual illustration of (a) coupling of waterjet application with a mechanical disc cutter, and (b) waterjet-assisted TBM tunneling.....	14
Figure 2.2: The primary idea of (a) the microwave-assisted drilling system, and (b) the microwave-assisted mechanical rock cutting system .....	16
Figure 2.3: (a) Scheme illustrating the principle underlying the operation of microwave-drill system. (b) Conceptual schemes of MWD applicators, including a basic MWD consists of a coaxial waveguide with a moveable center electrode, inserted into the softened hot spot to form the hole (left) and an advanced MWD for deeper holes (right).....	18
Figure 2.4: Effect of microwave treatment of basaltic rocks with an input power density of 1 W/g at different microwave exposure times on (a) samples' mean compressive strength and (b) penetration rate of basalt for the percussive drilling process (modified from Satish et al. [2006]) .....	23
Figure 2.5: Temperature dependency of dielectric constant (left) and dielectric loss factor (right) of basalt, granite, and sandstone in the temperature range of 25-1000 °C at a constant frequency of 2.45 GHz (data taken from table in Hartlieb et al. [2016]) .....	30
Figure 2.6: Effect of microwave treatments with different energy inputs and exposure times on the samples (data taken from table in Singh et al. [2017]) .....	31
Figure 2.7: Real and imaginary permittivity values of serpentine (left) and olivine (right) as a function of increasing temperature (image modified with permission from Forster et al. [2018]) .....	35
Figure 2.8: (a) Heating rate upon exposure to microwave radiation with respect to temperature for Pipe (▪,▫) and OK (●,○) ores; (b) imaginary permittivity, and (c) real permittivity for the Pipe and OK ores with increasing temperature at frequencies of 912 and 2466 MHz (image modified from Bobicki et al. [2018]) .....	36

## Chapter Three

Figure 3.1: Graphical illustration of the orientational (dipolar) polarization mechanism .....	57
--	----

Figure 3.2: Graphical illustration of ionic (conduction) polarization of electric field moving in a perfect conductor .....	58
Figure 3.3: Traveling of free electrical charges in a rock exposed to an external electric field ....	61
Figure 3.4: Schematic of the electromagnetic waves penetrating a lossy (dielectric) material .....	62
Figure 3.5: The propagation of an electromagnetic wave in a multi-layered dielectric .....	64
Figure 3.6: The response of permittivity due to electronic or atomic polarization (Figure modified from the plot given by Chen et al. [2004]).....	67
Figure 3.7: Response of $\epsilon'$ and $\epsilon''$ for all frequencies of the electromagnetic spectrum for a hypothetical dielectric (Figure modified from the plot given by Ramo et al. [1994]) .....	67
Figure 3.8: Graphical description of permeability as a function of frequency presented by Chen et al. (2004).....	68
Figure 3.9: Common values of conductivity/resistivity for various materials and rock types (Figure adapted from [Palacky, 1988]).....	70
Figure 3.10: Heat transfers in and out of a rock's surface with heat generation in the rock block .....	72
Figure 3.11: Detailed overview of a multi-mode microwave cavity system and its components...	74
Figure 3.12: Detailed overview of a single-mode microwave cavity system and its components..	76

## Chapter Four

Figure 4.1: Schematic illustration of the placement of (a) a cylindrical sample of UCS or BTS size in the multi-mode microwave and (b) stacked basalt specimens inside the single-mode microwave .....	79
Figure 4.2: Illustration of different dielectric property measurement methods specific to a range of frequencies and the material's complex permittivity (material loss) (Figure modified from [Begley, 2010]).....	80
Figure 4.3: Conceptual illustration of the coaxial probe method for measurement of a rock sample's dielectric properties.....	81
Figure 4.4: Conceptual illustration of a network analyzer connected to a resonant cavity where (a) shows the position of the specimen in the empty cavity, and (b) shows the perturbation frequency shifting from cavity ( $f_c$ ) to specimen ( $f_s$ ) when the specimen is inserted into the resonant cavity (Note that $Q_c$ and $Q_s$ are the quality factors of the empty cavity and the filled cavity.).....	82
Figure 4.5: Conceptual illustration of the parallel plate capacitor system's setup and its components .....	83
Figure 4.6: Conceptual illustration of the transmission line method for measurement of a small rock sample's dielectric properties .....	84

Figure 4.7: Conceptual illustration of the free space method with a network analyzer connected to two antennas and a furnace with a sheet sample for measurement of the sample’s dielectric properties.....85

Figure 4.8: The calculated mean values of the dielectric constant for the three rock types with respect to frequency ranges of 0.9-12 GHz .....88

Figure 4.9: The calculated mean values of the dielectric loss factor for the three rock types with respect to frequency ranges of 0.9-12 GHz .....88

Figure 4.10: The calculated mean values of loss tangent for the three rock types with respect to frequency ranges of 0.9-12 GHz.....88

Figure 4.11: Graphical representation of the processes of measuring electrical conductivity of rocks, where (a) is the Z-2405A power supply, (b) is the schematic of rock sample placed between two electrodes, and (c) is the FLUKE 18B+ digital multimeter for measurement of voltage.....89

Figure 4.12: Measurement of thermal properties of selected rock types with the KD2PRO thermal properties measurement device.....91

Figure 4.13: The process of thermal imaging by Fluke TiS65 IR camera after microwave treatment .....92

Figure 4.14: A schematic illustration of the method of calorimetry for novel thermal energy (absorbed heat) measurement in a rock sample after microwave treatment.....94

Figure 4.15: Image of (a) the Hitachi SEM-SU3500 Variable Pressure Scanning Electron Microscope (VP-SEM) instrument located at McGill University, Department of Mining and Materials Engineering, and (b) position monitoring of the rock sample inside the SEM cavity...95

Figure 4.16: The image of (a) the system of SKYSAN-1172 micro-CT scanner (Skyscan, Kontich, Belgium) with the X-ray tube operating at 50 kV located at McGill University, Department of Mining and Materials Engineering, and (b) placement and positioning of the sample in the micro-CT cavity for 3D X-ray imaging.....96

## Chapter Five

Figure 5.1: Industrial single-mode, variable high-power (up to 15 kW) microwave cavity system in the Geomechanics Laboratory at McGill University .....100

Figure 5.2: Conceptual illustration of the single-mode microwave cavity system with two different configuration of rock blocks: (a) rock block with changing volume where the length of the block,  $L$  (cm), changes according to the size of the rock and the distance from the horn antenna, and (b) rock block with a constant volume placed on two rectangular insulators installed on four rod-shaped insulators with a height,  $h$  (cm), changing according to the distance from the antenna .....101

Figure 5.3: The process of thermal imaging by a thermal camera from basalt specimens after single-mode microwave irradiation tests for surface temperature measurements: (a) nontreated specimens of basalt ready for irradiation; (b) thermal imaging from surface of the irradiated specimens (the distance from the microwave horn antenna is shown by a white arrow); and (c) post processing of thermal images using FLIR software .....104

Figure 5.4: Surface temperature profiles of the irradiated blocks of basalt after 60s microwave exposure from the results of thermal images, where the projection of temperature distribution is parallel to the width of the horn antenna’s aperture .....106

Figure 5.5: Surface temperature profiles of the irradiated blocks of basalt after 60s microwave exposure from the results of thermal images, where the projection of temperature distribution is perpendicular to the width of the horn antenna’s aperture .....107

Figure 5.6: Illustration of visible crack development at the surface of the topmost basalt specimens irradiated at 60s microwave exposure and different power levels and distances from the horn antenna .....108

Figure 5.7: Illustration of the block of basalt after 60s exposure to 15 kW power at 5 cm distance from the antenna: (a) shows the first irradiated specimen and spallation at its top center surface and (b) gives the dimensions of a piece of rock chipped from the top center of the specimen...109

Figure 5.8: Spallation mechanism of the topmost specimen of basalt after microwave irradiation .....110

Figure 5.9: Distribution of the surface temperature changes obtained at the top center of the topmost basalt specimens irradiated at 60s exposure and various distances from the horn antenna .....111

Figure 5.10: Schematic of the applied standing waves from the waveguide horn antenna to the surface of rock at different wavelengths and distances from the horn antenna where (a)  $d = 8.8$  cm, (b)  $d = 21$  cm, and (c)  $d = 33.2$  cm. Here it should be noted that the intersection of the solid (–) and dashed lines (--) is where the electromagnetic waves touch the surface of the topmost specimen, solid lines show how the waves propagate in air from the waveguide port to the rock surface, and dashed lines represent how the waves are absorbed and attenuated inside the rock block.....112

Figure 5.11: Effect of distance from microwave horn antenna on surface temperature change of basalt for three different volumes of blocks comprising 1 specimen, 2 specimens, and 3 specimens after their exposure to a 3 kW microwave power at 60s.....113

Figure 5.12: Effect of microwave power level on maximum surface temperate change in blocks of basalt irradiated at various distances from the horn antenna .....115

Figure 5.13: Effect of microwave induced power density on maximum surface temperate changes in the volume changing blocks of basalt irradiated at various distances from the horn antenna...116

Figure 5.14: Effect of microwave energy input on maximum surface temperate change in blocks of basalt irradiated at various distances from the horn antenna.....	117
Figure 5.15: The results of maximum temperate difference change on the rock blocks over distance from the horn antenna at 60s and 120s exposure times at 30 kW power level.....	117
Figure 5.16: Schematic illustration of (a) the single-mode microwave system setup with the specimens placed inside the cavity and below the horn and the process of drilling core sample with a dimension of $r = 0.5$ cm and $h = 2$ cm from the center of the topmost irradiated specimen, (b) the SEM equipment set-up with the core sample placed inside the SEM cavity for microcrack imaging .....	119
Figure 5.17: The results of SEM images from cylindrical cored samples under different experimental conditions .....	120
Figure 5.18: Effect of distance from horn antenna on overall crack length initiated at the surface of the topmost specimen after microwave irradiation tests with different operating parameters	122
Figure 5.19: Effect of input microwave power level on crack density when the distance from the antenna changes from 5 cm to 25 cm.....	123
Figure 5.20: The placement of a cylindrical core sample of an irradiated basalt specimen in the chamber of the micro-CT scanner (model SKYSAN-1172).....	124
Figure 5.21: The results of (a) the 3D model of the core sample after reconstruction operation on raw data of micro-CT images and (b) the 2D cut planes at vertical and horizontal middle planes of a core sample.....	125
Figure 5.22: The result of image processing of micro-CT scan on a nontreated core sample on the 2D (a) vertical cut plane and (b) horizontal cut plane captured from the middle of the core sample .....	126
Figure 5.23: The results of image processing on a core sample drilled from an irradiated specimen by single-mode microwave irradiation at 3 kW and 120s exposure: (a) the processed 2D micro-CT image shown at the horizontal cut plane, (b) the processed 2D micro-CT image shown at the vertical cut plane, and (c) the SEM image captured from the top center of the core sample .....	126
Figure 5.24: The results of image processing on a core sample drilled from an irradiated specimen by single-mode microwave irradiation at 9 kW and 120s exposure: (a) the processed 2D micro-CT image shown at the horizontal cut plane, (b) the processed 2D micro-CT image shown at the vertical cut plane, and (c) the SEM image captured from the top center of the core sample .....	127

## Chapter Six

Figure 6.1: Conceptual sketch of (a) a single-mode microwave cavity system with horn antenna and (b) a multi-mode microwave cavity system with an umbrella-shaped stirrer fan.....	130
--	-----

Figure 6.2: Industrial multi-mode, variable high-power (up to 15 kW) microwave cavity system in the Geomechanics Laboratory at McGill University .....	132
Figure 6.3: Experimental procedures for calorimetric studies.....	134
Figure 6.4: The results of calorimetric tests conducted with water to define microwave ramp-up time: (a) the absorbed energy in water with respect to the gross exposure times of microwaves and (b) the calculated ramp-up time as a function of microwave power level.....	135
Figure 6.5: The process of thermal imaging by a thermal camera from rock samples after multi-mode microwave irradiation tests: (a) nontreated rock samples of UCS and BTS sizes ready for irradiation, (b) thermal imaging from surface of the irradiated samples, and (c) post processing of thermal images using FLIR software.....	137
Figure 6.6: The plots of maximum surface temperature change with respect to various microwave exposure times for BTS size samples of basalt exposed to multi-mode microwave irradiation at the two power levels of 5 kW and 12 kW.....	138
Figure 6.7: The plots of maximum surface temperature change with respect to different microwave exposure times for UCS size samples of basalt exposed to multi-mode microwave irradiation at the two power levels of 5 kW and 12 kW.....	138
Figure 6.8: The plots of maximum surface temperature change with respect to various microwave exposure times for BTS size samples of granite exposed to multi-mode microwave irradiation at the two power levels of 5 kW and 7 kW.....	140
Figure 6.9: The plots of maximum surface temperature change with respect to various microwave exposure times for UCS size samples of granite exposed to multi-mode microwave irradiation at the two power levels of 5 kW and 12 kW.....	141
Figure 6.10: The plots of maximum surface temperature change with respect to various microwave exposure times for BTS size samples of kimberlite #1 exposed to multi-mode microwave irradiation at the two power levels of 5 kW and 7 kW .....	142
Figure 6.11: The plots of maximum surface temperature change with respect to various microwave exposure times for UCS size samples of kimberlite #1 exposed to multi-mode microwave irradiation at two power levels of 5 kW and 12 kW .....	143
Figure 6.12: Effect of input microwave energy on the total heat (energy) absorption after irradiating BTS (left) and UCS (right) size samples of basalt in the multi-mide microwave cavity .....	144
Figure 6.13: Effect of input microwave energy on the total heat (energy) absorption after irradiating BTS (left) and UCS (right) size samples of granite in the multi-mide microwave cavity .....	144

Figure 6.14: Effect of input microwave energy on the total heat (energy) absorption after irradiating BTS (left) and UCS (right) size kimberlite #1 samples in multi-mode microwave cavity .....145

Figure 6.15: Effect of microwave ramp-up time on the amount of heat (energy) absorption of BTS size samples of basalt after their irradiation in the multi-mode microwave cavity .....146

Figure 6.16: Schematic of (a) the multi-mode microwave cavity model comprising a waveguide port and an umbrella-shaped stirrer fan and (b) the actual multi-mode microwave cavity system used for the practical microwave irradiation tests .....148

Figure 6.17: Flowchart of the solver algorithm for modeling processes of multi-mode microwave irradiation using COMSOL-MATLAB interface depicting a novel simulation approach for rotational stirrer fan.....149

Figure 6.18: Analytical flowchart of the fully coupled numerical modeling approach representing the interaction between electromagnetic and thermal multiphysics where (a)→(b) is the input from electromagnetic to thermal multiphysics and (a)↔(b) represents the interactions between the two multiphysics .....150

Figure 6.19: Steps for model development.....154

Figure 6.20: An example of the results of the mesh independence study, showing the averaged dissipated power in the BTS size kimberlite #2 rock model after its irradiation at 10 kW power with respect to minimum mesh size (left) and maximum mesh size (right).....156

Figure 6.21: The novel strategy applied for the simulation of rotating stirrer fan in the multi-mode microwave cavity model where (a) shows the geometry of the multi-mode microwave cavity system and (b) shows the modeling of stirrer fan in the multi-mode microwave model.....158

Figure 6.22: Illustration of the electric field distribution obtained for different positions of the stirrer fan inside an empty multi-mode microwave cavity model with an input power level of 3 kW from to initial rotation angle of (a)  $\theta = 0^\circ$  to (b)  $\theta = 5^\circ$  until when (c)  $\theta = 55^\circ$ ; and finally, (d) the obtained averaged electric field distribution, which is the overall electric field distribution in the cavity from averaging of all the obtained electric field distribution. Both (i) 3D and 2D plots: (ii) xz cut plane and (iii) xy cut plane, are shown in the figure. ....156

Figure 6.23: Numerical model validation against experimental data from calorimetric measurements for BTS (left) and UCS (right) size samples of basalt .....161

Figure 6.24: Numerical model validation against experimental data from calorimetric measurements for BTS (left) and UCS (right) size samples of granite .....161

Figure 6.25: Numerical model validation against experimental data from calorimetric measurements for BTS (left) and UCS (right) size samples of kimberlite #1 .....161



Figure 6.26: Variation of the measured (a) dielectric constant ( $\epsilon'$ ) and (b) dielectric loss factor ( $\epsilon''$ ) for kimberlite #1 at the frequency of 2.45 GHz with respect to five different tests for one sample. Note that the numerical models of both BTS and UCS size samples with the values shown in red were found to give the minimum errors when compared with the experimental data.....163

Figure 6.27: Variation of the measured (a) dielectric constant ( $\epsilon'$ ) and (b) dielectric loss factor ( $\epsilon''$ ) for granite at the frequency of 2.45 GHz with respect to five different tests for one sample. Note that the numerical models of both BTS and UCS size samples with the values shown in red were found to give the minimum errors when compared with the experimental data .....163

Figure 6.28: The effect of variations of dielectric constant ( $\epsilon'$ ) on the average dissipated power by kimberlite #2 BTS size after its irradiation at 10 kW and 10s microwave exposure.....165

Figure 6.29: The effect of variations of dielectric constant ( $\epsilon''$ ) on the average dissipated power by kimberlite #2 BTS size after its irradiation at 10 kW and 10s microwave exposure.....165

Figure 6.30: The effect of variations of loss tangent ( $\tan \delta$ ) on the average dissipated power by kimberlite #2 BTS size sample after its irradiation at 10 kW and 10s microwave exposure .....166

**Appendix A**

Figure A.1: Effect of microwave ramp-up time on UCS size basalt .....188

Figure A.2: Effect of microwave ramp-up time on BTS size granite.....188

Figure A.3: Effect of microwave ramp-up time on UCS size granite .....189

Figure A.4: Effect of microwave ramp-up time on BTS size kimberlite #1.....189

Figure A.5: Effect of microwave ramp-up time on UCS size kimberlite #1 .....190

# List of Tables

## Chapter Two

Table 2.1: Classification of conventional and novel rock penetration methods (modified from Hartman and Mutmanský [2002]).....	13
Table 2.2: The results of highest surface temperatures achieved at recorded microwave exposure times in different rock samples after 3 kW microwave treatment (Peinsitt et al., 2010).....	25
Table 2.3: Categorization of different rock types from data in Hartlieb et al. (2018).....	34
Table 2.4: Secondary publications found through a chronological literature review on laboratory experiments of microwave treatment of rocks and minerals and the corresponding effects .....	39
Table 2.5: Publications on numerical simulations of microwave-assisted heating and pre-conditioning of rocks and minerals that were found through a chronological literature review (2010-2020).....	44
Table 2.6: Results of microwave treatment effects on strength reductions in rocks and minerals: a comparison between the amount of microwave energy input and the mechanical changes in different rock samples.....	47
Table 2.7: Estimated operating and cost parameters for industrial scale applicators (table modified from Bradshaw et al. [2007]).....	48

## Chapter Three

Table 3.1: Comparisons of microwave-assisted heating and conventional heating .....	56
---	----

## Chapter Four

Table 4.1: Details of the selected rock types in the present study and their characteristics .....	78
Table 4.2: List of advantages and disadvantages of dielectric property measurements methods and the selected rock types analyzed.....	86
Table 4.3: Calculated average values of real ( $\epsilon'$ ) and imaginary ( $\epsilon''$ ) parts of permittivity and loss tangent ( $\tan \delta$ ) for four selected rock types at the two frequencies of 0.9 GHz and 2.45 GHz .....	87
Table 4.4: Measured values of electrical conductivity of the selected rock types for both BTS and UCS sizes of the selected rock types .....	90
Table 4.5: Measured values of thermal properties of the selected rock types .....	91
Table 4.6: Measure emissivity values of the selected rock types .....	92

## **Chapter Five**

Table 5.1: The input operating parameters (conditions) for the experimental tests of single-mode microwave irradiation on the specimens of basalt.....103

Table 5.2: The designed case studies with their input microwave operating parameters for the single-mode microwave irradiation tests on the specimens of basalt .....119

Table 5.3: Results of crack quantification analysis from SEM images of the core samples .....121

## **Chapter Six**

Table 6.1: The experimental conditions for multi-mode microwave irradiation tests.....133

## Nomenclature

$\tan \delta$	Loss tangent	-
$\tan \delta_m$	Loss tangent (from magnetic permeability)	-
$\rho_e$	Volumetric electric charge density	C/m <sup>3</sup>
$\rho$	Density	Kg/m <sup>3</sup>
$I$	Absolute direct current	Ampere
$T$	Temperature	°C
$m$	Mass	kg
$\alpha$	Thermal diffusivity	m <sup>2</sup> /s
$\alpha_t$	Coefficient of thermal expansion	1/°C
$C_p$	Specific heat capacity	J/kg °C
$P_t$	Total polarization	C/m <sup>2</sup>
$T_0$	Room temperature	°C
$A$	Unit cross-sectional area	m <sup>2</sup>
$\alpha$	Atomic polarization	C·m <sup>2</sup> ·V <sup>-1</sup>
$\chi_e$	Dielectric susceptibility	-
$\chi_m$	Magnetic susceptibility	-
$\mathbf{P}$	Polarization	C/m <sup>2</sup>
$\mathbf{E}$	Electric field	V/m
$\mathbf{D}$	Electric displacement	C/m <sup>2</sup>
$\mathbf{H}$	Magnetic field	A/m
$\mathbf{B}$	Magnetic flux density	Tesla
$\epsilon$	Electrical permittivity	F/m
$\epsilon_r$	Relative permittivity	-
$\epsilon_0$	Permittivity of free space ( $\epsilon_0 = 8.86 \times 10^{-12}$ )	F/m
$R$	Electrical resistivity	$\Omega \cdot m$
$\mathbf{I}$	Electrical current	Ampere
$\mathbf{J}$	Electric current density	A/m <sup>2</sup>
$t$ or $t$	Time	s
$\epsilon''$	Dielectric loss factor	-

$\mu$	Magnetic permeability	H/m
$\mu_r$	Relative permeability	-
$\mu_0$	Permeability of free space ( $\mu_0 = 4\pi \times 10^{-7}$ )	H/m
$\sigma$	Electrical conductivity	S/m
$f$	Frequency	Hz
$\lambda$	Wavelength	m
$\lambda_0$	Wavelength of incident radiation	m
$c$	Speed of light in vacuum	m/s
$v$	Speed of wave	m/s
$\omega$	Angular frequency	rad/s
$P_0$	Incident surface power	W
$P_d$	Power density	W/m <sup>3</sup>
$P$	Dissipated power	W
$\beta$	Attenuation constant	m <sup>-1</sup>
$q$	Local heat flux density	W/m <sup>2</sup>
$k$	Thermal conductivity	W/mK
$V$	Volume	m <sup>3</sup>
$V$	Voltage	V
$L$	Length	m
$Q_R$	Heat absorbed by the rock sample	kJ
$Q_W$	Heat absorbed by the water	kJ
$Q_{Total}$	Total heat absorption	kJ
$h$	Height	cm
$d$ or $d$	Distance of rock from microwave horn antenna	cm
$r$	Radius	cm
$u$	Velocity	m/s
$Q_e$	Electromagnetic heat source	W/m <sup>3</sup>
$Q_{rh}$	Resistive heating losses	W/m <sup>3</sup>
$Q_{ml}$	Magnetic (ohmic) heat losses	W/m <sup>3</sup>

## List of Abbreviation

UCS	Unconfined Compressive Strength
SEM	Scanning Electron Microscopy
CT	Computed Tomography
ETM	Electromagnetic, Thermal, and Mechanical
FE	Finite Element
FEM	Finite Element Method
TAL	Thermally Assisted Liberation
TBM	Tunnel Boring Machine
ODC	Oscillating Disc Cutter
RBM	Raise Boring Machine
CAI	Cerchar Abrasivity Index
BWI	Bond Work Index
XRD	X-ray Diffraction
FT-IR or FTIR	Fourier Transform Infrared
UPV	Ultrasonic Pulse Velocity
HPGR	High Pressure Grinding Rolls
BTS	Brazilian Tensile Strength
PLS	Point Load Strength
FDTD	Finite-Difference Time-Domain
ISM	Industrial, Scientific and Medical
CW	Constant Wave
MWD	Microwave Drill
CADT	Council Committee on Advanced Drilling Technologies
DEM	Discrete Element Modeling
ANFO	Ammonium Nitrate Blasting Agent
RF	Radio Frequency
IR	Infrared
USV	Ultrasound Velocity
VHF	Very High Frequency

DSC	Differential-Scanning Calorimetry
TGA	Thermogravimetric Analysis
XRPD	X-ray Powder Diffraction
2D	Two dimensional
3D	Three dimensional
CW	Constant Wave
NMR	Nuclear Magnetic Resonance
XRF	X-ray Fluorescence
RMR	Rock Mass Rating
NIH	National Institute of Health
TGA	Thermogravimetric Analysis
DSC	Differential-Scanning Calorimetry
MLA	Mineral Liberation Analysis
PDE	Partial Differential Equation
RHS	Right Hand Side
LHS	Left Hand Side
UHF	Ultra High Frequency
WHO	World Health Organization
IEC	International Electrotechnical Commission
ICES	International Committee on Electromagnetic Safety
IEEE	Institute of Electrical and Electronic Engineers
CENELEC	European Committee for Electrotechnical Standardization
BDF	Backward Differentiation Formula
MUMPS	MUltifrontal Massively Parallel Sparse
RAM	Random Access Memory
GUI	Graphic User Interface

# Chapter 1

## Introduction

### Contents

---

<b>1.1 Background and motivation</b> .....	<b>1</b>
<b>1.2 Research objectives</b> .....	<b>4</b>
<b>1.3 Thesis outline</b> .....	<b>7</b>

---

### 1.1 Background and motivation

Over the years, mining companies have increased production rates due to increasing demand for raw materials from rapid growth in the global population and industrialization (Dutta et al., 2016). The mining industry is thus essential in order to ensure enough supply to support expansion. This expansion, improving production rates and reducing the footprint of mining operations, brings new opportunities to the mining industry’s development since necessity leads to major investment in new innovative technologies. Given that high-grade ore deposits on or near the surface are continuously depleting, the high demand for raw materials requires advances in mining and exploration techniques to enable more sustainable, automated, continuous, and deeper mining excavations. Continuous processes have been identified as a key factor for the improvement of productivity in the mining industry (Womack & Jones, 1997).

While today rock breakage is considered the most common operation in the civil and mining industries, there exist several challenges regarding the breakage of rocks in both rocks made up of different minerals and the mechanical cutting tools applied to them (Rostami, 2011). One of the main issues that a mining project might encounter during rock breakage processes is that the typical excavation machines available are operating at a limited level due to high disc wear and low rate of penetration in hard rocks (Hassani et al., 2016; Nienhaus et al., 2013). Conventional rock breakage methods such as drilling, blasting, ripping, jack hammers, explosives, hydro-demolition,



and heating through conduction produce high levels of noise, dust and/or vibration, which considerably affect the environment (Natanzi & Laefer, 2014). Consequently, there has been significant industrial interest in replacing conventional methods of rock breakage with novel systems, as the bigger picture also considered the potential of creating non-explosive continuous rock breakage operations (Haase, 1991; Murray et al., 1994; Res et al., 2003). These new systems are expected to be environmentally friendly and to enhance levels of safety and productivity. More importantly, the proposed alternatives should be feasible and cost-effective (Singh, 1998). They must achieve better rock stability, reduce induced seismicity due to the existence of high stresses, and maximize the extraction rate of the mechanical cutting tools. In this case, enormous efforts have been made in finding alternatives to reduce rocks' strength by affecting their mechanical and physical material properties prior to the use of mechanical tools (Hartlieb & Rostami, 2018; Jones et al., 2005; Shepel et al., 2018; Somani et al., 2017). This process of reducing rocks' strength is called "pre-conditioning". Various applications such as hydraulic splitting of rock, plasma blasting, thermal heating, chemical expansion powders, lasers, and electromagnetic induction (microwaves) have been introduced for rock pre-conditioning in recent decades (Hartman & Mutmanský, 2002). The technology of microwave treatment of rocks has recently been assessed as a potential approach for rock pre-conditioning prior to breakage by mechanical means such as the Tunnel Boring Machine (TBM) (Hartlieb et al., 2017; Nekoovaght, 2015). It has been shown that the total energy applied to the rocks could be decreased by combining microwave energy and one of the available excavation machines, e.g. Roadheader, TBM, or Oscillating Disc Cutter (ODC). The penetration rate also increases when an excavation machine is equipped with microwave technology (Hassani & Nekoovaght, 2011; Motlagh, 2009).

The idea of the employing microwaves was first proposed by Maurer (Maurer, 1968; Maurer, 1979) as a novel application to break natural rocks with no mechanical tools involved. Later in 1991, Lindroth et al. (1991) introduced the concept of rock pre-conditioning by microwaves prior to the use of mechanical discs as a potential alternative to conventional methods of rock breakage. Thereafter, several researchers have introduced the application of microwaves in the pre-conditioning of rocks as a novel technique in the future rock breakage operations (Jones et al., 2005, 2007; Kingman et al., 2003; Lovas et al., 2011; Vorster et al., 2001). In the context of the present thesis, the mechanism of the microwave-assisted rock pre-conditioning is defined as follows. When a rock mass is subjected to electromagnetic waves, the applied microwave energy

generates heat (Harrison, 1997). This phenomenon indicates that microwaves have the ability to increase the temperature distribution, creating several microcracks within the rock body due to the selective heating of the rock's mineral constituents, which results in weakening and therefore easier breakage. Hence, one of the significant applications of microwaves is to produce strong thermal gradients in rocks. The generation of these thermal gradients results in the creation of mechanical stresses through rock particles and finally leads to the formation of intergranular cracks (Isaka et al., 2019; Toifl et al., 2017). A conceptual illustration of the primary idea of microwave-assisted rock pre-conditioning system prior to breakage by mechanical tools (e.g. TBM, disc cutter, Roadheader) is depicted in Figure 1.1.

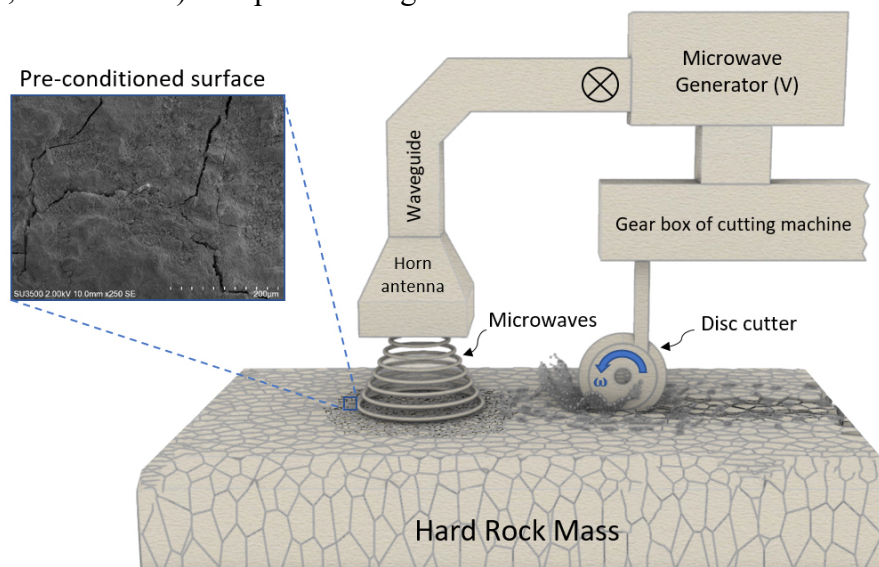


Figure 1.1: A conceptual illustration of microwave-assisted rock pre-conditioning system prior to breakage by a disc cutter

Since the 2000s, microwave-assisted rock heating and pre-conditioning have been found to be a potential new avenue to improve mining and civil engineering projects related to breakage of rocks and processing of minerals (Kingman, 2006; Whittles et al., 2003). The purpose of microwave treatment of rocks is to reduce their strength by weakening key material properties in a continuous manner and without explosives prior to the use of mechanical tools in order to facilitate the breakage operation (Liu, 2014; Lu et al., 2017; Peinsitt et al., 2010; Toifl, 2016). In general, microwaves involve two different types of applicators (cavities), single-mode and multi-mode, with different heating and pre-conditioning mechanisms. Single-mode microwave irradiation is typically used for localized microwave effects (heating and cracking) on the surface of materials under irradiation; it is more applicable when (a) coupled with one of the available

rock cutting tools such as drill and borehole, and/or (b) rock fragmentations needed for downstream processes (Feng et al., 2020; Morrison, 2013; Teimoori et al., 2019a, 2019b). On the other hand, multi-mode microwave irradiation is used for volumetric heating and pre-conditioning of rocks; it is more applicable in the mineral processing industry (Lu et al., 2020). Thus, an understanding of different mechanisms involved in the processes of rock heating and pre-conditioning by the two types of microwaves is important for successful and efficient implementation of a microwave-assisted rock breakage or mineral processing system. To this end, many other parameters should be accurately considered and evaluated to arrive at a proper design prior to its being economically viable, since the only use of microwave technology to break rocks without mechanical tools requires a large amount of energy (Bradshaw et al., 2007). It has been shown that the effect of microwaves on rocks composed of different minerals is highly affected by variations in thermo-physical and electrical properties (Forster et al., 2018; Hartlieb et al., 2016). However, among different properties, the rock's dielectric properties, which comprise both dielectric constant and loss factor, play an important role in the amount of heating and damage produced after irradiation (Li et al., 2019; Zheng et al., 2005). Today, there exist several challenges regarding the efficiency of microwaves that have to be resolved and properly addressed. The previous research serves as a foundation for this thesis and provides insight into the fundamental science of microwaves to bring the idea of applying microwaves to rocks/minerals one step closer to practical implementation. In the present thesis, the detailed concepts of single-mode and multi-mode microwaves are discussed; recent challenges in microwave irradiation of rocks are addressed; and the influences of both single-mode and multi-mode microwave irradiation on the thermal and mechanical changes in rocks with different material properties are quantified by both numerical models and laboratory experiments. The results contribute to better evaluating the impact of microwave technology on future rock breakage techniques, especially the energy-saving potential of such technologies, in both the mining and the processing of rocks. In terms of modeling and simulation, the present research project provides tools and insights into the design and performance of microwave-assisted rock breakage systems.

## **1.2 Research objectives**

The main objective of this research is to address various aspects of the novel application of microwaves in the heating and pre-conditioning of rocks and minerals for better facilitation of rock

breakage and mineral processing operations. To investigate the feasibility of microwave-assisted rock pre-conditioning, it is necessary to understand the mechanisms of different types of microwaves (single-mode vs. multi-mode) when applied to rocks. This can be achieved through laboratory experiments, advanced mathematical and numerical simulation techniques, or a combination of both. Thus, the present thesis has the following objectives:

- To understand how electromagnetic waves (microwaves) are generated in single-mode and multi-mode microwave cavity systems and induced into the rock under microwave exposure, influencing key physical and material properties of the rock after irradiation;
- To conduct several laboratory tests of single-mode and multi-mode microwave irradiation on four rock types, including basalt, granite, and two types of kimberlite, with different microwave operating parameters, e.g. power level, exposure time, and distance from microwave horn antenna (for single-mode microwave irradiation tests on basalt);
- To perform image processing on the irradiated basalt specimens in the single-mode microwave system at various experimental conditions using thermal image analysis for surface temperature measurements, the Scanning Electron Microscopy (SEM) image analysis for quantification of surface microcracks (length and density), and micro-CT scan for visualization of volumetric microcracks;
- To implement a calorimetric method for measurements of the heat (energy) absorption by the selected rock samples irradiated in the multi-mode microwave system at various power levels and exposure times in order to measure the efficiency of microwave energy conversion to heat using calorimetric analysis;
- To numerically develop a novel 3D model of the multi-mode microwave system with a rotational stirrer fan using the Finite Element Method (FEM) for simulating all the practical tests of multi-mode microwave irradiation on the selected rock types and validating the model with the experimental data;
- To conduct parametric studies for investigations on the effects of (a) single-mode microwave irradiation on the surface of a rock mass in terms of damage density and temperature distribution in order to establish more efficient cavity setups, (b) multi-mode microwave irradiation on the heating and energy absorption of rocks in different sizes to test the efficiency of the multi-mode microwave system, and (c) variations in the dielectric properties of rocks on their heat (energy) absorption using a validated numerical model.

In order to achieve the project's main goals, the following fundamental and applied research objectives are accomplished.

### **1.2.1 Fundamental research**

Fundamental research answers the initial question of how things work in the defined project. The fundamental aspects of the present thesis concern the understanding of microwave systems' characterizations in terms of how they are generated, their systematic mechanisms in the rock pre-conditioning process, and how they influence the rock samples after microwave treatments with different operating parameters. The answers to these concerns can be obtained and addressed by measuring the corresponding thermomechanical effects in the irradiated rock samples (i.e. temperature, mechanical stress, and thermally induced microcracks). As part of an overall research investigation on employing microwave irradiation for rock pre-conditioning and as an alternative to former conventional methods, both experimental tests and numerical models are carried out. Several experiments are conducted in order to determine microwave primary effects on heating and fracturing of rocks after microwave treatments in both single-mode and multi-mode microwave systems with different operating parameters (e.g. power level, exposure time, and distance from the horn antenna for single-mode microwave irradiation application) on various rock types with different electrical, thermal, and mechanical properties. In addition, several numerical models with the same experimental parameters are developed using the FEM to investigate the primary effects of multi-mode microwave irradiation on hard rocks. The models are validated against experimental data from calorimetric measurements. The numerical modeling approach is considered a strong mathematical tool that generates new insights into the integration of the fundamental concept of multiphysics interactions in rocks after their exposures to microwaves. With a validated numerical model, future investigations of the effects of microwave irradiation on various rocks and minerals can be achieved without costly experiments. Thus, the development of a validated numerical model is a crucial step of the present thesis which enhances the evaluation of microwave systems' efficiency.

### **1.2.2 Applied research**

Applied research is designed to answer specific questions aimed at solving technical and practical problems. Novel knowledge acquired from applied research has specific commercial objectives in the form of implementation of products, procedures or services (Kothari, 2004). In

this thesis, the results from fundamental research are extended through several investigations by changing key parameters (e.g. microwave operating parameters and material properties of rocks) that play significant roles during the microwave operation for its maximum efficiency. The applied aspects of the current research address optimization of the design of microwave-assisted rock pre-conditioning and breakage with maximum efficiency for both single-mode and multi-mode microwave cavity systems.

In summary, this thesis, in its fundamental aspect, advances rock mechanics science and engineering knowledge of microwave applications for the pre-conditioning of rocks and minerals. It also covers the applied aspects of successful implementation of this novel system for its future industrial-scale implementation. Hence, it can be inferred that the difference between the applied and fundamental research is straightforward—findings of applied research can be applied to resolve issues, whereas fundamental studies are used to explore elements and certain issues in a microwave-assisted rock pre-conditioning system. A quick summary of the fundamental and applied research objectives of the present thesis is given in Figure 1.2.

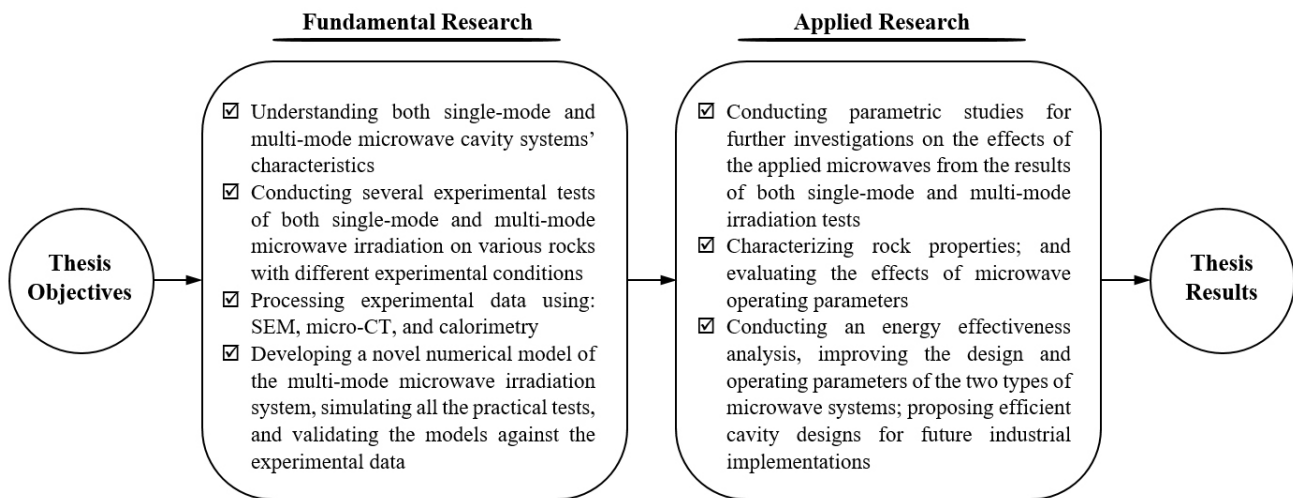


Figure 1.2: Flowchart of the thesis research objectives

### 1.3 Thesis outline

This thesis is divided into seven chapters and the outline is as follows:

**Chapter 1** is the primary guideline of the present thesis. It first discusses the background and gives a quick overview of microwaves and their potential applications in the heating and pre-conditioning of rocks as well as processing of minerals. Then, a general introduction, aim and

motivation for this thesis, and the objectives of the study follow. Finally, a brief summary of each chapter is given.

**Chapter 2** aims to give a comprehensive review of the work done in the context of rock heating and pre-conditioning methods for their easier breakage. It covers, in its beginning, a broad overview of the history of rock breakage techniques and the evolution of microwave applications in rock mechanics and rock engineering. Then, it presents a comprehensive literature review of previous experimental studies and modeling and simulation literatures published from 2000 to 2020. Finally, the chapter concludes with a technical and economic analysis of work done up to now in the area of microwave-assisted rock pre-conditioning and breakage.

**Chapter 3** introduces the fundamental principles of electromagnetic waves for heating and pre-conditioning of rocks. All mechanisms involved and influencing parameters in the microwave irradiation of rocks and minerals are defined. Various aspects of rock-microwave system characteristics from variations in the rocks' electrical and thermal properties to the type of the microwave system applied are discussed.

**Chapter 4** provides details of technical information about the physio-mechanical and mineralogical characteristics of the selected rock types in the present work for microwave irradiation experiments. Various experimental methods for measuring the electrical and thermal properties of the selected rock samples are then described and compared; and then, the measured values of material properties of the selected rocks are analyzed. The final section of the chapter introduces all the instrumental methods utilized for characterization of the irradiated rock samples after the microwave irradiation experiments.

**Chapter 5** introduces a multiphysics study of single-mode microwave irradiation effects on rock pre-conditioning and breakage. Rectangular specimens of basalt—intact blocks cut from quarries—are used in all experimental tests of this chapter. The aim of this chapter is to experimentally investigate the impact of single-mode microwave irradiation on the surface heating and pre-conditioning of rocks by implementing three research phases. In Phase I of the research, a thermal image analysis from surface temperature measurement of irradiated basalt specimens at different experimental conditions is presented and discussed. Then, in Phase II of the research, SEM image analysis from surface microcrack quantification is given and assessed. Finally, in Phase III of the research, volumetric microcrack visualization from the results of micro-CT scanning is presented and discussed. Parametric studies are conducted to investigate the influence

of microwave power level, exposure time, and distance from the horn antenna. Finally, the chapter ends with overall conclusions based on the findings of the experiments.

**Chapter 6** presents a comprehensive multiphysics study of multi-mode microwave irradiation effects on rock pre-conditioning and breakage. The chapter is divided into two main parts as follows. The first part presents experimental studies of multi-mode microwave irradiation on four rock types, basalt, granite, and two types of kimberlite, in two sizes of standard BTS and UCS. The following steps were implemented: (1) irradiation of the selected rock samples in the multi-mode microwave system at various power levels and exposure times, (2) thermal analysis of the irradiated samples from surface temperature measurements, and (3) calorimetric tests for calculating microwave ramp-up time and measuring heat (energy) absorption in the rock samples after microwave tests. The results of each step are presented and discussed separately. Parametric studies are conducted in the first part to examine the results of the experiments for investigating the effectiveness and energy saving potential of multi-mode microwave cavities for future industrial applications of rock pre-conditioning and breakage. In the second part of the chapter, the development of a novel 3D numerical model of the multi-mode microwave cavity system—with the same physics and geometry as in the experiment—with its numerical implementation is described. This model development section highlights the existing challenges in the modeling of rock-microwave systems and presents a novel simulation of the multi-mode microwave cavity system with a rotational stirrer fan. Discussion of the model validation follows. Finally, the results of the electric field distribution and power absorption by the irradiated rock models are discussed and the effects of variations in dielectric properties of rocks are numerically examined. Finally, the chapter ends with overall conclusions based on the findings of the experiments and the models.

**Chapter 7** presents the main conclusions of this work. It highlights the primary findings of individual chapters and projects an outlook concerning the main objectives of this study. In the end, it provides certain perspectives of the limitations of the current work and recommendations for future studies.



# Chapter 2

## Literature review

### Contents

---

2.1	History of rock breakage techniques.....	11
2.2	Review of recent research on microwave irradiation of rocks and minerals.....	19
2.3	Research gaps and outlook.....	49

---

### Preface (Linking Paragraph)

*This chapter provides a background and summary of the published literature related to the focus of this thesis. It reviews the state-of-the-art achievements in the literature regarding the fundamental and applied aspects of the microwave-assisted rock/mineral pre-conditioning and breakage systems for easier breakage of hard and abrasive rocks by mechanical means and for enhancement of the downstream processing of minerals. The first part of literature review, section 2.1, explains the history of rock breakage techniques, as follows.<sup>1</sup> In section 2.1.1, conventional rock breakage techniques are explained and compared with novel breakage methods. Then, in section 2.1.2, evolution of microwave applications in rock mechanics and rock engineering is discussed. Section 2.2, reviews recent studies from 2000 to 2020 on microwave irradiation of rocks and minerals that focus on different methodologies and analyses, as follows: experimental studies (section 2.2.1), modeling and simulation literatures (section 2.2.2), technical and economic analyses (section 2.2.3). Finally, section 2.3 discusses the challenges involved in this research area and the efforts that should be made regarding the potential practical implementation of microwaves in rock mechanics for the industry. The research gaps shape the basis of the current work that will be explicated in the subsequent chapters.*

---

<sup>1</sup> This chapter does not review all the techniques in the history of rock breakage. Only those that were within the scope of the thesis subject are discussed.

## **2.1 History of rock breakage techniques**

### **2.1.1 Conventional and novel rock breakage methods**

Since the Stone Age, humans have increasingly used various rock breakage techniques. The breakage of rocks has been a serious challenge for most civil and mining projects, such as tunneling and underground excavations. One of the historic forms of rock breakage is by explosives. Explosives are chemicals which react to cause the desired result and are considered one of the primary forms of breakage. They have been used for blasting purposes in civil engineering, military and mining applications (Murray et al., 1994). The other typical and historical form of rock breakage, which is considered the most efficient one, is the use of force via a mechanical device or tool. Mechanical rock breakage has been the dominant method since the transition to new manufacturing processes in Europe and the United States, which occurred in the period from about 1760 to sometime between 1820 and 1840—the Industrial Revolution. In the context of the present literature review, the definition of mechanical rock breakage is the process of creating a high-stress area within the rock by using a tool to cause failure and disintegration. In addition, mechanical excavation refers to the methods of breakage whereby the rock is entirely removed from the mine face by applying mechanical tools. There are three primary tools for mechanically breaking rocks: drag bits, indenters, and impact tools (Rostami, 2011). The majority of rock cutting tools are indenters, which include all cutters that roll, such as disc cutters, rolling cones, or button bits (Vogt, 2016). The most typical mechanical excavators are Tunnel Boring Machines (TBMs), Oscillating Disc Cutters (ODCs), Raise Boring Machines (RBMs), roadheaders, continuous miners, and longwall shearer drums (Hartman et al., 1994).

Today, there are very few methods available for the breakage of rocks. These methods are limited to the following techniques: conventional drilling and boring, blasting, ripping, and heating through conduction (Rostami, 2011). However, there exist several challenges; for instance, one of the significant issues during the breakage of rocks by mechanical excavators is that the typical excavation machines available operate at a limited level because of high disc wear and low rate of penetration (Nekoovaght, 2015). With increasing depth, rock drilling and boring encounter (1) high confining pressure or high stress state, (2) high temperature in the drill bits, and (3) energy transmission becoming less efficient in very long-hole drilling. These factors slow down drilling or boring processes and increase the overall cost of the project. From an energy point of view, in

rock drilling, blasting, crushing, and grinding, it has been shown that the effective energy used in rock breakage is relatively small in comparison to the total input energy (Zhang, 2016).

Since the mid-1900s, civil and mining companies have found that using high-energy explosives for breaking rocks has several disadvantages that limit the productivity and advancement rates of a mining project (Persson et al., 1994). Therefore, rock fracturing by mechanical means has remained the most efficient and economical. However, serious attempts at development of viable and novel alternative methods to explosives (e.g. chemical, thermal, fluid, sonic, laser, and electrical) started (Murray et al., 1994). In 1952, James Robbins developed the first modern TBM for the Oahe Dam Project in South Dakota, USA. The machine used drag bits and dumbbell-shaped cutters to successfully excavate weak shale rock (Bruland, 1999). Since the development of the modern hard rock TBMs in 1950s, they have become one of the most dominant tunneling techniques. TBMs began to seriously impact the use of explosives in large tunnel jobs (Zheng et al., 2016). TBM tunneling in hard rocks has shown several advantages compared to conventional drilling or blasting techniques because it achieves higher advance rates and better working conditions. When compared to the conventional breakage methods, other advantages of TBMs are higher levels of labor safety and possible saving of operation costs (Cigla et al., 2001; Maidl et al., 2008). Nevertheless, there is still a challenge when TBMs are applied to harder and more abrasive rocks, resulting in excessive cutter wear and low advance rates. In addition, modern drilling in underground excavations is primarily performed by TBMs. While they are very effective, their extended use wears down the equipment and results in costly replacements. Therefore, it is necessary to reduce the impact on drilling equipment by introducing an assisting method to pre-condition the surface of rock prior to the act of the mechanical tool. This pre-conditioning technique allows continuous mining operations without interruption and leads to the reduction of environmental impacts such as air blast, fly rock, or any damage to the surroundings (Singh, 1998).

Generally, hard rock contributes to the reduction of the efficiency and performance of the cutting tools and their life span. Conventionally, in explosive-free rock breakage applications, an improvement of machinery was the priority approach to increasing the efficiency and performance of the equipment. In tunneling and deep mining operations, the conventional methods, such as tunnel excavator or tunneling by TBMs, has faced multiple challenges: low penetration rate and long duration of project (Lu et al., 2016; Zheng et al., 2016). Consequently, mining companies

needed a more technical and innovative excavation technique to facilitate conventional hard rock excavation. The new design criteria for such techniques should be capable of breaking rocks, including harder and more abrasive types, more efficiently than the former methods. The proposed method was supposed to have achieved better rock stability, reduced induced seismicity due to the existence of high stress, and maximized the extraction rate of the mechanical cutting tools (Singh, 1998). In the history of various rock breakage techniques' development and improvement, enormous efforts have been made in finding alternative assistive methods to conventional rock breakage techniques. Over recent decades, to facilitate the breakage of rocks, various applications, such as chemical, thermal, fluid, sonic, laser, and electrical have been developed and applied (Res et al., 2003). Sometimes, these assistive methods of breakage were designed to be able to break rocks on their own capacity; however, in most cases, their developments were initially intended to be coupled with one of the available mechanical breakage machines, such as disc cutters or TBMs. These methods along with the previous rock breakage techniques can be divided into two major categories at the stage of development. In 2002, Hartman and Mutmansky (2002) classified methods of rock breakage into two major categories, conventional methods and novel techniques. Although they introduced two classifications of rock penetration methods, one based on form of attack and the other based on form of energy, the former penetration method can be considered more applicable after emergence of novel assisting methods of rock breakage in the past two decades (see Table 2.1).

Table 2.1: Classification of conventional and novel rock penetration methods (modified from Hartman and Mutmansky [2002])

Method	<i>Practical</i>			<i>novel</i>		
	Mechanical	Thermal	Fluid	Sonic	Chemical	Electrical
Percussion Drop tool Hammer	Flame Plasma	Jet Erosion	Vibration	Explosion Reaction	Electric arc or current Electron beam	Laser
Rotary, drag-bit Blade Stone-set Sawing	Hot fluid Fusion	Bursting Cavitation			Electromagnetic induction (microwaves)	
Rotary, roller-bit Rotary-percussion Hammer Rotary	Freezing					

Further studies on the conventional methods of rock breakage and comprehensive state-of-the-art reviews of current and emerging rock breakage technologies are presented in Vogt (2016), Dehkhoda (2017), and Ramezanzadeh & Hood (2010). A considerable amount of research on novel assisting rock breakage applications began at the end of the 1960s (Zheng, 2017). For example, the application of waterjet cutting technology for rock breakage was introduced. A waterjet cutter consists of a high-pressure pump, a jet nozzle, and an abrasive delivery system. It provides an impact on the designated area using a high velocity and high pressure jet. A commercial type of waterjet system can provide pressures up to 900 MPa. Although waterjets are capable of cutting rocks of any strength and hardness, the adjacent ribs produced between waterjet notches still have to be mechanically removed by a secondary method (Summers & Henry, 1972). A conceptual illustration of the primary idea of the coupling of waterjets with a mechanical disc cutter and a TBM is shown in Figure 2.1(a) and 2.1(b). On the basis of the form of attack, the waterjet-assisted cutting system can be considered a novel rock penetration method. There is a high-level of interest in the investigation of the application of high-pressure power to improve rock cutting for blast-hole drilling, as discussed by Pederick and Lever (2004). It is worth mentioning that a later study by Wilson et al. (1997) indicated that waterjets on their own are inefficient; however, they can be more efficient when combined with other techniques, e.g. coupled with mechanical tools (Vogt, 2016). A comprehensive review of the waterjet cutting history and its applications in direct and assisted rock breakage can be found in a study by Summers (2003).

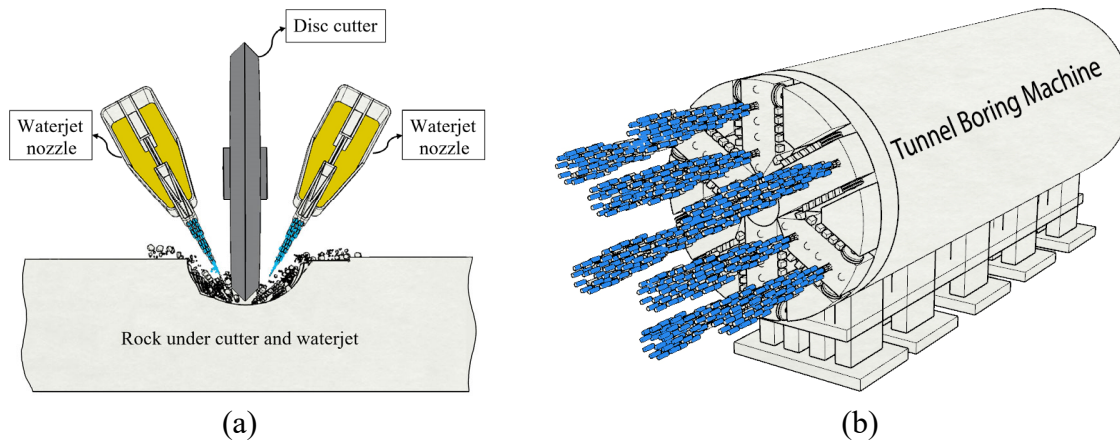


Figure 2.1: Conceptual illustration of (a) coupling of waterjet application with a mechanical disc cutter, and (b) waterjet-assisted TBM tunneling

Rocks are composed of different minerals. The difference between thermal expansion of the minerals in a rock sample creates fractures, which facilitate breakage and reduce the energy of size

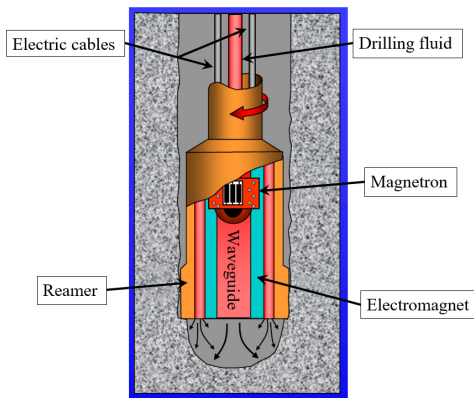
reduction (Fitzgibbon & Veasey, 1990). Therefore, thermally assisted breakage of rocks is another novel rock breakage technique. There are different sources of heating available for thermal treatment of rocks, including laser, plasma, flame, fusion, infrared radiation, and microwaves. The mechanism of thermal breakage is the same for almost all these heating applications; when heat is applied, the temperature gradients in the rock cause mechanical stresses that develop and expand existing microcracks (Ndeda et al., 2015). In 1990, Thermally Assisted Liberation (TAL), based on the consecutive heating and cooling of rocks, was suggested as a method to reduce comminution energy (Fitzgibbon & Veasey, 1990; Vorster et al., 2001). This method used cyclical expansion and contraction of minerals to create cracks between the grain boundaries. These fractures led to improvement of grinding and enhancement of mineral liberation. After the emergence of microwave technology, it was found that microwave treatment is more effective than TAL or other heating methods because it heats materials according to their dielectric properties; therefore, energy is not wasted (Kingman et al, 2000). Consequently, the application of microwaves in the rock breakage industry, in both mining and processing of rocks and minerals, started after subsequent studies confirmed that microwaves are more competitive than any other assistive rock breakage techniques, considering:

- Microwaves heat up rocks on the basis of their dielectric properties; therefore, energy is not wasted to warm up the whole rock body, since rocks are composed of various minerals with different dielectric properties (Kingman et al., 2000),
- Microwaves are faster as they rely on selective heating of minerals (some minerals have a rapid response to the applied electromagnetic waves) (Li et al., 2019),
- Microwaves have high a level of safety and automation (Haque, 1999).

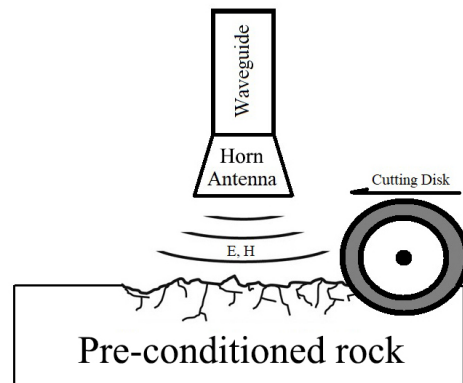
### **2.1.2 Evolution of microwave applications in rock mechanics and rock engineering**

Even though electromagnetic waves were discovered in the mid-1800s, microwaves were first predicted by James Clerk Maxwell in 1864. Later in 1888, Heinrich Hertz proved the existence of microwaves by building a device that produced and detected microwave radiation (Sengupta & Sarka, 2003). Microwaves comprising electric and magnetic fields, represent a form of electromagnetic energy. Materials that can absorb microwave radiation are called dielectrics and contain dipoles. When a dielectric material is subjected to microwaves, its dipoles align and flip

when the applied electromagnetic waves alternate. As a result, the stored internal energy is lost to friction and the dielectric materials heat up (Kingman & Rowson, 1998). Microwaves have been used for a variety of applications in the past six decades. These applications include food processing, power transmission, communications, weather control, medical science, vulcanization of rubber, as well as heating and drying (Antunes et al., 2017; Eastlund & Jenkins, 2008; Li et al., 2018; Reddy et al., 2013; Vorlíček et al., 2011). However, among different applications of microwaves, heating of materials has been considered one of the most common applications of microwaves for domestic and industrial purposes (Huang et al., 2020; Kingman, 1996), which therefore led to increased research into the applications of microwave irradiation in rock mechanics and the rock engineering field. The use of microwaves was first proposed by Maurer (Maurer, 1968; Maurer, 1979) as a novel application to break natural rocks with no mechanical tools involved. Maurer (1968) illustrated the potential of some novel conceptual drilling techniques, of which one was a microwave-assisted drill. In short, the method that Maurer (1968) introduced was drilling by only using microwave antenna at the end of the drill bit (see Figure 2.2(a)). Although Maurer’s (1968) design was novel, many parameters had to be accurately considered in a proper design of a microwave-assisted rock drilling system to be economically viable, since the sole use of microwave technology to break rocks without mechanical tools requires a large amount of energy. The pressure to remain with the *status quo* always conserves the main focus in any technological change (Constant, 2002).



(a) modified from Maurer (1968)



(b) modified from Lindroth et al. (1991b)

Figure 2.2: The primary idea of (a) the microwave-assisted drilling system, and (b) the microwave-assisted mechanical rock cutting system

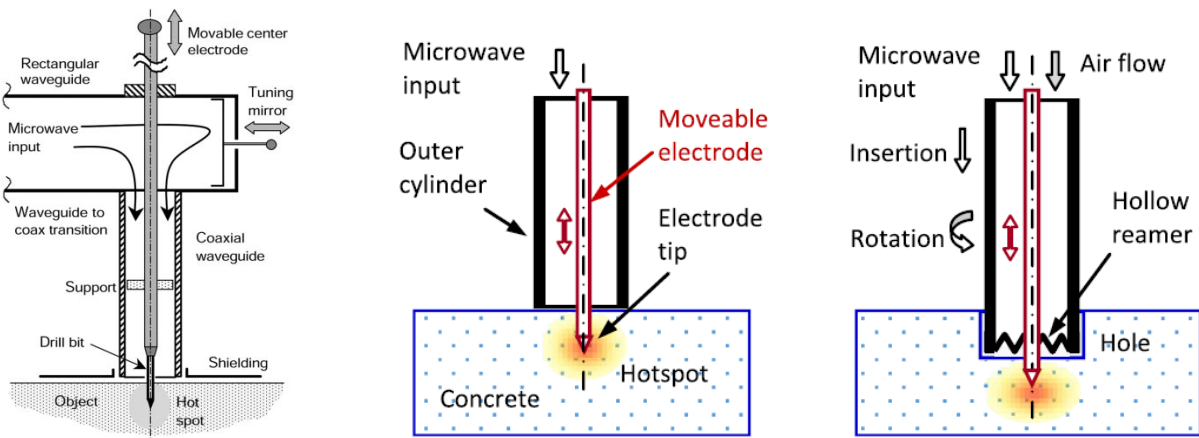
After rock breakage, the ore needs to be processed in order to provide a valuable concentrate (Ali, 2010). If the reduction in the wear on the drills is offset by determinantal effects on the

processing, then new protocols for the separation of valuable minerals from the waste will be required (Ali & Bradshaw, 2010). Previous work investigating the effects of microwave irradiation on the processing of minerals, including separation, grinding, and purification, has shown some promise results (Buttress et al., 2016, 2017; Ferrari-John et al., 2016; John et al., 2015; Kingman, 2006; Monti et al., 2016). From 1988 to 1991, it was discovered that ore minerals are great absorbers and gangue minerals are transparent to electromagnetic waves (Walkiewicz et al., 1988). It has been shown that under microwave irradiation, the differential heating or selective heating is created between minerals grain and surrounding transparent matrix (gangue minerals), which generate intergranular cracks through minerals' boundaries. Moreover, the thermal expansion of different minerals causes tensile stress along the grain boundaries, which finally results in several microcracks. These microcracks reduce the overall rock strength and improve rock breakage, grindability, and mineral liberation. More importantly, the pre-conditioned rock facilitates rock drilling, reduces bit wearing, and decreases energy consumption of size reduction in mineral processing (e.g. crushing and grinding) (Walkiewicz et al., 1988). These findings have been key focuses, since energy consumption and mineral recovery have always been two important issues in the mineral processing industry (Fitzgibbon & Veasey, 1990). The very first recorded attempt to expose minerals to microwave irradiation was a patented work by Zavitsanos and Bleiler (1978) in 1978 called "desulphurization of coal using microwaves". Subsequent research about this novel application of microwave irradiation on minerals was stimulated by a publication from Chen et al. (1984) concerning the relative transparency of minerals to microwave energy. The research on application of microwaves for the pre-conditioning and breakage of rocks was first introduced in 1991 by Lindroth et al. (1991b) and called "pre-conditioning of rocks by microwaves" as a potential alternative to conventional methods. Following this innovation, the technology of microwave-assisted rock breakage was considered potentially as one of the most important explosive-free technologies for pre-conditioning of rocks prior to breakage by a cutting machine. A schematic of the first proposed novel microwave-assisted mechanical rock cutting system is shown in Figure 2.2(b).

In 1994, the American National Research Council Committee on Advanced Drilling Technologies (CADT) published a report entitled "Drilling and Excavation Technologies for the Future" (National Research Council, 1994). In this report, Maurer's (1968) proposal on the use of the microwave-assisted drill was emphasized by the committee members. This report therefore



underlined the importance of improved conventional mechanical drilling technologies as well as avenues to assist such technologies with the use of microwave energy. Thereafter, several researchers introduced the use of microwaves in the pre-conditioning and breakage of rocks and processing of minerals as a novel approach in the future mining operations. Extensive research began in the 2000s. Several studies have outlined that the total energy applied to the rocks can be decreased by combining microwave energy and one of the available excavation machines, e.g. Roadheader, TBM, or Oscillating Disc Cutter (ODC) (Ouellet et al., 2013; Zheng et al., 2016). The penetration rate also increases when an excavation machine is equipped with microwave technology (F. Hassani & Nekoovaght, 2011). In 2000, Jerby and Dikhtiar (2000) presented their novel apparatus that drives the microwave energy from a 1 kW magnetron to a waveguide and, finally, into the material. The design is such that the applied microwaves are localized into a predetermined spot on the material. An extended project was later presented in 2003 which introduced a novel design of a Microwave Drill (MWD) system based on generating a hot spot on the surface of an object (Jerby & Dikhtyar, 2003). As shown in Figure 2.3(a), microwaves from a rectangular waveguide are transmitted to a coaxial waveguide. The central electrode (central antenna), which also function as a drill bit, concentrated the microwaves to a specific point. Therefore, the hot spot created on the surface weakened the rock's strength and resulted in easier drilling.



(a) (Jerby & Dikhtyar, 2003)

(b) (Jerby et al., 2018)

Figure 2.3: (a) Scheme illustrating the principle underlying the operation of microwave-drill system. (b) Conceptual schemes of MWD applicators, including a basic MWD consists of a coaxial waveguide with a moveable center electrode, inserted into the softened hot spot to form the hole (left) and an advanced MWD for deeper holes (right)

Following the design presented in 2003, Jerby and colleagues developed the basic design of a microwave drill capable of drilling holes with 26 cm (depth) by 12 mm (diameter) in concrete, as shown in Figure 2.3(b). Their technology can be performed silently to drill 1.5 cm holes at 2.45 GHz frequency. This apparatus has been successfully applied to a variety of materials such as glass, basalt, concrete, ceramics, and silicon, but it is still at the bench scale.

In conclusion, although tools operate on different scales, their penetration and fragmentation functions occur through the application of energy on similar rock failure mechanisms. In any rock destruction method, processes conducting a very rapid application of energy are critical to produce failure. In drilling, cutting, breaking, kerfing, boring, or any other similar applications, the penetration rate “R” is directly proportional to the amount of energy “P” applied to the process. Therefore, microwave energy in combination with a breakage machine raises the total energy applied to the rock and results in an easier failure of the rock.

## **2.2 Review of recent research on microwave irradiation of rocks and minerals**

Microwaves have been used for a variety of applications in the past two decades. However, there has been a significant and growing interest in the applications of microwaves in the rock breakage and mineral processing industries. The purpose of this section is to focus on these applications and to present a technical review of the state-of-the-art experimental studies, modeling and simulation literatures, as well as technoeconomic analyses introduced in the literature from 2000 to 2020. As a final contribution of this section, the challenges involved in this research area with some concluding remarks from the discussed literatures are debated. Moreover, the attempts that should be made to numerically model the process of microwave treatment of rocks via computer simulations for future predictions of the effects of microwaves on different rock types without costly (and sometimes impossible) experiments are discussed.

### **2.2.1 Experimental studies**

In the 2000s, several studies highlighted the effects of microwave treatment on different types of rocks and minerals by performing various experimental tests. The experimental approach is an ongoing methodology used by researchers to verify the potentiality of microwave energy in the pre-conditioning and breakage processes of rocks and in the processing of minerals. In this

section, the primary experimental studies related to the subject of the present thesis are extensively discussed and reviewed. Then, a summarized list of the results published in secondary experimental studies on laboratory experiments of microwave treatment of rocks and minerals is given in Table 2.4. Because of the scarcity of the literature, the following review is organized so that each paragraph discusses all publications for each well-known research group or studies with the same perspective in the field.

From the beginning of the 2000s, researchers from the University of Nottingham, UK, carried out a number of related studies on the effect of microwave irradiation on mineral processing, including minerals separation, grinding, purification, and the reaction mechanisms of microwaves on various types of rocks and ores with different morphologies. Kingman et al. (2000) investigated the grindability of ores according to the Bond Work Index (BWI). They experimentally irradiated four samples, including massive Norwegian ilmenite ore, massive sulphide, highly refractory gold ore, and open pit carbonatite, in a multi-mode microwave cavity with a variable power of 2.6 kW and a frequency of 2.45 GHz. From the results of microwave irradiation tests on the selected ore samples with an applied power level of 2.6 kW at different exposure times of 10s, 30s, 60s, 90s, 100s, and 120s, the authors concluded that microwaves can significantly reduce the BWI of ores, which implies that microwave treatment has the ability to decrease the energy required for fragmentation of ores. The same conclusion was later drawn in a study by Vorster et al. (2001) on the grindability response of a massive copper ore. This study showed that the work index of massive copper ore may be reduced by up to 70% after 90s of microwave exposure at a power level of 2.6 kW in a multi-mode cavity. Later, Jones et al. (2002) presented a review of microwave heating applications in environmental engineering and surveyed all related conclusions in studies prior to 2002. Jones et al.'s (2002) study concluded that an efficient design of microwave heating equipment is not possible without a proper knowledge of the material's dielectric properties. The authors further pointed out that a detailed fundamental knowledge of microwave engineering is needed for the development of an efficient design of microwave cavities to reduce the energy input for a pilot test or economically feasible industrial commercialization. Furthermore, in an investigation on the influence of microwave treatment on andesite specimens, Znamenáková et al. (2003) exposed three individual cored samples. These samples were melted completely after being subjected to 1.35 kW at a frequency of 2.45 GHz after 10 minutes microwave exposure and 30 minutes with 2.7 kW at the same frequency in a multi-mode cavity. To investigate the results

from this experiment, the same authors later performed a characterization method, an X-ray Diffraction (XRD) analysis, which revealed that the basic chemical composition of andesite remained unchanged; nevertheless, its structure became amorphous after the microwave experiments (Lovás et al., 2010; Lovás et al., 2011).

In 2004, Kingman et al. (2004) experimentally studied the influence of short-term microwave treatments of copper carbonatite ores, up to 1 kg in weight, with power levels of 3 kW to 15 kW in a single-mode cavity. They conducted point load, drop weight, grindability, and liberation tests on the treated and untreated ores. According to the results of these experiments, the authors reported that by treating the samples for 0.2s exposure at 15 kW microwave power with an energy input of 0.83 kWh/t, 30% reduction in impact breakage parameters was achieved. Kingman et al. (2004) further pointed out that by using a microwave-assisted comminution process, reduced plant size, potentially reduced wear costs per tonne, lowered water usage, and produced smaller downstream recovery circuits could be considered as benefits of microwave usage. In another study, Kingman and colleagues (2004) experimentally tested the effects of microwave power on the breakage of lead-zinc ore samples by employing both single-mode and multi-mode microwaves with an operating frequency of 2.45 GHz at different power levels of 5, 10, and 15 kW for various exposure times of 1s, 5s, and 10s. The authors performed comparative tests on the results of their single-mode vs. multi-mode microwave irradiation tests and on their treated vs. untreated samples. From the results of multi-mode microwave tests, Kingman et al. (2004) found that the strength of their samples was reduced rapidly at higher microwave power levels (e.g. 15 kW). However, multi-mode microwave irradiation tests with lower power levels were observed to be less effective. Subsequently, by using drop weight tests for quantification of the changes in the strength of the treated ore samples, up to 40% reduction in required comminution energy was achieved for ore particles of a mean size of 14.53 mm. Likewise, after single-mode microwave irradiation experiments at 10 kW, strength reduction of 50% was observed in the irradiated ores with a residence time of only 0.1s, which implies that for both single-mode and multi-mode microwave applications, a high input power level of microwave plays an important role for strength reduction and ore failure.

In 2005, experimental investigations on the effects of microwave treatment on the fracturing and grinding of kimberlite ore samples were studied by Didenko et al. (2005). They employed continuous wave magnetrons with power levels of 0.6 kW and 5 kW at a frequency of 2.45 GHz.

The authors specifically mentioned that they used resonator-type rather than waveguide-type microwaves to elevate the microwave-energy density, which allowed them to reduce the heating time of samples. After exposure of kimberlite samples of a size 3-4 cm<sup>3</sup> into the cylindrical  $H_{111}$  resonator for several seconds at a microwave power of 0.6 kW, the samples' temperature reached hundreds of degrees Celsius. Didenko et al. (2005) mentioned that the heating process was done alongside a series of explosions, and the samples were split into 2-4 pieces. They further used a vapor bath method to investigate the effect of pressure rise due to the vaporization of water in the pores on the fracturing process; and found thermal shock fracturing could occur because of either linear expansion of solids in the heating process or the rapid evaporation of water in the rock pores.

Another study by Wang and Forssberg (2005) presented microwave-assisted comminution and liberation tests on various minerals, including dolomite, limestone, copper ore, and quartz. Although it is not mentioned which types of microwave applicators were used for microwave irradiation tests in the article, it can be inferred that the authors employed a multi-mode microwave applicator for treatment of their samples. They employed a microwave system with a volume of 2.5 m<sup>3</sup>, a frequency of 2.45 GHz, and variable power levels of 3 kW and 7 kW for the following microwave exposures: 0, 5, 10, and 30 minutes. To investigate the influences of microwave treatments on the samples, dry ball milling tests for grindability evaluations and UCS tests for samples' strength measurements were performed. By comparing the results of the untreated with treated (7 kW/10 min) samples, the authors observed that the uniaxial compressive strength of quartz and limestone decreased from 50 MPa to 25 MPa and 40 MPa to 35 MPa, respectively. On the contrary, the UCS size of dolomite was found to be incremented. Then Wang and Forssberg (2005) concluded that the coarser particles ( $-9.50 + 4.75$  mm) of limestone and quartz were affected by microwave heating to varying degrees. In terms of liberation, the authors remarked from the grindability tests that the initiation of cracks by microwave heating would favor the reduction of energy consumption in comminution processes. In addition, a better and cleaner liberation of the mineral particles from the ore matrix can be obtained when a selective fracturing along the grain boundaries occurs. Overall, the study by Wang and Forssberg (2005) indicated that minerals' particle size had a significant effect in both mineral pre-treatment by microwaves and comminution and liberation processes; therefore, the result was an increased fineness of the ground product. A similar investigation by Amankwah et al. (2005) on improved grindability and gold liberation by microwave pre-treatment of a free-milling gold ore also verified the above findings.

In 2006, the influence of applying microwave irradiation with low power levels of 100 W to 150 W on basaltic rock was experimentally investigated by Satish et al. (2006). A multi-mode microwave cavity with an input power density of 1 W/g and an operating frequency of 2.45 GHz was used to irradiate cylindrical samples with a diameter of 38.1 mm and a height of 40 mm at exposure times of 60s, 120s, 180s, and 240s. The temperatures of the samples were recorded by using an Infrared (IR) camera after microwave treatments. Moreover, a standard point load tester was used for further mechanical and physical investigations on the amount of compressive and tensile strengths in the irradiated samples. The authors found that an increased exposure time resulted in increased temperatures, cracks, local spallation, and, subsequently, reduction of the rock's final strength. The trend of this reduction in the samples' compressive strength with respect to microwave exposure is shown in Figure 2.4(a).

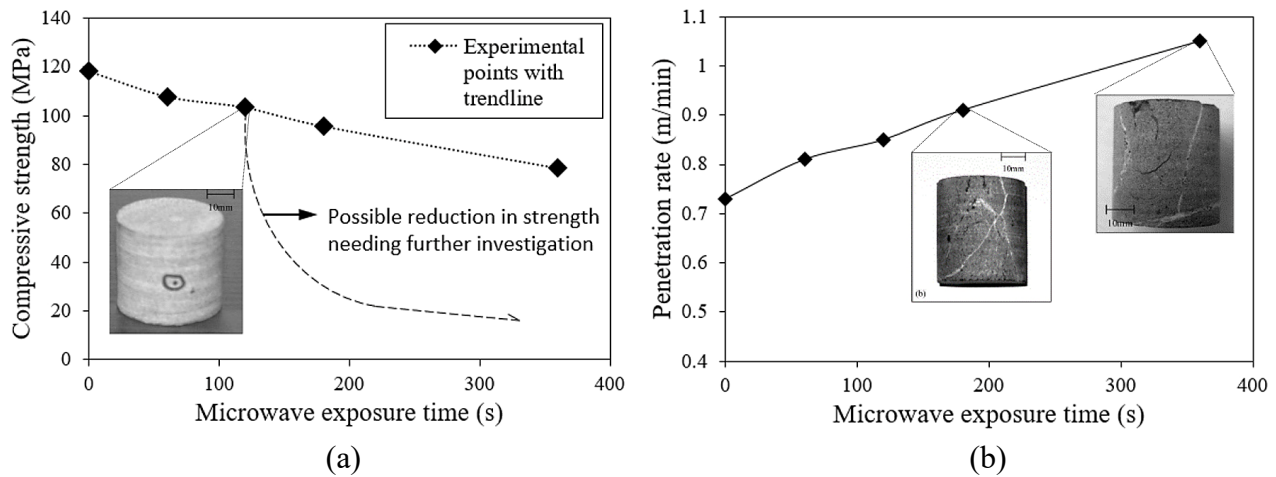


Figure 2.4: Effect of microwave treatment of basaltic rocks with an input power density of 1 W/g at different microwave exposure times on (a) samples' mean compressive strength and (b) penetration rate of basalt for the percussive drilling process (modified from Satish et al. [2006])

Satish et al.'s (2006) study provides a plot of microwave exposure times in regard to penetration rate for the percussive drilling process. It has been shown that at 360s microwave exposure, a 42% increase in penetration resulted compared to nontreated samples. Furthermore, thermally induced cracks visually appeared only when samples were treated for 180s and 360s exposures (see Figure 2.4(b)). In conclusion, this study verified that basaltic rock is very responsive to microwave exposures with low power levels as its temperatures linearly increase with time of irradiation.

Can and Bayraktar (2007) studied the influences of microwave irradiation on the floatability and magnetic susceptibilities of different sulfide minerals including pyrite, chalcopyrite, galena and sphalerite. These selected minerals were irradiated in a multi-mode microwave system at power levels of 600 W, 950 W, and 1300 W and exposure times of 5s, 20s, 60s, 90s, 120s and 240s. The authors performed microfloatation and magnetic separation tests to investigate the effects of the applied microwaves on the minerals. From the results of the experiments, Can and Bayraktar concluded that the sulfide minerals were unequally affected by microwaves; the floatability of pyrite, chalcopyrite and galena was negatively affected by microwave treatment; the floatability of sphalerite became unchanged after microwave treatment; and finally, the magnetic susceptibilities of the sulfide and the oxide compounds formed on pyrite surfaces were higher than untreated pyrite. Later, a similar study by Waters et al. (2008) also verified that thermal treatment has a considerable effect on the magnetic recovery of pyrite.

In 2009, the effect of mechanical property variation and the cutting rate on the microwave-treated granite samples were experimentally studied by Sikong and Bunsin (2009). They used a variable-power (up to 1000 W) multi-mode microwave oven with a frequency of 2.45 GHz for the treatment of orthorhombic shape granite samples with sizes of 15 mm × 50 mm × 70 mm at power levels of 600 W and 850 W and different exposure times. The results of this study show that the compressive strength of granite was reduced by 60% after 30 min at 850 W; the compressive strength of treated and quenched samples was reduced by 70% after 30 min at 850 W; and finally, the cutting rate of treated and quenched samples was reduced by 38% after 10 min microwave exposure at 600 W power. In a similar study, Peinsitt et al. (2010) investigated the effect of microwave treatments on UCS, wave velocities, and heating characteristics of basalt, granite, and sandstone in their dry and water-saturated states using a multi-mode microwave oven with a power level of 3 kW and a frequency of 2.45 GHz. The researchers irradiated cylindrical shape samples, 5 cm in height and diameter, which were positioned in the center of the microwave cavity. After microwave treatments with different exposure times, the authors investigated the effects of microwave irradiation on their samples by measurements of temperature using an IR camera, visible modifications on the surface, UCS, and Ultrasound Velocity (USV). The results of surface temperature measurements are shown in Table 2.2. The main conclusion that should be drawn from the results of Peinsitt et al.'s (2010) study is that severe damage (including large cracks and breakage) occurred in the samples when higher energy inputs produced high temperatures in

the samples' interior. This conclusion shows that the generation of microwave-induced damage of rocks is mainly due to the large discrepancies between the temperatures of the interior and the outer surface of an irradiated rock.

Table 2.2: The results of highest surface temperatures achieved at recorded microwave exposure times in different rock samples after 3 kW microwave treatment (Peinsitt et al., 2010)

Rock sample	Sample's state	MW* exposure time (s)	Highest surface temperature achieved (°C)
Basalt	dried	330	60
	water-saturated	325	60
Granite	dried	220	300
	water-saturated	295	300
Sandstone	dried	255	300
	water-saturated	125	30

\* In this table, the word microwave is abbreviated as MW.

In 2010, Kobusheshe (2010) experimentally investigated the effects of both single-mode and multi-mode microwave treatments on two kimberlite ores consisting of significant amounts of hydrated minerals. Point Load Strength (PLS) tests and Ultrasonic Pulse Velocity (UPV) measurements were used to evaluate the intensity of the damages induced within the samples because of microwave treatment. The author noticed high variability in the results and significant discrepancies between the mean and median values of the measured properties. It was noted that these variations were due to the anisotropic nature of the rocks and inconsistencies in electric field properties within the cavity. After different microwave power levels and exposure times were implemented, the results from the PLS tests were used to measure the strength of two kinds of copper and kimberlite ore samples. The results revealed that the stronger the ore samples, the higher the reduction. In addition, better results were achieved in the kimberlite samples that were treated for longer exposure times. The author concluded that the presence of hydrated minerals led to this phenomenon, which demonstrates the value of implementation of the right method of power delivery over higher power levels and microwave energy inputs. Furthermore, because of the incapacity of the point load test in observing the damage prior to and after the microwave experiments on the sample particle, UPV tests were conducted on the copper and kimberlite ore samples. As a result, Kobusheshe (2010) noticed that a 10% reduction in the mean UPV in the kimberlite particles was promoted by using 6.81 kWh/t microwave energy input.



In another study, the grindability of microwave treated iron ore samples was experimentally evaluated by Kumar et al. (2010). To this end, a variable power (up to 900 W) multi-mode microwave system with a frequency of 2.45 GHz was employed. After microwave treatment of iron ore at a constant power level of 900 W and various exposure times, the authors observed an increase in the ore's temperature. Consequently, the grindability of the iron ore was observed to increase significantly, with the specific rate of breakage rising by an average of 50%. Therefore, the authors pointed out that the grindability of microwave treated iron ores was accomplished much more rapidly than for untreated samples. In conclusion, it can be inferred from the results of Kumar et al.'s (2010) study that microwave energy induces thermal stress cracks and, subsequently, decreases the energy required for grinding of iron ore.

In 2011, the potential application of microwaves in hard rock drilling, cutting, and breakage was introduced and analyzed by Hassani and Nekoovaght (2011). This study aimed at the development of microwave-assisted machineries to break hard rocks by investigating the effects of both single-mode and multi-mode microwave irradiation on temperature profiles and strength reduction (with UCS and BTS tests) in hard rocks for different power levels and exposure times. The authors inferred that only single-mode microwave applicators are able to provide high electric field intensity in order to break hard and abrasive rocks. Hassani and Nekoovaght's article indicates that by combining the microwave energy and one of the available excavation machines—Roadheader, Tunnel Boring Machine (TBM), or Oscillating Disc Cutter (ODC)—the total energy applied to the rocks can be decreased. The penetration rate consequently increases when an excavation machine is equipped with microwave technology. These results opened a new horizon for future breakage operations by one of the available rock excavation machines, i.e. drilling and/or full-face TBM, combined with rock pre-conditioning using microwave energy to perform a continuous non-explosive rock excavation. In another study, Rizmanoski (2011) investigated microwave-assisted pre-treatment with modulated power levels on the breakage of copper ore. In this study, a single-mode microwave applicator with a frequency of 2.45 GHz was employed for microwave treatments of copper ore samples with different particle sizes. By performing comparative drop weight tests, the author found that the microwave-treated samples for 5s exposure at a modulated 5 kW power level break more easily than untreated samples. The objective of this study was to minimize the applied microwave energy using modulated power in order to obtain designated thermal stresses at a shorter exposure time. As a result, the modulated

microwaves compared to continuous microwaves were observed to be energy savers in inducing the desired thermal stresses. Therefore, modulated microwave irradiation of ores can be effective at enhancing mineral processing. Three other studies (Amankwah & Ofori-Sarpong, 2011; Kingman et al., 2004; Vorster et al., 2001) also verified this conclusion. In addition, a similar publication by Wang, Shi, and Manlapig (2011) on pre-weakening of mineral ores by high voltage pulses also showed that pulsed waveforms can reduce energy consumption in the downstream grinding processes of ore minerals.

In 2012, Chen et al. (2012) experimentally examined the behavior of ilmenite ores under microwave treatments with 3 kW power and a frequency of 2.45 GHz at exposure times of 10s, 20s, and 30s. After microwave irradiation tests, the irradiated samples were ground for 60s with a laboratory crusher. Chen et al. (2012) characterized their treated ore samples by using the following methods: XRD, Scanning Electron Microscopy (SEM), and Fourier Transform Infrared (FT-IR) analysis. They found that, in general, ore minerals (e.g. basalt) responded more favorably to microwaves than gangue minerals. More significantly, their characterization results showed that the behavior of minerals with microwave irradiation was compositionally dependent. Therefore, the study demonstrated that the temperature dependency of the rocks' material properties plays an important role in the heating and pre-conditioning processes by microwaves. In another study, Hartlieb et al. (2012) treated cylindrical samples of basalt experimentally in a multi-mode microwave cavity system to investigate the amount of heating and microwave-induced damage. After microwave treatments of basalt with 3.2 kW power at 10s, 20s, 30s, 40s, 60s, and 120s exposure times, the samples' surface temperatures reached 100 °C after 30s, 280 °C after 60s, and 450 °C after 120s of irradiation. Additionally, Hartlieb et al. (2012) further indicated that the temperature in the samples' center reached 250 °C and 440 °C after 60s microwave exposure. From the results of the samples' heating and cracking behaviors, the authors concluded that the development of cracks in basalt is governed by macroscopic temperature gradients and the geometry of the sample instead of its mineralogical composition.

In another research project Jerby, Meir, and Faran (2013) experimentally and theoretically demonstrated the thermal-runaway instability induced by localized microwaves in basalt. By employing a single-mode microwave cavity with a power level of 0.9 kW and a frequency of 2.45 GHz, a cubic sample of basalt was irradiated at different exposure times (up to 10 min). At 10 min microwave exposure, the sample's surface temperature was reached to slightly more than 1200 K,

and the authors recorded the melting temperature value of basalt at approximately 1300 K. In another study, Swart and Mendonidis (2013) evaluated the effect of radio-frequency pre-treatment of granite for comminution purposes. By comparing the results from SEM analysis of the untreated and treated granite samples, no significant changes in the form of fracture along the mineral grain boundaries were found in the treated samples in comparison to the untreated samples. Therefore, Swart and Mendonidis (2013) concluded that electromagnetic waves within the Very High Frequency (VHF) range do not significantly weaken the mineral grain boundaries; and hence, the mineral liberation process is of no benefit.

In 2014, a review on the applications of microwave energy in cement and concrete was presented by Makul, Rattanadecho, and Agrawal (2014). Similarly, another review of microwave processing of materials and applications in manufacturing industries was presented by Singh et al. (2014). In another publication, Irannajad et al. (2014) experimentally tested the floatability of ilmenite ores after microwave treatments in a multi-mode microwave cavity with different power levels (up to 1000 W) and an operating frequency of 2.45 GHz. To optimize microwave irradiation time of the ores, several experiments for different exposure times (up to 600s) at the highest power level of 1000 W were carried out. The authors observed that the flotation recovery of ilmenite was improved by increasing the microwave exposure and a maximum recovery of ilmenite (94%) after irradiation for 150 seconds was obtained. Longer exposures had no significant impact on ilmenite flotation recovery. However, it should be noted that when considering the potential for microwave-enhanced liberation of flotation recovery, several other factors, such as the mineral's grain size, grind size and valuable mineral associations, must be well understood (Batchelor et al., 2016; Tungpalan et al., 2015). In other experimental work, Like, Jun, and Pengfei (2015) exposed a UCS size sample of granite to microwave treatments with a power density of  $8 \times 10^6 \text{ W/m}^3$  at different microwave irradiation times. Following the results of the experiments, a linear decrease in rock mass strength was achieved with increasing microwave irradiation time and power density. From microwave irradiation time changing from 0s to 60s, the mass strength of granite was decreased from 50.6 MPa to 29.6 MPa, which is 41.5% in strength reduction. Thus, the researchers concluded that microwave irradiation effectively reduces rock mass strength; therefore, the longer the microwave exposure time, the lower rock mass strength.

In 2016, a technical research study investigating the effects of different microwave power levels and exposure times on temperature profiles and strength reduction in hard rocks was

presented by Hassani et al. (2016). They treated cylindrical and disc-shaped samples from three different rock types (two types of basalt from different places, mafic norite, and granite) under microwave treatments with power levels of 1.2, 3, and 5 kW for 10s, 65s, and 120s in a multi-mode microwave cavity. They used cylindrical disks, 50 mm in diameter, to perform strength tests on their samples. The disks were 100 mm high for UCS tests, and shorter disks at the height of 25 mm were used for BTS tests. According to their work, the maximum energy of 740 kWh/t was added to the disks during the microwave pre-treatment. The authors observed that low exposure times of about 10s did not lead to any significant impact on the tensile strength of the samples. Microwave treatment did not affect the UCS of the granite samples, and the basalt samples showed a 30% decrease under 65s irradiation with an input power of 5 kW. The results of the BTS tests showed that increasing the exposure time had the same effect on strength reduction, although the energy input to the samples was increased. Moreover, microwave treatment had a better effect on norite than granite and basalt in terms of strength reduction. Hassani et al. further conducted single-mode microwave experiments—in addition to multi-mode microwave experiments—to measure the surface temperature distribution on a rock positioned at different distances from microwave horn antenna. They performed several tests on slab-shaped basalt specimens ( $40 \times 40 \times 40 \text{ cm}^3$ ) at a constant 3 kW power for 60s and 120s exposures and at six distances of 3.5, 6.5, 9, 12, 15, and 19.5 cm. The local damage spread approximately 3 cm in depth, whereas the global damage exceeded 10 cm. Hassani et al.'s (2016) study shows that exposure of rocks to high-power microwaves results in increased temperature and formation of mechanical damages to the rock surface, better facilitation of breakage operations for the mechanical disc cutter of an excavation machine, and reduction of disc cutter wear. According to the results presented by Hassani et al. (2016), a combination of microwaves with one of the available breakage machines, such as the TBM, could improve the rate of penetration, thereby increasing the lifetime of the cutter and saving on the overall cost of the project.

Another research project by Hartlieb, Toifl, Kuchar, Meisels, and Antretter (2016) experimentally addressed the temperature dependency of the electrical, thermal, and mechanical properties of basalt, granite, and sandstone. The authors measured thermo-physical properties of their selected rocks, such as specific heat capacity, thermal diffusivity, thermal expansion, thermal conductivity, and dielectric properties, in the temperature range of 25 °C to 1000 °C, thus showing how phase transitions influence the rock's texture and stability. According to Hartlieb et al.'s

(2016) measurements, the strong variation of microwave effects depends mainly on the rocks' dielectric properties. To better illustrate how dielectric properties of the selected rocks varied at different temperatures, Hartlieb et al.'s (2016) tabular findings are plotted in Figure 2.5. As shown, both plots of the dielectric constant and the loss factor of basalt achieved higher values than granite and sandstone. Moreover, a similar behavior can be observed from the plots of granite and sandstone samples, which means that the responses of these two rocks to microwave treatment should not vary significantly temperature wise.

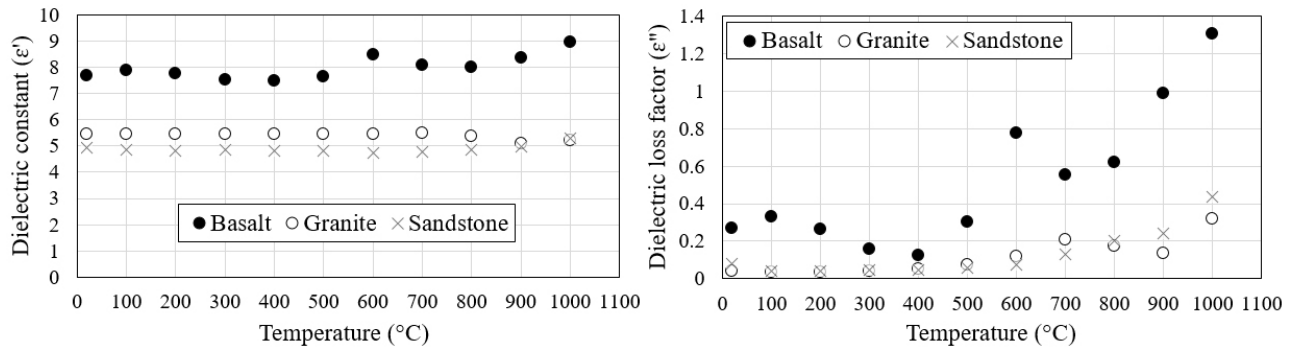


Figure 2.5: Temperature dependency of dielectric constant (left) and dielectric loss factor (right) of basalt, granite, and sandstone in the temperature range of 25-1000 °C at a constant frequency of 2.45 GHz (data taken from table in Hartlieb et al. [2016])

Overall, the data of Hartlieb et al.'s (2016) study shows the impact of the rock forming minerals on the structure and thermal behavior of selected hard rocks; and therefore, selective heating by microwave irradiation is possible when rocks are made up of different minerals (absorbents) with different dielectric properties.

In 2017, a study by Hartlieb, Grafe, Shepel, Malovyk, and Akbari (2017) addressed the crack patterns caused by microwave irradiation and the effect of these cracks on subsequent breakage. Their results included crack pattern and damage propagation, cutting force distribution, specific energy consumption, and particle size distribution for nontreated and treated granite samples for 30s and 45s. Hartlieb et al. (2017) used  $50 \times 50 \times 30 \text{ cm}^3$  sized Neuhauser granite and exerted a UCS of 210 MPa and Cerchar Abrasivity Index (CAI) of 4.2. The authors reported that the local damage spread approximately 3 cm in depth, whereas the global damage exceeded 10 cm. They also noted a 22.5% reduction in average cutting forces due to the microwave treatment of the sample for 45s when the cutting forces were reduced from 6.04 kN and 6.26 kN to 4.26 kN and 5.22 kN for 8 mm and 12 mm cutting spacing, respectively. Their experiments included treatment of 18 spots on the granite samples with a 24 kW microwave system operating at 2.45 GHz for 30s

and 45s. Their results showed a 4.7 kWh/t conservation of cutting energy achieved because of the reduction in cutting force, in the best case, at a treatment time of 45s. Hartlieb et al. (2017) also used a 24 kW microwave with a frequency of 2.45 GHz to create a network of cracks on the surface of granite with a UCS of 210 MPa and a CAI of 4.2. The authors demonstrated that the local damage (created around the microwave treated area) and global damage (generated in the area next to the treated surface) after 45s of irradiation decreased the cutting forces and drilling energy consumption dramatically, equaling to a greater penetration rate. Other studies (Hartlieb et al., 2017; Hartlieb & Grafe, 2017; Hartlieb & Rostami, 2018) have also verified this conclusion. In addition, a comparative analysis on the effect of microwave irradiation on the milling and liberation characteristics of minerals with different morphologies was carried out by Singh et al. (2017). The study shows how different microwave energy inputs affect minerals and their processing operations. To this end, three different types of minerals, including a coal sample, iron ore, and manganese ore, were treated in a multi-mode microwave cavity with an operating frequency of 2.45 GHz at different power levels of 180, 540, and 900 W and exposure times of 1, 3, and 5 minutes. After irradiation tests, the samples' overall temperatures were recorded by a thermocouple and reported by the authors. However, for a better understanding of how the different samples in Singh et al.'s (2017) study responded to microwave treatments with different energy inputs and exposure times, the results in their table of temperature data are plotted in Figure 2.6 for different microwave testing conditions.

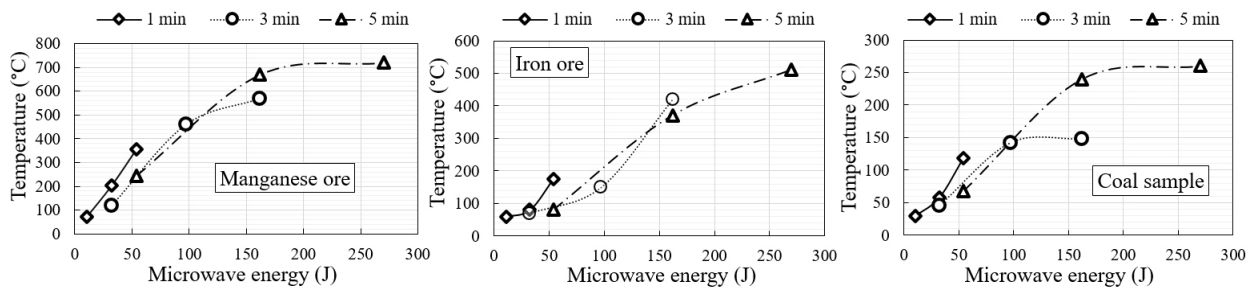


Figure 2.6: Effect of microwave treatments with different energy inputs and exposure times on the samples (data taken from table in Singh et al. [2017])

By comparing the plots, it can be seen that the temperatures of all three samples increase with increasing microwave energy inputs. However, with the same amount of microwave energy input, manganese ore heated more than the other two samples. The best operating ranges of input microwave energy for treatment of coal, iron ore, and manganese ore were found to be 1 Wh to 30 Wh, 5 Wh to 45 Wh, and 15 Wh to 40 Wh, respectively. The authors concluded from the results

of the sample characterizations that microwave treatment improved the grinding of coal, manganese ore, and iron ore. Moreover, liberation studies demonstrated that microwave treatment can lead to a 17.1% increase in carbon recovery for coal and a 42.46% increase in manganese recovery, but the iron ore did not show any improvement in mineral liberation.

In addition, a possible design of several single-mode microwave antennas on breakage machines such as cutting discs and TBMs for microwave-assisted excavation was developed and proposed by Zheng (2017). The study demonstrates that it is feasible to install several microwave applicators on a cutterhead. However, there might be a challenging problem for a rotating cutterhead because of the very short exposure time of microwaves, which reduces the amount of heating and the subsequent micro fracturing effects. Another significant result from Zheng's study is his recommendation to use a horn applicator in order to have better directionality when microwave applicators (antennas) are installed on TBM cutterheads. In an extended work, Zheng et al. (2017) experimentally investigated the effect of microwave treatment on thermal and ultrasonic properties of gabbro using a 2 kW single-mode microwave at a frequency of 2.45 GHz. Zheng et al.'s (2017) study shows the effects of microwave irradiation with variable power levels of 0.5-2 kW and exposure times of 30-120s on the temperature, microcracks, and p-wave velocity of the samples using an infrared camera, an X-ray microscope, and an ultrasonic pulse transmitter. From IR images, a linear increase in both maximum and average temperatures with microwave power level and exposure time was observed. The same conclusion was drawn for the specimen surface temperature and its heating rates. In terms of microcracking analysis of the irradiated specimens, the evolution of cracks at 2 kW power started as the microwave duration increased from 30s to 120s. The authors also stated that they observed both intergranular and transgranular cracks; however, intergranular cracks were more dominant. Another significant conclusion was that the density of both macro- and micro-cracks increased with increasing microwave exposure, which indicates that a considerable reduction in the mechanical strength of the rock was achieved. From the data of p-wave velocity tests, Zheng et al. (2017) observed that the overall p-wave velocity in their samples was reduced by up to 55%, which implies a significant reduction in the strength of the samples. Finally, it is concluded that a pulsed microwave with a high power level at a short exposure time yields better rock heating and pre-conditioning, and this can be considered as an alternative method of rock breakage with continuous microwave irradiation.

In 2018, in an extended research project, Hartlieb and Rostami (2018) presented initial results of their laboratory-scale microwave irradiation experiments on a block of granite using a high power (24 kW) microwave apparatus. The objective of this study was to present innovative concepts for improving the breakage of hard and abrasive rock types by pre-conditioning and inducing micro-cracks with high power microwaves. The authors introduced the Rock Mass Rating (RMR) system to quantitatively express the condition of the irradiated rock mass related to its strength and mechanical behavior. From the results of applying high power microwave irradiation on granite, the authors concluded that (1) an extended network of cracks occurs in hard rocks such as granite, basalt, quartzite, etc., because of high power irradiation, (2) induction of micro and large cracks reduces RMR values and can influence both rolling and normal forces of the cutting discs, and (3) the reduced cutting forces and power consumption lead to an increased penetration rate of the breakage machine, which ultimately increases cutter life. These findings are good indicators for evaluating the feasibility and possibility of applying high power microwaves on future breaking machines such as TBMs. In another project, Hartlieb, Kuchar, Mosar, Kargl, and Restner (2018) performed low power (3.2 kW) multi-mode microwave irradiation tests on various types of rocks (hard and abrasive) to assess their physical and chemical changes before and after microwave treatments with different exposure times. To this end, cylindrical rock samples with the same size ( $d = 50$  mm,  $h = 50$  mm) were used. The selection of the given rocks for microwave irradiation experiments was based on different considerations i.e. rocks in terms of hardness and abrasivity and the rocks' ability to absorb microwaves. In this case, a quick overview of Hartlieb et al.'s (2018) categorization of rocks is given in Table 2.3. After microwave irradiation experiments on the selected rock types, the authors conducted XRD analyses, p-wave velocity measurements, and surface temperature and ultrasound velocity measurements from the treated rock samples, which resulted in the following findings. Samples of basalt heated up from their initial temperature and, therefore, microscopical damage (crack) occurred after 40s of microwave exposure. Extensive and wide cracking was observed in the treated samples after 120s of irradiation; and therefore, ultrasound velocity of the samples significantly decreased. Similarly, an increase in average surface temperature of the irradiated gabbro sample was observed with increasing irradiation times. This surface temperature rise was accompanied by a decrease in the gabbro's p-wave velocity.



Table 2.3: Categorization of different rock types from data in Hartlieb et al. (2018)

<b>Rock name</b>	<b>Rock mineralogical type/texture</b>	<b>Microwave absorbability</b>	<b>Dielectric constant, <math>\epsilon'</math></b>	<b>Dielectric loss factor, <math>\epsilon''</math></b>
Granite	Mafic volcanic, coarse-grained texture	low absorber	5.0-5.8	0.03-2
Sandstone	Mafic volcanic, medium-grained texture	low absorber	4.93	0.08
Copper ore	Hard and tough	good absorbed under specific circumstances	High	High
Basalt	Greenstones, fine-grained texture	relatively good absorbers	5.4-9.4	0.08-0.88
Diabase	Greenstones, fine- to medium-grained texture	relatively good absorbers	5.4-9.4	0.08-0.88
Gabbro	Medium-grained texture	good absorber	5.4-9.4	0.08-0.88

Hartlieb et al. (2018) concluded that rocks with similar absorption properties are strongly influenced by rock texture. They further pointed out that coarse grained rocks (i.e. gabbro) showed cracks along grain boundaries, but random crack networks were found to be in the fine-grained rocks, such as basalt. Similarly, the grain size of each rock type played an important role in the rock's heating, as highly absorbing copper ore was not influenced by microwaves in comparison to the fine-grained and readily heated ore. Further analyses and investigations on quantification of cracks in rocks after microwave treatment and a comprehensive review of different techniques for characterizing cracks induced in rocks with can be found in a review study by Nicco et al. (2018). Another study by Forster, Maham, and Bobicki (2018) experimentally performed microwave heating tests and high-temperature dielectric property (real and imaginary permittivity) analysis on magnesium silicate minerals. The findings showed how microwave irradiation affects the microwave heating properties of serpentine and olivine (the primary components of ultramafic nickel ores and constituent minerals). The authors experimentally irradiated cylindrical samples of serpentine and olivine (with a diameter of 16 mm, a mass of 7.5 g, and heights of 17.5 mm and 15mm, respectively) in a multi-mode microwave cavity with a power level of 1200 W and a frequency of 2.45 GHz. Then, by using the cavity perturbation technique, they measured samples' dielectric properties, involving real and imaginary primitivities at different frequencies and different temperatures. The dielectric properties of olivine and serpentine were found to be frequency dependent, especially in the serpentine curves at low temperatures (below 500 °C). In addition, frequency dependence was also observed for the imaginary permittivity of serpentine at temperatures above 800 °C. Comparatively, the imaginary permittivity values for serpentine were

significantly higher than those for olivine across the temperature range 0-1200 °C (see Figure 2.7). The results of Forster et al.'s study demonstrate that for serpentine, the imaginary permittivity ( $\epsilon''$ )—or simply the loss factor—largely decreased with increasing temperature in the microwave heating tests, resulting in a decreased heating rate. For olivine, the imaginary permittivity was nearly zero in the range of temperatures; thus, the heating rate was also close to zero.

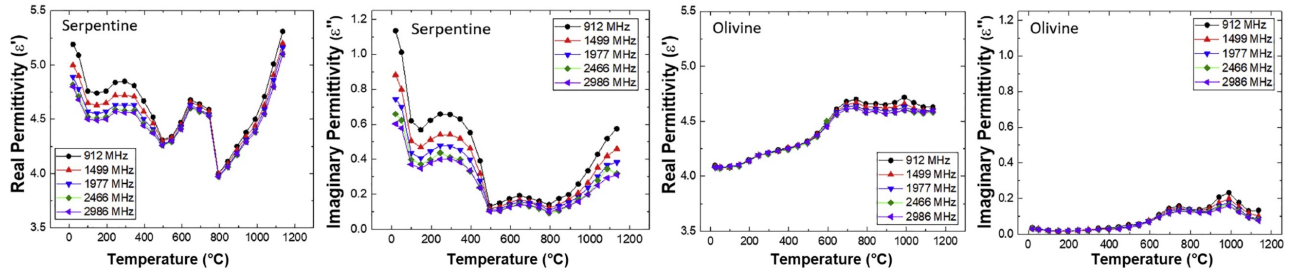


Figure 2.7: Real and imaginary permittivity values of serpentine (left) and olivine (right) as a function of increasing temperature (image modified with permission from Forster et al. [2018])

A similar work by Bobicki, Liu, and Xu (2018) focused on the effects of microwave treatment of two types of ultramafic nickel ores: Okanogan nickel (OK) ore and Pipe ore—obtained from the Vale-owned Pipe deposit—on the overall process improvements, including grindability, rheology, flotation, material handling, dewatering and tailings treatment. To this end, the authors employed a 1000 W multi-mode microwave with a frequency of 2.45 GHz. The ore samples were then treated with 100% microwave power capacity. The temperature results of the OK and Pipe ores with respect to microwave heating time are illustrated in Figure 2.8(a). The plot indicates that the OK ore sample has a high initial heating rate that declined with increasing temperature and microwave exposure time. The same trend can be observed from the plot of the Pipe ore up to 8 min microwave heating time. However, it is important to note that the authors mentioned that after 8 minutes of exposure, a partial melting was observed in the Pipe ore sample. This occurrence resulted in a change in the trend. To investigate why there were differences between the obtained heating rates in the two ores, Bobicki et al. further experimentally measured imaginary and real permittivities of the ores with increasing temperatures at frequencies of 912 and 2466 MHz, as shown in Figure 2.8(b) and 2.8(c). It can be seen that both imaginary and real permittivity of the ores vary with increasing temperature. However, the measured values for Pipe ore at the frequencies of 912 MHz and 2466 MHz are higher than the OK ore at temperatures between 0-400 °C and 800-1100°C, respectively. Therefore, as power dissipation in rocks is highly

influenced by the rock dielectric properties, the obtained variation in imaginary and real permittivity of the two ores is the main reason for the difference in their heating rates.

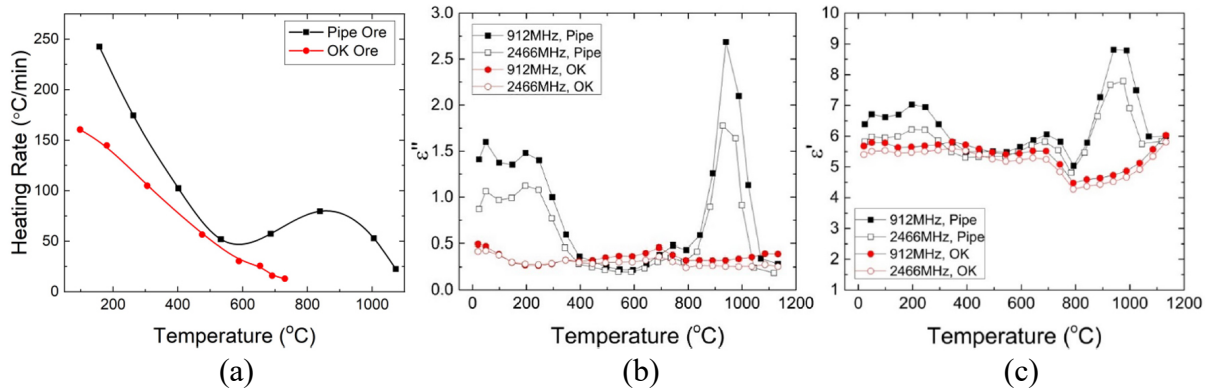


Figure 2.8: (a) Heating rate upon exposure to microwave radiation with respect to temperature for Pipe (■, □) and OK (●, ○) ores; (b) imaginary permittivity, and (c) real permittivity for the Pipe and OK ores with increasing temperature at frequencies of 912 and 2466 MHz (Bobicki et al. [2018])

Further analyses on the treated ore samples were conducted by Bobicki et al. using the following techniques: X-ray Fluorescence (XRF) spectroscopy, quantitative XRD analysis, Fourier Transform Infrared (FTIR) spectroscopy, and SEM methods. From the results of ore characterizations after microwave treatment, the authors concluded that by microwave irradiation: (1) the grindability of ore with consistent texture (OK ore) improved; (2) the grindability of ore with inconsistent texture (Pipe ore) decreased; and (3) the specific surface area of both ores improved. Ultimately, the authors reported that since microwave pretreatment did not decrease the energy required for grinding under the specified microwave conditions, the energy savings might only be realized for overall process improvements (e.g. grindability, rheology, and flotation).

Ong and Akbarnezhad (2018) experimentally investigated various effects of microwave irradiation on samples of concrete. According to the results of their study, the variations in concrete's dielectric constant and its loss factor for a typical specimen with water content and microwave frequency were observed. Both dielectric constant and loss factors of the concrete increased significantly with an increase in the microwave frequency or water content, leading to a higher heating potential when exposed to microwaves. For a sample of concrete, there was an inverse relationship between the penetration depth of microwaves in the concrete and microwave frequency. This means that the higher the microwave frequency, the less the penetration depth. Therefore, at higher microwave frequencies, the microwave energy is expected to be dissipated within the surface layer of the concrete rather than penetrating deeply into the specimen; the higher

the microwave frequencies, the thinner the affected surface layer. A review of the applications of microwave energy in rock and concrete processing is given by Wei et al. (2019).

In 2019, structural changes in samples of granite (cube of 20 mm) at high temperatures (300-800 °C) induced by microwave irradiation were studied (Zeng et al., 2019). In this case, an adjustable multi-mode microwave (1.4 kW) with a frequency of 2.45 GHz was used for irradiation tests. The microwave treated samples were then characterized by SEM analysis, Thermogravimetric Analysis (TGA), Differential-Scanning Calorimetry (DSC) tests, X-ray Powder Diffraction (XRPD) analysis, and UCS tests. Thus, from the results of these rock characterization analyses, Zeng et al. (2019) concluded that (1) granite samples were observed melted and cracked at 600 °C and completely melted at 800 °C, (2) both transgranular and dominant intergranular cracking modes were observed by the SEM, (3) the results from TG-DSC tests indicated moisture releasing, (4) feldspar and biotite melted at 800 °C according to the XRPD results, and finally (5) the uniaxial compressive strength of granite decreased from 88.17 MPa at 25 °C to 18.61 MPa at 800 °C. The results presented in a similar publication by Li et al. (2019) also arrived at the same conclusions. Additionally, Lu, Feng, Li, Hassani, and Zhang (2019) developed a research study to examine experimentally the effects of different microwave power levels on the mechanical strength, burst time, and fragmentation of compact basalt samples comprising plagioclase, enstatite, olivine, and a small amount of ilmenite. A continuous wave multi-mode microwave cavity with a power range of 1 kW to 6 kW and the frequency of 2.45 GHz was used to treat the basalt samples at different power levels and exposure times. Cylindrical samples (50 × 100 mm) for the UCS, discs (50 × 50 mm) for the BTS and the PLS tests, and cube samples with four different length sizes of 30, 50, 75, and 100 mm for fragmentation tests were used. The microwave treated specimens were cooled to room temperature and placed for the tests in a loading direction perpendicular to the main crack direction in the BTS and PLS tests. A faster reduction in strength was observed at the higher microwave power levels. The authors concluded that lower energy consumption was needed to burst the specimens at higher power levels. Overall, Lu et al.'s (2019) work reveals that all the measured values of UCS, BTS, and PLS tests on basalt were decreased by increasing the microwave irradiation time. In an extended study, Lu, Feng, Li, and Zhang (2019) examined the microwave-induced fracturing of hard rocks for underground engineering applications by developing a novel (open-type) microwave-induced fracturing apparatus with an operating frequency of 2.45 GHz and variable power levels of up to 15 kW.

Their microwave apparatus comprised single-mode microwave applicators to investigate the subsurface and borehole fracturing effects on basalt samples. The researchers performed both laboratory-scaled microwave experiments and field tests. Therefore, the uniqueness of this study was its field tests of microwaves at 15 kW power level on rock masses. From the results of laboratory-scaled microwave experiments, the authors concluded that the longer microwave exposures resulted in greater reduction in p-wave velocity. From the results of the field tests, the borehole fracturing mode rendered a favorable fracturing effect on boreholes. Moreover, a reduction in the sound velocity around the borehole and between the boreholes was observed. Overall, Lu et al.'s (2019) study demonstrated a real application of microwaves in the field, which had never before been implemented to this extent. In the studies mentioned above, microwave-induced fracturing of basalt was successfully surveyed and analyzed. However, the only lack in the two studies might be energy and economical analyses for industrial implementations.

In 2020, several researchers and research groups have investigated the impact of microwave treatment on hard rock pre-conditioning and fracturing. For example, by using the same microwave system explained in the study by Lu et al. (2019), the response of compact basalt samples under different confining pressures was surveyed by Lu, Feng, Li, and Zhang (2020). The study enhances the understanding of microcracking behavior of basalt after microwave treatments with different power levels (1 kW to 5 kW) and exposure times (up to 300s). Kahraman et al. (2020) studied the effect of microwave treatment on the compressive and tensile strength of nine different igneous rock samples consisting of six granites, two syenites, and one gabbro. UCS and BTS tests on these samples before and after microwave treatments with power levels of 1 kW, 2 kW, and 6 kW at different exposure times ranging from 60s to 420s were performed. Kahraman et al. observed that the UCS values of a granite sample, including a small but significant amount of microwave absorber minerals, decreased at surface temperatures above 200 °C. However, the BTS test values started to decline at temperatures above 100 °C for the same granite sample. The authors observed inconsistency and fluctuations in average temperature plots of the treated samples in their analysis of the experiments using an infrared gun after the microwave treatment. They further concluded that depending upon the mineral contents of each rock type, the heating degrees of the rocks differ from one type to another. Furthermore, the strength of the treated igneous rocks decreased with increasing microwave power and exposure time. However, the rate of the losses depended mainly on the varying mineral contents.

As surveyed in this section, many studies have highlighted the existing challenges and potential applications of microwaves in the rock breakage and mineral processing industries in order to increase mineral compound liberation as well as potential reduction of energy usage. Below, a technical summary, including the details of applied experimental methods and the main findings of secondary experimental studies not discussed in this section, but that have made significant contributions in the application of microwaves in rock mechanics and mining industries, is given in Table 2.4.

Table 2.4: Secondary publications found through a chronological literature review on laboratory experiments of microwave treatment of rocks and minerals and the corresponding effects

Microwave operating parameters and sample info	Subject of study	Experiment methods	Main findings and highlights
MW treatment of small coal samples (19.05–12.7 mm) with a power level of 900 W; <b>M</b>	The influence of microwave pre-treatment on the grindability of coal	<u>Sahoo et al. (2011)</u> Grindability tests, SEM, XRD	The MW treated coal was grinded more rapidly than untreated coal. With the specific rate of breakage increased by an average of 15% after MW heating, the grindability of coal increased significantly.
MW treatment of a porphyry copper ore with different sizes; with a power level of 15 kW (approximately 2 kWh/t); <b>S</b>	Study on how increasing grind size effectively influences liberation and flotation of the ore by MW treatment	<u>Batchelor et al. (2016)</u> MLA, PLS test, crushing and grinding	An indirect reduction in specific comminution energy by grinding the ore for a shorter time might occur as a result of increase in grind size of the ore.
MW treatment of granite block samples with different sizes with a power level of 24 kW and 2.45 GHz frequency; <b>S</b>	Investigating the strength reduction of the rock by artificially induced crack patterns via MW pre-conditioning	<u>Hartlieb et al. (2017)</u> X-ray CT, UCS, CAI, linear cutting test rig	After exposure of the block sample to 24 kW and 45s MW irradiation, the mean cutting forces were reduced as follows: from 6.04 and 6.23 kN down to 4.26 and 5.22 kN.
MW treatments of coal core samples (50 mm diameter and 60 mm height) with various power levels (2-10 kW); <b>M</b>	Evolution of pore structure under MW heating for coal with different water saturation conditions (from 1% to 15%)	<u>Li et al. (2017)</u> NMR, X-ray CT, p-wave	The study shows the total porosity of coal rose linearly with MW power, while it increased exponentially with greater water content (1% to 15%).
MW treatment of granite cube samples (20×20×20 mm <sup>3</sup> ) with an adjustable power level of 1.4 kW and 2.45 GHz frequency; <b>M</b>	Determining the pre- and post-microwave microcracking and strength reduction of the samples at high temperatures induced by MW treatments	<u>Zeng et al. (2019)</u> XRF, SEM, TGA, DSC	Both transgranular and intergranular cracking modes were observed from SEM images, but the latter dominated. The moisture releasing and $\alpha$ - $\beta$ quartz transition was detected from TG-DSC result.
MW treatment of various ore particles at different sizes with a power level of 1.2 kW for 12s exposure and 2.45 GHz frequency; <b>M</b>	Investigating the position- and cross-dependencies of the rock particles in MW cavity for maximum heating; and the effect of particle properties (particle size, magnetic properties, thermal response) on the heating of adjacent particles	<u>Jokovic et al. (2019)</u> MLA analysis, IR imaging	“If two highly MW responsive particles were in electrical or magnetic contact, they would be much more effective at absorbing energy than either particle on its own and cause even larger distortions in the applied MW field” (p. 6).
MW treatment of three igneous rocks (gabbro, monzonite, and granite) (W84×L41×H30 mm <sup>3</sup> ) with various power levels (0.5-2 kW) for various exposures (30, 60, 90, and 120s) at 2.45 GHz; <b>S</b>	Investigating the thermal, mechanical, and cracking behavior of igneous rocks after MW treatments with different power levels and exposure times	<u>Zheng et al. (2020)</u> Ultrasonic s-wave and p-wave velocity measurements, UCS, UV, IR, and PPL imaging	Gabbro and monzonite specimens were thermally cracked and melted at MW treatment with 2 kW for 120s. Heating at higher power levels for shorter durations resulted in a more weakening.

\*Note: In the table the term “microwave” is abbreviated as MW; and the two MW applicator types of single-mode and multi-mode are denoted by **S** and **M**, respectively.

## 2.2.2 Modeling and simulation literatures

Computers have evolved and advanced significantly over the decades since they originated. As a result, numerical modeling techniques have become stronger in recent years for simulation of the process of microwave treatment of materials. In tandem with experimental research, computational studies have come to play an important role in understanding how different mechanisms are involved in microwave-assisted rock pre-conditioning and breakage processes. Numerical models can be used to predict the coupled Electromagnetic, Thermal, and Mechanical (ETM) multiphysics interactions in rocks under microwave treatments with different operating parameters including power levels, exposure times, and distances from the antenna (for single-mode microwaves). Moreover, the numerical modeling approach has been considered a useful comparative tool that allows quantification of the relationships between the material properties of rocks made up of different absorbent minerals and microwaves with different operating parameters. Therefore, the development of numerical models is considered an enhancement in understanding microwave-assisted rock breakage systems and their thermomechanical characteristics, i.e. temperature changes and initiation of mechanical stresses. In the 2000s, several studies have tried to numerically simulate the process of microwave heating and pre-conditioning of rocks and minerals to predict microwave effects. These modeling studies and their analyses for solving applied problems are now essential for a proper design and practical implementation of a functional microwave-assisted rock pre-conditioning system. The following literature review shows how evolution of computers and simulation techniques have significantly improved numerical modeling of microwave irradiation of rocks over the past two decades.

In 2002, a very simple numerical simulation of the microwave-assisted drilling process in alumina was developed by Grosplik, Dikhtyar, and Jerby (2002). They employed the FDTD method for their modeling in MATLAB software. However, because of the lack of computation capacity at the time of this work, only temperature and electric field at a concentrated point were shown. Later in 2003, by using the FLAC 2D commercial software, Whittles et al. (2003) numerically modeled 2D coupled electromagnetic, thermal, and mechanical multiphysics to predict the influence of microwave power density (2.6 kW and 15 kW) and exposure time on the strength change of rocks after microwave treatment using the finite difference method. Their study used a “theoretical” ore consisting of a microwave absorbing pyrite mineral in a low-absorbing calcite matrix and considered the following two different numerical scenarios applied at the same

frequency of 2.45 GHz. In the first scenario, it was assumed that samples of pyrite were already exposed to multi-mode microwave treatments at 1s, 5s, 10s, 15s, and 30s and a varied power density from  $3 \times 10^9 \text{ W/m}^3$  at 300 K to  $9 \times 10^9 \text{ W/m}^3$  at temperatures greater than 600 °C. Secondly, to study the effect of higher power levels of microwaves on temperature distribution, uniaxial compressive strength, and shear plane development within the ore samples, the study assumed that the samples were already exposed to single-mode microwave irradiation with a power density of  $1 \times 10^{11} \text{ W/m}^3$  (15 kW at 2.45 GHz). Because of the higher power density, Whittles et al. (2003) found that the strength of their simulated rock model dropped as the time of irradiation increased. The results presented in the Whittles et al.'s numerical study demonstrate that higher power density generates a considerably larger reduction in strength with much lower energy inputs, thus reducing energy requirements. Satish (2005) built upon the work of Whittles et al. (2003) by modifying the source of irradiation from a power density to an energy density to show the generation of stress within the grain boundaries of a single pyrite hosted calcite with the same material that had been defined by Whittles et al. (2003). The results of Satish's (2005) work showed that a large amount of potential stress could be generated at the particle boundaries of pyrite because of the transparency difference between the two minerals. In addition, Jones et al. (2005) developed a numerical model to study the effects of microwave power density and particle size on microwave treatment of ores prior to grinding. In contrast to the normal constant microwave energy previously used by Whittles et al. (2003), the influence of pulsed microwave energy at five different irradiation times from 0.1s to 10s was employed by Jones et al. (2005). The results of their study illustrate that (1) the obtained stresses along the mineral boundary were predominantly shear and tensile in nature; (2) by increasing microwave power density, minerals absorb more heat, resulting in better mineral liberation due to the creation of more thermal stress through the minerals' particles; and (3) by varying mineral particle size, the overall fracturing process was influenced. Jones et al.'s (2005) study concluded that a decrease in mineral size and an increase in input microwave energy are required for sufficient fracturing. In a later publication, Jones, Kingman, Whittles, and Lowndes (2007) studied numerically and extensively the effects of microwave power density and exposure time on the mineral weakening process by microwaves. By using FLAC 2D software, the researchers developed 2D simulation of a simplified two-phase mineral ore comprising pyrite particles randomly disseminated in a matrix of calcite. The models were undertaken with both continuous and pulsed wave simulations. The authors simulated six power



densities, varying between  $1 \times 10^9$  and  $1 \times 10^{10}$  W/m<sup>3</sup> for heating times varying between 0.1s and 10s in their continuous wave simulations. For pulsed wave simulations, the power density was varied between  $1 \times 10^{13}$  and  $2 \times 10^{15}$  W/m<sup>3</sup> with pulsed duration between 0.1s and 10 $\mu$ s. According to the results of Jones et al.'s (2007) study, with pulsed microwave, lower temperature was required to achieve the same reduction in a sample's strength and was observed as a result of continuous wave simulation. Furthermore, with increasing power density, mechanical stresses increased, which resulted in a greater damage within the ore and, in turn, a lower UCS.

In 2006, to test the potential application of multiple ports in traveling waveguide applicators, Balbastre et al. (2006) presented a simple numerical simulation of microwave heating in a cylindrical sample (5 cm diameter and 1 cm height) made up of a high loss material. By using the commercial ANSYS software and employing the finite element method, the authors were able to obtain the electric field amplitude in a closed region. Then, they found that a variable feed, such as ore particles in the design of microwave applicators, can be optimized for a specific load property, which enhances physical processes, such as the separation of minerals. The authors concluded that because of the limited electrical field uniformity within the material under microwave heating, the heating of high loss materials is a complex task. Typically, the limited electrical field uniformity is observed in large samples of low thermally conductive materials, as the homogeneity of microwave heating will be completely controlled by electrical field distribution, which increases the chance of hot-spots development or thermal runaway (Rizmanoski & Jokovic, 2016). Ali and Bradshaw (2009) numerically investigated the effect of ore texture on the amount of damage in a microwave treated ore model. By using FLAC 2D commercial software and employing the finite difference method, two binary ore models made up of galena-calcite and magnetite-dolomite were constructed. The models were then simulated according to the following two different input power densities: one simulation with a power density of  $1 \times 10^{10}$  W/m<sup>3</sup> with a high power pulsed source, and a series of simulations at a power density of  $1 \times 10^9$  W/m<sup>3</sup> to represent the power density in a 30 kW source microwave with 2.45 GHz applicator. The authors found that, at  $1 \times 10^9$  W/m<sup>3</sup> input energy and 0.01s microwave exposure, the amount of grain boundary damage was less than 50%. However, at a higher value of  $1 \times 10^{10}$  W/m<sup>3</sup> and lower exposure of 0.001s, the grain boundary damage increased to 74.3%, which confirms that the influence of microwave power density on the degree of ore liberation is high. The practical implication of the results presented in Ali and Bradshaw's (2009) study is that

for ores that are less amenable to continuous wave microwaves with low power densities, very high power pulsed microwave systems could be used for an economical treatment. The authors further extended their investigations to characterize the amount of microcracks induced in a conceptual binary ore consisting of 10% galena and 90% calcite by microwaves and to study the effect of applied power density and ore texture on the quantity of microcracks by using a bonded-particle modeling approach (Ali & Bradshaw, 2010). The results of this study demonstrated that through the implementation of higher microwave power density, more microcracks could be induced at the same energy input. A pulsation mode of microwaves also helps to liberate the absorbent minerals of the original size. Ultimately, the study shows that for the treatment of fine-grained ores at economical energy inputs, a higher power density is needed. Later, in another publication, Bradshaw et al. (2011) showed that with finer textured mineral ores, the required specific energy input had to be greater to produce the same amount of damage. For the same power density and exposure time of the applied microwave, smaller thermal stresses generate a finer textured ore.

In 2010, using COMSOL multiphysics software a numerical modeling of microwave heating of an insulated sphere with a radius of 3 cm was presented by Lovás et al. (2010). The aim of this study was to investigate the effects of microwave irradiation on temperature distribution in the samples of andesite, siderite, magnesite, chalcopyrite, and pyrite. From the results of the models, the authors concluded that the response of a mineral when it is subjected to a microwave treatment depends greatly on the material's electromagnetic and thermal properties, such as its dielectric properties, specific heat capacity, and thermal conductivity. Therefore, Lovás et al.'s work verified that different material properties of a mineral have a great impact in the heating and breakage processes of the rock under microwave irradiation.

Now, it can be seen from the discussed literatures that almost all numerical studies have been focusing on investigating the effects of microwave irradiation on heating of rocks and minerals to compare the results obtained from experiments with computer modeling data. To make this section more concise, a summary list with technical details of other published numerical works that were found in the literature from 2010 to 2020 is provided in Table 2.5.

Table 2.5: Publications on numerical simulations of microwave-assisted heating and pre-conditioning of rocks and minerals that were found through a chronological literature review (2010-2020)

Numerical methods, modeling approach, software	Microwave type and geometry, MW input numerical parameters	Rock/mineral name, Sample input model parameters	Main findings and highlights
FDM, coupled 2D electromagnetic and thermal model, MATHEMATICA 7.0	N/A, MW power densities (0.5-4 MW/m <sup>2</sup> ) for 60s exposure at 0.915 GHz; and power density (1 MW/m <sup>2</sup> ) for various exposure times (1, 60, 300, and 600s) at 2.45 GHz	Peng et al. (2011) Coal, homogeneous magnetite block with a varying dimension of 2L x 2L m (L=0.2, 0.15, 0.1, and 0.05 m)	Microwave heating of coal at 0.915 GHz exhibited better heating uniformity than the same irradiation at 2.45 GHz because of the larger penetration depth of the MW. Under the same MW conditions applied to the same material, a MW irradiation with 2.45 GHz would dissipate in the area closer to the surface than that at 0.915 GHz.
FEM, 3D thermal and thermomechanical model, ABAQUS v6.10	Multi-mode; MW power level (3.2 kW), applied power density of 16.8×10 <sup>6</sup> W/m <sup>3</sup> at 2.45 GHz; and exposure times (up to 900s)	Hartlieb et al. (2012) Basalt, cylindrical (h=50 mm, r=25 mm) sample; various temperature dependent values of <i>k</i> (W/mK), <i>c<sub>p</sub></i> (J/kgK), <i>E</i> (GPa), and <i>ν</i> (1) applied in FE simulations	For a slow MW absorption process (when the heating rate is small compared to the heat transfer rate in grains and between the sample and its surrounding), a fine-grained rock like basalt does not show effects of differential heating and thermal expansion of individual grains.
FDTD, 3D electromagnetic and thermal model, QuickWave 3D	Multi-mode; Pentagonal and rectangular cavity, MW power levels (15, 20 kW), at various frequencies (2.45 and 0.915 GHz); and various exposure times	Jokovic (2012) various ore particles, e.g. including monzonite ore, modeled with different dielectric properties applied to the rock models	Rectangular cavity provided more uniform and efficient heating than the pentagonal cavity. The study shows although multi-mode MW heating should provide, in the best case, uniform heating throughout the cavity, optimization of feed positions must be completed for maximum efficiency.
FEM, 2D electromagnetic, thermal and mechanical model, ANSYS	N/A, MW power densities (10 <sup>10</sup> , 10 <sup>11</sup> W/m <sup>3</sup> ); frequency (2.4 GHz); and exposure times (0.00043s, 0.00044s, 0.00045s, 0.00046s)	Wang and Djordjevic (2014) a single disc-shaped grain of pyrite surrounded by a larger disc of calcite, various particles grain sizes for the ores	The size and thermal properties of the rock under microwave exposure can significantly affect thermal heating and subsequent thermal stress. The study suggests that a high-power density combined with a short heating interval offers the best energy efficiency.
FDTD, 2D electromagnetic, thermal and mechanical model, ABAQUS v6.12	Single-mode, MW power level 25 kW and assumed losses of 30% resulting in a power input of 17.5 kW	Meisels et al. (2015) Basalt, Gabbro and Granite, a block (15 × 15 × 20 cm <sup>3</sup> ) rock sample at 30 cm distance from MW from antenna	Different morphologies resulted in a change to the maximum stress and the initiation of cracks. Temperature gradients and induced stresses will occur on short distances.
DEM, (a) 2D and (b) 3D micromechanical and thermal models, PFC2D/PFC3D	Single-mode, MW power density (10 <sup>10</sup> W/m <sup>3</sup> ) representing a power density in a 6 kW power cavity with a frequency of 2.45 GHz; and various exposure times (0.01-4s)	Charikinya (2015) Massive sulfide ores, (a) 2D rectangular specimen (W15 × L20 mm <sup>2</sup> ) (b) 3D parallelepiped specimen (15 × 15 × 20 mm <sup>3</sup> )	The results from 2D models suggest that model resolution had a great impact on the magnitude of simulated crack damage. From 3D models, the author found that the majority of the cracks observed were tensile cracks with very few shear cracks.
FEM, coupled 3D electromagnetic and thermal model, COMSOL Multiphysics	Multi-mode; cavity (W267×L270×H188 mm <sup>3</sup> ), MW power levels (0.5-3 kW); frequencies (2.4-2.5 GHz); and exposure times (up to 300s)	Hong et al. (2016) Coal, a cylindrical (h = 50 mm, r = 12.5 mm) sample	MW heating behavior of the coal samples was highly affected by the samples' positioning in the cavity and the MW frequency and power level.
FEM, coupled 3D electromagnetic and thermal model, COMSOL Multiphysics	Multi-mode; cavity (W630×L650×H660 mm <sup>3</sup> ), MW power levels (0.5-6 kW); frequencies (2.4-2.5 GHz); and exposure times (0-600s)	Lin et al. (2017) Coal, cylindrical (h = 60-100 mm, d = 50 mm) samples; various samples' permittivities (dielectric constants and loss factors) applied	(1) Better thermal heterogeneity of coal was obtained with larger MW power levels, (2) coal sample temperature increased while thermal heterogeneity decreased with loss factor, and (3) efficient heating was found to be achieved at an optimal frequency of 2.45 GHz.

\*Note: In the table the term “microwave” is abbreviated as MW.

Table 2.5 continued

Numerical methods, modeling approach, software	Microwave type and geometry, MW input numerical parameters	Rock/mineral name, Sample input model parameters	Main findings and highlights
FEM, coupled 3D: (a) electromagnetic, heat and mass transfer model; (b) electromagnetic, thermal and mechanical model, COMSOL Multiphysics	Multi-mode; cavity (W267×L270×H188 mm <sup>3</sup> ); (a) MW power levels (0.5-2 kW); frequencies (1.95-3.7 GHz); specific moisture capacity (0.5-10%); and exposure times (0-60s); (b) MW power level 500 W; frequency 2.45 GHz; and exposure times (0-300s)	Huang et al. (2018) Coal, a cylindrical sample (h = 60 mm, r = 25 mm); various samples' permittivities (dielectric constants and loss factors) applied	(a) Microwave heating of a coal sample was responsive to input MW power level and frequency; and the best MW heating effect was found in the coal with low water saturation. (b) The results showed that the average permeability of coal rose by 2.2 times after 300s MW exposure with 500 W input power level at the frequency of 2.45 GHz.
FEM, coupled 3D electromagnetic and thermal model, COMSOL Multiphysics	Multi-mode; cavity (W630×L650×H660 mm <sup>3</sup> ), MW power level 1 kW at 2.45 GHz frequency; and exposure times (10-300s)	Li et al. (2019) Coal, cylindrical sample (h = 100 mm, d = 50 mm)	Variation in electric field norms was observed because of nonuniform electromagnetic distribution that resulted in a selective heating of the coal sample. When water evaporation was included, temperature increased nonlinearly.
FEM, coupled 3D electromagnetic, thermal and mechanical model, COMSOL Multiphysics & AutoCAD	Multi-mode, MW power level 3 kW applied at 2.45 GHz frequency; for 120s exposure time	Li et al. (2019) Pegmatite, cylindrical samples (h = 100 mm, d = 50 mm); a thin section (0.34 × 0.47 in <sup>2</sup> ) sliced from the center of the rock for 2D analysis	Dielectric constants, coefficients of thermal expansion, and sizes of mineralogical boundaries in minerals have a significant impact on the effects of MW treatment. By increasing MW exposure time, the rate of generation of von Mises stresses increases rapidly along the interfaces between different minerals. All the stress-strain curves showed elastic deformation behavior.
FEM, coupled 3D electromagnetic and thermal model, COMSOL Multiphysics	Multi-mode; cavity (W630×L650×H660 mm <sup>3</sup> ), MW power levels (1-6 kW); at 2.45 GHz frequency; and exposure times (60s, 120s, 180s, 240s, 300s)	Li et al. (2019) Coal, cylindrical sample (h = 30 mm, d = 25 mm)	By increasing the input MW power level, the electric field intensity and temperature of coal and the spatial heterogeneity of the electric and thermal fields all increased. MW heating can induce interconnection of pores and fractures in coal.
FEM, coupled 3D electromagnetic, thermal, and mechanical model, COMSOL Multiphysics	Multi-mode; cavity (W267×L270×H188 mm <sup>3</sup> ), MW power level 500 W; at 2.45 GHz frequency; and exposure times (0-300s)	Jinxin et al. (2019) Coal, a cylindrical sample (h = 60 mm, r = 25 mm)	The average permeability of coal increased from 1.65×10 <sup>-16</sup> m <sup>2</sup> to 3.63×10 <sup>-16</sup> m <sup>2</sup> after MW irradiation of 500 W at 2.45 GHz and 300s exposure.
FEM, coupled 3D electromagnetic, thermal, and mechanical model, MATLAB & COMSOL Multiphysics	Multi-mode; cavity (W267×L270×H188 mm <sup>3</sup> ), MW power level 3 kW; at 2.45 GHz frequency; and exposure times (10-90s)	Yuan and Xu (2019) Basalt, a cylindrical sample (h = 100 mm, d = 50 mm)	The uneven distribution of temperature caused damage because of the different thermal stresses produced in the rock sample. Tensile failure at the surface of rock was observed. Finally, radial cracks were observed from both the numerical models and the experiments.
FEM, coupled 2D electromagnetic, thermal, and mechanical model, COMSOL Multiphysics	Single-mode; cavity (W300×L500 mm <sup>2</sup> ), MW power level 100 kW; at 2.45 GHz frequency; and 45s exposure time	Zhang et al. (2019) Granite & Limestone, rectangular samples (W300mm) at various distances (12, 14, 16 cm) from MW from antenna	The distance from MW antenna has a great influence on the electromagnetic field, temperature, mechanical stress, and plastic zone distribution in rock. At the same distance, limestone showed higher electromagnetic field intensity than granite; instead, the rock surface temperature of granite was higher.
FEM, coupled 3D electromagnetic and thermal model, ANSYS v17	Multi-mode, MW power levels (0-3 kW & 5.55 kW); at 2.45 GHz frequency; and exposure times (up to 240s)	Hidayat et al. (2020) Ilmenite, cylindrical samples (r = 0.035 m, L = 0.015, 0.03, 0.045, and 0.06 m) slab samples (L0.07 × W0.07 m) and various thickness (b = 0.015, 0.03, 0.045, 0.06 m)	Hotspot location in ilmenite changed as the thickness of sample varied. Higher temperature distribution was observed in thinner samples.

\*Note: In the table the term “microwave” is abbreviated as MW.

### 2.2.3 Technical and economic analyses

This section aims to give an overview of the published studies related to energy-related (consumption, savings, etc.) investigations and to present techno-economic analyses on the results of microwave irradiation of rocks and minerals discussed in earlier sections, for future possible implementation of a pilot-scale microwave in industrial usage. As discussed by Napier-Munn et al. (1996), the mechanical size reduction of solids (comminution) is one of the most energy intensive processes for mineral processing plants. Thus, there have been serious efforts in the past two decades for improving the efficiency of comminution processes. Through investigations in the findings of experimental research studies, it can be confirmed that reduced comminution energy and improved recovery processes are practically achievable at economically viable microwave energy inputs (Kingman et al., 2004; Kingman et al., 2004b). However, depending upon which types of microwave applicators are used, single-mode or multi-mode, the outcome varies significantly. For example, a single-mode microwave cavity provides relatively high power densities in the absorbing phases of minerals. It was found that 1 kg batches of copper carbonatite ore treated at 15 kW and 0.1s microwave exposure (or 0.4 kWh/t) showed a reduction in strength of over 50%; and little improvement was achieved for longer microwave exposures as discussed by Kingman et al. (2004). The copper ore recovery after microwave treatment was found to be increased by 85% to 89.5% (Scott et al., 2008). In addition, comparative batch flotation experiments by Sahyoun et al. (2005) on copper ore samples microwaved with power levels of 5-12 kW at 0.1-0.5s exposure times demonstrated that improvements in copper recovery of between 6-15% could be achieved when the results of treated ores were compared with untreated samples. On the other hand, several studies on microwave irradiation of minerals in multi-mode cavities have shown promising results. For instance, after microwave treatments of 20 grams chalcopyrite in a multi-mode microwave cavity with 3 kW power level and the frequency of 2.45 GHz for 0, 5, 10, and 20s of microwave exposures, Da Silva et al. (2018) found that microwave treatment increases the mineral's specific surface area and porosity and changes the pore size distribution. Therefore, the authors concluded that chalcopyrite's leaching kinetics process could be improved by multi-mode microwave irradiation. The same conclusion was also drawn in a study by Zhu et al. (2018) in which the effects of microwave heating parameters on the pore structure of oil shale samples were evaluated. In conclusion, these results verify that today microwave treatment of ores can be done economically. However, depending upon the objective of the project,

a wise selection between the two different microwave applicators, single-mode or multi-mode, should be considered. For further technical investigation on the reported experimental data discussed in the literature review, Table 2.6 is given as an overview of the amounts of rock/ore strength reduction from different measurement techniques with respect to different microwave input operating parameters. It can be seen that the amount of microwave energy input has a direct relation to the strength reduction of rocks and minerals.

Table 2.6: Results of microwave treatment effects on strength reductions in rocks and minerals: a comparison between the amount of microwave energy input and the mechanical changes in different rock samples

Reference	Type of rock/mineral	MW operating parameters and type (M or S*)	Result (UCS, Cracking, energy)
(Vorster et al., 2001)	Massive copper ore	P = 2.6 kW, t = 90s, <b>M</b>	BWI of the ore reduced up to 70%
(Kingman et al., 2004)	Copper carbonite ore	P = 15 kW (0.83 kWh/t). t = 0.2s, <b>S</b>	30% reduction in impact breakage parameters
(Kingman et al., 2004)	Lead-zinc ore	P = 10 kW, t = 0.1s, <b>S</b>	Up to 50% reductions in strength of the ore
(Charikinya, 2015)	Sulfide ore	Input MW energies (2.11-2.65 kWh/t), <b>S</b>	Cracks volume increased by 500%
(Kumar et al., 2010)	Iron ore	P = 900 W, t = up to 120s, <b>M</b>	Specific rate of breakage increased by an average of 50%
(Wang & Forssberg, 2005)	Quartz and limestone	P = 7 kW, t = 10 min, <b>M</b>	UCS decreased from 50 MPa to 25 MPa and 40 MPa to 35 MPa for quartz and limestone
(Satish et al., 2006)	Basalt	Power density 1 W/g, t = 360s, <b>M</b>	42% increase in penetration of cutter
(F Hassani et al., 2016)	Basalt	P = 5 kW, t = 65s, <b>M</b>	30% reduction in uniaxial compressive strength
(Sikong & Bunsin, 2009)	Granite	(a) P = 850 W, t = 30 min; (b) P = 600 W, t = 10 min (quenched sample), <b>M</b>	(a) 60% reduction in samples' compressive strength (b) 38% reduction in cutting rate
(Zeng et al., 2019)	Granite	P = 1.4 kW, <b>M</b>	UCS of granite decreased from 88.17 MPa at 25 °C to 18.61 MPa at 800 °C
(Kobusheshe, 2010)	Kimberlite	Input MW energy of (a) 9 kWh/t; and (b) 6.81 kWh/t, <b>S &amp; M</b>	(a) 40% reduction in point load strength and (b) 10% reduction in the mean UPV
(Singh et al., 2017)	(a) Coal sample; and (b) Manganese ore	(a) P = 180 W; (b) P = 900 W, t = 1, 3, 5 min, <b>M</b>	(a, b) 17.1% average increase in carbon recovery for coal
(Zheng et al., 2017)	Gabbro	P = 2 kW, t = 30-120s, <b>S</b>	55% reduction in the overall p-wave velocity

\*Note: In the table the term “microwave” is abbreviated as MW; and the two MW applicator types of single-mode and multi-mode are denoted by **S** and **M**, respectively.

The feasibility and economical potential of microwave irradiation of rocks and minerals was demonstrated after a techno-economic study by Bradshaw and colleagues (2007) looked into the potential profitability of microwave-assisted comminution and liberation of mineral ores. The preliminary economic analyses presented in this study showed that the overall cost of the microwave equipment was found to be in a range between \$0.16 US to \$0.85 US per ton of ore.

In a detailed investigation, the study tabulated the estimated data of operating and cost parameters for industrial scale applicators for two appropriate ISM frequencies, 433 and 915 MHz (see Table 2.7). It should be noted that the estimated values were only provided for a Constant Wave (CW) operation and do not involve pulsed or other types of microwaves.

Table 2.7: Estimated operating and cost parameters for industrial scale applicators (table modified from Bradshaw et al. [2007])

Frequency, MHz	433		915	
	Most expensive scenario	Least expensive scenario	Most expensive scenario	Least expensive scenario
Power kW	500		100	
Estimated feed top size (mm)	90		50	
Cross section of applicator m <sup>2</sup>	0.32		0.07	
Critical energy density Jm <sup>-3</sup> <sub>abs</sub>	1×10 <sup>8</sup>	0.5×10 <sup>8</sup>	1×10 <sup>8</sup>	
Microwave energy consumption kWh/t	1.11	0.55	1.11	
Order of magnitude unit capital cost US\$/kW	20,000	10,000	7,000	4,000
Electricity cost US\$/kWh	0.035		0.035	
Annual operating hours	8,150		8,150	
Order of magnitude capital cost US\$	10,000,000	5,000,000	700,000	400,000
Amortized cost US\$/yr	2,983,155	996,260	208,820	79,700
<b>Overall cost US\$/t</b>	<b>0.85</b>	<b>0.16</b>	<b>0.14</b>	<b>0.06</b>

In Table 2.7, the estimated capacity, cost, and other operating parameters for the most appropriate ISM frequencies, 433 and 915 MHz, for industrial scale operation are given. It is clearly estimated that for large-scale operations, an appropriate capacity can be achieved at 433 MHz frequency, while for smaller operations, parallel units at 915 MHz might be feasible. Overall, Bradshaw et al.'s (2007) study estimated that the overall cost of microwave equipment was found to vary in a range from lower bound (\$0.06 US/t) to upper bound (\$0.85 US/t) on the total amortized capital and operating expenditure. This study initiated for the first time a concluding remark for possible future industrial implementation of an economic microwave usage for rock breakage and mineral processing industries.

As discussed earlier, the high consumption of energy in the process of microwave treatment of rocks and ores before their processing is the primary challenge that must be appropriately addressed before the technology becomes feasible and economical. Assuming that microwave treatment reduces 50% of the UCS of the rocks and \$0.28/kWh to be the cost of electricity, \$8.66/t is the electricity cost of implementation of the microwave treatment system working with 0.76 UCS reduction per energy rate (i.e. MPa per kWh/m<sup>3</sup>). However, by increasing this rate to ten times its initial value, the electricity cost of the microwave treatment system can be reduced to \$0.89/t, which is much smaller in comparison to the total mining cost, e.g. higher economic feasibility. Therefore, in order to achieve these higher rates, higher power densities are required. But there are other researchers, like Didenko et al. (2005) and Hartlieb et al. (2017), who used  $1.71 \times 10^5$  kW/m<sup>3</sup> and  $8.47 \times 10^4$  kW/m<sup>3</sup> power densities; however, these power densities led to low UCS reduction per energy rates. Thus, to investigate feasibility of microwaves in the reduction of the overall rocks' strength, many parameters, including the role of material properties' variation, input microwave operating parameters, experimental conditions, etc. should be accurately determined. As indicated in almost all recent research studies on microwave irradiation of rocks and minerals, the key to techno-economically feasible implementation of any microwave-assisted rock treatment system for the industry is to reduce energy intensity effectively; and therefore, by selecting an optimal microwave power density, a feasible design of microwave-rock pre-conditioning systems can be achieved.

## **2.3 Research gaps and outlook**

Taking all the discussed literature into account, several experimental studies have been carried out in recent years to investigate and address the effects of microwave irradiation on various types of rocks and minerals. These studies were able to successfully identify the importance of microwave energy as a prospective application in future rock breakage operations and mineral processing applications in the civil and mining industries. In addition, in tandem with experimental research, computational studies have come to play an important role in understanding how different mechanisms are involved in microwave-assisted rock pre-conditioning and breakage processes. The development of a numerical model is considered an enhancement of the understanding of microwave-assisted rock pre-conditioning and breakage and thermomechanical characteristics of rocks after their exposure to microwaves at different microwave operating



parameters, either in single-mode or multi-mode microwave cavity systems. As discussed and reviewed in this chapter, today, the vital role of computer simulations in the field of mining and civil engineering is recognized for researchers and even the industry. Serious efforts have been made by researchers for developing a reliable and trustworthy numerical model that mimic the correct electromagnetic wave propagation in the multi-mode microwave system. However, although several studies have been done in recent years to investigate the effects of multi-mode microwave irradiation on rocks with the numerical modeling approach (e.g. finite element method), no numerical model of multi-mode microwave irradiation was found that: (1) is fully coupled for electrical and thermal multiphysics interactions, (2) represents a correct electromagnetic wave propagation inside the multi-mode microwave cavity as in the experiment, and more importantly (3) is validated against experimental data of microwave irradiation tests on various rock types with different microwave settings. Therefore, given the above picture of the gaps in the literature, the present thesis takes into account all the previous efforts and aims to study the effects of both single-mode and multi-mode microwave irradiation on various rock types with several experimental tests and by different rock characterization methods. In addition, the current thesis presents a novel numerical model of the multi-mode microwave irradiation system with a rotational stirrer fan that is validated against experimental data. The validated numerical model is used to accurately predict the effects of multi-mode microwave irradiation on rocks with different dielectric properties. The numerical modeling approach is the initial step to gain more in-depth information into phenomena occurring inside rocks and/or minerals under microwave irradiation. A numerical model that is validated with experimental data is a novel contribution that can be employed for future investigations without costly experiments. It can also be a promising tool for design, optimization (improving heating and pre-conditioning capacity), and even innovation in the implementation of large-scale microwave-assisted rock breakage systems.

# Chapter 3

## Fundamental principles of microwaves for heating of rocks

### Contents

---

3.1	Electromagnetic wave theory .....	52
3.2	Mechanisms of microwave heating of materials .....	55
3.3	Influencing parameters in rock heating and pre-conditioning by microwaves....	65
3.4	Summary and conclusions .....	76

---

### Preface

*Since rocks are made up of dielectric materials that can be heated when exposed to electromagnetic waves (microwaves), a thorough understanding of the fundamental mechanisms involved in a microwave-assisted rock heating process is needed. Therefore, it is necessary to introduce the concept of electromagnetic wave theory and to define the influencing parameters involved in the process of rock heating and pre-conditioning by microwaves. This chapter first introduces the fundamental principles of electromagnetic wave theory (section 3.1). Then, various mechanisms of microwave heating of materials are explicated (section 3.2). The influencing parameters in rock heating and pre-conditioning by microwaves are defined and explained (section 3.3). Finally, there are a summary of the discussed fundamentals and conclusions (section 3.4). The outcome of this chapter will form a foundation for the present thesis. By accurately defining the parameters discussed above, the mechanisms of rock heating by microwaves can be easily understood.*

## 3.1 Electromagnetic wave theory

Electromagnetic waves occur in many varieties, including radio waves, from the long-wave band through VHF, UHF, and beyond; microwaves; infrared, visible and ultraviolet light; X-rays, gamma rays etc. In electromagnetics there are several theorems and principles that are fundamental to the understanding of electromagnetic generation, radiation, propagation, scattering, and reception (Balanis, 1999). Most of these concepts are usually used to facilitate the solution of interrelated problems such as microwave-assisted heating of dielectric materials (e.g. rocks in the present study), which consists of an electromagnetic energy source (magnetron) and a dielectric material that absorbs the produced electromagnetic waves (microwaves) and transforms them into heat. Given this, all the known laws of electricity and magnetism that were brought together by James Clerk Maxwell in the 1860s are introduced in the following section.

### 3.1.1 Introduction to Maxwell's equations

In 1862-64 James Clerk Maxwell brought together all the work that had been done by brilliant physicists such as Oersted, Coulomb, Gauss, and Faraday, and added his own insights to develop a set of four partial differential equations (PDEs) that was later called “Maxwell's equations” (Balanis, 1999). A brief summary of the former attempts prior to the discovery of Maxwell's equations are given as follows:

- *Gauss's law for electricity* gives the electric field produced by electric charges:  $\nabla \cdot \mathbf{D} = \rho_e$  (3.1)
- *Gauss's law for magnetism* states that individual magnetic charges cannot exist:  $\nabla \cdot \mathbf{B} = 0$  (3.2)
- *Faraday's law* gives the electric field produced by a changing magnetic field:  $\nabla \times \mathbf{E} = -\partial \mathbf{B} / \partial t$  (3.3)
- *Maxwell-Ampère's law* gives the magnetic field produced by electric currents:  $\nabla \times \mathbf{H} = \mathbf{J} + \partial \mathbf{D} / \partial t$  (3.4)

In the above equations,<sup>2</sup> the following parameters are given.  $\mathbf{E}$  (V/m) and  $\mathbf{D}$  (C/m<sup>2</sup>) denote electric field and electric displacement;  $\mathbf{H}$  (A/m) and  $\mathbf{B}$  (Tesla) represent magnetic field and magnetic flux density;  $\mathbf{J}$  (A/m<sup>2</sup>) and  $\rho_e$  (C/m<sup>3</sup>) are given as electric current density and volumetric electric charge density (Civelek & Bechteler, 2008). Equations (3.1) to (3.4) constitute a set of coupled, first order, PDEs for electric ( $\mathbf{E}$ ) and magnetic ( $\mathbf{B}$ ) fields. In free space, referred to as a vacuum, zero electric charge density,  $\rho_e = 0$ , can be assumed. This condition also applies for the electric current density,  $\mathbf{J}$  (A/m<sup>2</sup>), in the equation of continuity that is given in equation (3.5). The

---

<sup>2</sup> By convention, vector quantities are denoted by bold-faced characters.

following assumptions also apply to free space:  $\mathbf{B} = \mu_0 \cdot \mathbf{H}$  and  $\mathbf{D} = \epsilon_0 \cdot \mathbf{E}$ , where  $\mu_0$  and  $\epsilon_0$  are the permeability and permittivity of free space (Griffiths, 2017).

$$\nabla \times \mathbf{J} = -\frac{\partial \rho}{\partial t} \quad (3.5)$$

Now, by taking the curl of equations (3.3) and (3.4) of the Maxwell's equations, they become decoupled and yield the following equations,

$$\nabla^2 \mathbf{E} = \mu_0 \epsilon_0 \frac{\partial^2 \mathbf{E}}{\partial t^2} \quad (3.6)$$

$$\nabla^2 \mathbf{B} = \mu_0 \epsilon_0 \frac{\partial^2 \mathbf{B}}{\partial t^2} \quad (3.7)$$

A closer look at these equations reveals that both vector functions  $\mathbf{E}$  and  $\mathbf{B}$  satisfy the wave equation with speed  $v = 1/\sqrt{\mu_0 \epsilon_0} \approx 3.00 \times 10^8$  m/s, which is the speed of light in a vacuum ( $v = c$ ) (Panofsky & Phillips, 2005). The solutions to equations (3.6) and (3.7) can be written in the form of plane waves, as given in equations (3.8) and (3.9),

$$\tilde{\mathbf{E}} = \tilde{\mathbf{E}}_0 e^{i(\mathbf{k} \cdot \mathbf{r} - \omega t)} \quad (3.8)$$

$$\tilde{\mathbf{B}} = \tilde{\mathbf{B}}_0 e^{i(\mathbf{k} \cdot \mathbf{r} - \omega t)} \quad (3.9)$$

where  $\tilde{\mathbf{E}}_0$  and  $\tilde{\mathbf{B}}_0$  are the complex amplitudes and  $\mathbf{k}$  is the vector of wave propagation that is given in equation (3.10) (David K. Cheng, 1989),

$$\mathbf{k} = k \hat{\mathbf{n}} = \frac{2\pi}{\lambda} \hat{\mathbf{n}} = \frac{2\pi v}{c} \hat{\mathbf{n}} = \frac{\omega}{c} \hat{\mathbf{n}} \quad (3.10)$$

in which  $\lambda$  (m) is the wavelength and  $\hat{\mathbf{n}}$  is a unit vector in the direction of wave propagation.

### 3.1.2 Electromagnetic waves in materials

When there are conductors and dielectrics involved, the form of Maxwell's equations change along with their solutions (Griffiths, 2017). For a conductive material, the free electric charge density,  $\rho$ , immediately flows to the surface of the material; and for insulators where no free charge density is available, the charge density becomes zero, as it is tightly limited to atoms and molecules. For linear, isotropic, and non-dispersive materials, the following assumptions apply:  $\mathbf{B} = \mu \cdot \mathbf{H}$ ,  $\mathbf{D} = \epsilon \cdot \mathbf{E}$ , and  $\mathbf{J} = \sigma \cdot \mathbf{E}$ , where  $\mu$ ,  $\epsilon$ , and  $\sigma$  are the permeability, permittivity, and electrical conductivity of the material (Cheng, 1989). By implementing these assumptions in Maxwell's equations (3.1) to (3.4) and by taking the curl to equations (3.3) and (3.4), the new wave equations for a linear medium (e.g. rock) are formed as follows,

$$\nabla^2 \mathbf{E} = \mu \varepsilon \frac{\partial^2 \mathbf{E}}{\partial t^2} + \mu \sigma \frac{\partial \mathbf{E}}{\partial t} \quad (3.11)$$

$$\nabla^2 \mathbf{B} = \mu \varepsilon \frac{\partial^2 \mathbf{B}}{\partial t^2} + \mu \sigma \frac{\partial \mathbf{B}}{\partial t} \quad (3.12)$$

Both equations (3.11) and (3.12) are plane-wave solutions where the wave number  $\mathbf{k}$  is complex, as in equations (3.6) and (3.7).

### 3.1.3 Electromagnetic spectrum, safety, and compliance

*Electromagnetic spectrum:* Microwaves are high frequency radio waves (radiofrequency fields) and, like visible radiation (light), are part of the electromagnetic spectrum. They are a form of electromagnetic radiation with frequencies ranging from several hundred MHz to several hundred GHz and wavelengths ranging from approximately 1 to 20 centimeters (Pozar, 2012). Because of their high frequencies, microwaves have the advantage of being able to carry more information than ordinary radio waves and are capable of being beamed directly from one point to another. In addition to their telecommunications applications, microwaves are used in cooking, police radar, and certain military applications. Microwave heating applications usually perform on the 0.915 GHz (0.896 GHz in the UK) and 2.45 GHz frequencies in order to minimize interference with communication band microwaves. Of these, 2.45 GHz is the frequency most used (Meredith, 1998).

*Microwave safety and compliance*<sup>3</sup>: Microwave energy can be absorbed by the body and, therefore, produce heat in exposed tissues. There is a high risk of damage from heat to the organs with a poor blood supply and temperature control, such as the eye, or temperature-sensitive tissue like the testes. However, thermal damage may only happen from long microwave exposures to very high levels of microwaves, well in excess of those measured around microwave ovens. In terms of health and safety, although numerous research studies have been conducted in the 21<sup>st</sup> century regarding the hazards of microwave exposure for human health, no concrete conclusions have yet been found. In this case, several countries, as well as the International Electrotechnical Commission (IEC), the International Committee on Electromagnetic Safety (ICES) of the Institute of Electrical and Electronics Engineers (IEEE), and the European Committee for Electrotechnical Standardization (CENELEC), have set a product emission limit of 50 (W/m<sup>2</sup>) at any point 5 cm

---

<sup>3</sup> The content of this paragraph is according to the safety report by the World Health Organization ((WHO), 2005)

away from the external surfaces of the microwave oven. In practice, it is reported by the World Health Organization (WHO) that while the microwave is on, emissions from modern domestic microwave ovens are substantially below this international limit standard and have interlocks that prevent people from being exposed to microwaves. Moreover, exposure decreases rapidly with distance; for example, a person who has a distance of 50 cm from the oven receives about one one-hundredth of the microwave exposure of a person who exposed at the distance of 5 cm away.

### **3.2 Mechanisms of microwave heating of materials**

The system of “microwave heating of materials” consists of two main components: microwaves and matter. Microwaves as part of the electromagnetic spectrum carry energy through space at the speed of light. Other characteristics of microwaves, such as penetration depth into materials and their microscopic polarization effect upon frequency and power used, make them a prime candidate for producing heat within dielectric materials. In general, all materials can be classified into three main groups: (i) conductors, which reflect microwaves; (ii) insulators, through which microwaves pass with no effect; and (iii) absorbers, which absorb part of the microwaves and produce heat (Pozar, 2012).

Materials that absorb microwave radiation are called dielectrics. Dielectrics have two main important properties: a) they have very few charge carriers—when an external electrical field is applied, there is very little electric charge carried through the material matrix—and b) the molecules or atoms comprising the dielectric exhibit a dipole movement. Contrary to convective heating with steam, hot air, or via any other heat sources and even radiation heating in general, dielectric heating by microwaves generates heat directly inside the exposed material. The conversion of electric energy to heat results from the dielectric losses of the electric nonconductive material, which is usually also a poor thermal conductor. In convective heating of materials with poor thermal conductance properties, the surface has to acquire high temperatures so that the temperature gradient, i.e., the transport of heat, will be as high as possible and account for the material’s rapid heating. Thus, the major advantages of microwave heating when compared to the other techniques are the precise control on specifications and volumetric heating, rapid heating, selective heating of materials composed of different parts with different dielectric properties, and the high level of safety and automation (Haque, 1999). A summary list of the comparisons between the conventional heating and microwave-assisted heating is given in Table 3.1.

Table 3.1: Comparisons of microwave-assisted heating and conventional heating

<b>Microwave treatment</b>	<b>Conventional heating</b>
Selective heating is possible according to the variations of the material's properties	Non-selective heating
Rapid and efficient heating	Slow and inefficient heating
Hot spots can be obtained if desired (usually by single-mode microwaves for surface pre-conditioning)	Impossible to create hot spots
Controlled heating (no inertia): When the microwave is switched off, the source of heat is immediately removed from the object	Less controllable
Heating by conversion of energy (irradiation, conduction, etc.)	Heating by transfer of energy

### 3.2.1 Polarization in linear dielectrics

Microwave heating, which is also called dielectric heating, depends on the interaction between polar groups in molecules of nonconductive materials and the alternating electric field of electromagnetic oscillation. The atomic carriers of charges prevailing in fluid and solid materials are not able to move upon imposing an electric field  $\mathbf{E}$ ; instead, they may only be slightly dislodged from their initial position. The effective force is proportional to the electric field strength, and because of this displacement, negative and positive surface charges arise at the terminal sites (Ramo et al., 1994). This phenomenon is referred to as polarization,  $\mathbf{P}$  ( $\text{C}/\text{m}^2$ ), and is related to the product of atomic polarizability,  $\alpha$ , and electric field,  $\mathbf{E}$  ( $\text{V}/\text{m}$ ), as given in equation (3.13).

$$\mathbf{P} = \alpha\mathbf{E} \quad (3.13)$$

All atoms, ions, and dipoles in materials tend to reorient themselves so as to align with an externally applied electric field. Thus, each atom, ion, and dipole obtains a dipole moment that is proportional to the electric field and has its own polarizability (A. C. Metaxas & Meredith, 2011). Therefore, materials become polarized by one or a combination of the following three different polarization mechanisms within an electromagnetic field (Gabriel et al., 1998):

- (a) Orientational (dipolar) polarization,
- (b) Ionic (conduction) polarization,
- (c) Interfacial or Maxwell-Wagner polarization.

When a bulk material (e.g. rock sample) polarizes, all the small dipoles caused by individual atoms, ions, and dipoles align in the same direction. Therefore, the polarization vector,  $\mathbf{P}$ , in a bulk

material (e.g. rock sample) can be defined as the dipole moment per unit volume and the total polarization,  $\mathbf{P}_t$ , can be calculated by adding the realignment contributions of all atoms, ions, and dipoles as shown in equation (3.14),

$$\mathbf{P}_t = \mathbf{P}_a + \mathbf{P}_i + \mathbf{P}_o \quad (3.14)$$

where the a, i, and o correspond to atomic, ionic, and orientational polarization, respectively.

### 3.2.1.1 Orientational (dipolar) polarization

Dipolar polarization is a phenomenon that is responsible for most microwave heating in materials that have a pronounced dipole (water, acids, solvents). In this case, either the displacement of electrons around nuclei (called electronic polarization) or the relative displacement of atomic nuclei as a consequence of the unequal distribution of charges in molecule formation (called atomic polarization) causes induced dipoles. In the presence of microwave irradiation with rapidly changing electric fields, the molecules try to orient themselves in the direction of the field lines, as depicted in Figure 3.1. This results in a loss of energy from the dipole by molecular friction and collisions when the frequency of the applied electric field is such that molecules simply lag behind the field polarity, giving rise to dielectric heating. In cases where high electric field intensity applies, although the molecules try to follow the field, intermolecular inertia prevents any significant movement before the field has been alternated (reversed). Moreover, it is noteworthy to mention that the molecules will be polarized uniformly, if the frequency of the oscillation is very low (Chen et al., 2004).

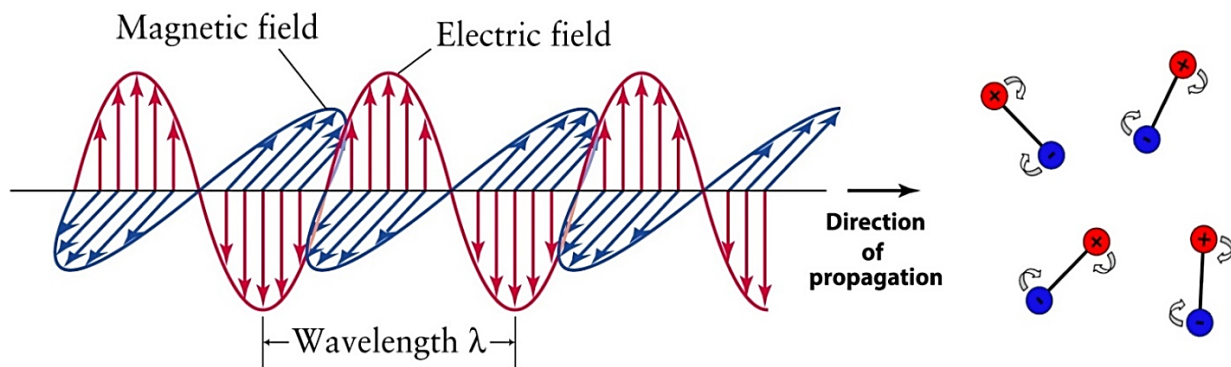


Figure 3.1: Graphical illustration of the orientational (dipolar) polarization mechanism



### 3.2.1.2 Ionic (conduction) polarization

When the material under irradiation is an electrical conductor, a different type of polarization can be observed in molecular groups with two different atoms that combine with a molecule (ion). But, in their entirety, these atoms do not reveal any external polarization because the centers of positive and negative charges have become identical. Thus, the charge carriers (electrons, ions, etc.) oscillate back and forth, move through the material under the influence of the electric field,  $E$ , and collide with the adjacent molecules or atoms, which cause agitation and excitation and, therefore, heat creation (see Figure 3.2). When a highly conductive material (e.g. metal) is exposed to microwave irradiation, most of the microwave energy does not penetrate the surface of the material and is therefore reflected. However, high surface voltages, which may still be induced, are in charge of the arcing that is usually observed on metals under microwave irradiation (Chen et al., 2004). For instance, if there is a part of the metal that is very thin, such as with aluminum foil or a fork, a high voltage could build up that exceeds the breakdown voltage of air and cause a spark (arcing).

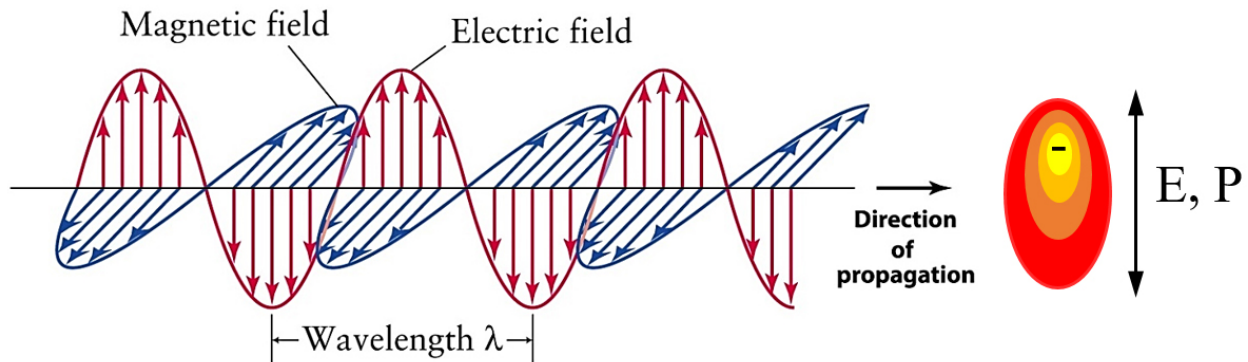


Figure 3.2: Graphical illustration of ionic (conduction) polarization of electric field moving in a perfect conductor

Both of the mechanisms, orientational (dipolar) polarization and the ionic (conduction) polarization, are influenced by various factors such as wavelength, physical properties of the material (e.g. dielectric constant, temperature, and thermal capacity), and ion characteristics (e.g. size, concentration, charge, and mobility). A combination of both conduction and dipolar polarizations results in an interfacial polarization which is explained in the following section.

### 3.2.1.3 Interfacial polarization

This type of polarization occurs in systems consisting of two different types of materials, a conductive and a nonconductive material, and is caused by polarization from charges developed between components in the heterogeneous materials (Chen et al., 2004). This mechanism is an important mechanisms for systems composed of conducting and nonconducting materials. An example would be a dispersion of metal particles in some rocks.

### 3.2.2 Definition of relative permittivity of materials

The permittivity of an isotropic material is related to its polarization and can be defined as,

$$\mathbf{D} = \epsilon_0 \mathbf{E} + \mathbf{P} = \epsilon_0 \mathbf{E} + \epsilon_0 \chi_e \mathbf{E} = \epsilon_0 (1 + \chi_e) \mathbf{E} = \epsilon_0 \epsilon_r \mathbf{E} \quad (3.15)$$

where  $\epsilon_0$  is the permittivity of free space ( $\epsilon_0 = 8.854 \times 10^{-12}$  F/m),  $\mathbf{E}$  (V/m) and  $\mathbf{D}$  (C/m<sup>2</sup>) are electric field and electric displacement,  $\mathbf{P}$  is the polarization field, and  $\chi_e$  is the dielectric susceptibility of the material (Pozar, 2012). The permittivity of the material is also related to both the permittivity of a vacuum,  $\epsilon_0$ , and the relative permittivity,  $\epsilon_r$ , of the material, as shown in equation 19. However, it should be noted that equation (3.16) is for *lossless material*.

$$\epsilon = \epsilon_0 \epsilon_r \quad (3.16)$$

For a material with a *lossy behavior*, which is a material that dissipates electromagnetic energy passing through it, the permittivity becomes complex as

$$\epsilon_r = \epsilon' - j\epsilon'' \quad (3.17)$$

where  $j = \sqrt{-1}$ ,  $\epsilon'$  is defined as the dielectric constant of the material; and the imaginary part,  $-\epsilon''$ , is called the dielectric loss factor. The dielectric loss factor accounts for the loss in the medium (heat) due to damping of the vibrating dipole moments. This term must be negative ( $\epsilon''$  is positive) because of energy conversion. Lossless dielectric materials (e.g. free space) have a zero imaginary part. There is another important parameter that can be defined from the real and imaginary terms of equation (3.17). This parameter is called the dielectric loss tangent,  $\tan \delta$ , of the material, which corresponds to a ratio between the dielectric constant and the loss factor of the material and is defined in equation (3.18) (Griffiths, 2017).

$$\tan \delta = \frac{\epsilon''}{\epsilon'} \quad (3.18)$$

In microwave engineering, the use of relative permittivity is more common because it is a dimensionless quantity (Chen et al., 2004). Thus, by substituting equation (3.18) into equation (3.16) and by using equation (3.17), the following relation can be obtained,

$$\epsilon_r = \frac{\epsilon}{\epsilon_0} = \frac{\epsilon - j\epsilon''}{\epsilon_0} = \epsilon' - j\epsilon'' = \epsilon'(1 - j \tan \delta) \quad (3.19)$$

### 3.2.3 Definition of relative permeability of materials

Magnetic permeability,  $\mu$ , is the corresponding property for magnetic fields, which relates the magnetic flux density,  $\mathbf{B}$ , of a material to the magnetic field intensity,  $\mathbf{H}$ , and magnetization,  $\mathbf{M}$ , of the material. Thus, interaction of the material in the presence of an externally applied magnetic field can be introduced by the following relation (Cheng, 1989):

$$\mathbf{B} = \mu_0 (\mathbf{H} + \mathbf{M}) = \mu_0 (\mathbf{H} + \chi_m \mathbf{H}) = \mu_0 (1 + \chi_m) \mathbf{H} = \mu_0 \mu_r \mathbf{H} \quad (3.20)$$

where  $\chi_m$  is the magnetic susceptibility. Just as with the permittivity,  $\mu$  equals the product of the permeability of the vacuum,  $\mu_0$ , and the relative permeability,  $\mu_r$ . In general,  $\mu$  can be defined in a complex form as

$$\mu_r = \mu' - j\mu'' \quad (3.21)$$

in which  $\mu'$  and  $\mu''$  are real and imaginary parts of the complex permeability,  $\mu_r$ . Therefore, as in the case of complex permittivity, the ratio of the imaginary to the real part of the complex permeability is called the loss tangent,  $\tan \delta_m$ , which is given in equation (3.22). The subscript  $m$  distinguishes the loss tangent obtained from permeability from that obtained from permittivity.

$$\tan \delta_m = \frac{\mu''}{\mu'} \quad (3.22)$$

### 3.2.4 Definition of electrical conductivity and resistivity of materials

Electrical conductivity,  $\sigma$  (S/m), is a physical property of materials that describes how easily electric currents can flow through a medium when they are subjected to an external electric field (Pozar, 2012). More specifically, the relationship between the electrical current density,  $\mathbf{J}$  (A/m<sup>2</sup>), within a material, and the electric field,  $\vec{E}$  (V/m), is referred to as electrical conductivity.

$$\mathbf{J} = \sigma \cdot \mathbf{E} \quad (3.23)$$

When a material, such as a rock sample, is exposed to an electric field, because of the existence of free electrical charges within the rock, these charges experience an electric (Coulomb) force. This

force causes the free charges in the rock to move along the direction of the applied field through the sample, with positive charges traveling parallel to the direction of electric field and negative charges traveling in the opposite direction, as shown in Figure 3.3.

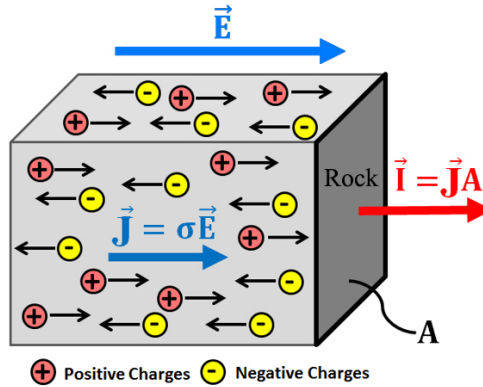


Figure 3.3: Traveling of free electrical charges in a rock exposed to an external electric field

As shown in Figure 3.3 by red, the size of the flow of electrical charges through a rock, referred to as electrical current,  $\mathbf{I}$  (A), is equal to the product of current density and unit cross-sectional area,  $A$  ( $\text{m}^2$ ), of the surface acted upon (Cheng, 1989). Thus, current density represents the amount of current flowing per unit across a cross-sectional area, as given in equation (3.24).

$$\mathbf{J} = \frac{\mathbf{I}}{A} \quad (3.24)$$

In conductive materials (with larger  $\sigma$ ), free charges move more easily; and, therefore, strong currents may be induced by relatively weak electrical fields. On the contrary, resistive materials (with smaller  $\sigma$ ) need strong electrical fields to produce strong electrical currents. The relationship between the electrical conductivity of a material,  $\sigma$  (S/m), and its dielectric loss factor,  $\epsilon''$ , is a function of the electromagnetic frequency,  $f$  (Hz), as shown in equation (3.25) (Gabriel et al., 1998).

$$\sigma = \omega \epsilon_0 \epsilon'' = 2\pi f \epsilon_0 \epsilon'' \quad (3.25)$$

In this equation,  $\omega$  is the angular frequency in (Hz),  $\epsilon_0$  is the electrical permittivity of free space ( $\epsilon_0 = 8.86 \times 10^{-12}$  F/m), and  $\epsilon''$  is the material's loss factor at the appropriate frequency. An equivalent physical property of materials in relation to their conductivity is their resistivity,  $R$  ( $\Omega \cdot \text{m}$ ). By definition, the resistivity of a material is the reciprocal of its conductivity,

$$R = \frac{1}{\sigma} \quad (3.26)$$

However, one should note that both electrical resistivity and conductivity are sometimes used interchangeably, as they are acceptable for describing the conductive properties of materials. Depending upon the specific measurement technique used, either property can be selected as an input electrical property in a numerical model, for instance.

### 3.2.5 Calculation of penetration depth

In the application of microwaves at industrial scale, it is essential to determine an important factor called “penetration depth”. This factor appears when the amplitude of the wave affecting a dielectric material diminishes as the electromagnetic wave enters the dielectric until it disappears. The mechanism is that the wave enters and penetrates a lossy (dielectric) material (e.g. a rock sample); propagates into the material because of power absorption, i.e. the associated power dissipates exponentially after traversing some distance; and finally, the wave is attenuated (Griffiths, 2017). For a better visual understanding of this phenomenon, Figure 3.4 is presented in which an electromagnetic wave enters from air to a conductive material and exits. It is noticeable that whereas the electric and magnetic fields are in phase in free space (the air), once they enter a conductive material, they become out of phase, according to the constraints of Maxwell’s equations.

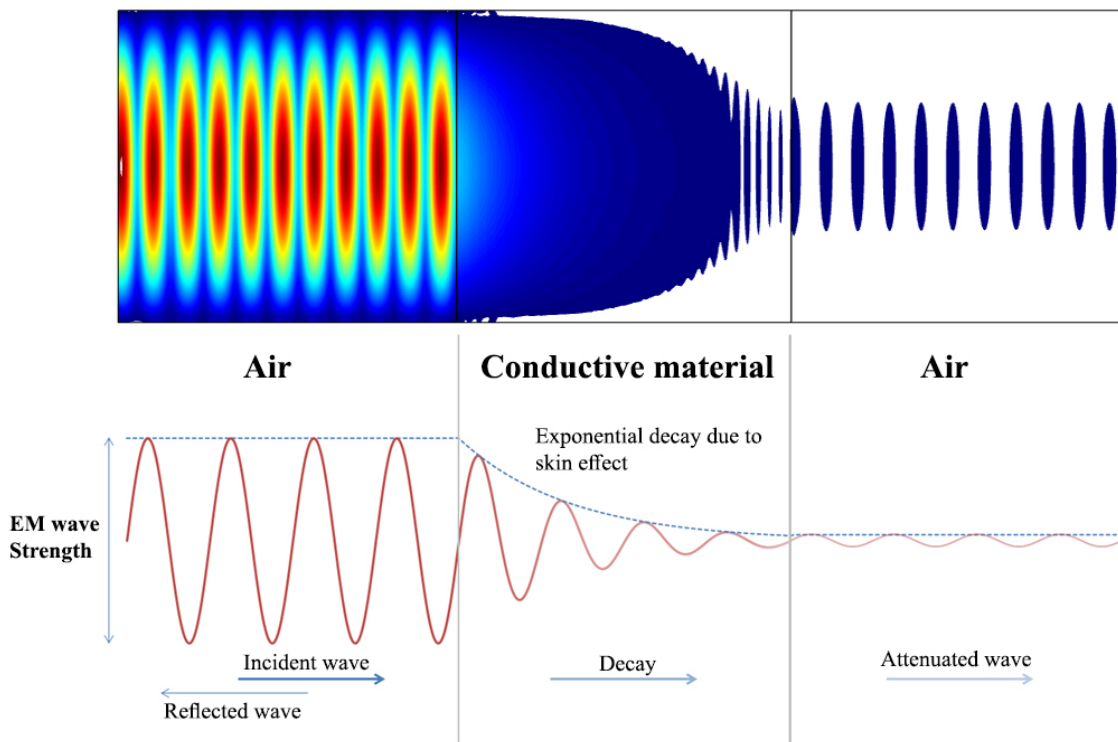


Figure 3.4: Schematic of the electromagnetic waves penetrating a lossy (dielectric) material

A simplified approach to calculate the microwave power dissipation in a dielectric material is given by Lambert's law. According to this law, incident energy is normal to the surface and dissipates energy exponentially as it travels through the dielectric material (see Figure 3.4) (Yang & Gunasekaran, 2004). Therefore, there is an exponential relation for the dissipation of power within the dielectric material as given in equation (3.27),

$$P(x) = P_0 e^{-2\beta x} \quad (3.27)$$

where  $P(x)$  is the power dissipation at depth  $x$  in (W),  $P_0$  is the incident power at the surface in (W), and  $x$  is the depth from the surface in (m).  $\beta$  is the attenuation constant in ( $m^{-1}$ ); and its value is a function of frequency (Hz), velocity of radiation (m/s), and loss tangent. The penetration depth,  $D_p$ , can then be defined as the distance (the depth into the material) after which the power drops to  $1/e = 0.368$  of its surface value, and its value can be obtained by using equation (3.28),

$$D_p = \frac{\lambda_0}{2\pi\sqrt{2\varepsilon'}} \frac{1}{\sqrt{\left[1 + \left(\frac{\varepsilon''}{\varepsilon'}\right)^{0.5}\right] - 1}} \quad (3.28)$$

where  $\lambda_0$  is the wavelength of incident radiation (Meredith, 1998). In most materials,  $\varepsilon'' \ll \varepsilon'$ ; and therefore, equation (3.28) can be Taylor expanded and reduced to equation (3.29).

$$D_p = \frac{\lambda_0 \sqrt{\varepsilon'}}{2\pi\varepsilon''} \quad (3.29)$$

The penetration depth,  $D_p$ , increases proportionally with the frequency  $f$  and the dielectric constant  $\varepsilon'$ . The attenuation depth depends on the dielectric loss factor,  $\varepsilon''$ .

In a mixed dielectric, the processes are very complicated; so ultimately, the experiment has to decide on the actual prevalent penetration depth. Furthermore, there are influences of the material's conductivity properties that are quite obvious in a multi-layered dielectric (Griffiths, 2017). As shown in Figure 3.5, one part of the incoming waves will be reflected from the surface if the characteristic impedance of air does not correspond to the corresponding impedance of the dielectric material. The same happens at the joint boundary of the two dielectrics I and II if both differ in their characteristic impedance. Reflections will also occur at this interface. The reflected wave interferes in dielectric I with the propagating wave and forms a standing wave field with maximal and minimal values, which will cause an uneven temperature distribution. In general, a change of the material's property constants goes along with a temperature rise so that no

disadvantageous temperature distribution occurs; instead, the maximum and minimum values become blurred.

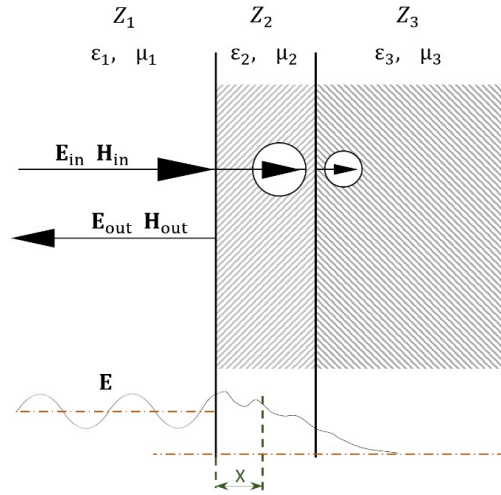


Figure 3.5: The propagation of an electromagnetic wave in a multi-layered dielectric

### 3.2.6 Energy in electromagnetic waves

Metaxas and Meredith (1983) provided an in-depth analysis of the energy that electromagnetic waves carry; this is considered one of the most crucial aspects of electromagnetic waves. By definition, energy is transported through space by electromagnetic waves. The power flow through a closed surface can be quantified by the power density that is generated by the applied electric and magnetic fields. Although the determination of the electric field inside a material can be quite difficult, it can be approximated by assuming that it is constant in the area under consideration. Thus, the rate at which heat is absorbed in the dielectric material can be expressed as power density, which is given in equation (3.30),

$$P_d = 2\pi f \epsilon_0 \epsilon'' E_{\text{rms}}^2 \quad (3.30)$$

where  $P_d$  is the power density in ( $\text{W}/\text{m}^3$ ),  $f$  is the frequency in (Hz),  $E_{\text{rms}}^2$  is the root mean square value of the electric field inside the material,  $\epsilon_0$  is the permittivity of free space, and  $\epsilon''$  is the dielectric loss factor. According to equation (3.30), the power density is in direct relation to the electric field; it increases with the square of the electric field's strength. This means that if the electric field's strength is doubled, then four times ( $4\times$ ) more power density is achieved. For example, if a 6 kW microwave can induce  $1 \times 10^9 \text{ W}/\text{m}^3$ , then a 12 kW microwave will induce  $4 \times 10^9 \text{ W}/\text{m}^3$ . In conclusion, it can be inferred that very high power densities can be generated by increasing microwave power.

### 3.2.7 Coupling of electromagnetics theory and heat transfer in materials

The first law of thermodynamics implies that the power that is dissipated and absorbed within a material with a specific mass causes an increase in the temperature of that material to temperature  $T$  (°C) after  $t$  seconds from an initial temperature of  $T_0$  (°C) at an initial time of  $t_0$  (s). The heat rate is then equal to  $\Delta T/\Delta t$  (Meredith, 1998), and the dissipated power can be calculated by using the following formula,

$$P_d = m \cdot C_p \left( \frac{\Delta T}{\Delta t} \right) \quad (3.31)$$

where  $P$  is the dissipated power in (W),  $m$  is the mass of the material in (kg), and  $C_p$  is the specific heat capacity of the material in (J/kg°C). By combining equations (30) and (31), the temperature increase in a material by microwave can be expressed as,

$$\frac{dT}{dt} = \frac{2\pi f \epsilon_0 \epsilon'' E_{rms}^2}{m \cdot C_p} \quad (3.32)$$

From equation (3.32), it can be seen that the increase in temperature of a material during microwave-assisted heating depends on the material's dielectric properties, which often vary with the temperature. Furthermore, it is more convenient to use an average power density value for any analysis of the results evaluating the microwave efficiency.

### 3.3 Influencing parameters in rock heating and pre-conditioning by microwaves

The way a rock sample is heated and pre-conditioned by microwaves depends on the rock's electrical and thermal properties, mineralogical and physical characteristics (i.e. rock composition, size, and shape), and the nature of the microwave used (Xu, 2015). Since rocks are composed of various minerals with different material properties, including electrical, thermal, and physical properties, they behave differently when exposed to electromagnetic waves (microwaves), because some minerals absorb, some reflect, and some transmit the waves. Those minerals that absorb the microwave energy emitted into the mineral transform that energy into heat. Those that transmit the waves and are in the vicinity of others that absorb them are heated by heat (or thermal) conduction. For instance, when the combination of calcite and pyrite is exposed to the microwave field, the pyrite absorbs the energy and heats, while the calcite transmits the energy and will not heat up



until the conduction of heat from one to the other heats both minerals. Because of the fact that rocks expand when they heat, there will be fractures produced along the grain boundaries of the minerals forming the rock; as the two minerals expand at different rates because of the differential heating. This process of reducing rocks' strength and producing fractures (i.e. macro and micro cracks) inside a rock composed of different minerals is called rock pre-conditioning. Because of the fractures along the grains, the energy required to break the pre-conditioned rock, crush the ore, and liberate the mineral grains will be reduced. Another factor that can affect the process of microwave-assisted heating and pre-conditioning of rocks is the state of the rock (in dried or moisture state) when pre-conditioned by microwaves. This is because water is very high-loss substance; and therefore, the existence of water in a rock/ore sample increases permittivity and makes the ore heat better. Thus, a little absorbed water in the rock/ore sample causes the rock/ore to undergo bulk cracking because the water vapor tries to escape from the sample (Motlagh, 2015; Peinsitt et al., 2010). Hence, the amount of pre-conditioning has a direct relationship with the amount of dielectric heating; and therefore, it is very important to identify all determining factors, i.e. electrical and thermal properties, in the process.

### **3.3.1 Electrical and thermal properties of rocks**

#### **3.3.1.1 Factors affecting rocks' dielectric properties**

Among different factors that can affect dielectric properties of rocks, frequency and temperature are the most important. Because water has a high dielectric constant value (78.2 at room temperature), the moisture content of rocks is considered a less important contributing factor. Below, the frequency and temperature dependency of rocks' dielectric properties and their variations are explained separately in the two subsequent parts.

##### ***-Frequency dependency of rocks' dielectric properties***

One of the most important factors that influences rocks' dielectric properties is frequency. The permittivity of rock varies in strength with the frequency of an alternating electric field (Balanis, 1999). This is because of the ability of the atoms, ions, and dipoles to align and realign with the alternating electric field. Figure 3.6 presents the behavior of permittivity in the vicinity of resonance frequency  $\omega_0$ ; it shows the response of  $\epsilon'$  and  $\epsilon''$  near a resonance frequency. In this figure, the contribution of higher resonance to  $\epsilon'$  at the present frequency range is shown by A, whereas the contribution of the present resonance to lower frequencies is shown by  $2B/\omega_0$ . It can

be seen that  $\epsilon''$  obtains a maximum value around the resonance. It is therefore these frequencies that are coupled most in the rock with the electromagnetic waves and produce the most heat. Usually, the imaginary term of permittivity (the dielectric loss factor) is small; yet when the system approaches resonance, the dielectric loss factor assumes its maximum value.

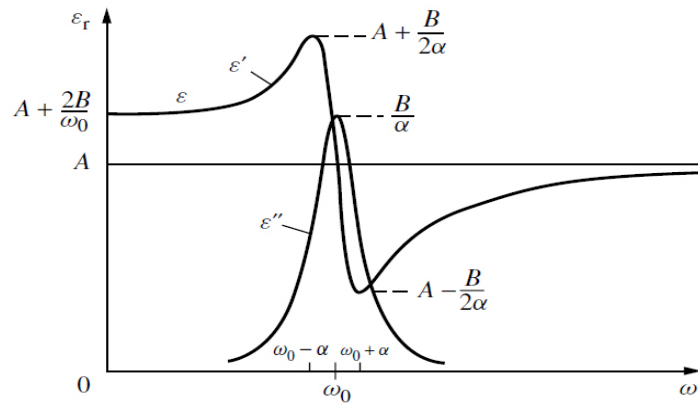


Figure 3.6: The response of permittivity due to electronic or atomic polarization (Figure modified from the plot given by [(Chen et al., 2004)])

Figure 3.7 demonstrates a typical behavior of both dielectric constant,  $\epsilon'$ , and loss factor,  $\epsilon''$ , as a function of frequency. According to this figure, the permittivity of a material is related to different physical phenomena (i.e. ionic conduction, atomic polarization, and dipolar relaxation).

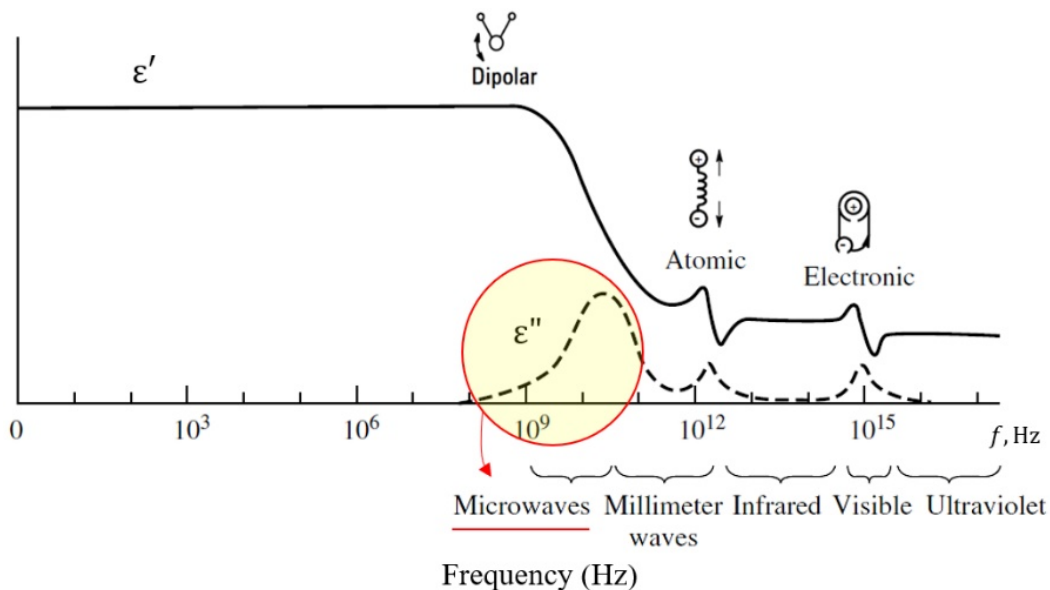


Figure 3.7: Response of  $\epsilon'$  and  $\epsilon''$  for all frequencies of the electromagnetic spectrum for a hypothetical dielectric (Figure modified from the plot given by Ramo et al. [Ramo et al., 1994])

Figure 3.7 shows that the material's permittivity is more or less constant for low frequencies. In general, it might be sufficient to measure the permittivity of a rock sample at a single frequency in the regime of interest and that will give a fairly good overview of the permittivity; but, nevertheless, this value may not be a good representation for all 0.4-40 GHz frequencies. Therefore, for high frequency applications, the dielectric permittivity values (both constant and loss factor) should be measured for different frequencies (Ramo et al., 1994). As can be seen in Figure 3.7, there are three main areas of resonance caused by the electronic, atomic, and dipolar polarizations. These three different polarization mechanisms are located at the microwave, millimeter waves, infrared, visible, and ultraviolet frequencies. This plot can be applied to most materials (Chen et al., 2004). Moreover, as shown by the red circle, there is a high resonance peak of value  $\epsilon''$  around the area of microwave frequencies. This clearly explains why microwaves are so useful for heating of rocks.

Like permittivity of materials, permeability is a property that depends on the material's atomic dipoles (Arfken et al., 2013). The main difference between the permittivity and permeability of rocks is that the permeability of a rock is highly dependent on frequency in such a way that the permeability value may vary strongly with different frequencies (Chen et al., 2004). Thus, it is impossible in general to use constant approximation for permeability, but this is not the case for the permittivity of rocks. Figure 3.8 shows a graphical description of permeability as a function of frequency presented by Chen et al. (2004).

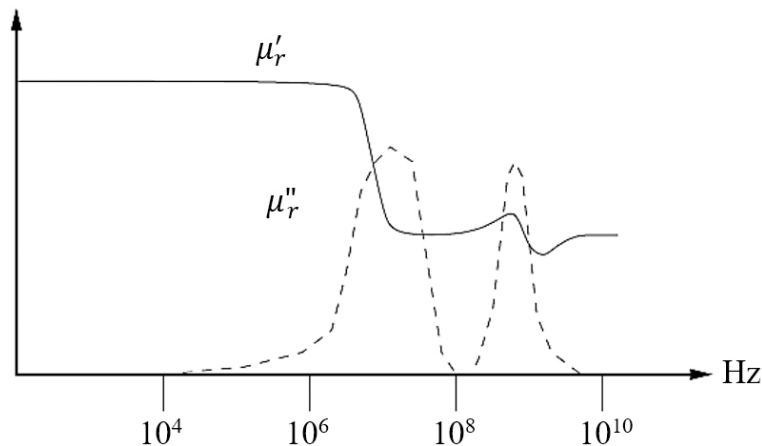


Figure 3.8: Graphical description of permeability as a function of frequency presented by Chen et al. (2004)

### ***-Temperature dependency of rocks' dielectric properties***

The dielectric loss factor of rocks determines the part of the applied microwave energy that is lost in the material and transferred to heat. Both dielectric constant and loss factor of rocks are temperature dependent. This temperature dependence is a function of the dielectric relaxation processes operating under particular conditions and the specific frequency applied. Generally, dielectric relaxation can be defined as the time taken for dipoles to return to a random orientation when the electric field is removed (Pozar, 2012). By increasing the temperature, the relaxation time decreases, but the dielectric constant of rock increases.

In conclusion, since both frequency and temperature dependency of dielectric properties of most rocks is very complex to determine, it is almost always recommended to measure rocks' dielectric properties at the frequencies and conditions desired.

#### **3.3.1.2 Factors affecting rocks' electrical conductivity and resistivity**

To understand how and why electrical conductivity or resistivity of rocks differs from one type to another, the following factors should be considered<sup>4</sup>:

- 1. Rock Porosity, Pore Saturation, and Pore Fluid:** Most of rocks are made up of pore spaces, which are partially saturated with ionic fluids such as fresh water, brackish water, ocean water etc. Therefore, electrical currents generally prefer to flow through the pore spaces of rocks because pore fluids have a higher conductivity than most rock-forming minerals. As a result, the bulk conductivity of the rock depends mainly on the rock's porosity, fluid saturation, and type of fluid contained within the pore spaces. On the other hand, there are some rocks that are unsaturated (usually referred to dry rocks) in which the pore spaces are occupied solely by air. In this case, because the air is highly resistive, it forces the electrical currents to flow through the minerals comprising the rock. Consequently, unsaturated rocks are considered to be poorly conductive.
- 2. Rock Tortuosity:** The connectivity and complexity of a rock's network of pore spaces are defined as the rock's tortuosity. For rocks with low tortuosity values, the electrical current's path within and through the pore spaces is simple, creating an efficient conduction of electrical charges. On the other hand, in rocks with high tortuosity values, the electrical

---

<sup>4</sup> Discussions of this section about factors affecting rocks' electrical conductivity and resistivity are adapted from "Geophysics for the mineral exploration geoscientist", (Dentith & Mudge, 2014)

current flows through the rock in an indirect path. Thus, the rock is more resistive because conduction is inefficient.

- 3. Mineralization:** If the minerals forming a rock are more conductive, electrical currents within the rock tend not to flow through the rock's pore spaces. This phenomenon occurs most frequently in ore-bearing rocks, including magnetite, ilmenite, specular hematite, because of the presence of metal oxides, metal-sulphides (e.g. pyrite, pyrrhotite, galena), and metals (e.g. gold, silver, copper). One exception is graphite, which is very conductive. As expected, the conductivity increases as the concentration of conductive minerals within the rock increases.

A chart showing the range of electrical conductivity/resistivity values for common rock types is shown in Figure 3.9. It should be noted that the scale of the chart is logarithmic, which indicates a huge amount of variability in conductivity/resistivity among different rocks.

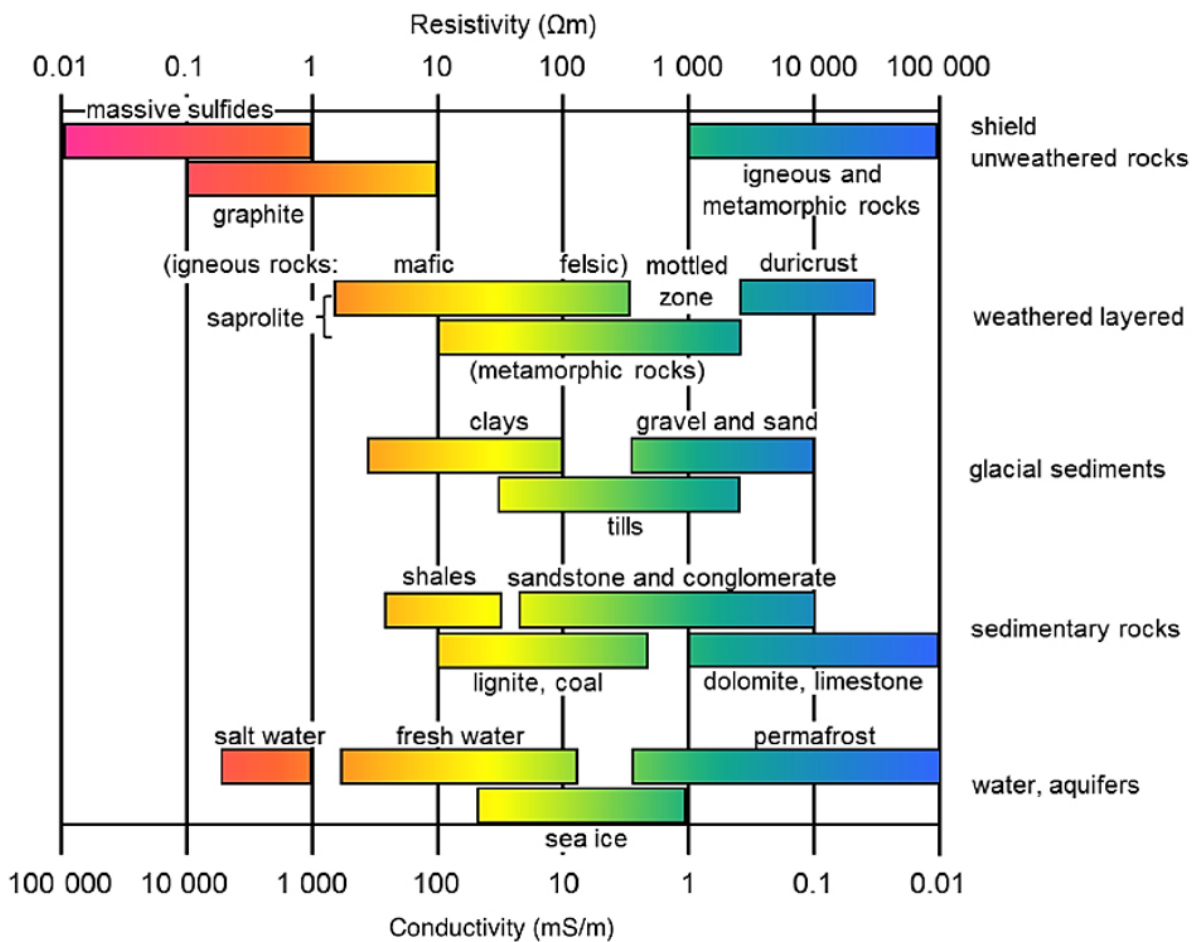


Figure 3.9: Common values of conductivity/resistivity for various materials and rock types (Figure adapted from [Palacky, 1988])

From the chart given in Figure 3.9, it can be inferred that:

- Massive sulphide and graphite-bearing rocks are by far the most conductive,
- Carbonate rocks and unconsolidated sediments are high resistive rocks,
- Weathered igneous and metamorphic rocks are more conductive than untethered igneous and metamorphic rocks,
- Sedimentary rocks containing clays are generally more conductive than other rock types.

### 3.3.1.3 Variations of rocks' thermal conductivity and specific heat capacity

Once the heat is dissipated in a rock sample because of the applied microwave and its dielectric heating effect, the atomic lattices and structures interact in such a way that this heat is dispersed throughout the rock. Therefore, the study of these processes and the mechanisms involved in the microwave-assisted heating of rocks is crucial.

When there is a temperature difference (which is called temperature gradient) within a rock, there is an energy transfer from the high-temperature regions to the low-temperature regions according to the second law of thermodynamics. The heat is then transferred through the rock sample by a process called conduction. This conduction of heat is governed by Fourier's law and can be stated as

$$q = -kA\nabla T \quad (3.33)$$

where  $q$  is the heat transfer rate (local heat flux density),  $A$  is the cross-sectional area, and  $T$  is the temperature distribution in ( $^{\circ}\text{C}$ ) (Incropera et al., 2007). The constant of proportionality,  $k > 0$ , is the thermal conductivity (W/mK) of the rock. Thermal conductivity is one of the key thermophysical properties of rocks (Abdulagatov et al., 2006). Several studies have been conducted to measure the conductivity of various rock types and rock-forming minerals at high temperatures and confirmed that the conductivity is a temperature-dependent property, especially at high temperatures (Abdulagatova et al., 2009; Čermák & Rybach, 1982; P. Hartlieb et al., 2016; Seipold, 1990; Vosteen & Schellschmidt, 2003).

A more complicated system involves the temperature of the rock sample changing with time and heat sources, as depicted in Figure 3.10.

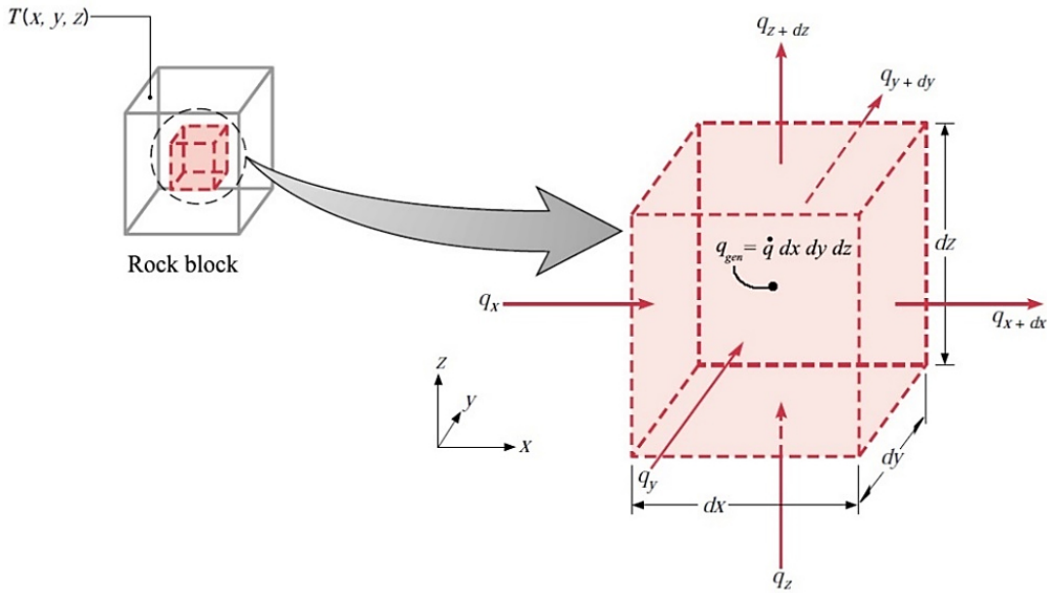


Figure 3.10: Heat transfers in and out of a rock's surface with heat generation in the rock block

As shown in Figure 3.10, infinitesimal heat transfers in and out of the rock through the three orthogonal axes ( $x, y, z$ ) and heat generation,  $\dot{q}$ , occurs within the rock. Hence, by using conversion of energy, the governing heat transfer phenomenon can be expressed as a three-dimensional heat conduction equation:

$$\frac{\partial}{\partial x} \left( k \frac{\partial T}{\partial x} \right) + \frac{\partial}{\partial y} \left( k \frac{\partial T}{\partial y} \right) + \frac{\partial}{\partial z} \left( k \frac{\partial T}{\partial z} \right) + \dot{q} = \rho C_p \frac{\partial T}{\partial t} \quad (3.34)$$

where  $\rho$  is the density and  $C_p$  is the specific heat capacity of the rock. In most cases, the thermal conductivity,  $k$ , can be assumed to be constant; and therefore equation (3.34) changes to equation (3.35) as

$$\nabla^2 T + \frac{\dot{q}}{k} = \frac{1}{\alpha} \frac{\partial T}{\partial t} \quad (3.35)$$

where  $\alpha (= k/\rho C_p)$  denotes the thermal diffusivity of the material with an SI unit of ( $m^2/s$ ). By definition, thermal diffusivity is the rate of transfer of heat in a material from the hot side to the cold side. Equation (3.35) reveals that its solution is highly dependent on parameter  $\alpha$ ; the larger the value of  $\alpha$ , the quicker heat diffuses through the rock. However, since  $\alpha$  depends on both thermal conductivity,  $k$ , and the specific heat capacity,  $C_p$ , of the rock, any variation of these two parameters directly affects  $\alpha$  and, thereby, influences the overall rock-heating process. It can be inferred from the literature that metamorphic rocks possess high thermal conductivities, ore minerals have extremely high values of thermal conductivity, and the group of mica, mepheline, and polyhalite possess low values of thermal conductivity (Schön, 2015).

### **3.3.2 Mineralogy and physio-mechanical characteristics of rocks**

The effects of the structure (size, shape, and distribution of the pores) and mineralogical compositions on the rock heating and pre-conditioning by microwaves have been studied by several researchers. Since rocks are composed of different minerals with different textures, material properties, and responses to microwave irradiation and heat generation, it is very important to take into account the effect of the material property variations in the constituent minerals, i.e. electrical and thermal property variations, when the rock is going to be exposed to microwave irradiation. It is very important to notice that a homogeneous rock is heated more uniformly than a nonhomogeneous (heterogeneous) rock when exposed to microwaves. This is due mainly to the variation in the material properties of the nonhomogeneous rock. For example, by comparing basalt, which is a fine-grained rock that can be assumed to be homogeneous, and granite, which is a coarse-grained rock and assumed to be heterogeneous, under the same microwave irradiation, basalt heats more uniformly than granite. Moreover, the shape, size, and distribution of pores in a rock sample affects the overall temperature of the rock after microwave treatments. Natural rocks have various porosity (hard igneous rocks have 0.5-1% porosity) according to their texture and mineralogy and, therefore, respond differently when treated by microwaves (Nasseri et al., 2009).

### **3.3.3 Microwave system characteristics**

One of the major factors in rock heating and pre-conditioning by microwaves is the type of microwave systems (the applicator) used to treat a rock sample. Typically, there are two types of microwave system applicators: single-mode and multi-mode. Mode is defined as the pattern of distribution of the electric and magnetic field components of an electromagnetic wave excited in a closed cavity (Bradshaw et al., 2004). These two types of microwave applicators are systematically different in inducing microwave energy into the rock under treatment. The details of the multi-mode and single-mode microwaves with the differences of their systematic heating mechanisms are explained in the following two sections.



### 3.3.3.1 Multi-mode microwave cavities with stirrer fans

In the case of microwave-assisted heating, a multi-mode microwave cavity can be used. Multi-mode microwave cavities are designed to deliberately spread their electromagnetic energy uniformly across the cavity. They do not have a single standing wave and therefore achieve a thermal heating effect evenly in a rock under treatment (Kingman, 2009). These multi-mode cavities are very useful for processing a wide range of workloads, in both size and electrical properties (Meredith, 1998). A schematic illustration of an industrial multi-mode microwave is given in Figure 3.11.

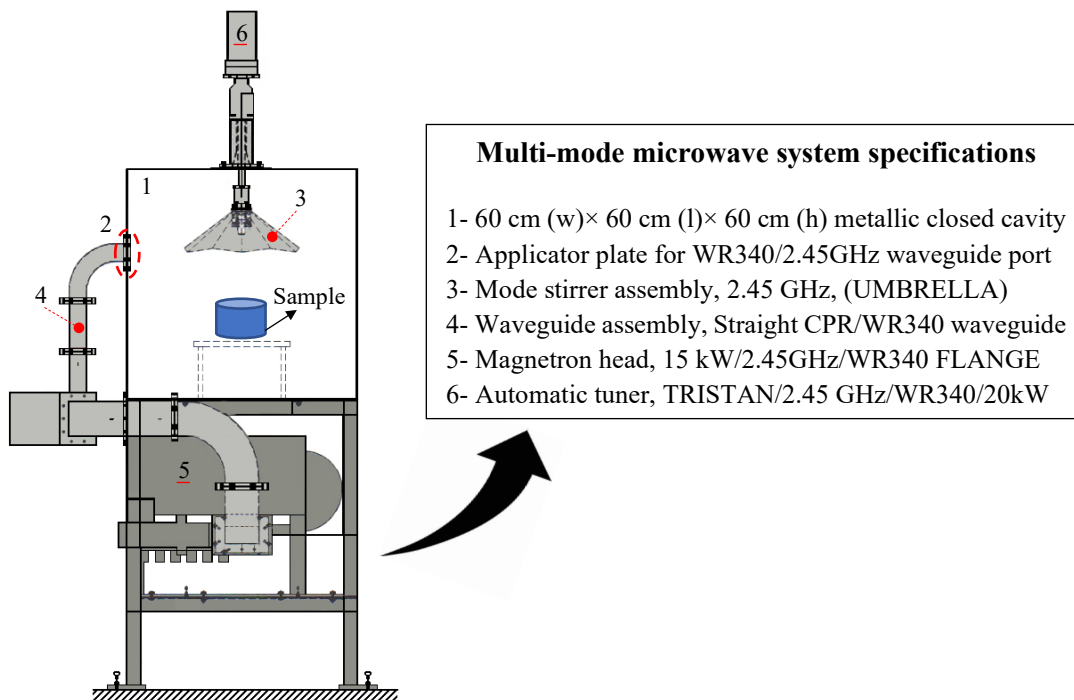


Figure 3.11: Detailed overview of a multi-mode microwave cavity system and its components

As shown in Figure 3.11, a multi-mode microwave system contains a metallic cavity into which a rock sample is placed, a waveguide that directs the generated electromagnetic waves into the cavity, and a mode stirrer (which is called a stirrer fan in the present thesis) that propagates the incoming waves for maximum mixture of the waves inside the cavity. The stirrer fan is usually a metallic blade rotating inside the cavity in order to perturb the electromagnetic field distribution. Since the blades are continuously rotating inside the cavity, the incident energy is constantly reflected, causing the field distribution to change continuously and, on average, become closer to uniformity. The mechanism of rock heating by a multi-mode microwave system is as follows. The

electromagnetic energy (microwaves) is first generated by the magnetrons and the waves are then transmitted from the magnetrons to the multi-mode cavity by waveguides. Waveguides are long, hollow rods, made of dielectric material (e.g. aluminum) to reflect all the waves inside the cavity, thus guiding them towards their destination (i.e. the rock for heating and pre-conditioning). The cavity has a small aperture (commonly called a port) where the waveguide deposits the electromagnetic waves into the multi-mode cavity. Several studies have conducted research trials (both experimentally and numerically) on the effectiveness of multi-mode cavities for heating and pre-conditioning of various rocks and minerals (Kingman, 2009). According to the results of these studies, multi-mode microwaves are very useful because they support such a large number of resonant modes that superpose to create high electric fields permeating the cavity. Each mode resonates when the length of the cavity is a multiple of  $\lambda/2$ , where  $\lambda$  is the wavelength of the electromagnetic wave. A single mode leads to a sinusoidal electric field distribution inside the cavity, leaving many nodes (areas where the electric field is zero). This leads to non-uniform heating and further complicates predicting heat input. It is precisely for this reason that multi-mode cavities are used to excite many modes, enabling a more homogeneous electric field distribution and more uniform and volumetric heating.

### **3.3.3.2 Single-mode microwave cavities with horn antennas**

In the application of microwaves for heating and pre-conditioning of rocks, there are times when high electric field strengths are required. Therefore, a single standing wave can be used in a system that is called a single-mode microwave. This single standing wave then has maximum and minimum power density that depends mainly on the position of the sample in the cavity. As for the multi-mode microwave system, a single mode microwave system contains a metallic cavity in which the rock sample is placed and a waveguide that directs the generated electromagnetic waves from the magnetron into the cavity. However, the only difference between this system and the preceding one, multi-mode microwave system, is that there is no rotating stirrer fan in the single-mode microwave system; but instead, there is a horn antenna that is installed on the port just after the end of the waveguide in order to direct the standing electromagnetic waves into the microwave cavity. As shown in Figure 3.12, these standing waves directly touch the surface of the rock sample inside the cavity and, therefore, cause heating and pre-conditioning to start from the surface and move downwards into the rock. By comparison, it can be inferred that the multimode microwave

system has a volumetric heating and pre-conditioning effect, whereas the single-mode microwave affects the surface of the rock.

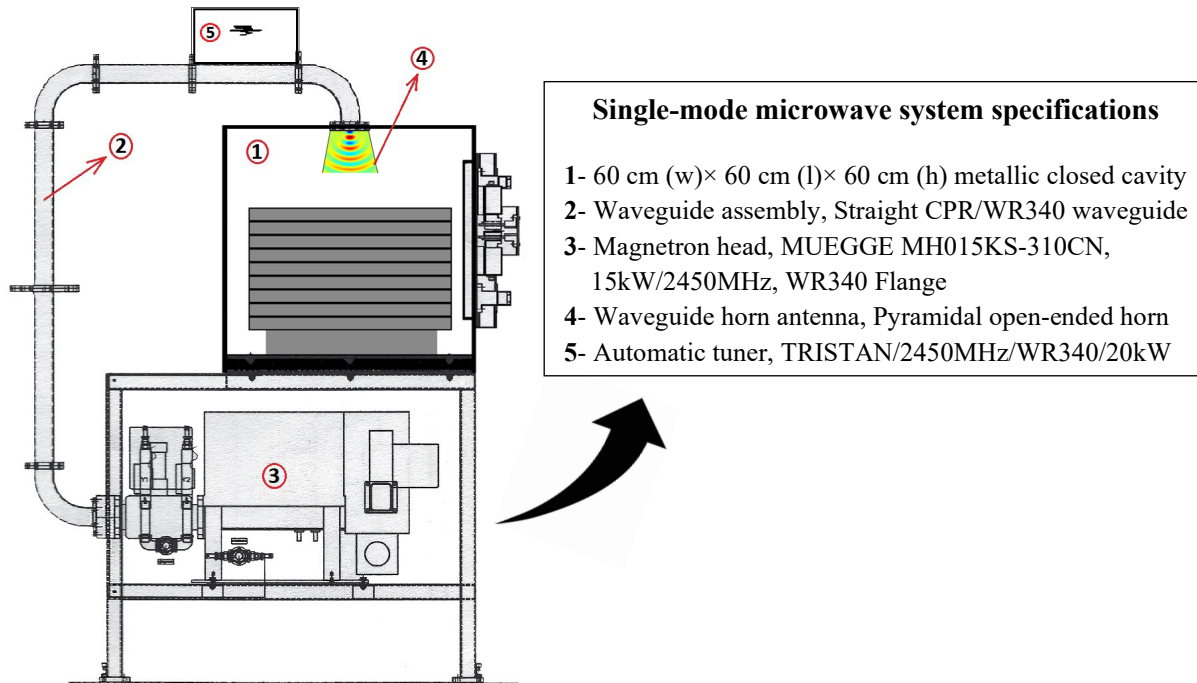


Figure 3.12: Detailed overview of a single-mode microwave cavity system and its components

### 3.4 Summary and conclusions

In this chapter, a theoretical foundation and fundamental principles of microwaves for heating of rocks have been introduced. All the parameters that are involved in a microwave-assisted rock heating process are introduced and discussed. Moreover, the chapter introduces all the influencing parameters in the microwave-assisted rock heating from both the theoretical and experimental aspects. In conclusion, it can be seen that the process of heating rocks by microwaves depends on several parameters. The nature of the rock being irradiated strongly influences the effect of microwave treatment on its heating and subsequent pre-conditioning. Therefore, in order to conduct an efficient microwave-assisted rock heating and pre-conditioning experiment, it is necessary first to recognize all the factors involved in the process and to design the various factors of the microwave system appropriately. The influencing factors (e.g. material properties) need to be accurately analyzed in terms of the microwave system's parameters (power, time, etc.) in order to arrive at an efficient design.

## Chapter 4

# Rock-microwave system characterization methods and procedures

### Contents

---

4.1 Rock samples utilized .....	78
4.2 Measurement methods for rocks' material properties .....	80
4.3 Instrumental methods utilized .....	91

---

### Preface

*This chapter introduces and presents all the methods employed in the present thesis for the measurement of rocks' electrical and thermal properties and the instrumental methods applied for characterization of the selected rocks after microwave treatment tests with different experimental conditions, in the following order. The selection of the rock samples and their descriptions, including rocks' technical info (i.e. material properties, compositions, morphological details, and textural appearance) are first justified (section 4.1). Then the chapter introduces all of the common methods for measurement of rocks' electrical and thermal properties, including dielectric constant, loss factor, electrical conductivity, thermal conductivity, thermal resistivity, thermal diffusivity, and specific heat capacity; and it, additionally, presents tables of measured corresponding data for each specific property introduced (section 4.2). Finally, the chapter ends by introducing the different instrumental methods utilized for thermo-physical and morphological characterization of the microwave-treated rock samples (section 4.3). The measured emissivity values of the selected rock types are also given this last section.*

## 4.1 Rock samples utilized

In nature, there exist various types of rocks with different textures and morphologies. Each rock type consists of different minerals and compositions, which make it behave differently when compared to other rock types or even other samples within the same type. In general, rocks are classified into three main classes (Kahraman & Gunaydin, 2009): sedimentary (e.g. sandstone and limestone), metamorphic (e.g. gneiss and schist), and igneous (basalt, granite, and kimberlite) (Mitchell, 2013). To study the effects of microwave irradiation on natural rocks—especially harder and more abrasive rocks—various types of rocks are needed to conduct an appropriate and reliable comparative study. Therefore, in the present thesis, four different rock types, i.e. basalt, granite, and two different kimberlites #1 and #2, were chosen. The details of these rocks, including their origin (location and country), and some of their physical characteristics are given in Table 4.1.

Table 4.1: Details of the selected rock types in the present study and their characteristics

Rock sample	Location	Country	Density (kg/m <sup>3</sup> )	Type	Grain size	Uniformity	Homogeneity
<b>Basalt</b>	Chifeng, (Inner Mongolia)	China	2800-2900	Igneous	Fine	Yes	Yes
<b>Granite</b>	Northwest Territories	Canada	2600-2700	Igneous	Coarse	Yes	Yes
<b>Kimberlite #1</b>	Victor mine	Canada	2300-2400	Igneous	Medium	Yes	Yes
<b>Kimberlite #2</b>	Gahcho Kué mine	Canada	2400-2500	Igneous	Medium	Yes	Yes

Among the rocks listed in Table 4.1, granite and two types of kimberlite, kimberlite #1 and #2, were received from active mines either as cores or as boulders extracted by drill and blasting methods. The basalt rock was already available in the Geomechanics lab at McGill University in the form of intact blocks cut from quarries located in Chifeng, China. Where needed, the intact blocks of basalt were drilled to obtain cylindrical core samples or rectangular slab-shaped specimens. The blocks and/or boulders were cored by using a radial drilling machine. The cored samples, which were either received directly from the mine sites as cores or drilled by the drill machine in the lab, were cut precisely into several same-size cylinders (with the same shapes) for the microwave irradiation tests of the present research. This process of cutting the samples to prepare them in an appropriate shape and dimensions was done by using a 4-inch wet diamond

saw according to standard procedures. Since the geometry of the samples, such as their shapes, sizes, and dimensions, might have an impact on the results of microwave heating and pre-conditioning experiments, the core samples were prepared and cut into two different sizes: UCS size and BTS size. The UCS-sized samples were prepared in a cylindrical shape respecting a height to diameter ratio of 2:1, and the BTS-sized samples were prepared in a disc shape (small cylinders) respecting the rule of  $0.5D < L < D$  (see Figure 4.1(a)). According to the standards of ISRM suggested techniques (1978, 1979) and ASTM, the cylinder ends were cut and polished (Ulusay, 2015). Both ends of the samples were exactly flattened by using a diamond wheel grinder machine. All these processes were done to have sets of the same-dimension samples for microwave irradiation tests to be repeated three times for each experimental condition.

Aside from the cylindrical samples that were mainly prepared for multi-mode microwave irradiation tests, a set of rectangular slab-shaped basalt specimens was prepared for exposure to microwave irradiation from a pyramidal open-ended horn antenna (single-mode microwave apparatus) to simulate the conditions of single-mode microwave treatments (e.g. at the tunnel face). These specimens were cut into 40 cm (l) × 40 cm (w) × 2 cm (h) and then stacked on top of each other to simulate a rock mass. The goal of testing these specimens was to determine the amount of rock pre-conditioning by single-mode microwave treatments with different operating parameters and, especially, at various distances of the top surface of the rock from the horn antenna. Figure 4.1(b) depicts the single-mode microwave system with the stacked basalt slabs.

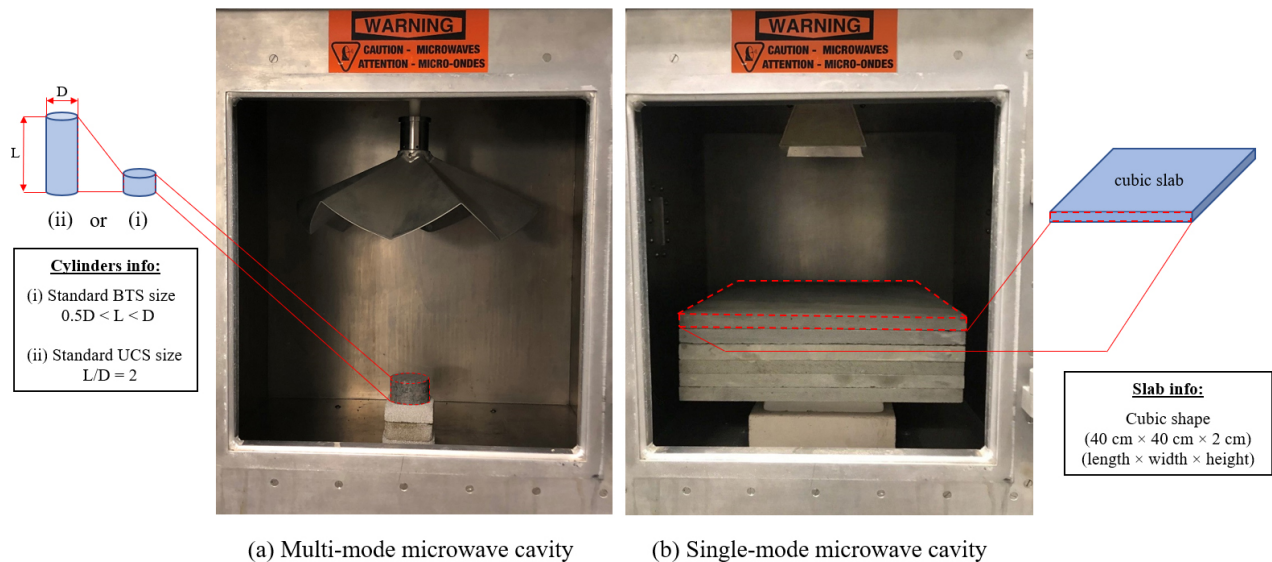


Figure 4.1: Schematic illustration of the placement of (a) a cylindrical sample of UCS or BTS size in the multi-mode microwave and (b) stacked basalt specimens inside the single-mode microwave

## 4.2 Measurement methods for rocks' material properties

### 4.2.1 Measurement methods of dielectric properties

Today, there are five common methods for measuring the dielectric properties of materials (e.g. rocks); they are shown in Figure 4.2 with respect to a range of frequencies and material loss.

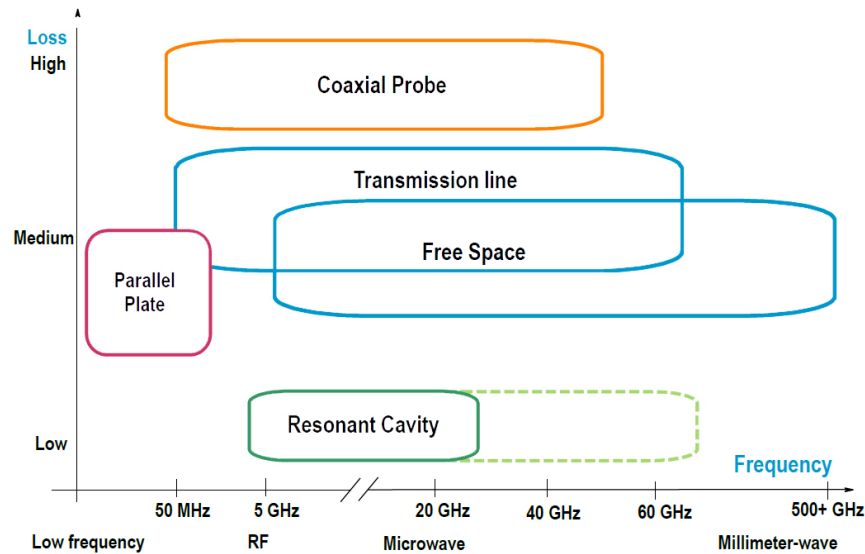


Figure 4.2: Illustration of different dielectric property measurement methods specific to a range of frequencies and the material's complex permittivity (material loss) (Figure modified from [Begley, 2010])

Although the aim of employing all of the presented methods in Figure 4.2 is to measure a material's dielectric properties, the choice of the best among the five different techniques depends on the following factors: frequency of interest, expected value of relative permittivity, required measurement accuracy, material properties (i.e. homogeneous, isotropic), form of material (e.g. liquid, powder, solid), size restrictions, and temperature. Therefore, it is very important to account for these factors and then decide upon which dielectric property measurement method will be chosen. In the following sections, all of the five methods are introduced and explained and a comparative analysis between them specific to the rock samples of the present study is given at the last section (see section 4.2.1.6).

#### 4.2.1.1 Coaxial probe method

Coaxial probe method is one of the most typical methods for the measurement of the dielectric properties of rocks—from medium to high loss rocks—at the microwave frequency

range. Although this method of measuring the rocks' dielectric properties gives very accurate results, it is important to use a specially designed low thermal expansion probe for high-temperature applications (Andrade et al., 1992). In order to employ this method, the following material assumptions have to be applied: no air gaps or bubbles, homogeneous, non-magnetic, isotropic, and effectively infinite thickness. Moreover, since electromagnetic energy is transmitted and arced within the sample during the test, the smoothness of the sample's surface highly influences the accuracy of the measurement; and therefore, it is important to minimize the air gaps between the coaxial probe and the sample's surface (Agilent, 2006). As a result, all measurements of dielectric properties of selected rock types by the method of coaxial probe in the present thesis were performed in such a way that one end of the rock samples was polished to an accuracy of 5-10  $\mu\text{m}$  of surface roughness before testing. In addition, on the basis of past experience with this method of measuring dielectric properties, the rock sample must be at least 1.5 times thicker than the diameter of the probe. A typical system of dielectric properties measurement by the method of coaxial probe consists of a network analyzer, a dielectric (coaxial) probe, and an external computer for data acquisition, as shown in Figure 4.3. The coaxial probe can measure the dielectric properties of materials over a wide range of frequencies from 500 MHz to 120 GHz (Brodie et al., 2016).

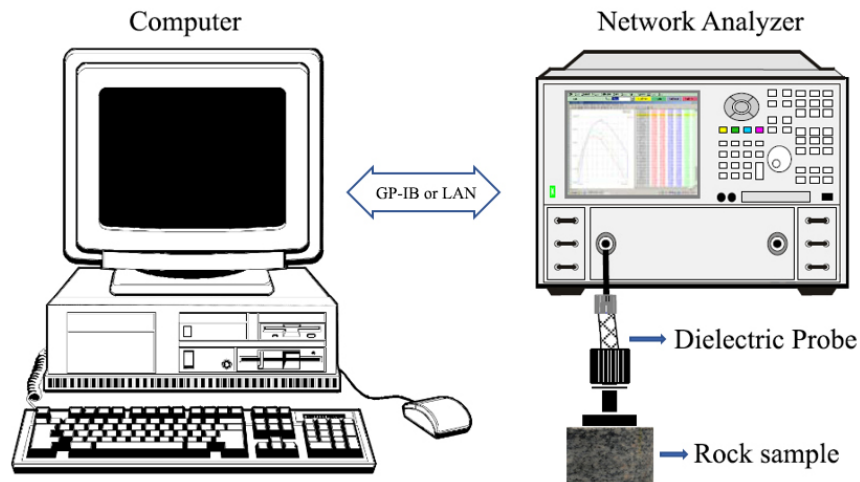


Figure 4.3: Conceptual illustration of the coaxial probe method for measurement of a rock sample's dielectric properties

The process of measuring a rock's dielectric properties by coaxial probe is as follows. First, the dielectric probe is firmly pressed to the smooth, flattened surface of the rock sample. Then, the dielectric properties of the rock can be measured by sending a signal from the probe to the rock



and analyzing the reflected signal (phase and amplitude). In this study, the frequency range on the network analyzer was set to measure the real and imaginary parts of the rock permittivity, dielectric constant ( $\epsilon'$ ) and loss factor ( $\epsilon''$ ), between 500 MHz and 12 GHz frequencies. Moreover, multiple dielectric property measurements were recorded for each rock type from different locations at a constant ambient temperature of 20 °C and the mean values are calculated and reported.

#### 4.2.1.2 Resonant cavity (cavity perturbation) method

Among different methods of measuring dielectric properties, the resonant cavity (cavity perturbation) method is considered one of the best methods to measure the complex permittivity of low-loss materials, hard rocks in particular (Sheen, 2005; Ulaby et al., 1990). In this method, the cavity is designed according to the wavelength of a specific frequency. Moreover, a rock specimen needs to be prepared as small, thin, and rod-shaped in order to be inserted into an empty cavity called the resonant cavity, as shown in Figure 4.4.

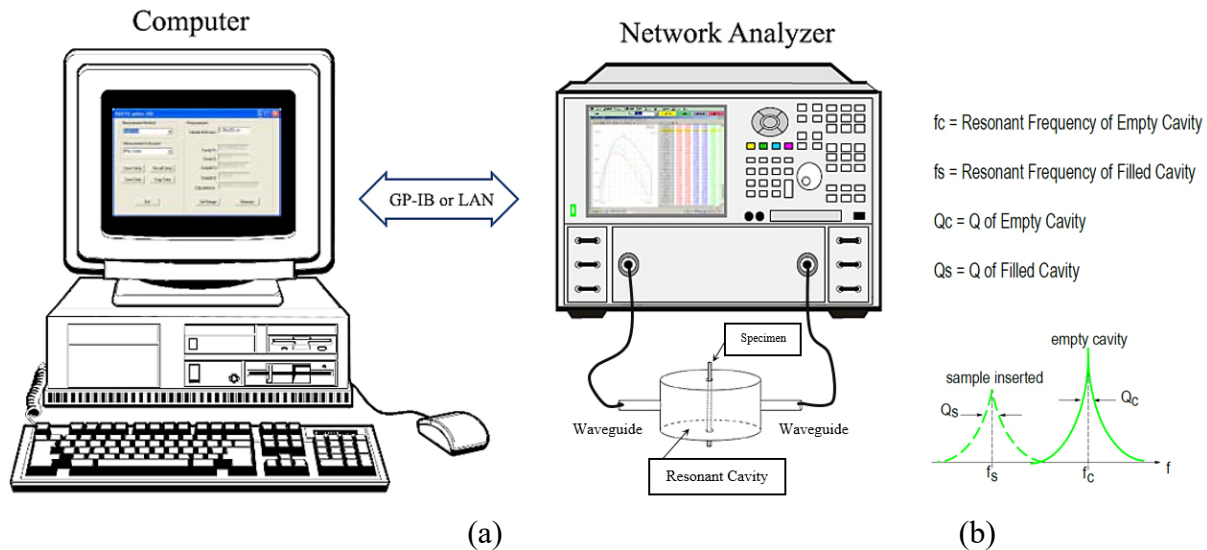


Figure 4.4: Conceptual illustration of a network analyzer connected to a resonant cavity where (a) shows the position of the specimen in the empty cavity, and (b) shows the perturbation frequency shifting from cavity ( $f_c$ ) to specimen ( $f_s$ ) when the specimen is inserted into the resonant cavity (Note that  $Q_c$  and  $Q_s$  are the quality factors of the empty cavity and the filled cavity.)

The mechanism of measuring the specimen's dielectric properties by the method of resonant cavity is as follows. When electromagnetic waves are passed from the data analyzer into the resonant cavity, a peak is observed at the exact frequency of the empty cavity (see Figure 4.4(b)). Immediately after placement of the specimen in the cavity, the resonance of the cavity changes, as

the impurity of the empty cavity has changed. As a result of this change in the cavity's resonance, the peak of the graph shifts to another phase, which indicates another frequency. Consequently, by calculating the changes in the cavity resonance and frequency, the dielectric properties of the specimen can be obtained. However, it is extremely important to know the exact volumes of the empty cavity and of the specimen because their physical dimensions influence the final result. To measure dielectric properties of the same specimen at another specific frequency, other cavities must be designed and built according to the specific frequency needed. Thus, it can be concluded that the resonant cavity method (1) is good for a single frequency, (2) has high accuracy, and (3) is best for low-loss or very thin specimens.

### 4.2.1.3 Parallel plate method

The parallel plate method is one of the most widely used methods in measurement of the dielectric properties of solid materials or liquids. In this method, a very thin disc-shaped specimen has to be prepared and inserted between two plates that are connected to a data analyzer. The dielectric properties of the specimen can then be calculated by knowing the default parameters of the aperture—which simulates the functionality of a capacitor filled with the specimen—and transmitting the electromagnetic energy. This method of dielectric property measurement is an appropriate method for low frequencies and best for thin flat sheets (Agilent, 2006). The system used in this method is also suitable to study the effect of different temperatures on the dielectric properties of materials if it changes to an enclosed system in a temperature controlled area. Figure 4.5 shows a conceptual illustration of this method and its opponents.

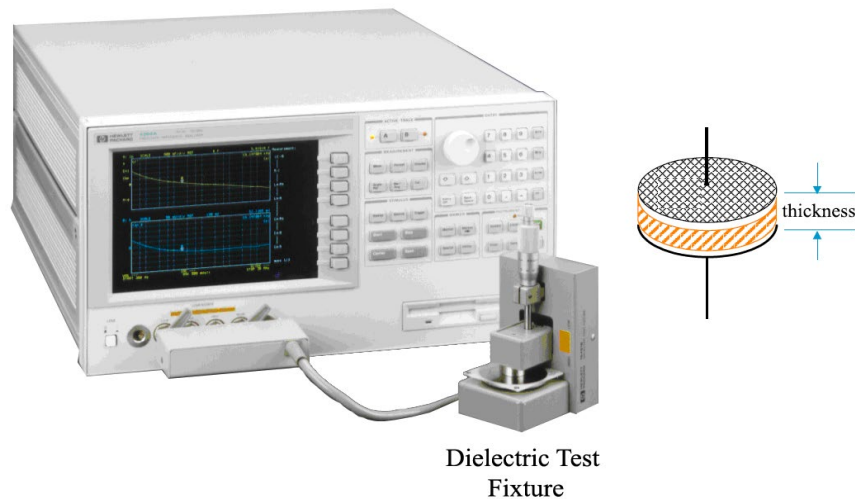


Figure 4.5: Conceptual illustration of the parallel plate capacitor system's setup and its components

#### 4.2.1.4 Transmission line method

In this method, a small cylindrical sample is cut precisely to the size of the waveguide, which is designed to contain and hold the small sample. The sample is then inserted into the closed-end waveguide, as shown in Figure 4.6. Upon being subjected to electromagnetic energy inside the waveguide, the sample reflects, absorbs, and transmits some of the incoming energy. By computing the difference between impedances, the amount of energy reflected, transmitted, and absorbed can be calculated, resulting in obtaining the sample's dielectric properties. The material assumptions for the method of transmission line are as follows: (1) sample fills fixture cross section, (2) no air gaps at fixture walls, and (3) flat face, perpendicular to long axis (Begley, 2010).

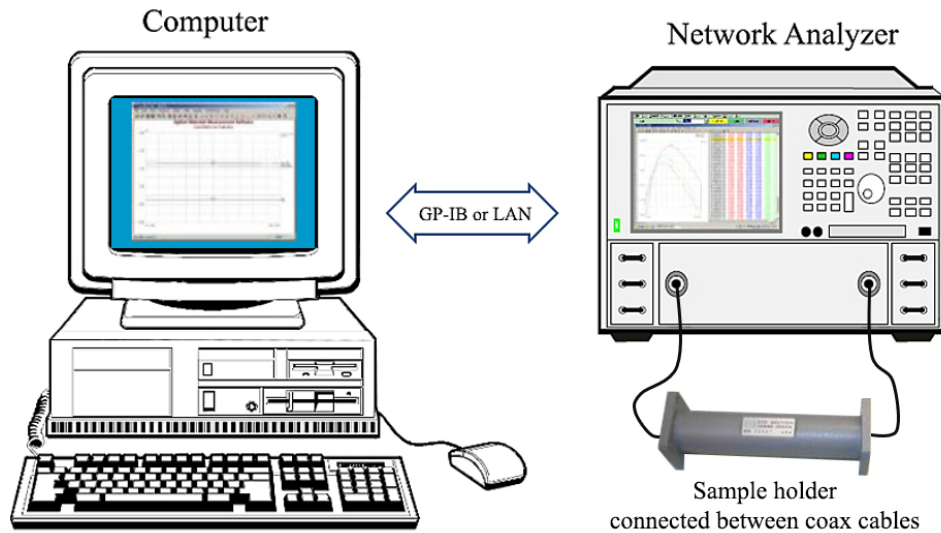


Figure 4.6: Conceptual illustration of the transmission line method for measurement of a small rock sample's dielectric properties

#### 4.2.1.5 Free space method

The free space method for measuring materials' dielectric properties can be considered one of the most complex methods when compared to the others. In this method, a sample must be far enough away from the antenna to be out of the reactive regions; therefore, it should be located at a distance close to  $2d^2/\lambda$  from the antenna, where  $d$  is the largest dimension of the antenna and  $\lambda$  is the wavelength of the electromagnetic wave. The thickness of the test sample must be large enough to contain the 3 dB beam spot (Ghodgaonkar et al., 1989). This method is very similar to the transmission line method described above; dielectric properties are measured by computing the difference between the transmitted and reflected electromagnetic waves. However, the only

difference between the two methods is that in the free space method, the sample's thickness must be small compared to its length, and its surface area must be larger than the cross section of the antenna. The material assumptions for the free space method are (1) sample in non-reactive region, (2) flat parallel face samples, and (3) beam spot contained in sample. This method is also suitable to study high or low temperature effects on the dielectric properties of a sample if the system uses an enclosed furnace in which the sample is installed in a temperature controlled environment. To better understand this system, a conceptual illustration of the free space method with furnace is shown in Figure 4.7.

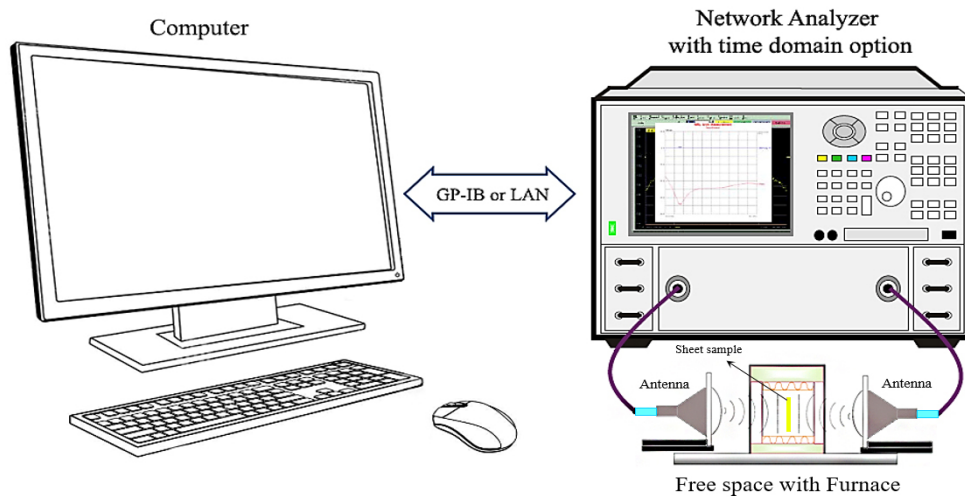


Figure 4.7: Conceptual illustration of the free space method with a network analyzer connected to two antennas and a furnace with a sheet sample for measurement of the sample's dielectric properties

#### 4.2.1.6 Analysis of the methods and variations of the measured dielectric properties of selected rocks

Dielectric properties of a rock sample, which include dielectric constant and loss factor, are the main parameters influencing the microwave-assisted rock heating process (Marland et al., 2001). They are essential information needed for a numerical model to produce a valid result. Thus, it is very important to choose the best method for measuring the dielectric properties of the selected rocks before microwave irradiation experiments and subsequent numerical models with the same conditions. To this end, before choosing a method, the advantages and disadvantages of all five methods of measuring dielectric properties are analyzed and listed in Table 4.2. The table also shows the specific method employed to measure dielectric properties for each selected rock

type, i.e. basalt, granite, kimberlite #1, and kimberlite #2. Because of the variations in the texture, composition, and/or other parameters that might affect the overall result of the dielectric properties, two samples, basalt and granite, were tested by different methods, coaxial probe/resonant cavity and coaxial probe/parallel plate/free space, respectively, to arrive at a valid, trustworthy result.

Table 4.2: List of advantages and disadvantages of dielectric property measurements methods and the selected rock types analyzed

<b>Method</b>	<b>Advantages</b>	<b>Disadvantages</b>	<b>Selected rock type analyzed</b>
Coaxial probe	<ol style="list-style-type: none"> <li>1. Wide range of frequencies</li> <li>2. Easy sample preparation</li> <li>3. High accuracy for high-loss materials</li> </ol>	<ol style="list-style-type: none"> <li>1. Air gaps/bubbles between probe and sample creates errors</li> <li>2. Difficult calibration</li> </ol>	Basalt, Granite, Kimberlite #1, and Kimberlite #2
Resonant cavity	<ol style="list-style-type: none"> <li>1. Suitable for low-loss materials</li> <li>2. High accuracy</li> <li>3. Useful in high temperatures</li> <li>4. Easy calibration</li> </ol>	<ol style="list-style-type: none"> <li>5. Useful for low-loss materials</li> <li>6. High accuracy</li> <li>7. Useful in high temperatures</li> <li>8. Easy calibration</li> </ol>	Basalt
Parallel plate	<ol style="list-style-type: none"> <li>1. Suitable for high-loss materials</li> <li>2. High accuracy at low frequencies</li> <li>3. Easy application</li> </ol>	<ol style="list-style-type: none"> <li>1. Unsuitable at high frequencies</li> </ol>	Granite
Transmission line	<ol style="list-style-type: none"> <li>1. Useful for anisotropic materials</li> <li>2. Suitable at high frequencies</li> </ol>	<ol style="list-style-type: none"> <li>1. Difficult sample preparation</li> <li>2. Not applicable at low frequencies</li> </ol>	None
Free space	<ol style="list-style-type: none"> <li>1. Wide range of frequencies</li> <li>2. Easy sample preparation</li> <li>3. No contact</li> <li>4. Suitable for high temperatures</li> <li>5. Unsuitable for high or low loss materials</li> </ol>	<ol style="list-style-type: none"> <li>1. Diffraction error</li> </ol>	Granite

\*Note that the following references were used to list the advantages and disadvantages of the methods for measurement of rocks' dielectric properties (Agilent, 2006; Khan & Ali, 2012; Ouellet et al., 2013)

As shown in Table 4.2, the method of coaxial probe was the only method used in the present study to measure the dielectric properties of all four rock types. In addition, the dielectric properties of granite were measured by the two other methods: parallel plate and free space; and the method of resonant cavity was enrolled to measure the dielectric properties of basalt at two frequencies of 0.9 GHz and 2.45 GHz. Because there was a variation in the values obtained for the real ( $\epsilon'$ ) and

imaginary ( $\epsilon''$ ) part of permittivity ( $\epsilon$ ) for the four selected rock types, the averages of the test results are reported in this section. Table 4.3 shows the calculated average values of real and imaginary permittivity and loss tangent for the selected rocks at the two frequencies. Further discussion and detailed analyses of the variations in the obtained experimental dielectric properties of the selected rock types will be provided, separately, in Chapter 6 where the results of the numerical models of multi-mode microwave irradiation are discussed in terms of the different input values of the rocks' dielectric properties.

Table 4.3: Calculated average values of real ( $\epsilon'$ ) and imaginary ( $\epsilon''$ ) parts of permittivity and loss tangent ( $\tan \delta$ ) for four selected rock types at the two frequencies of 0.9 GHz and 2.45 GHz

Rock type	0.9 GHz			2.45 GHz		
	$\epsilon'$	$\epsilon''$	$\tan \delta$	$\epsilon'$	$\epsilon''$	$\tan \delta$
Basalt	8.7	1.3	0.149	8.1	0.7	0.086
Granite	5.60	0.06	0.011	5.54	0.18	0.032
Kimberlite #1	6.60	0.97	0.147	6.11	0.75	0.123
Kimberlite #2	7.92	0.68	0.086	7.61	0.67	0.088

It should be remarked that materials/rocks with a high complex permittivity absorb electromagnetic energy and heat at high temperatures, whereas materials/rocks with a low complex permittivity are transparent to electromagnetic waves and do not heat readily. According to the results given in Table 4.3, it can be seen that at both frequencies, the complex permittivity was highest for basalt and lowest for granite. Thus, basalt is expected to have the highest capacity to transform electromagnetic energy into heat, while granite has a low capacity. Given this, and as expected, the value of loss tangent, which represents a measure of dissipation of electromagnetic energy, for granite was the lowest in comparison to the other rock types. Furthermore, the method of coaxial probe was employed to study the effect of frequency variations on the dielectric properties of granite and the two kimberlites. The results of these tests are shown in Figures 4.8 to 4.10. Because of different mineral compositions of the selected rocks, the real part of the complex permittivity showed a declining trend in the frequency range of 0.5-12 GHz for all three rock types (see Figure 4.8). Following this trend, lower sensitivities to changes at higher frequencies (> 8GHz) can be observed. For all the rock types, the imaginary part of relative (complex) dielectric

permittivity and loss tangent showed an incremental trend at frequencies of 2-7 GHz, as shown in Figures 4.8 and 4.10. The trend becomes decremental at frequencies above 7 GHz.

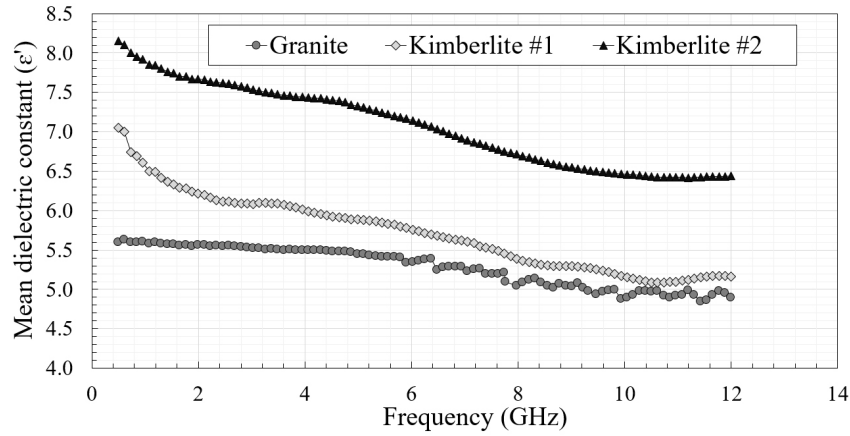


Figure 4.8: The calculated mean values of the dielectric constant for the three rock types with respect to frequency ranges of 0.9-12 GHz

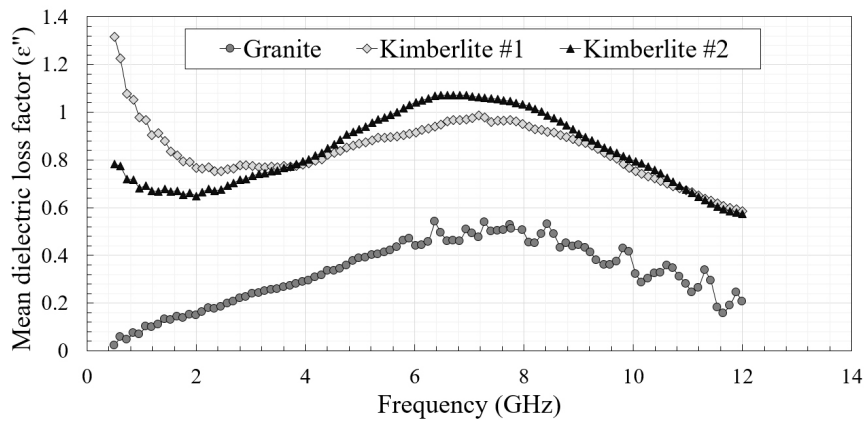


Figure 4.9: The calculated mean values of the dielectric loss factor for the three rock types with respect to frequency ranges of 0.9-12 GHz

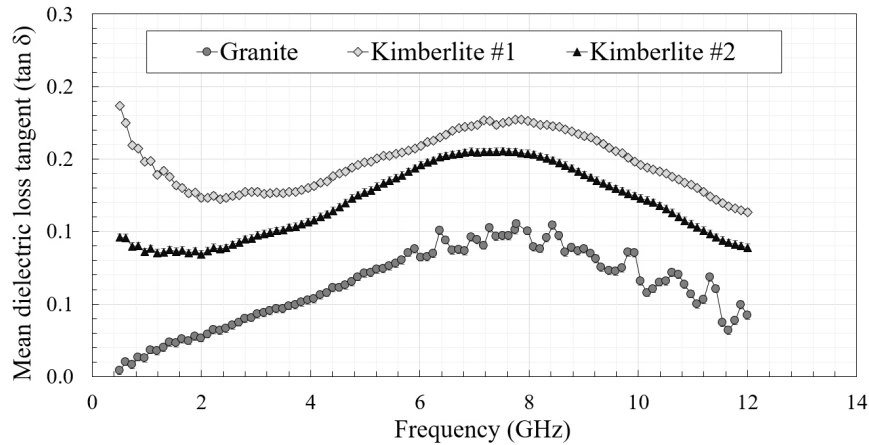


Figure 4.10: The calculated mean values of loss tangent for the three rock types with respect to frequency ranges of 0.9-12 GHz

## 4.2.2 Measurement of electrical conductivity of selected rocks

The aim of this section is to describe a method for measuring the electrical conductivity of rocks and to provide the obtained values of electrical conductivity of the selected rock types in the present study. Accordingly, the following procedures were performed to measure the electrical conductivity values. First, a cylindrical core sample was placed in a sample holder between two copper/graphite electrodes to construct a resistive element for a circuit. Then, a regulated DC power supply was used to drive direct current,  $I$  (Amp), through the core sample. A graphical representation of the processes involved and the instruments used to measure electrical conductivity is given in Figure 4.11.

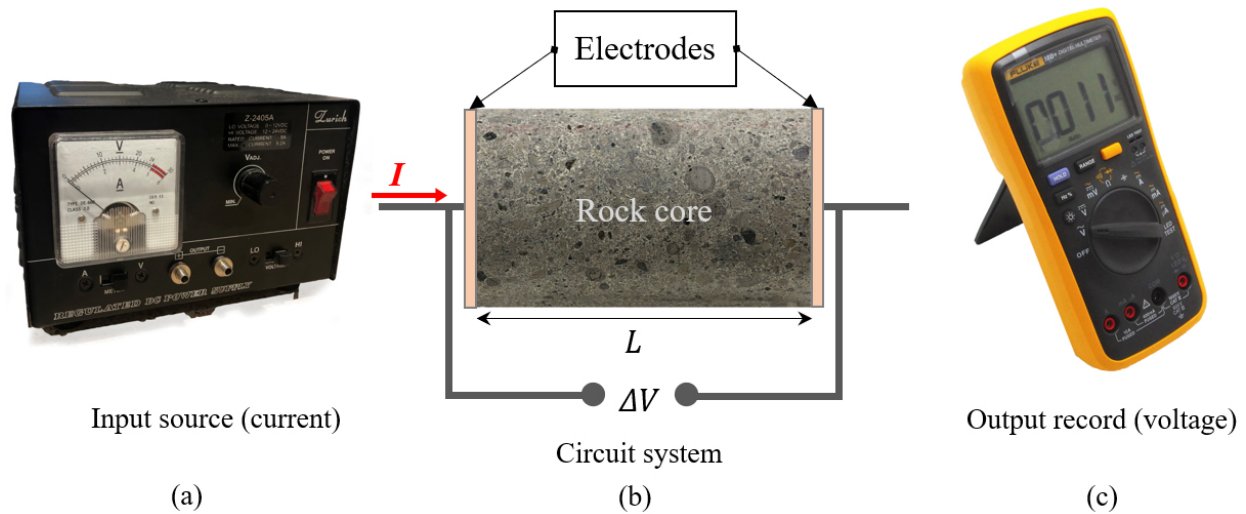


Figure 4.11: Graphical representation of the processes of measuring electrical conductivity of rocks, where (a) is the Z-2405A power supply, (b) is the schematic of rock sample placed between two electrodes, and (c) is the FLUKE 18B+ digital multimeter for measurement of voltage

Finally, by measuring the voltage drop,  $\Delta V$  (V), across the length of the sample, Ohm's law can be used to determine the circuit resistance,  $R$  ( $\Omega$ ), caused by the rock:

$$R = \frac{\Delta V}{I} \quad (4.1)$$

The measured resistance increases proportional to the length,  $L$  (m), of the core sample. Consequently, the values of electrical conductivity for samples with different sizes are expected to differ slightly because of the change in their lengths. This increase was expected, given that the current must flow through more of the resistive rock. The measured resistance is also inversely proportional to the cross-sectional area,  $A$  ( $m^2$ ), of the rock sample. This relationship can be





understood by comparing the net resistance of two identical resistors in parallel to a single resistor in series. Ultimately, the resistivity of the rock sample can be obtained from the measured resistance, the length of the core, and the sample's cross-sectional area by using Pouillet's law (Cheng, 1989):

$$\rho = \frac{RA}{L} \quad (4.2)$$

It was shown by (Coster & FRS, 1948) that the electrical conductivity of rocks changes only at high temperature values (around 450 °C and above). Therefore, the electrical conductivity of the selected rock types in the present study is considered to be constant and measured at room temperature. Table 4.4 gives the measured values of electrical conductivity of the selected rock samples. It should be noted that since length is the parameter that influences the rocks' electrical conductivity value, both BTS and UCS sizes of the selected rock types were measured. Each test was repeated three times to obtain a reliable value; and therefore, averaged values of the tests are given in the table.

Table 4.4: Measured values of electrical conductivity of the selected rock types for both BTS and UCS sizes of the selected rock types

Rock type	Electrical conductivity (S/m)	
	BTS size 	UCS size 
Basalt	0.00005	0.000057
Granite	0.0000004	0.00000043
Kimberlite #1	0.00052	0.00043
Kimberlite #2	0.00057	0.00049

### 4.2.3 Measurement of thermal properties of selected rocks

The specific heat capacity,  $C_p$  (J/g °C), and the coefficient of thermal expansion,  $\alpha_t$  (1/°C), of the selected rock types were experimentally measured by using a heat flux differential scanning calorimeter (KD2 PRO) thermal properties analyzer (see Figure 4.12). With the same method, the thermal conductivity,  $k$  (W/m°C), of the samples was measured, and the obtained values were verified against the values reported in the literature.

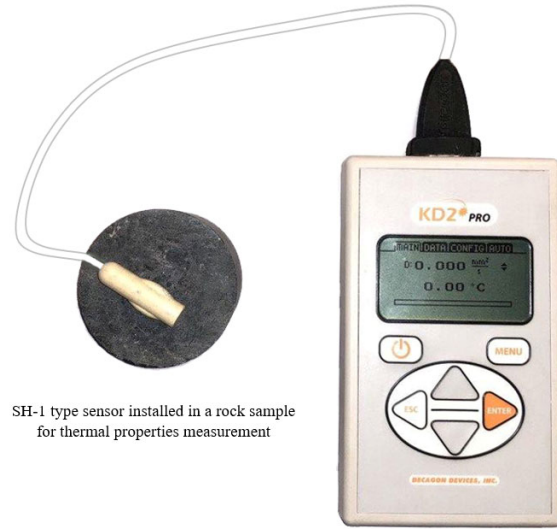


Figure 4.12: Measurement of thermal properties of selected rock types with the KD2PRO thermal properties measurement device

Table 4.5 shows the obtained thermal properties of the selected rock types. To accurately measure these thermal properties, each test was repeated three times for a given sample from each type and an average value was calculated and is shown in the table.

Table 4.5: Measured values of thermal properties of the selected rock types

Rock type	Thermal conductivity (W/m·°C)	Thermal resistivity (°C·cm/W)	Thermal diffusivity (mm <sup>2</sup> /s)	Specific heat capacity (J/kg·°C)
Basalt	1.55	69.30	1.6	850
Granite	2.47	40.91	1.03	670
Kimberlite #1	2.108	47.44	0.72	960
Kimberlite #2	1.369	73.01	0.56	980

## 4.3 Instrumental methods utilized

### 4.3.1 Method of thermal imaging for temperature data acquisition

The thermal imaging method can be described as the process of converting Infrared (IR) radiation (heat) into visible images that depict the spatial distribution of temperature profiles by a thermal imaging camera (Havens & Sharp, 2015). Real-time observations of temperature distribution on the surface of an irradiated rock sample after microwave treatments can be captured by a thermal imaging camera to record final temperature profiles and the maximum or minimum temperature achieved. Moreover, the obtained data from the thermal camera can also be used to

determine heat generated at the crack tips when cracking has occurred. Therefore, the method of thermal imaging for temperature data acquisition is a powerful tool to obtain temperate data of rocks after microwave treatments. The present study employs this method and a Fluke TiS65 IR camera to obtain temperature data of the selected rocks after microwave treatments and to compare them under different experimental conditions. Figure 4.13 shows the process of temperature data acquisition by the method of thermal imaging.

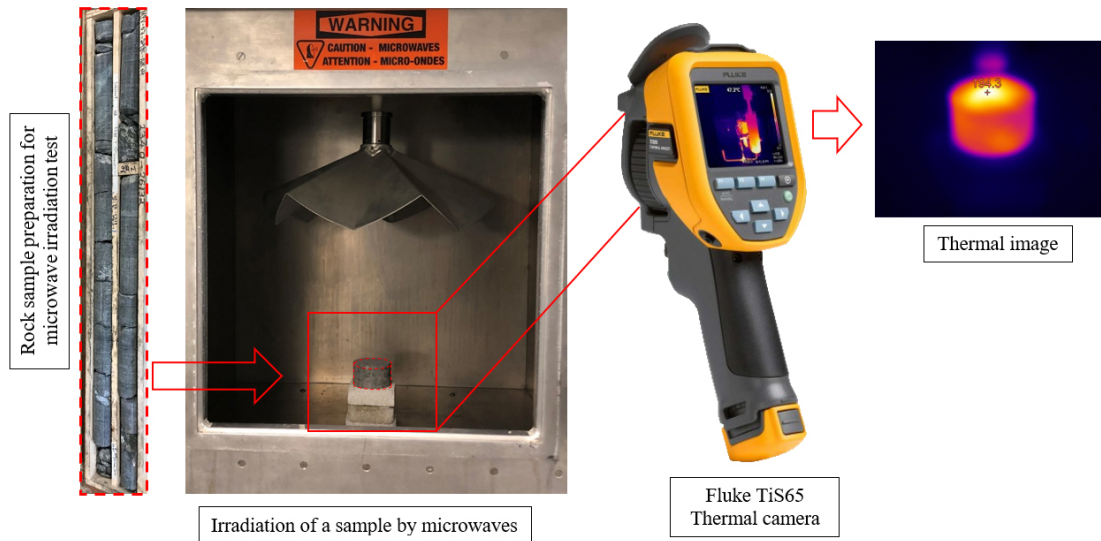


Figure 4.13: The process of thermal imaging by Fluke TiS65 IR camera after microwave treatment

The main factor when using a thermal imaging camera (IR camera) is the setting of its emissivity. Emissivity is defined as the ratio of the energy radiated from a material’s surface to that radiated from a black body (a perfect emitter) under the same viewing conditions and at the same temperature and wavelength (Madding, 1999). This is an essential parameter in capturing the correct thermal image of a sample. Hence, the corresponding emissivity values of each selected rock type was experimentally measured using the method described in (Rakrueangdet et al., 2016). Table 4.6 gives the measured values of emissivity for the selected rock types in the present study. All IR thermal images obtained from the experiments (microwave treatments of selected rocks) were then analyzed using the thermography software SmartView® 4.3 provided by Fluke Co.

Table 4.6: Measure emissivity values of the selected rock types

Rock type	Basalt	Granite	Kimberlite #1	Kimberlite #2
Emissivity	0.74	0.95	0.91	0.88

### 4.3.2 Method of calorimetry for thermal energy (absorbed heat) measurement

In this thesis, the method of calorimetry is used for the measurement of heat/energy absorption of the selected rock types after the microwave irradiation experiments were completed. This method was adopted from a recent innovative study by Hassani et al. (2020). By using this method, the amount of heat/energy absorbed by the rock samples can be obtained and compared with the amount of energy induced by the microwave system. The measured heat values are also used to validate the numerical models. The application of the calorimeter for thermal energy measurement of selected rocks after microwave treatment is described below.

Initially, there is a high-temperature substance—that is the rock sample after microwave treatment—denoted by (R) and a low temperature substance that is the cool water (W). By immersing the irradiated (hot) rock into an insulated bath filled with water, heat will flow from R to W. The temperature of R will decrease, and the temperature of W will increase by the time the two substances reach thermal equilibrium. Under an ideal circumstance in which all of the heat transfer occurs between the two substances, with no heat gained or lost by either the calorimeter or the calorimeter's surroundings, the net heat exchange between the rock and the water equals zero:

$$Q_R + Q_W = 0 \quad (4.2)$$

where  $Q_R$  denotes the heat absorbed by the rock sample, and  $Q_W$  is the heat absorbed by the water. In line with the law of thermodynamics, the relationship given in equation (4.2) can be rearranged as equation (4.3), showing that the heat gained by the rock is equal to the heat lost by the water:

$$Q_R = -Q_W \Rightarrow (m C_p \Delta T)_R = -(m C_p \Delta T)_W \quad (4.3)$$

The magnitude of the heat change will, therefore, be the same for both substances, the rock sample and the water. Moreover, the negative sign merely shows that  $Q_R$  and  $Q_W$  are opposite in the direction of heat flow (gain or loss); nevertheless, it does not indicate the arithmetic sign of either  $Q$  value (that is determined by whether the substance in question gains or loses heat, by definition). In the situation described,  $Q_R$  is a negative value and  $Q_W$  is positive, since heat is transferred from the rock to the water. A schematic illustration of the method of calorimetry for novel thermal energy (absorbed heat) measurement in a rock sample after microwave treatment is given in Figure 4.14.

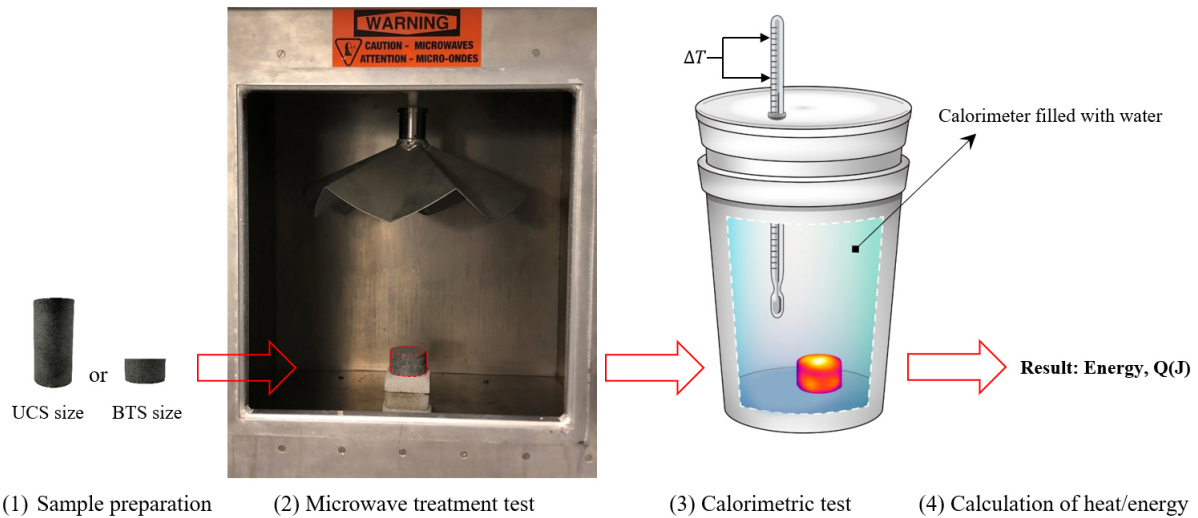


Figure 4.14: A schematic illustration of the method of calorimetry for novel thermal energy (absorbed heat) measurement in a rock sample after microwave treatment

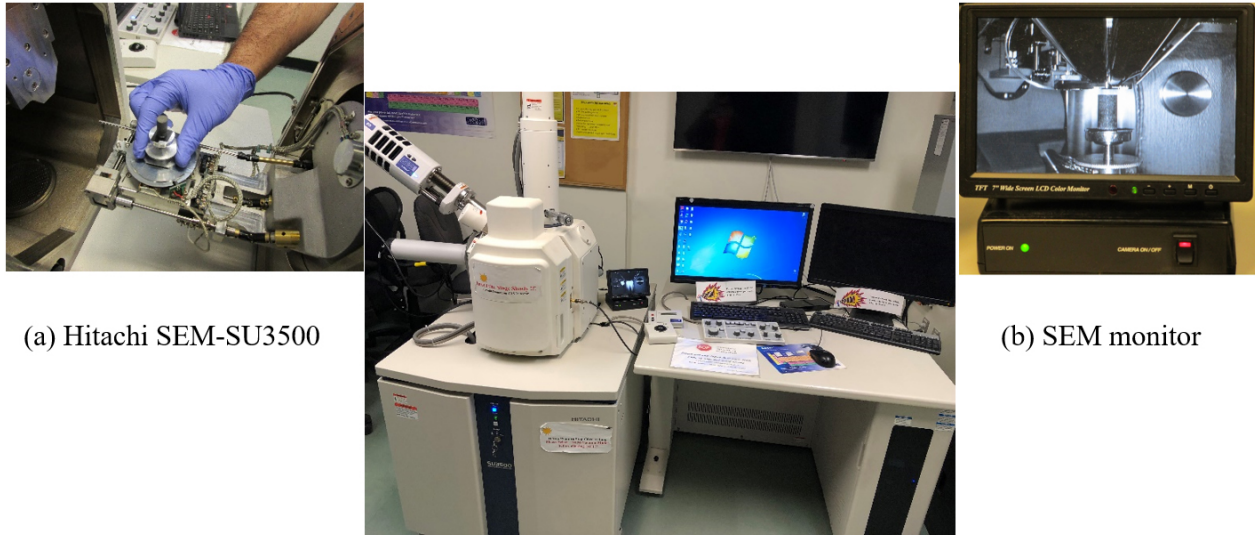
By recording all parameters, i.e. initial temperature of the rock and the water in the calorimeter and the final equivalent temperature of the rock and the water, the total heat/energy produced in the calorimeter can be calculated as

$$Q_{\text{Total}} = Q_{\text{R}} + Q_{\text{W}} \quad (4.4)$$

### 4.3.3 Method of Scanning Electron Microscopy for rock surface characterization

Scanning electron microscopy (SEM) is one of the most advanced technologies for the quantification and analysis of microstructural responses of solid materials (e.g. rocks). SEM analysis is comparatively more useful in studies that investigate quantification of microstructural properties such as microcracks and voids. The Hitachi SU3500 Variable Pressure Scanning Electron Microscope (VP-SEM) used in the present study can provide up to 7 nm SE images with a resolution at 3 kV, 10 nm, and backscattered electron (BSE) image resolution at 5 kV. It is equipped with an 80 mm 2X-Max SDD EDS detector with the EBSD Aztec HKL Advanced system. The high probe of this microscope with 1  $\mu\text{A}$  current allows the automatic EDS-EBSD mapping to create a montage of all the regions of a given specimen at very high speed (Brodusch et al., 2018). The BSE detector can produce quantitative three-dimensional maps of the surface of a specimen to quantify complicated and rough surfaces. The low vacuum mode characterizes non-

conductive materials without coatings. Fig. 4.15 shows the Hitachi SEM SU-3500 instrument used for SEM imaging in the present thesis.



(a) Hitachi SEM-SU3500

(b) SEM monitor

Figure 4.15: Image of (a) the Hitachi SEM-SU3500 Variable Pressure Scanning Electron Microscope (VP-SEM) instrument located at McGill University, Department of Mining and Materials Engineering, and (b) position monitoring of the rock sample inside the SEM cavity

In the present thesis, the SE images were captured with a resolution at 2 kV and 200  $\mu\text{m}$ . Then, ImageJ software developed by the National Institute of Health (NIH) was employed to conduct image processing on the raw data (Abramoff et al., 2004). This software has the capability of performing various operations such as binary thresholding and area measurement based on Java language.

#### 4.3.4 Method of micro-Computed Tomography for rock volumetric characterization

From recent developments in the micro-focusing capability of X-ray Computed Tomography (CT) scanning technology, researchers are now able to visualize the patterns of cracks (i.e. crack density, crack size, etc.) in rocks to study the fracture mechanism according to microstructural observations. The X-ray micro-CT scan is a nondestructive tool to investigate the internal microstructure of rocks that can provide quantitative data about the morphology of three-dimensional rock samples. Several studies have verified the potential application of the CT imaging technique in the microstructural analysis of rocks (Mathews et al., 2011; Saif et al., 2016; Zhu et al., 2019). These studies showed that micro-CT is a powerful tool to visualize and quantify



the microcracks and morphological changes in rocks after microwave treatments. For example, Meng et al. (Meng et al., 2019) studied the effect of microwave-assisted heating on the microstructure of oil shale samples. They demonstrated that micro-CT scanning is a powerful imaging technique to quantify the changes in the microstructure of oil shale samples after microwave irradiation experiments. Several other studies reported that CT imaging provides a valuable way to understand the changes in the microstructure of hard rocks after microwave treatment. Thus, by taking into account the features related to this method, the present study employs it and investigates the effects of applying microwave irradiation on the microstructural behavior of hard rocks by using three-dimensional volume renderings. To this end, a high resolution micro-CT scanner (SKYSAN-1172, Skyscan, Kontich, Belgium), with the X-ray tube operating at 50 kV, 200  $\mu$ A, 1600 ms exposure time with a 0.5 mm aluminum filter and a focal spot size of 5  $\mu$ m, was used to obtain high-resolution volumetric reconstructions at a maximum voltage of 150 kV and maximum light power of 10 W with three different magnification lenses (4 $\times$ , 10 $\times$ , 20 $\times$ ). SKYSAN-1172 features two X-ray camera options: a high-performance 10 megapixel option and an economy 1.3 megapixel option. The former allows maximum scanning versatility with an image field width of 68 mm (in dual image camera shift mode) or 35 mm (in standard single camera image mode). A resolution (pixel size) of lower than 1  $\mu$ m is also attainable. The scannable height of approximately 70 mm allows for either large samples or automatic batch scanning of a column of smaller samples. Pictures of the micro-CT scanner and the sample placement inside the device chamber are shown in Figure 4.16(a) and 4.16(b).

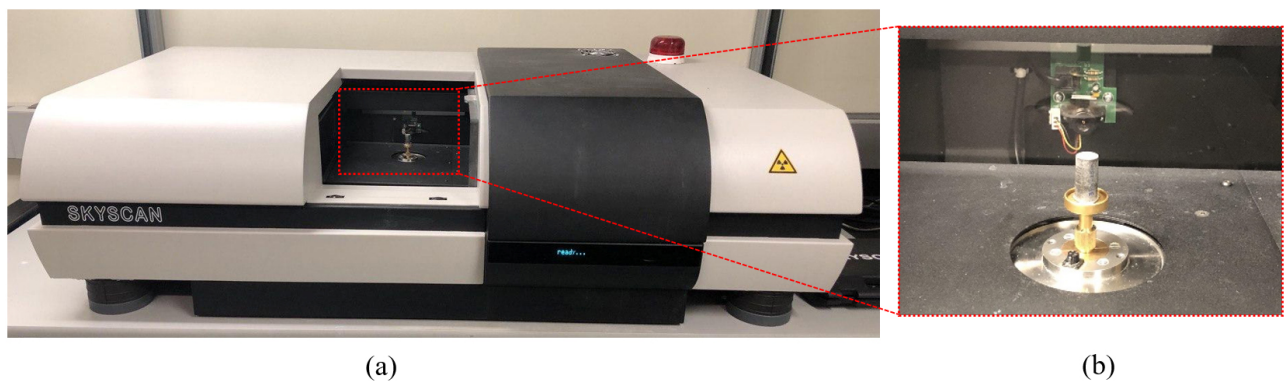


Figure 4.16: The image of (a) the system of SKYSAN-1172 micro-CT scanner (Skyscan, Kontich, Belgium) with the X-ray tube operating at 50 kV located at McGill University, Department of Mining and Materials Engineering, and (b) placement and positioning of the sample in the micro-CT cavity for 3D X-ray imaging

## Chapter 5

# Multiphysics study of single-mode microwave irradiation effects on rock pre-conditioning and breakage

### Contents

---

5.1	Introduction.....	98
5.2	Phase I: Thermal image analysis from surface temperature measurement .....	103
5.3	Phase II: SEM image analysis from surface microcrack quantification .....	118
5.4	Phase III: Volumetric microcrack visualization from micro-CT scan.....	124
5.5	Conclusions .....	128

---

### Preface

*Rock pre-conditioning and breakage by single-mode microwave irradiation are well-known for their intensive influences on rock surfaces. A conventional design of a single-mode microwave system for maximum pre-conditioning (microcracking) effects on the surface of a rock under irradiation is based on several parameters, including microwave power level, exposure time, and distance from microwave horn antenna. The aim of this chapter is to experimentally investigate the effects of these parameters on the pre-conditioning and breakage of hard rocks by implementing three research phases. The organization of the chapter is as follows. First, an introduction to single-mode microwave systems and their application in rock pre-conditioning and breakage is given; details of experimental setups and conditions are described (section 5.1). Then, in Phase I of the research, a thermal image analysis from surface temperature measurement of irradiated rock specimens at different experimental conditions is presented and discussed (section 5.2). In Phase II of the research, SEM image analysis from surface microcrack quantification is given and discussed (section 5.3). Afterwards, in Phase III of the research, volumetric microcrack visualization from the results of micro-CT scanning is presented and discussed (section 5.4). Finally, the chapter ends with a summary of findings and overall conclusions on the effectiveness of single-mode microwave-assisted rock pre-conditioning and breakage (section 5.5).*



## 5.1 Introduction

The pre-conditioning of hard rocks by single-mode microwave irradiation consists of the following two main components: the microwave system's characteristics and the rock specimens' specifications.<sup>5</sup> Microwaves occupy the most significant part of the electromagnetic wave spectrum, where the magnitude of wavelength,  $\lambda$  (m), and frequency,  $f$  (GHz), vary from 0.001 to 1 m and from 0.3 to 30 GHz. The role of microwaves is to carry energy (from the magnetron) through space (waveguide) at the speed of light to affect rock specimens in the microwave cavity. When a single-mode microwave cavity system starts to irradiate a rock specimen, the process of energy transmission continues until heat is generated in the specimen and, subsequently, because of temperature differences in the rock particles, several microcracks are thermally induced within the rock. These microcracks are created mainly at the surface of the irradiated specimens because of the intrinsic nature of the single-mode microwave irradiation effect.

One of the main advantages of using a single-mode microwave cavity system is that the correct electromagnetic field polarization undergoes multiple reflections through the waveguide and directly touches the surface of a rock specimen facing the waveguide horn's outlet (microwave antenna). The superposition of the reflected and incident electromagnetic waves from the waveguide to the microwave cavity gives rise to a standing electromagnetic wave pattern that is well defined in the cavity. By using a single-mode microwave system and considering the position at which a dielectric material absorbs maximum electric field strength, maximum heating and pre-conditioning can be achieved (Whittles et al., 2003). However, to set the best positioning of a rock specimen in a single-mode microwave cavity for maximum impact, there is a distance from the rock surface to microwave horn antenna—where the travelling electromagnetic waves in the waveguide are guided by the horn to enter the cavity—which is the primary parameter that needs to be accurately defined and selected. In addition, microwave power level and exposure time are secondary parameters in the study of single-mode microwave irradiation effects on rock heating and pre-conditioning (microcracking/fracturing). Although several experimental studies have recently employed single-mode microwave systems for irradiation of hard rocks, there is still no comprehensive study on the influencing parameters, i.e. microwave power level, exposure time,

---

<sup>5</sup> In this chapter, the term 'specimen' refers to rectangular basalt extractions of size 40 cm × 40 cm, while the term 'sample' refers to cylindrical basalt extractions of size  $r = 0.5$  cm from the center of the irradiated specimens to further characterize the effects of the microwaves.

and distance from the horn antenna, in a single-mode microwave-assisted rock pre-conditioning and breakage application. The present study extensively investigated these determining parameters by first conducting several microwave irradiation tests on rectangular-shape specimens of basalt in an industrial high power single-mode microwave cavity system at different experimental conditions (parameters) and then analyzing the results of the experiments in the following steps: (1) thermal image analysis from surface temperature measurements obtained by a thermal camera, (2) SEM image analysis from surface microcrack quantification, and (3) volumetric microcrack visualization from micro-CT scanning. These three steps are called phases in the present research study, and their extensive details are explained explicitly at the end of section 5.1.2. The overall discussion and conclusions provided at the end of this chapter will help prospective users of single-mode microwave cavity systems in an industrial application better set their microwave systems' operating parameters for efficient pre-conditioning and breakage of hard rock types to create maximum damage.

### **5.1.1 Experiments of single-mode microwave irradiation on basalt specimens**

In the present study, the experimental tests of single-mode microwave irradiation of basalt rock were performed at a constant frequency of 2.45 GHz by an industrial, high-power (up to 15 kW), single-mode microwave cavity system located in the Geomechanics Laboratory of McGill University. A schematic of this microwave system, comprising its components, is shown in Figure 5.1. The figure illustrates a power level gauge for adjustment of the input power levels of the microwave system, a 480 V power supply, a magnetron, and a closed 60 cm × 60 cm × 60 cm cubic cavity with a pyramidal horn antenna. The antenna is located at the end of waveguide, inside the microwave cavity, and prevents the incoming electromagnetic waves from randomly scattering in all directions. The purpose of the horn aperture is to allow microwaves to gradually enter a larger area—which is the cavity space—after leaving the rectangular waveguide. In the present study, the radiation of microwaves is from the waveguide into a much larger space (large cubic cavity); therefore, a simple “plane wave” form occurs because electromagnetic waves would look the same in any plane at right angles to the direction of propagation. With the described microwave system that provides up to 15 kW power and has a large cavity, it was possible to study the effects of different microwave parameters, including power level and exposure time, and arrangement of the specimens in the cavity, i.e. distance from the horn antenna, for maximum pre-conditioning.



Figure 5.1: Industrial single-mode, variable high-power (up to 15 kW) microwave cavity system in the Geomechanics Laboratory at McGill University

In the following section, the microwave system setup and research procedures for single-mode microwave tests, including the novel approach employed to investigate the single-mode microwave irradiation effects in rock pre-conditioning and breakage, are presented and discussed.

### 5.1.2 Microwave system setup and research procedures

The experimental tests of single-mode microwave irradiation were performed in the following steps. First, the basalt rock, intact and without visible cracks, was cut into several rectangular-shape specimens, each having a side-length of  $40 \text{ cm} \times 40 \text{ cm}$  and a height of 2 cm. The dimensions of these specimens were designed in such a way that they were larger than the largest dimension of the microwave horn antenna (see Figure 5.2). The specimens were then placed on top of each other (stacked together) inside the cavity and formed blocks of basalt to reach the desired distances from the horn antenna, depending upon the experimental condition. However, it should be noted that both the blocks with a constant volume and the blocks with changing volumes were used in the experiments of the single-mode microwave irradiation on basalt. To adjust the heights according to the desired distances from the horn aperture, the rock blocks with a constant volume were installed on four rod-shaped insulators and two rectangular-shape insulators (polypropylene), as shown in Figure 5.2(b). The aim of the experimental tests with this

configuration was to investigate the effects of various distances from the horn antenna on the surface temperature changes in basalt. However, the experimental tests with the blocks of changing volumes were designed to study the effects of various rock sizes and microwave input operating parameters (power level and exposure time) on the surface temperature changes. A conceptual illustration of the experimental single-mode microwave system's setup with its components and the placement of basalt specimens in the cavity is shown in Figure 5.2.

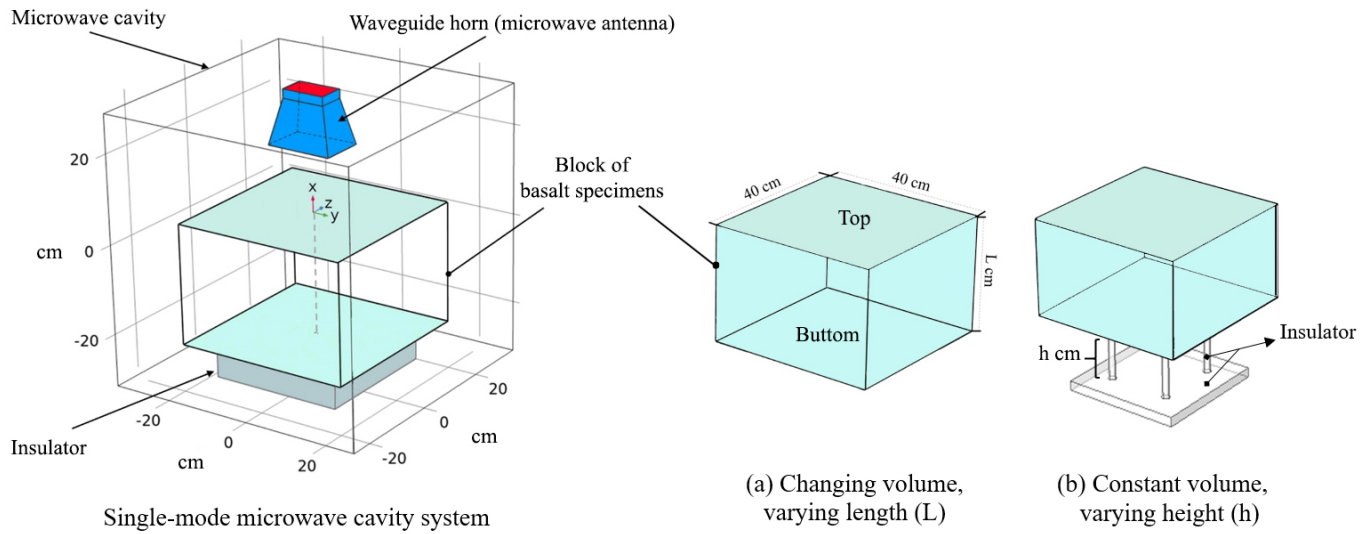


Figure 5.2: Conceptual illustration of the single-mode microwave cavity system with two different configuration of rock blocks: (a) rock block with changing volume where the length of the block,  $L$  (cm), changes according to the size of the rock and the distance from the horn antenna, and (b) rock block with a constant volume placed on two rectangular insulators installed on four rod-shaped insulators with a height,  $h$  (cm), changing according to the distance from the antenna

The above figure shows that the placement of the block of basalt is in such a way that its top surface faces the horn's outlet and the centroids of the block and the horn antenna are in the same direction. After the geometry of the single-mode microwave cavity system and the placement of the blocks of basalt in the cavity were established, various microwave operating parameters, including power level, exposure time, and distance from the horn antenna, were designed as microwave conditions, for the microwave irradiation tests on the specimens of basalt. To investigate the influence of each of these microwave operating parameters on the heating, pre-conditioning, and subsequent breakage of basalt, the present study implemented the following three research phases.

In phase I of the research, several blocks of basalt were experimentally irradiated in the

single-mode microwave cavity at different power levels, exposure times, and distances from the horn antenna. The experimental tests were performed on both the blocks with changing volumes and the blocks with constant volumes. After the microwave irradiation tests, thermal images from the surface of the irradiated specimens were captured by a thermal image camera (IR camera) for analysis. The results from thermal images were then presented and compared for different operating parameters to obtain the best condition of the single-mode microwave cavity system for maximum pre-conditioning effect, based on thermal analysis. Finally, the results of the conducted parametric study are discussed and analyzed.

In phase II of the research, a novel approach was employed for quantification of surface microcracks created in irradiated specimens of basalt at different microwave operating parameters (here called case studies) by the method of SEM imaging. The approach involved drilling cylindrical core samples from the topmost irradiated specimens after single-mode microwave experiment with different operating parameters, defining a specific location at the top center of the core samples for capturing SEM images, and conducting microcrack quantification from the SEM images to analyze the effect of microwave operating parameters from the parametric study. After processing the captured SEM images from the irradiated specimens, the images of microcracks specific to each case study are provided and the results of surface microcracking analysis are compared for various microwave operating parameters to arrive at the best condition of the single-mode microwave cavity system for maximum pre-conditioning effect based on SEM analysis.

In phase III of the research, single-mode microwave irradiation tests were performed on specimens of basalt at the four microwave operating parameters that had already been identified in phase II as the best conditions of the single-mode microwave system for maximum surface microcracking effect in basalt. Then, as in the novel approach employed for the SEM image analysis on the irradiated specimens of basalt in phase II of the research, cylindrical core samples were drilled from the center of the topmost irradiated specimen after single-mode microwave experiments. The core samples were then scanned by a micro-CT apparatus, and 3D volume renderings were generated after the micro-CT images were processed. Finally, volumetric propagation of microcracks in the core samples are presented at a 2D cut plane. The aim is to visualize microcracks created within the core samples to investigate how many microcracks are created volumetrically by the single-mode microwave irradiation on the specimens of basalt.

## 5.2 Phase I: Thermal image analysis from surface temperature measurement

### 5.2.1 Methodology and procedures

In the first phase of experimental investigations on the effects of single-mode microwave irradiation on hard rocks, by using a thermal camera, thermal images were captured from the surface of blocks of basalt irradiated at different experimental conditions (note that one block contains one or more specimens). In addition, the following two conditions were implemented in experimental setups: blocks with changing volumes and blocks with a constant volume. As mentioned earlier, in some experiments, the volume of the rock block was changed according to the corresponding distance from the horn antenna; and in the other experiments, the rock volume was kept constant. To adjust the desired distances from microwave antenna, four rod-shaped insulators at various heights were placed beneath the blocks to arrive at the desired distances based on various experimental conditions (see Figure 5.2(b)). These experimental conditions, including various input microwave operating parameters, are listed in Table 5.1.

Table 5.1: The input operating parameters (conditions) for the experimental tests of single-mode microwave irradiation on the specimens of basalt

no.	Distance from MW* horn antenna, d (cm)	Rock volume, $V$ (m <sup>3</sup> )	MW power level, P (kW)	MW exposure time, t (s)
1.	5	0.059	3, 9, 15	60
2.	10	0.051	3, 9, 15	60
3.	15	0.043	3, 9, 15	60
4.	20	0.035	3, 9, 15	60
5.	25	0.027	3, 9, 15	60
6.	30	<b>0.019<sup>a</sup></b>	3, 9, 15	60

\* In this table, the word microwave is abbreviated as MW.

<sup>a</sup> This volume, which contains six specimens stacked up together, was used for the experiments at constant rock volume in the investigation of the effect of MW power level.

As given above, the experimental tests of phase I were implemented on the specimens of basalt at 60 second microwave exposure, three power levels of 3, 9 and 15 kW, and six distances of 5, 10, 15, 20, 25, and 30 cm from the microwave horn antenna. In accordance with the six distances from the antenna, six case numbers (or simply case studies) were assigned for the experimental

conditions listed in Table 5.1. In addition, for every case study, its corresponding volume of the block of basalt, which consists of certain numbers of specimens stacked up to reach the desired distance from the horn antenna, is given for later calculation of the power densities for different experimental conditions. The purpose of this experimental design was to study first the effect of the distance of the rock from the microwave horn antenna and, subsequently, the other two operating parameters of microwave on the surface temperature (thermal heating) of the specimens. (Note that for some test conditions, the specimens of basalt were also irradiated at 120s to test the effect of exposure time.)

Figure 5.3 depicts the process of capturing thermal images from the surface of the irradiated basalt specimens at different experimental conditions. The temperature distributions at the top surface of the irradiated specimens were experimentally captured using a Fluke TIS65-30Hz thermal image camera with IR-Fusion technology and a resolution of  $260 \times 195$  pixels. The emissivity value of basalt was set at 0.74 in the thermal camera before thermal imaging (see section 4.3.1 for more details about the emissivity setting) (Meredith, 1998). Post processing of thermal images was done using FLIR software provided by FLUKE Connect™ (FLUKE, 2020).

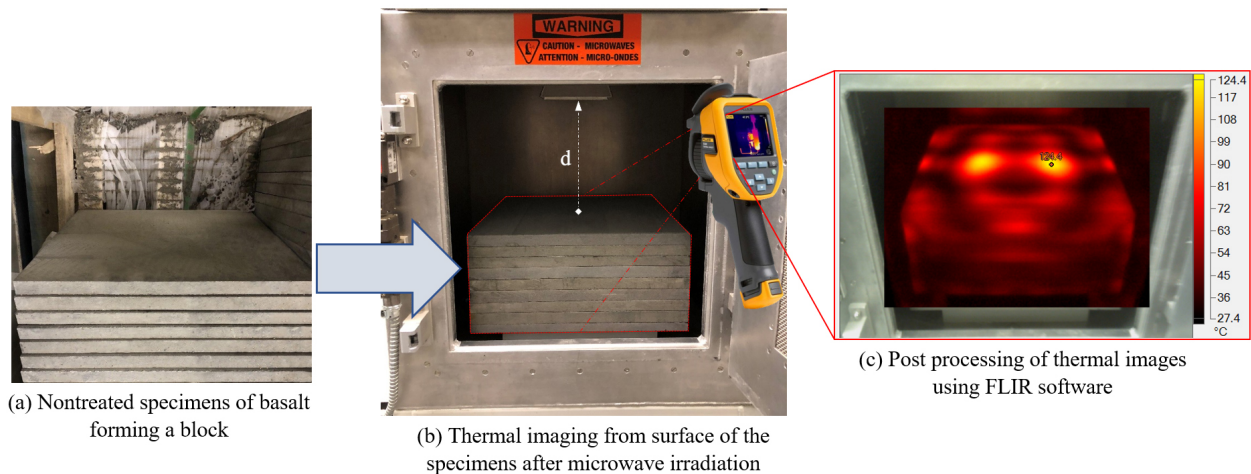


Figure 5.3: The process of thermal imaging by a thermal camera from basalt specimens after single-mode microwave irradiation tests for surface temperature measurements: (a) nontreated specimens of basalt ready for irradiation; (b) thermal imaging from surface of the irradiated specimens (the distance from the microwave horn antenna is shown by a white arrow); and (c) post processing of thermal images using FLIR software

## 5.2.2 Results and discussion

In this section, first the results of thermal images from the surface of the irradiated basalt specimens at different experimental conditions are presented. The amount of structural damages on basalt, such as major cracking, spallation, fractures, etc., which occurred as a result of temperature changes mainly at the surface of the topmost specimen after the single-mode microwave irradiation tests, are then provided for a better visual understanding of the pre-conditioning mechanisms, i.e. crack development and breakage, on the surface of irradiated specimens. The results section continues with thermal analyses conducted using a parametric study of the effect of various microwave operating parameters on the surface temperature distribution and measurements in the irradiated basalt specimens. A final discussion is provided as an energy effectiveness analysis of single-mode microwave irradiation effects on hard rock heating and pre-conditioning.

Figures 5.4 and 5.5 show the temperature profiles of irradiated blocks of basalt at various experimental conditions where the volumes of blocks were changed with respect to different distances from the horn antenna. It should be noted that the distribution of surface temperature profiles differs among the plots; a considerable influence of different distances from the horn antenna can be observed on the patterns of the rock surface temperature. The physical dimensions of the highest thermally affected area and their respective directions play an important role. As the electromagnetic wave propagates, different nodes/modes of microwave energy in which more energy is concentrated are created by the waves' alternations. Different distances from the horn antenna's aperture affect thermal distribution at the top surface of the rock blocks. The distance between each mode is directly related to the wavelength of the standing electromagnetic wave. When the distance from the horn antenna was set at a value between 0 to 8.8 cm, the direction of the affected area at the top surface of the specimens was parallel to the direction of the horn's width. According to theory, the electromagnetic wavelength at 2.45 GHz is approximately 12 cm. From the experimental tests of the present study, the exact number of the electromagnetic waves at 2.45 GHz for the microwave system used in the irradiation tests was found experimentally at 12.2 cm. Thus, the first wavelength of the electromagnetic waves was at a distance between 0 cm to 8.8 cm, and the second wavelength occurred when the distance from the horn antenna passed the 8.8 cm up to the distance of 21 cm (12.2 cm + 8.8). Consequently, the affected area became perpendicular to the horn's width when the distances were set at values between 8.8 cm to 21 cm.



The next change of shape to the affected area occurred after 33.2 cm (12.2 cm + 21 cm) distance from the horn antenna. Using this mechanism, the same repetitive alternations follow.

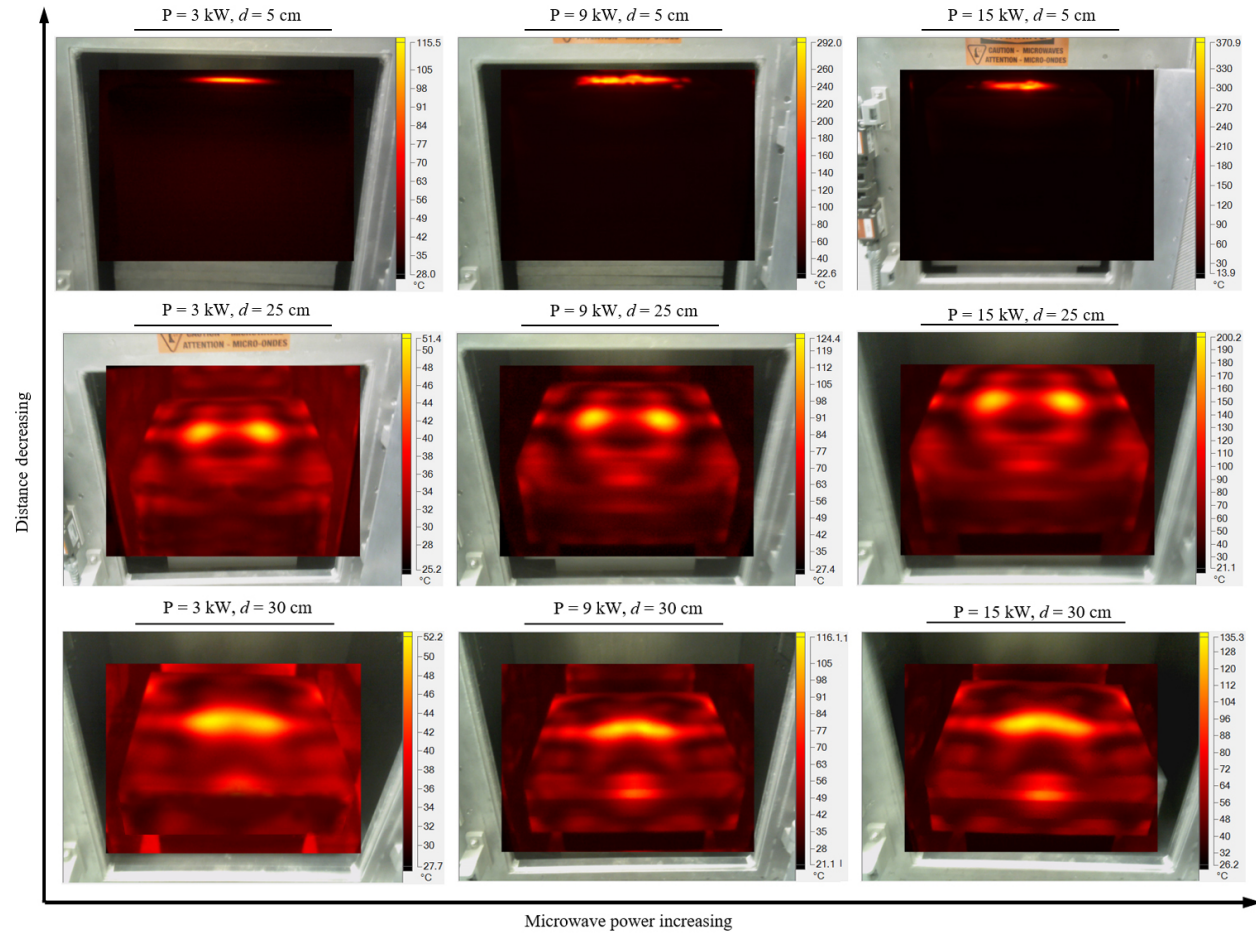


Figure 5.4: Surface temperature profiles of the irradiated blocks of basalt after 60 s microwave exposure from the results of thermal images, where the projection of temperature distribution is parallel to the width of the horn antenna's aperture

The plots shown in Figure 5.4 indicate that for the distances of 5 cm, 25 cm, and 30 cm the obtained high-temperature area on the top surface of the irradiated specimens is in a direction parallel to the horn's width. The direction of the high-temperature distributed area becomes perpendicular to the horn's width when the distances of the rock blocks from the horn antenna are set at 10 cm, 15 cm, and 20 cm, as shown in Figure 5.5. The plots presented in both figures follow the same trend of change according to their input microwave operating parameters; by increasing the input microwave power level, the obtained surface temperature of the irradiated specimens increases. Similarly, by decreasing the distance from the horn antenna, the obtained surface temperature of the irradiated specimens increases.

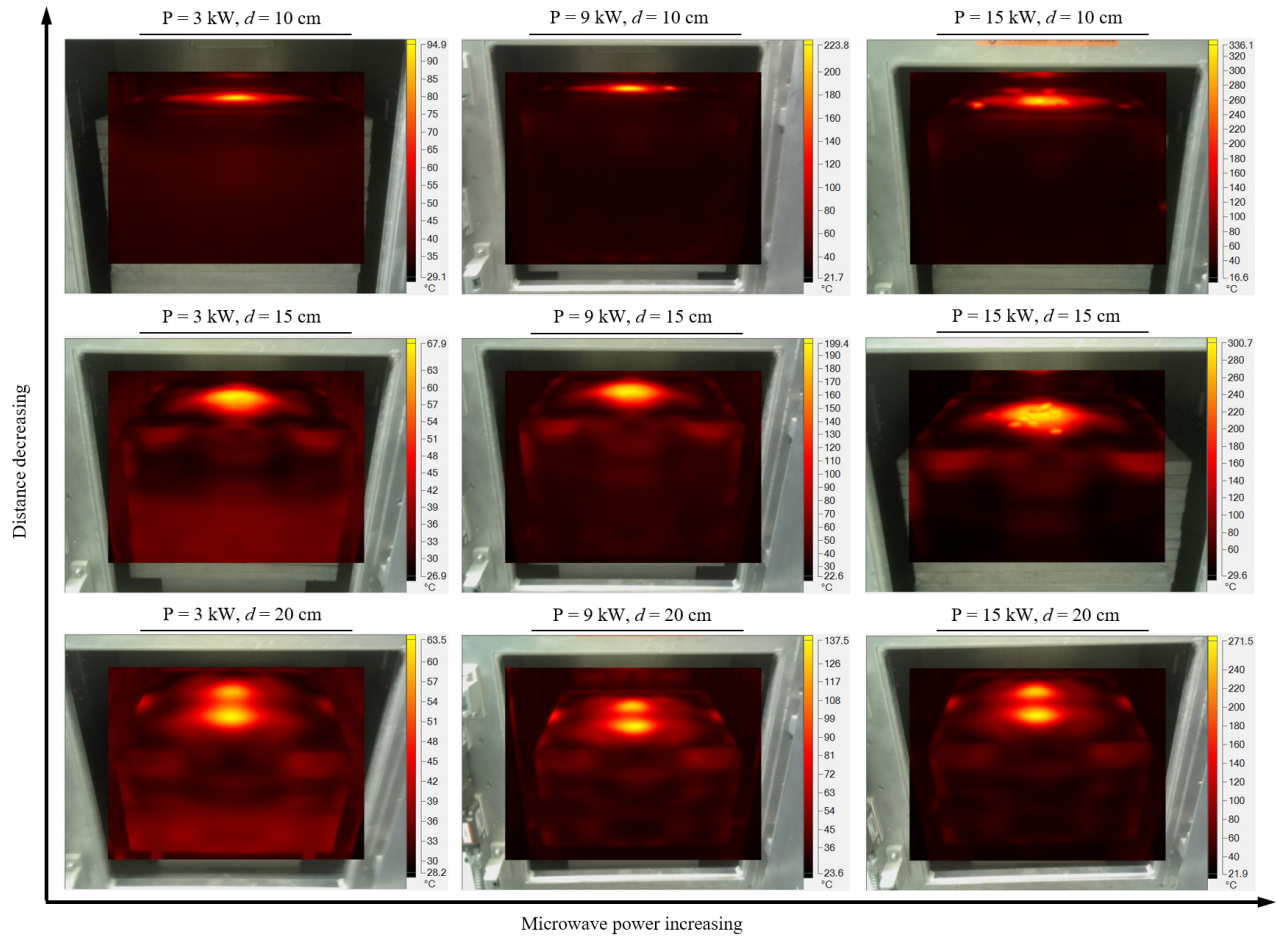


Figure 5.5: Surface temperature profiles of the irradiated blocks of basalt after 60s microwave exposure from the results of thermal images, where the projection of temperature distribution is perpendicular to the width of the horn antenna's aperture

The specimens of basalt in each irradiated block at different microwave operating parameters were predicted to have invisible microcracks and visible cracks mainly on the surface of the topmost specimen facing the horn's aperture. However, the intensity and severity of cracking were dependent on the applied microwave power level, exposure time, and the distance of the rock surface from the horn antenna. To better illustrate the effect of surface temperature changes on the irradiated specimens and their subsequent pre-conditioning (fracturing/spallation), for every experiment, an image of the topmost specimen in which the greatest damage occurred was captured and is shown in Figure 5.6. As mentioned, in addition to the visible cracks, several invisible microcracks occurred in the specimens as a result of single-mode microwave treatments. Thus, in phase II of the research, the invisible microcracking behavior of basalt with respect to different microwave conditions was studied by conducting SEM image analysis.



Figure 5.6: Illustration of visible crack development at the surface of the topmost basalt specimens irradiated at 60 s microwave exposure and different power levels and distances from the horn antenna

When the blocks of basalt were irradiated at 3 kW power, no visible cracking was observed until the distance from the antenna was 5 cm. A similar result, no visible cracks in the topmost specimen, was observed for the following microwave operating parameters:  $P = 9 \text{ kW}$ ,  $d = 20 \text{ cm}$ ;  $P = 9 \text{ kW}$ ,  $d = 25 \text{ cm}$ ;  $P = 9 \text{ kW}$ ,  $d = 30 \text{ cm}$ ;  $P = 15 \text{ kW}$ ,  $d = 25 \text{ cm}$ ; and  $P = 15 \text{ kW}$ ,  $d = 30 \text{ cm}$ . In addition, for the irradiated specimens under  $P = 3 \text{ kW}$ ,  $d = 5 \text{ cm}$ ;  $P = 9 \text{ kW}$ ,  $d = 15 \text{ cm}$ ; and  $P = 15 \text{ kW}$ ,  $d = 20 \text{ cm}$ , cracks scarcely occurred on the four sides radiating out from the center (see the yellow tracking lines in Figure 5.6). A more severe case occurred when the specimens were exposed to microwave treatments with the following input operating parameters:  $P = 9 \text{ kW}$ ,  $d = 10 \text{ cm}$ ;  $P = 9 \text{ kW}$ ,  $d = 5 \text{ cm}$ ;  $P = 15 \text{ kW}$ ,  $d = 15 \text{ cm}$ ;  $P = 15 \text{ kW}$ ,  $d = 10 \text{ cm}$ ; and  $P = 15 \text{ kW}$ ,  $d = 5 \text{ cm}$ . In all these conditions, hot spots on the top surface of each specimen were created (see Figures 5.4 and 5.5). Because of these hot spots, temperature changes occur at the surface of an irradiated rock specimen, which later result in thermally-induced microcracks and subsequent fracturing. In some cases, because of the high temperature differences between rock particles, a spallation at the area of the highest temperature region resulted. For example, it can be seen that for the cases in which the blocks of basalt were irradiated at 9 kW power level and 60s exposure, a spallation was initiated



only at 5 cm and 10 cm; and for the cases where the blocks were irradiated at 15 kW power level and 60s exposure, a spallation was initiated only at 5 cm, 10 cm, and 15 cm. (Refer to the thermal images given in Figures 5.4 and 5.5; strong surface temperature changes at the top center of the irradiated specimens can be observed from the surface temperature distributions for these cases.) However, the disintegrated segments had various thicknesses of 0.2 to 9 mm that varied in size and shape. For example, as a result of the irradiation at  $P = 15$  kW and  $d = 5$  cm, an area of  $10.5$  cm  $\times$   $6.5$  cm was separated from near the center of the topmost specimen. By changing it to 9 kW and 10 cm, the disintegrated area became smaller, with an area of  $4.1$  cm  $\times$   $3.2$  cm. In some cases, not only the topmost specimen showed spallation and visual cracking, the second specimen located beneath the first specimen was also cracked. However, since the second specimen was located beneath the first, confinement pressure from the weight of the first specimen kept the first specimen intact. Figure 5.7 illustrates the spallation mechanism of a block exposed to a microwave irradiation at 15 kW power level and 60s exposure time.

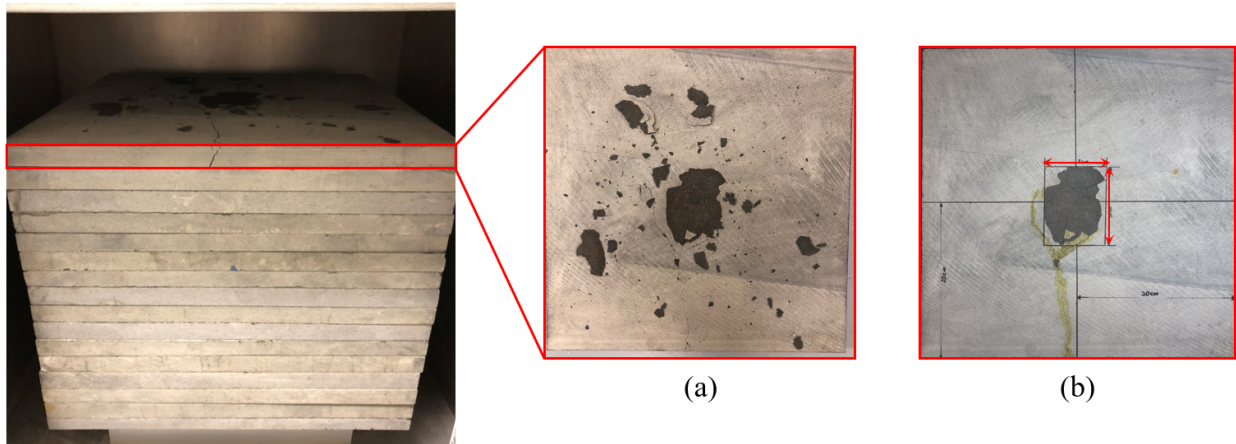


Figure 5.7: Illustration of the block of basalt after 60s exposure to 15 kW power at 5 cm distance from the antenna: (a) shows the first irradiated specimen and spallation at its top center surface and (b) gives the dimensions of a piece of rock chipped from the top center of the specimen

The mechanism of spallation in the irradiated specimens is as follows. The thermal expansion of the high temperature affected area tends to expand more toward the weakest confinement regions around the area, which results in creating a tension stress region in the center of the irradiated specimen and a shearing stress zone around the edge of the chip to be potentially disintegrated from the rock's surface. To better understand this mechanism, a conceptual illustration of the mechanism of spallation is given in Figure 5.8.

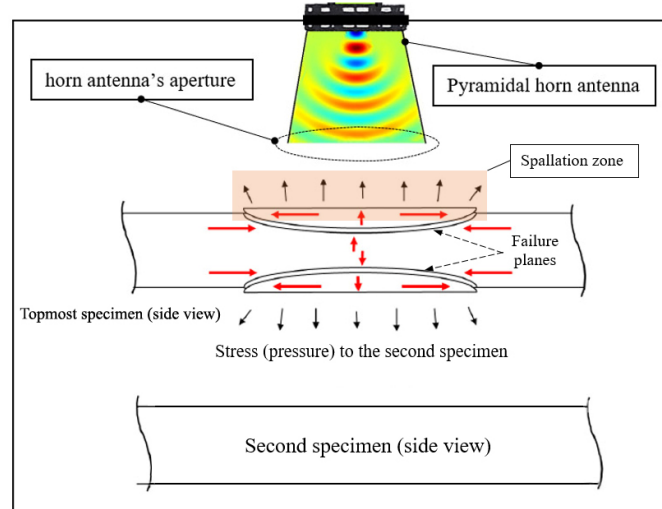


Figure 5.8: Spallation mechanism of the topmost specimen of basalt after microwave irradiation

From the conceptual figure above, it can be inferred that the mechanism of rock breakage by single-mode microwaves acts according to one or more of the following behaviors: (1) initiation of diagonally cracking from the center of the rock surface to the edge, (2) spallation from the center of the surface of the rock specimen facing the microwave horn antenna's aperture, and in harsh conditions (3) severe breakage and shattering as the specimen bursts from its center.

In conclusion, it can be deduced from the above results that all three operating parameters of the microwave system, i.e. input power level, exposure time, and distance from the microwave horn antenna, contribute to the process of rock heating and pre-conditioning by single-mode microwave irradiation. In following sections, the effects of each of these parameters on the heating of the specimens are presented and discussed, separately, to reach a better overall conclusion.

### 5.2.2.1 Effect of distance from microwave horn antenna

To study the effect of the distance of the rock blocks from the microwave horn antenna, first the results of thermal images (surface temperature distribution) from the blocks of basalt with changing volumes (see Figures 5.4 and 5.5) are compared and analyzed for different distances from the horn antenna. To this end, the temperatures at a point located at the top center surface of the topmost specimen were recorded for all irradiated specimens under different microwave conditions. Then, the recorded values were subtracted from the initial temperature of the rock before the experiment to represent the actual surface temperature change in the basalt specimens. The obtained values of temperature changes in the irradiated specimens, at different distances from the horn antenna, are plotted for the three power levels of 3, 9, and 15 kW, as shown in Figure 5.9.

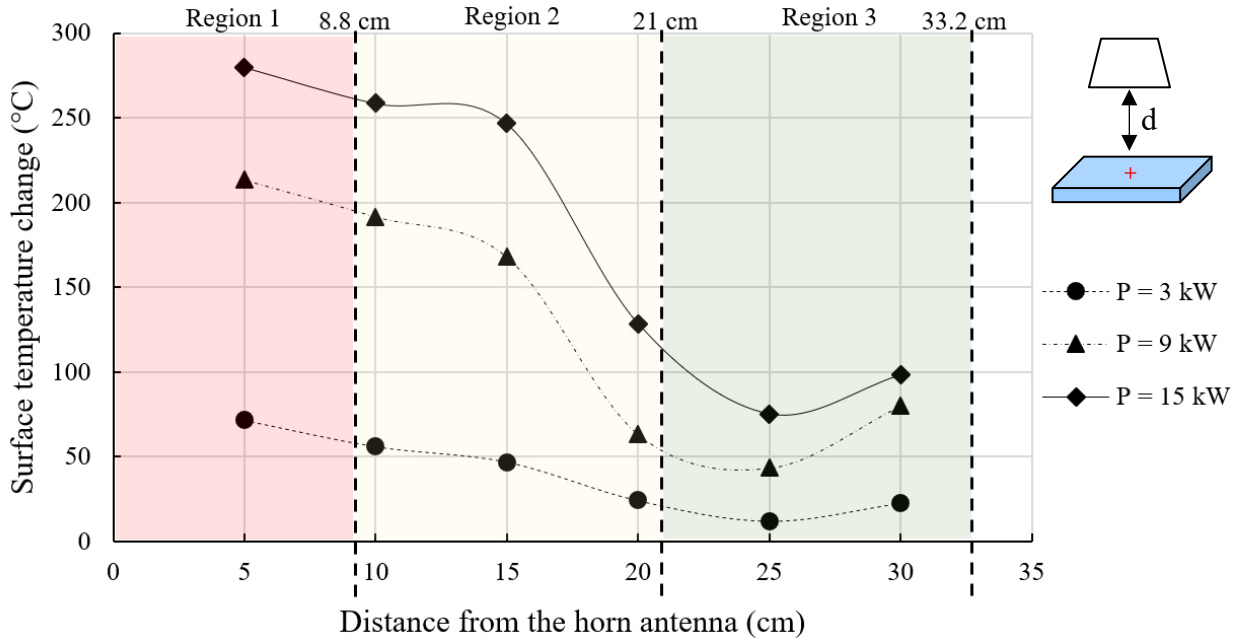


Figure 5.9: Distribution of the surface temperature changes obtained at the top center of the topmost basalt specimens irradiated at 60s exposure and various distances from the horn antenna

It can be seen that the behavior of the surface temperature changes in the blocks with changing volumes is directly related to the attenuation of waves in a dielectric material (see section 3.2.5 for more details). As the electromagnetic wave propagates, different nodes/modes of microwave energy in which more energy is concentrated are created by the waves' alternations. Different distances from the horn antenna's aperture affect electric field distribution and subsequently temperature distribution at the top surface of the rock blocks. To discuss this matter in detail, the following three different regions are assigned and shaded in Figure 5.9. Region 1 is when the distance from the horn antenna was set at a value between 0 to 8.8 cm, and the direction of the affected high-temperature area at the top surface of the specimens was parallel to the direction of the horn's width (see thermal images of 5 cm distance in Figure 5.4). Region 2 is when the distance from the horn antenna was set at a value between 8.8 to 21 cm, and the direction of the affected high-temperature area at the top surface of the specimens was perpendicular to the direction of the horn's width (see Figure 5.5). Region 3 is when the distance from the horn antenna was set at a value between 21 to 33.2 cm, and the direction of the affected high-temperature area at the top surface of the specimens was again parallel to the direction of the horn's width (see thermal images of 25 cm and 30 cm distances in Figure 5.4). As discussed earlier, the distance between each mode is directly related to the wavelength of the standing electromagnetic wave. An

analytical schematic of the attenuation of waves in the blocks of basalt with changing volumes is depicted in Figure 5.10.

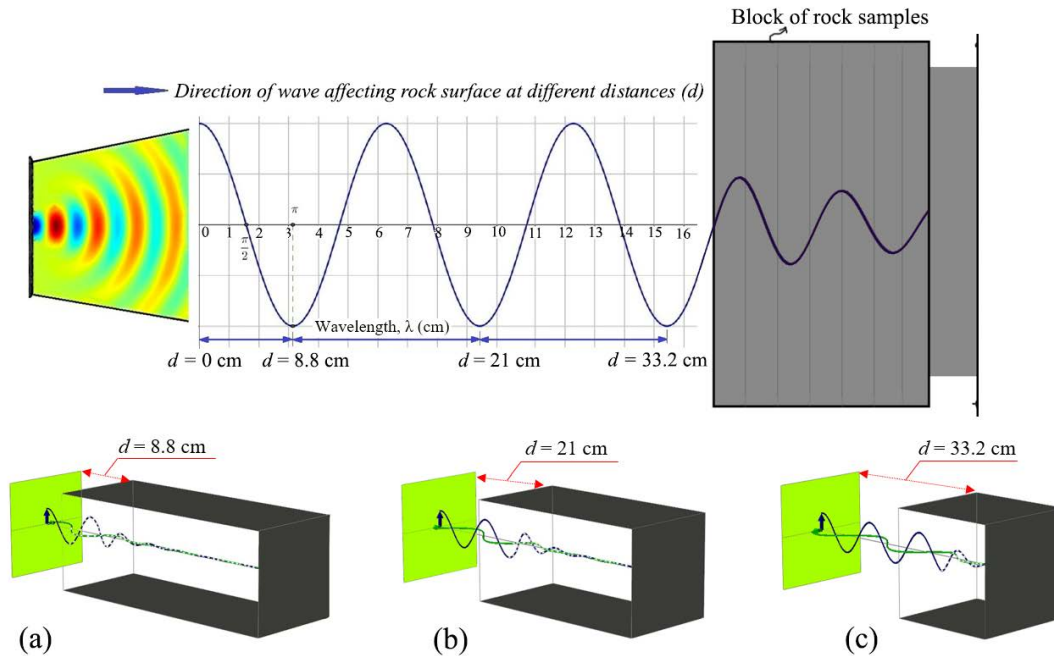


Figure 5.10. Schematic of the applied standing waves from the waveguide horn antenna to the surface of rock at different wavelengths and distances from the horn antenna where (a)  $d = 8.8$  cm, (b)  $d = 21$  cm, and (c)  $d = 33.2$  cm. Here it should be noted that the intersection of the solid (-) and dashed lines (--) is where the electromagnetic waves touch the surface of the topmost specimen, solid lines show how the waves propagate in air from the waveguide port to the rock surface, and dashed lines represent how the waves are absorbed and attenuated inside the rock block.

From the results discussed above, it can be concluded that the distance of 5 cm from the microwave horn antenna achieves the highest heating and pre-conditioning in cases where the volumes of the rock blocks are changed according to the desired distances from the horn antenna. An overall conclusion can also be drawn; the closer the distance of the rock's surface to the wavelength of the standing electromagnetic waves, the more heat dissipates at the surface of the rock and its pre-conditioning (cracking, spallation, and breakage).

Now, it is time to investigate the effect of distance from the microwave horn antenna on surface temperature changes with blocks of basalt kept at constant volumes and exposed at different distances from the horn antenna. To this end, three blocks with the following specifications were prepared: block of 1 specimen, block with 2 specimens stacked up, and block with 3 specimens stacked up. Then, these three volumes of basalt were separately irradiated in the

single-mode microwave cavity at a constant 3 kW power level and 60s microwave exposure and various distances from 5 cm to 20 cm. It should be noted that the reason why these experiments were performed at 3 kW for the study of the effect of distance from the horn antenna was that at 60s exposure, the only power level at which no major cracking and/or spallation occurred was 3 kW. While at all the other power levels at 60s, cracking at the top center was observed. In most cases, the surface cracking on a rock specimen affected the temperature distribution/profile captured by the thermal image camera. Since this was not the intent of the present investigation, the 3 kW power level was found to be the most appropriate power level for 60s microwave exposure.

After microwave irradiation tests, with the same procedure as outlined in the beginning of this section, a center point at the top surface of the irradiated blocks was chosen for measuring the surface temperature values by the thermal camera. For each test condition, a “surface temperature change” was calculated from the measured values of the top center surface temperature values subtracted from the initial temperature of the rock to conduct a valid, trustworthy thermal analysis. Figure 5.11 shows the results of experimental tests of single-mode microwave irradiation on the blocks of basalt at 3 kW power and 60s microwave exposure. The data presented in this figure are the averaged top center surface temperatures from triplicate measurements calculated for each test condition. In total, twelve experiments were conducted to obtain the following plots.

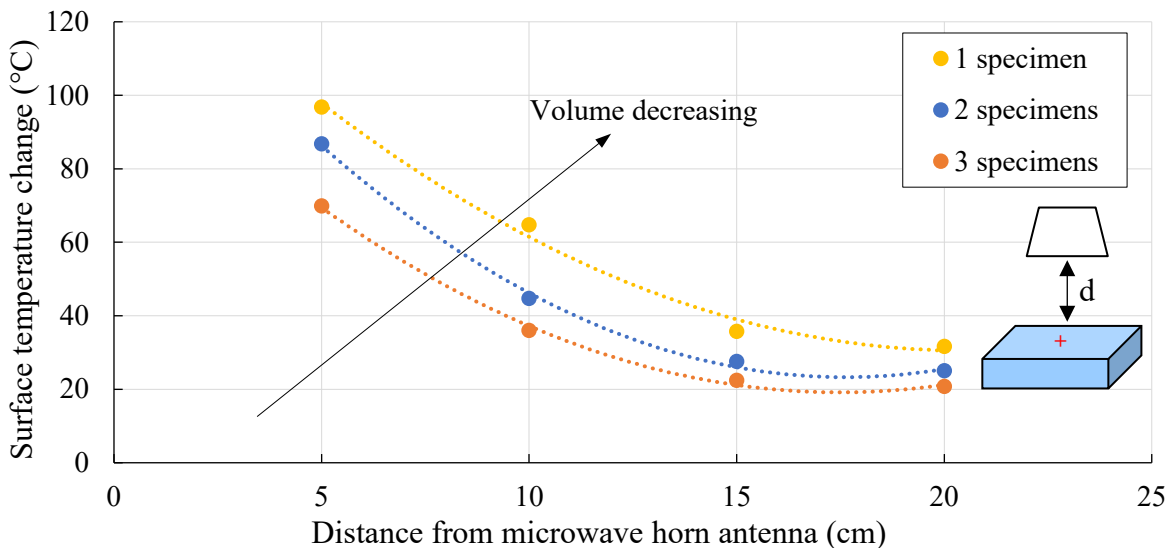


Figure 5.11: Effect of distance from microwave horn antenna on surface temperature change of basalt for three different volumes of blocks comprising 1 specimen, 2 specimens, and 3 specimens after their exposure to a 3 kW microwave power at 60s



At the 3 kW power level, the temperature change at the top center of the rock surfaces decreased linearly when the distance from the antenna decreased from 5 cm to 15 cm. However, for distances of more than 15 cm, the temperature changes evened out. This indicates that the effect of the distance from the horn antenna is very important at short distances where the first wavelength of the microwaves occurs. Higher distances from the microwave horn antenna result in low heating at the rock surface. Thus, it can be assumed that the overall tendency of the trend is exponential; but at short distances (5-15 cm) from the microwave horn antenna, the heating rate of the rock behaves linearly; and rock temperature increases at distances closer to the horn antenna's aperture. It can be seen that with higher rock volumes, less temperature change was effected at the surface of the basalt. This is directly related to the dissipation of heat with respect to the applied electromagnetic waves. The surface of rock absorbs much of the energy emitted; therefore, by increasing rock volume, the change in surface temperature decreases according to the law of thermodynamics.

#### **5.2.2.2 Effect of microwave power level**

It has already been observed that higher power levels result in higher electric and magnetic field intensity, which further contributes to better microwave heating and pre-conditioning within the same exposure time. However, an economic benefit should be considered for industrial applications. In the application of single-mode microwave irradiation for hard rock heating and pre-conditioning, an investigation on the effect of microwave power levels should be conducted simultaneously with the effect of the distance from the microwave horn antenna. This means that by deliberate selection of the input power level of the microwave and a distance at which a rock block absorbs maximum electric field intensity, less energy is needed for maximum heating and pre-conditioning effect. Figure 5.12 illustrates a reasonable thermal analysis from the results of surface temperature measurements at rock blocks irradiated at two high-power microwave treatments and various distances from the microwave horn antenna. The figure shows the maximum temperature change, which is obtained by subtracting the maximum temperature values captured at the surface of the irradiated blocks from their initial temperatures, with respect to different input microwave power levels at a constant 60s microwave exposure. The two plots are obtained for the blocks of basalt with a constant volume of 0.019 (m<sup>3</sup>) irradiated at two power levels of 3 kW and 9 kW and set at various distances from the horn antenna in the single-mode

microwave cavity system (see Table 5.1). The figure itself provides very important information about the combination of power level and distance from the antenna on the dissipation of heat at rock surfaces.

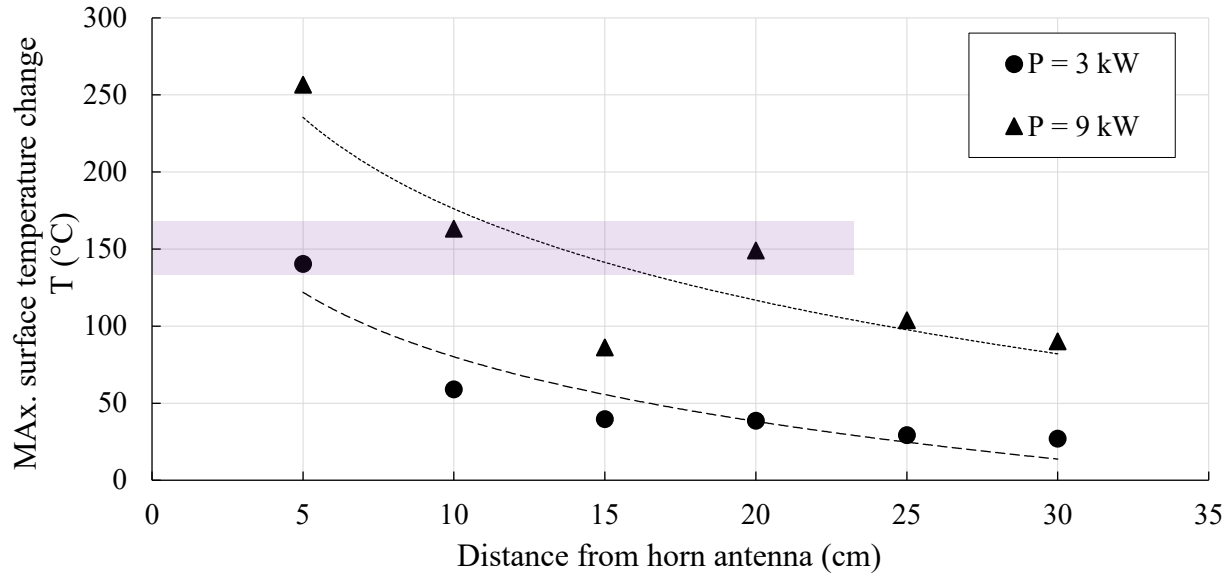


Figure 5.12: Effect of microwave power level on maximum surface temperature change in blocks of basalt irradiated at 60s microwave exposure and various distances from the horn antenna

It can be inferred that (1) as the shaded area in Figure 5.12 shows, the heat dissipated at the surface of the rock blocks and the temperature change achieved in the irradiated basalt at 9 kW power and distances of 10 cm and 20 cm are almost the same when compared with the block irradiated at 3 kW and 5 cm; (2) the effect of distance from the horn antenna is less important at low microwave power levels (e.g. 3 kW), whereas high microwave power levels (e.g. 9 kW) result in a significant variation when the distance from the horn antenna changes from 5 cm to 25 cm. Thus, it can be concluded comprehensively that the treatment of a hard rock with high microwave power level at a distance in which the rock surface is located at the wavelength of the electromagnetic waves gives maximum heating and pre-conditioning of the rock surface exposed to single-mode microwave treatment.

Additionally, Figure 5.13 shows a more in-depth analysis on the effect of input microwave power density for various experimental conditions on the maximum surface temperature change of the volume changing blocks of basalt. The plots are depicted with respect to different distances from the horn antenna; therefore, one can observe that as the distance from the antenna increased, fewer maximum surface temperature changes were obtained.

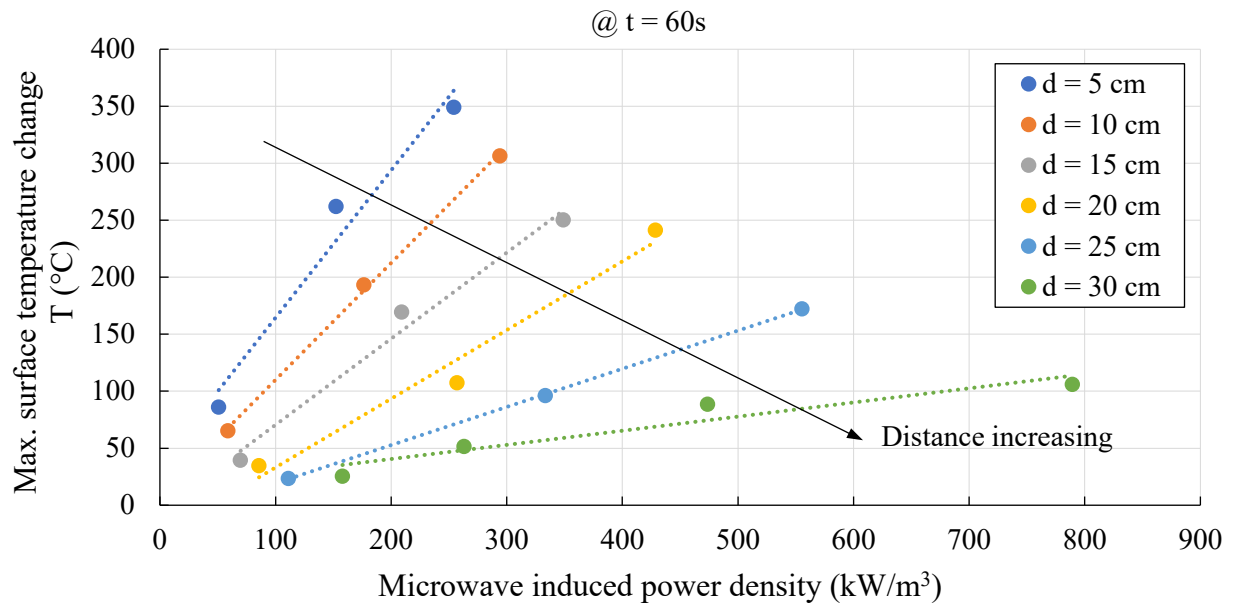


Figure 5.13: Effect of microwave induced power density on maximum surface temperature changes in the volume changing blocks of basalt irradiated at various distances from the horn antenna

### 5.2.2.3 Effect of microwave exposure time: an energy effectiveness analysis of single-mode microwave irradiation

The investigation of the energy effectiveness of microwave irradiation on hard rocks is usually analyzed by the two important operating parameters of microwave systems: power level and exposure time. However, when single-mode microwave cavity systems are employed, the effect of the distance from the microwave horn antenna is another factor to consider in analyzing the energy effectiveness of the single-mode microwave irradiation effect on hard rock heating and pre-conditioning. Thus, in this section, the results of experimental tests of single-mode microwave irradiation of basalt at various input microwave energy inputs and distances from the horn antenna are presented. The effect of microwave energy inputs on the maximum surface temperature changes of the volume changing blocks of basalt is depicted in Figure 5.14. The results confirm that at 5 cm distance from the horn antenna, the obtained surface temperature change was the highest compared to the other distances. Moreover, the trend changes show that regardless of the microwave energy inputs, with increasing distances from the horn antenna, less maximum surface temperature was achieved on the rock blocks. Furthermore, in Figure 5.15, two microwave exposure times of 60s and 120s were compared for the heating rates at the surface of the rock blocks obtained at different distances from the microwave horn antenna.

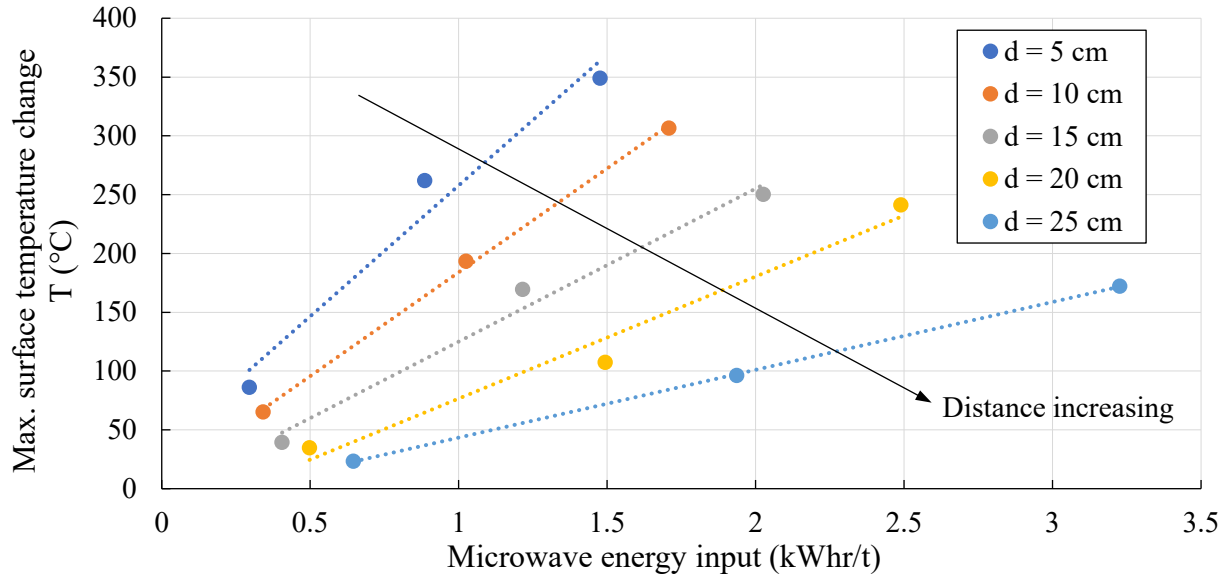


Figure 5.14: Effect of microwave energy input on maximum surface temperature change in blocks of basalt irradiated at various distances from the horn antenna

The power absorbed and dissipated in a rock is directly related to the heating rate of the specimens. Thus, without taking into account the exposure time, the heating rate decreased linearly with distance from the horn antenna. This behavior makes sense because microwave energy dissipates quickly and loses its intensity once the electromagnetic waves exit the waveguide and enter the open air in the cavity.

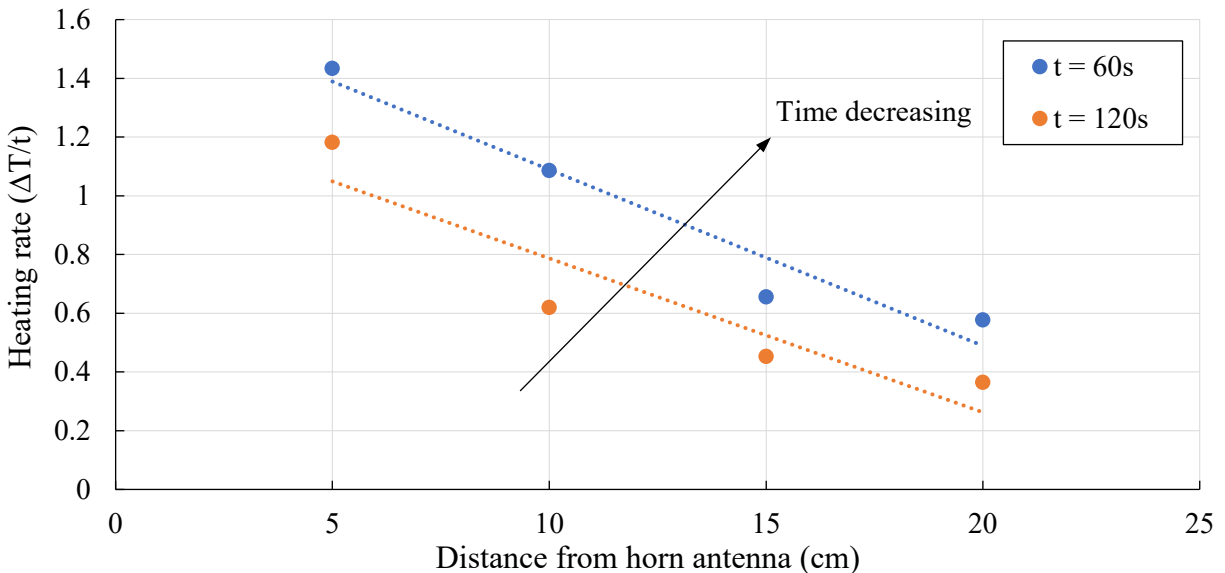


Figure 5.15: The results of maximum temperature difference change on the rock blocks over distance from the horn antenna at 60s and 120s exposure times at 30 kW power level

## **5.3 Phase II: SEM image analysis from surface microcrack quantification**

### **5.3.1 Methodology and procedures**

The present phase of the research investigates the microstructural responses of the specimens of basalt after single-mode microwave treatments by using the SEM image analysis. Scanning electron microscopy is one of the most advanced technologies for the quantification and analysis of microstructural responses of various materials (Brodusch et al., 2018), especially hard rocks and minerals (Rodriguez1 et al., 2014). SEM analysis is comparatively more useful in studies that investigate quantification of microstructural properties such as microcracks and voids. The SEM images of microcracks help the user get a visual and conceptual understanding of the mechanism of microcrack development in the irradiated rock specimens with different microwave conditions in terms of the number/length and density of microcracks created in the irradiated specimens at one specific area captured for all case studies.

The methods utilized in this phase of the research involve the following four steps:

- 1- Irradiating the blocks of basalt in the single-mode microwave cavity system at different microwave operating parameters,
- 2- Preparing cylindrical core samples from the center of the topmost specimens of each irradiated block using a drill bit with an inner radius of 0.5 cm,
- 3- Capturing SEM images from the top center of the cylindrical core samples,
- 4- Performing image processing and analyzing the captured SEM images using ImageJ software for the quantification of surface microcracks.

The details of the above-listed procedures for the quantification of surface microcracks in the basalt specimens irradiated at different microwave operating parameters are explained as follows. First, several specimens of basalt were placed on top of each other in the microwave cavity—forming a block of basalt—until they reached the desired distance from the microwave horn antenna, depending upon each experimental configuration. Then single-mode microwave irradiation tests were performed for a total of eleven case studies. The information about these case studies and their corresponding microwave operating parameters for the irradiation tests are given in Table 5.2. In this table, a nontreated cylindrical core sample was drilled from a nontreated specimen and the case no. 0 was assigned to it in order to better compare the results of microcracks.

Table 5.2: The designed case studies with their input microwave operating parameters for the single-mode microwave irradiation tests on the specimens of basalt

Case no.	0	1	2	3	4	5	6	7	8	9	10	11
MW* power level, P (kW)	Nontreated	3	3	3	3	9	9	9	15	15	3	9
MW exposure time, t (s)	Nontreated	60	60	60	60	60	60	60	60	60	120	120
Distance from the MW horn antenna, d (cm)	Nontreated	5	15	20	25	15	20	25	20	25	5	15

\* In this table, the word microwave is abbreviated as MW.

After sequentially irradiating the specimens according to the conditions listed in Table 5.2, in every experiment, the topmost irradiated specimen was used to drill cylindrical core samples for later SEM imaging. Therefore, in total, eleven core samples from the irradiated specimens and one core sample from a nontreated specimen were prepared for SEM image analysis. Figure 5.16 shows an overview of the process of microwave irradiation of the specimens and subsequent process of drilling core samples from the center of the topmost specimen for SEM imaging.

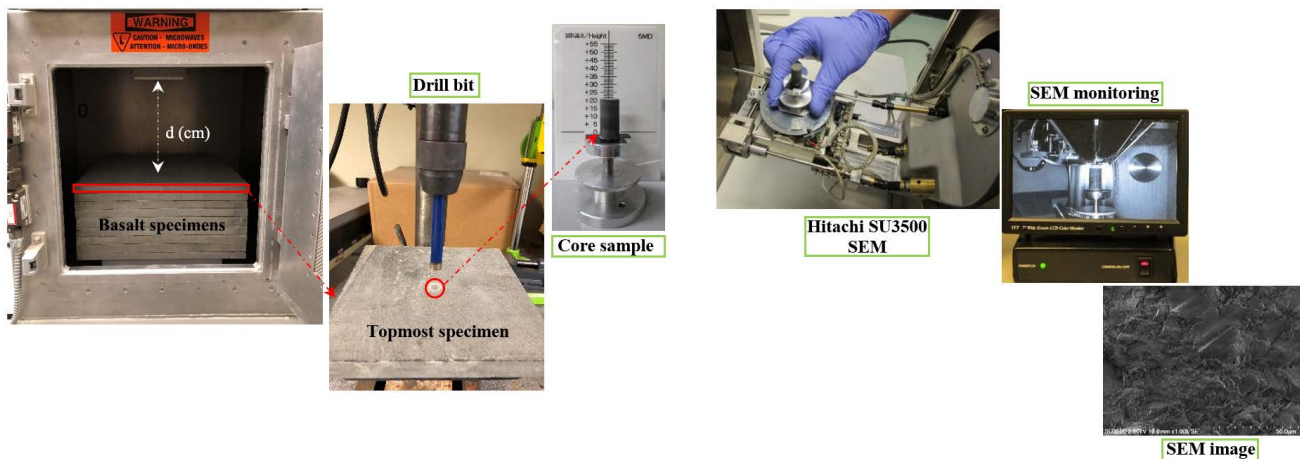


Figure 5.16: Schematic illustration of (a) the single-mode microwave system setup with the specimens placed inside the cavity and below the horn and the process of drilling core sample with a dimension of  $r = 0.5$  cm and  $h = 2$  cm from the center of the topmost irradiated specimen, (b) the SEM equipment set-up with the core sample placed inside the SEM cavity for microcrack imaging. In this study, after microwave treatment of the specimens and preparation of cylindrical core samples from the top center of the specimens for all eleven case studies, SEM images were captured from the center point of the core samples with a resolution at 2 kV and 200  $\mu\text{m}$ . ImageJ



software developed by the National Institute of Health (NIH) was then used to conduct image processing on the SEM images (Abramoff et al., 2004). This software has the capability to perform various operations, such as binary thresholding and area measurement based on Java language. The obtained data from SEM images was analyzed and compared for different microwave conditions; the results are provided in the following section and a parametric study based on data from microcrack quantification is discussed.

### 5.3.2 Results of SEM images and discussion

The results of the SEM images are shown in Figure 5.17. The plots follow the case studies listed in Table 5.2. The specified case numbers are shown under each plot. It can be seen that the intensity of microcracks reduces when the power level decreases from 15 kW to 3 kW, the exposure time decreases from 120s to 60s, and the distance from the antenna increases from 5 cm to 25 cm.

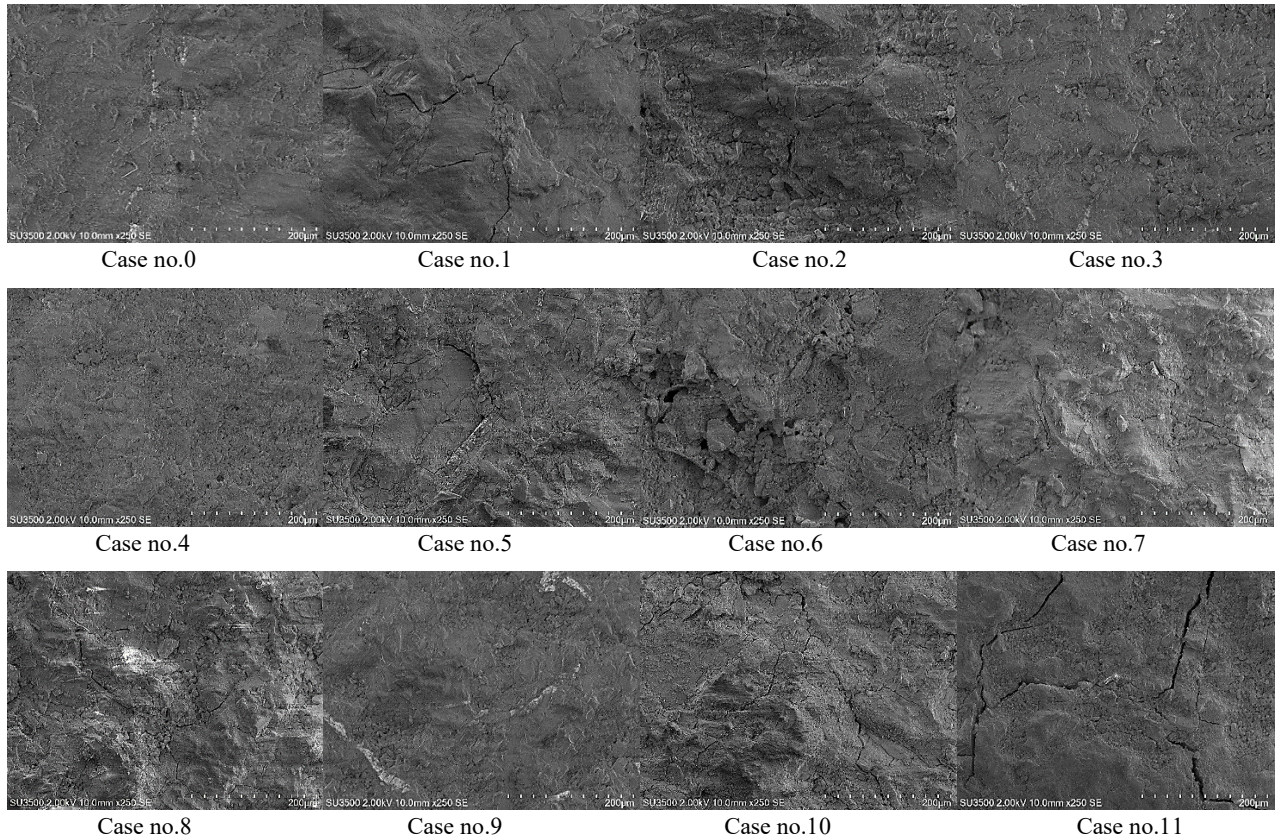


Figure 5.17: The results of SEM images from cylindrical cored samples under different experimental conditions

The first step of image processing was to conduct segmentation of the images into binary images through the brightness thresholding approach. This makes the SEM images black and white. By this process, ImageJ changes the intensities of image pixels that will highlight the regions of interest—in this study, are microcracks. For each plot of Figure 5.17, the low threshold level was set at zero and the best threshold level was determined by comparing the original gray image with the image after application of manual thresholding on the binary image. After being converted to the binary mode, all the SEM images were manually mapped, and the total number of crack lengths and crack density for all the case studies was obtained. However, it is worth mentioning here that microcracks are very elongated structures; therefore, length to width (referred to as shape factor) analysis was applied for different geometries. The corresponding data obtained for the length and density of cracks for the different case studies/numbers after image processing on the SEM images are summarized in Table 5.3.

Table 5.3: Results of crack quantification analysis from SEM images of the core samples

Case no.	Cracks length ( $\mu\text{m}$ )	Image field ( $\mu\text{m}^2$ )	Crack density ( $\mu\text{m}/\mu\text{m}^2$ )
0	432.15	192,482	0.002245145
1	1310.64	192,482	0.006809156
2	1182.07	192,482	0.006141198
3	943.74	192,482	0.004903004
4	780.42	192,482	0.004054509
5	1670.72	192,482	0.008679877
6	1322.91	192,482	0.006872902
7	1107.085	192,482	0.005751629
8	1432.11	192,482	0.007440228
9	1216.32	192,482	0.006319136
10	1540.02	192,482	0.008000852
11	1861.81	192,482	0.009672645

The above results indicate the presence of microcracks in the given core samples of every case study. Maximum lengths of cracks were 1670.72  $\mu\text{m}$  and 1861.81  $\mu\text{m}$ , for 60s and 120s exposure times, respectively. These two values were achieved when a 3 kW power level was applied at the 5 cm distance from the microwave horn antenna. Therefore, it can be concluded that the effect of exposure time was significant; longer exposure times were responsible for more



extensive cracks. In addition, for a better understanding of the cracking mechanism, a crack quantification analysis was done on the nontreated sample compared to the treated samples. The result for the nontreated sample is shown in case no.1 in Table 5.2. When comparing results from the irradiated samples with the nontreated sample, the effect of microwave input operating parameters is more visible. For example, by comparing cases 4 and 5, in which the crack length was under 1000  $\mu\text{m}$ , the effect of the distance from the horn antenna can be observed. As the distance from the antenna increases, the number of microcracks declines. The results from crack quantification analysis yield a better understanding of the mechanism of crack propagation in regard to differently applied microwave operating parameters.

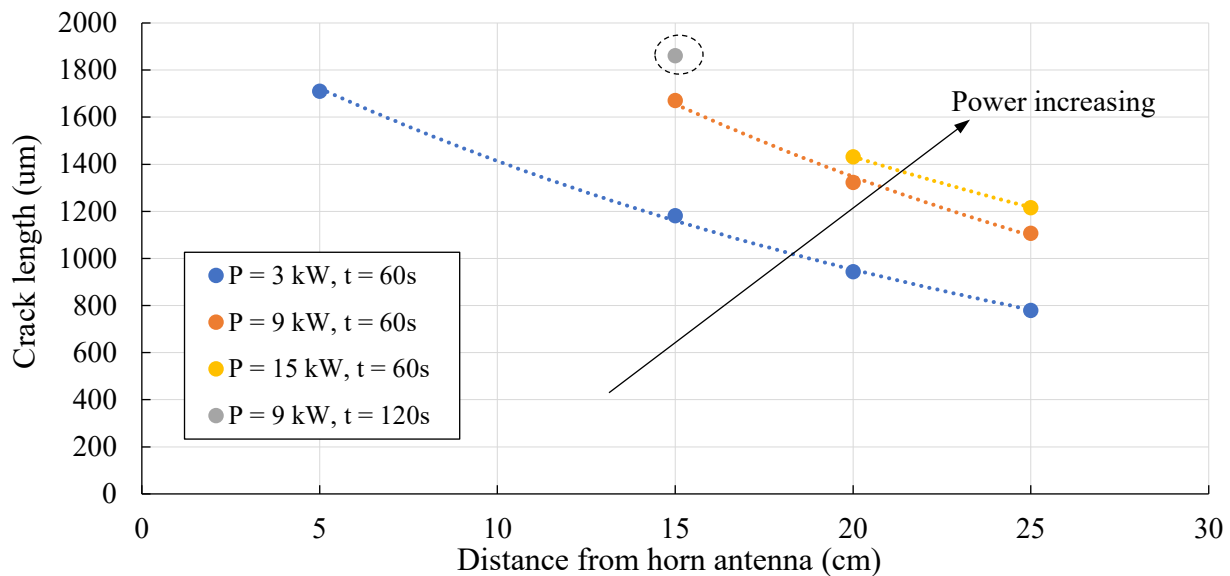


Figure 5.18: Effect of distance from horn antenna on overall crack length initiated at the surface of the topmost specimen after microwave irradiation tests with different operating parameters

The results of the crack quantification analysis shown in Figure 5.18 verify that the intensity of cracking was greatly dependent on the input power. It can be observed that a higher level of microwave power ( $P = 15 \text{ kW}$ ) results in greater crack lengths and densities. However, a longer exposure time, when  $t = 120\text{s}$ , was responsible for more extensive cracks created at the surface of the irradiated sample. This can also be seen visually from the results of SEM image provided in case no.11 of Figure 5.17; the longer exposure time, created denser and more extensive cracks. Moreover, a higher input microwave power contributes to complex physical and mechanical reactions, which include the elevation of internal pressure and decomposition of rock particles.

Figure 5.19 better illustrates how the input microwave power level affects the crack density results. It shows that the density of microcracks at the captured area differs, depending upon the applied microwave operating parameters and, particularly, the distance of the rock surface from the horn antenna.

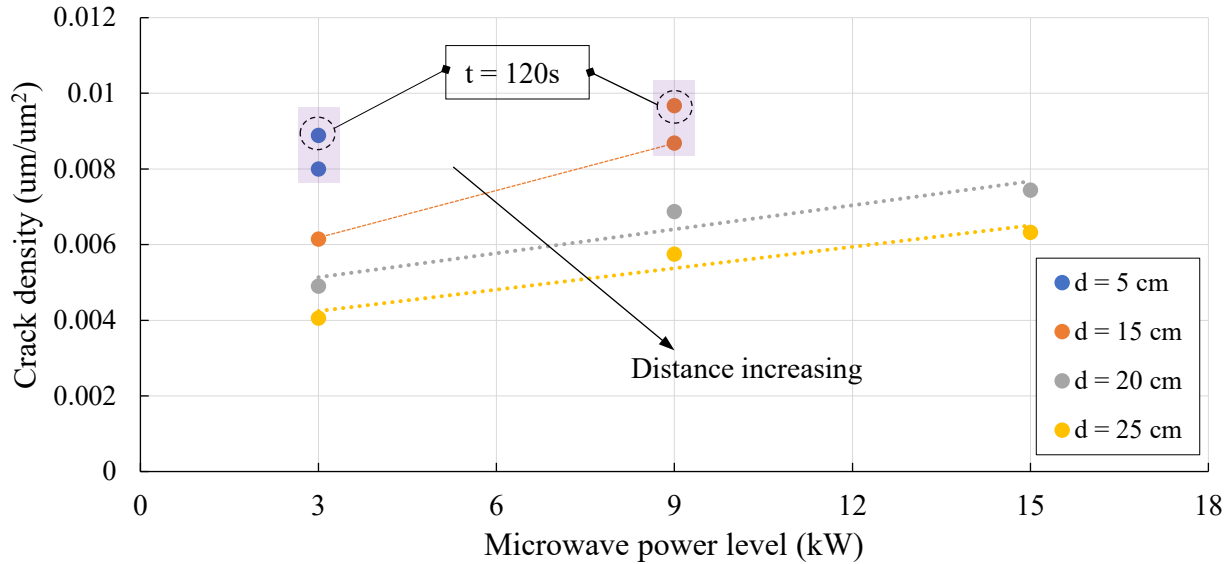


Figure 5.19: Effect of input microwave power level on crack density when the distance from the antenna changes from 5 cm to 25 cm

By comparing the data provided in Table 5.2, it can be seen that a higher level of microwave power results in greater crack lengths and densities. On closer inspection, however, at the same power level, a shorter distance from the antenna results in denser cracking. These observations can also be confirmed from the plots shown in Figure 5.19. With increasing distances from the horn antenna, the obtained crack density decreases regardless of the input microwave power. Moreover, as shown by the purple shaded area, increasing the microwave exposure duration increases the crack density in basalt, and this can be observed in the SEM images as well. Overall, from the results of the SEM analysis, it was found that the greater the microwave exposure time, the greater the number of microcracks created in the rock, and vice versa. More importantly, with short exposures to single-mode microwave irradiation and high input power levels, denser cracking was observed in the specimens when they were kept at the same distances from the horn antenna. In the following section, the results from micro-CT scans are provided.

#### 5.4 Phase III: Volumetric microcrack visualization from micro-CT scan

In this phase of the research, the specimens of basalt are first subjected to single-mode microwave irradiation tests at 5 cm distance from the horn antenna and power levels of 3 kW and 9 kW, respectively, under the same 120s microwave exposure. These microwave conditions were already tested and found to have most pre-conditioning (microcracking) effects on the surface of the specimens from the results of both thermal and SEM analyses. The purpose of conducting micro-CT scans, in addition to the SEM images, is to visually illustrate the microcracks created in the volume of the core samples that were drilled from the topmost specimens irradiated under different microwave conditions and to investigate how much the induced microcracks differ from one sample to another. To this end, the same core samples that were already drilled from the irradiated specimens and used in the SEM images were used to capture micro-CT images. It is worth mentioning that the maximum object size for the micro-CT chamber used in the present study was 27 mm in diameter and maximum 70 mm in length. A schematic illustration of the core sample placement in the vacuum chamber of the micro-CT scanner is shown in Figure 5.20.

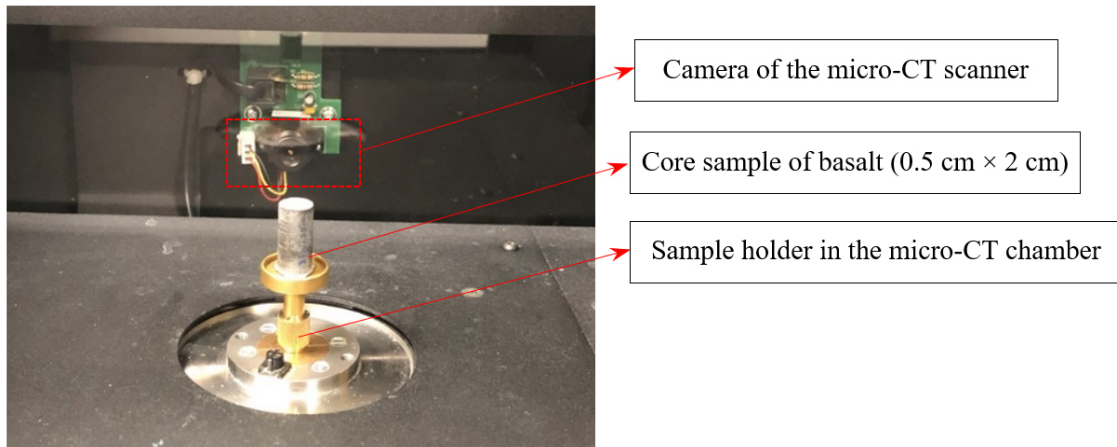


Figure 5.20: The placement of a cylindrical core sample of an irradiated basalt specimen in the chamber of the micro-CT scanner (model SKYSAN-1172)

As shown above, after adjusting the placement of the cylindrical core sample at a position directly in front of the micro-CT camera, micro-CT images were captured with the X-ray tube operating at 70 kV, 142  $\mu$ A, 1600ms exposure time, and a focal spot size of 5  $\mu$ m. The micro-CT images were then imported into an image-processing software, Bruker micro-CT reconstruction software, for processing, including 3D rendering and volume reconstruction. Volumetric reconstructions from the X-ray micro-CT data before and after microwave irradiation conditions were performed by

conducting the following image processing technique. First, the data obtained from the X-ray micro-CT scans, consisting of approximately 1500 2D slices, were categorized. The 3D models (volume renders) were then reconstructed from the 2D images with CTAn software from the FEI Company. The 3D images were processed by using a nonlocal filter and segmented to generate a binarized representation of the rock sample so that the network of cracks could be visualized in the cylindrical core model. A schematic illustration of a 3D image of a core sample of basalt after the reconstruction operation using Brucker micro-CT reconstruction software is shown in Figure 5.21(a). Moreover, to better illustrate and compare the results of volumetric microcracking in the core samples from the micro-CT scans, the results of the micro-CT images (volumetric renders) are depicted at one 2D vertical cut plane (bedding direction) and one 2D circumferential horizontal cut plane both captured from the middle of the core samples (see figure 5.21(b)).

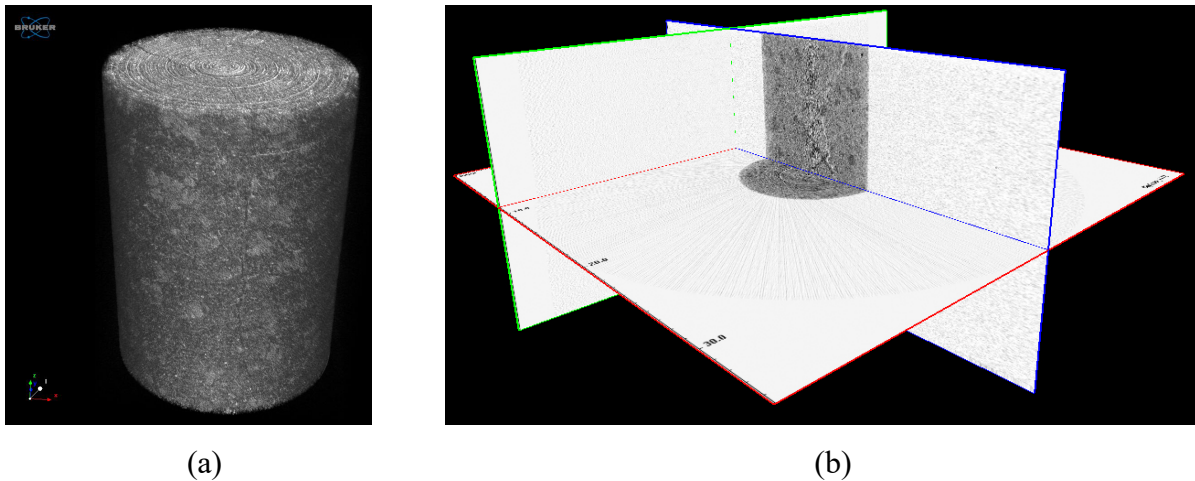


Figure 5.21: The results of (a) the 3D model of the core sample after reconstruction operation on raw data of micro-CT images and (b) the 2D cut planes at vertical and horizontal middle planes of a core sample

After the micro-CT images were processed as explained above, the results are shown in two different cut planes captured at the middle of the irradiated core samples. In order to compare the results of the irradiated specimens with a reference, a nontreated sample was also captured by the micro-CT scanner and its results are depicted in Figure 5.22. The figure shows that although some black spots can be observed in the micro-CT images of the nontreated sample (as this was also observed in the SEM images), these spots are referred to as voids instead of microcracks; therefore, no microcrack in the nontreated sample was found in its micro-CT image.

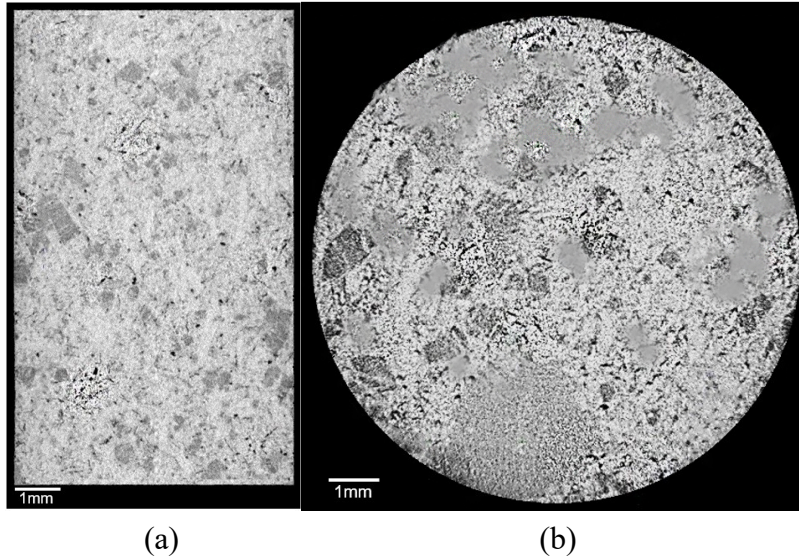


Figure 5.22: The result of image processing of micro-CT scan on a nontreated core sample on the 2D (a) vertical cut plane and (b) horizontal cut plane captured from the middle of the core sample. By comparing the image of the nontreated sample with the core sample irradiated at 3 kW microwave power under 120s exposure and 5 cm distance from the antenna, it can be seen that major microcracking occurred both at the vertical and horizontal cut planes in the irradiated core sample. To better compare the results of the micro-CT scan with the SEM image of the same core sample, Figure 5.23(c) is provided.

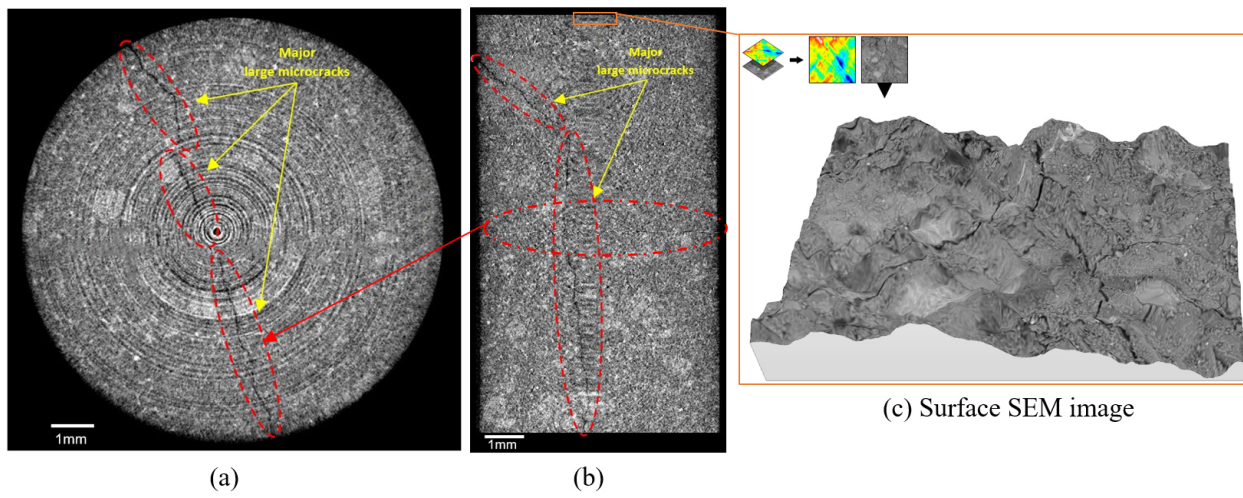


Figure 5.23: The results of image processing on a core sample drilled from an irradiated specimen by single-mode microwave irradiation at 3 kW and 120s exposure: (a) the processed 2D micro-CT image shown at the horizontal cut plane, (b) the processed 2D micro-CT image shown at the vertical cut plane, and (c) the SEM image captured from the top center of the core sample



Figure 5.24 shows the results of the irradiated specimen at 9 kW power level, 120s exposure, and the same distance of 5 cm. The 3D demonstrations of the SEM images were performed using the Mountains software from DIGITAL SURF. As expected, longer and denser cracks were created inside the core sample after this microwave treatment because of the higher power level. This confirms that the higher the microwave power input, the denser the microcracks created at the surface and in the volume of the rocks. Also, the cracks tend to be distributed vertically in a longitudinal direction.

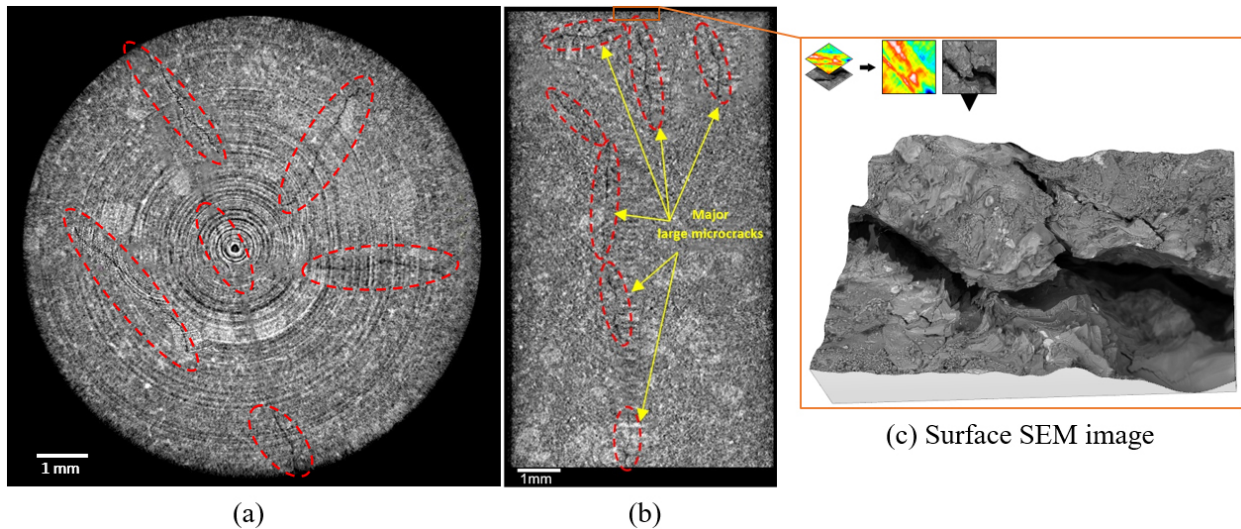


Figure 5.24: The results of image processing on a core sample drilled from an irradiated specimen by single-mode microwave irradiation at 9 kW and 120s exposure: (a) the processed 2D micro-CT image shown at the horizontal cut plane, (b) the processed 2D micro-CT image shown at the vertical cut plane, and (c) the SEM image captured from the top center of the core sample

The results of the phase III verify that the intensity of cracking depends greatly on the input power level of the microwave and the distance at which a rock is located in the single-mode microwave cavity. Moreover, a higher input microwave power level contributes to complex physical and mechanical reactions, which include the elevation of internal pressure and decomposition of particles. In fact, the mechanism of cracking comes from the unstable growth of cracks by shear forces (due to thermal strains), which propagate from the tips of pre-existing cracks towards the maximum principal (compressive) stress. This is the fundamental mechanism that produces microcracks in a rock specimen under microwave treatment.

## 5.5 Conclusions

In the present chapter, the effects of single-mode microwave irradiation with different operating parameters on specimens of basalt positioned at various distances from the horn antenna were investigated by thermal image analysis, SEM image analysis, and micro-CT scanning. In the single-mode microwave irradiation application for rock heating and pre-conditioning, this chapter demonstrated that the maximum impact from the applied electromagnetic waves occurred only when the rock blocks were positioned at distances on or close to the wavelengths of the traveling electromagnetic waves from the waveguide into the closed cavity. Thus, it is very important for potential users of the single-mode type of microwave cavity systems to find the distances where the wavelengths of the electromagnetic waves occur so that their rock samples have to be positioned at those distances or at least close to them for maximum heating and pre-conditioning. For the single-mode microwave cavity system used in the present study, it was experimentally found from all three investigating methods that at 5 cm distance from the horn antenna, maximum surface heating and pre-conditioning was obtained on the irradiated specimens regardless of the microwave input power level and exposure time set at different values. However, for the same distance from the horn antenna and power level, a longer microwave exposure duration was achieved: the greater the temperature change at the surface of the irradiated specimens, the less dense the microcracks but the greater their number.

The thermal images in this study reveal various aspects of rock heating by single-mode microwave irradiation, and the SEM images point to the determination of the effects of different microwave operating parameters on the surface pre-conditioning of basalt and possible creation of microcracks by the single mode microwave treatment. The results of the present study show that there is a significant difference between the number of microcracks present in samples irradiated at different power levels and distances from the antenna, and that a longer exposure time resulted in more severe cracks being created.

## Chapter 6

# Multiphysics study of multi-mode microwave irradiation effects on rock pre-conditioning and breakage

### Contents

---

<b>6.1 Introduction.....</b>	<b>130</b>
<b>6.2 Experimental tests of multi-mode microwave irradiation.....</b>	<b>132</b>
<b>6.3 Numerical modeling of multi-mode microwave irradiation.....</b>	<b>147</b>
<b>6.4 Conclusions .....</b>	<b>167</b>

---

### Preface

*This chapter presents a comprehensive study of multi-mode microwave irradiation effects on the pre-conditioning and breakage of four different rock types: basalt, granite, and two types of kimberlite, made up of different electrical and thermal properties. By employing both experimental methods and a numerical modeling technique, the chapter itself covers multi-mode microwave irradiation effects on rock heating and pre-conditioning and its energy-saving potential for future industrial applications. To this end, the chapter begins with an introduction to multi-mode microwave systems and their application in heating and pre-conditioning of rocks (section 6.1). Details of the experimental methods utilized and the procedures conducted for multi-mode microwave irradiation tests on the selected rock types are described (section 6.2). The chapter then introduces a novel approach for numerically simulating a multi-mode microwave cavity with a rotational stirrer fan, presents numerical models of the selected rocks irradiated at the same microwave conditions applied to the practical tests, validates the models with data obtained from the experimental calorimetric tests, and conducts a parametric study on the effect of variation in dielectric properties of the selected rock samples (section 6.3). Finally, the chapter ends with overall conclusions based on the findings of the experiments and the models (section 6.4).*



## 6.1 Introduction

The application of standard multi-mode microwave cavities, similar to those found in conventional kitchen microwave ovens, is very common, but an industrial application of this type of microwave cavity is still being investigated for maximum electric field strength and maximum efficiency as energy-saving potential. Multi-mode microwave cavities are closed metal boxes consisting of two dimensions with several wavelengths that support many modes (Kingman, 2009). The mechanism of a multi-mode microwave cavity is as follows. When electromagnetic waves propagate, nodes of energy (each known as a mode) are created by the constantly alternating wave. The distance between the nodes (modes) is directly related to the wavelength of the standing wave. There are always two dimensions specific to the waveguide that are usually smaller than the wavelength and cause the electromagnetic waves to travel in a third direction. Therefore, only one mode is generated if the end of the waveguide is closed and a specimen is located at an energy node either exactly in front of the waveguide outlet or at a distance farther from it, a single-mode cavity is created (see figure 6.1(a)).

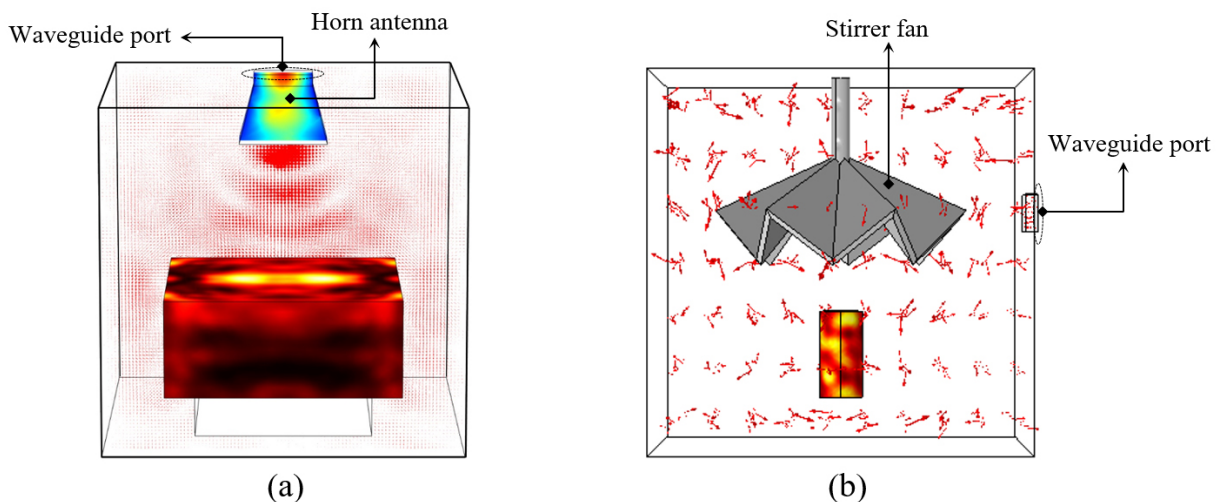


Figure 6.1: Conceptual sketch of (a) a single-mode microwave cavity system with horn antenna and (b) a multi-mode microwave cavity system with an umbrella-shaped stirrer fan

When two or more dimensions of a closed cavity are longer than one wavelength, more than one mode of energy is created; and therefore, a multi-mode cavity is constructed. The common way to achieve these dimensions for creating a multi-mode microwave system is by the use of a mode stirrer, which is usually called a “stirrer fan”. A stirrer fan is a metallic object, which is usually made up of the same material as the cavity, that has several blades with different angles

and is sometimes in the shape of an umbrella. The role of the stirrer fan is to be positioned in front of the waveguide outlet (port) inside the cavity in such a way that its blades face the waveguide port (see Figure 6.1(b)). When the stirrer fan rotates around its center line the incoming electromagnetic waves touch the blades at different angles; and, therefore, the direction of the standing electromagnetic waves changes according to the respective angle of the blade. A conceptual illustration of how the stirrer fan changes the direction of the electromagnetic waves from the waveguide port into the cavity is given in Figure 6.1(b).

The power density or electromagnetic energy absorption of a rock sample<sup>6</sup> under microwave irradiation depends on the electrical field strength,  $E$  (V/m), the frequency of microwaves,  $f$  (GHz), and the dielectric properties of the sample. The calculation of the power density is according to the following formula:

$$P_d = 2\pi f \varepsilon_0 \varepsilon'' E_{\text{rms}}^2 + 2\pi f \mu_0 \mu'' E_{\text{rms}}^2 \quad (6.1)$$

where  $f$  is the electromagnetic wave frequency,  $\varepsilon_0$  is the dielectric permittivity of a vacuum,  $\varepsilon''$  is imaginary part of complex permittivity (dielectric loss factor),  $E_{\text{rms}}$  is the electrical field,  $\mu_0$  is the magnetic permeability of a vacuum, and  $\mu''$  is the complex magnetic permeability (see section 3.1 for more comprehensive definitions of some of these terms). Since  $\mu''$  is equal to zero in nonmagnetic materials, the second part of equation (6.1) is not considered in the power density calculation. According to this equation, the heating rate increases with a stronger electric field intensity. In the application of multi-mode microwave cavities, the factors that influence the heat generated through dielectric materials (e.g. rock samples) are related to the sample's size, shape, and the microwave system's configuration ( Kingman et al., 2004). Thus, the aims of this chapter are to present the results of experimental tests of multi-mode microwave irradiation on various rock types with two different sample sizes and various microwave configurations. More importantly, the chapter presents the development of several numerical models whose results are validated against experimental data from calorimetric measurements for further investigations on the effects of multi-mode microwave irradiation on various rock types. The process of validating the numerical models with experimental calorimetric measurements is considered a novel approach, something never before published in the literature.

---

<sup>6</sup> In this chapter, the term 'sample' refers to cylindrical-shaped rock extractions of standard BTS and UCS sizes. In addition, it should be noted that the term 'specimen' refers only to the rectangular block-shaped basalt extractions used in the previous chapter.

## 6.2 Experimental tests of multi-mode microwave irradiation

### 6.2.1 Experimental conditions and procedures

In the present study, all microwave irradiation experiments on the selected rock types were performed in an industrial multi-mode microwave cavity system at a frequency of 2.45 GHz and different power levels ranging from 0 to 15 kW and at various exposure times. A schematic illustration of the multi-mode microwave system with its different components is provided in Figure 6.2. The figure shows a power level gauge for adjustment of the input power of the microwave system, a 480 V power supply, a magnetron, and a closed 60 cm × 60 cm × 60 cm cubic cavity with an umbrella-shaped stirrer fan located in front of the waveguide outlet (port) for propagating the incoming electromagnetic waves from the waveguide into the cavity; and therefore, causing maximum chaos to achieve a perfect multi-mode microwave cavity system.

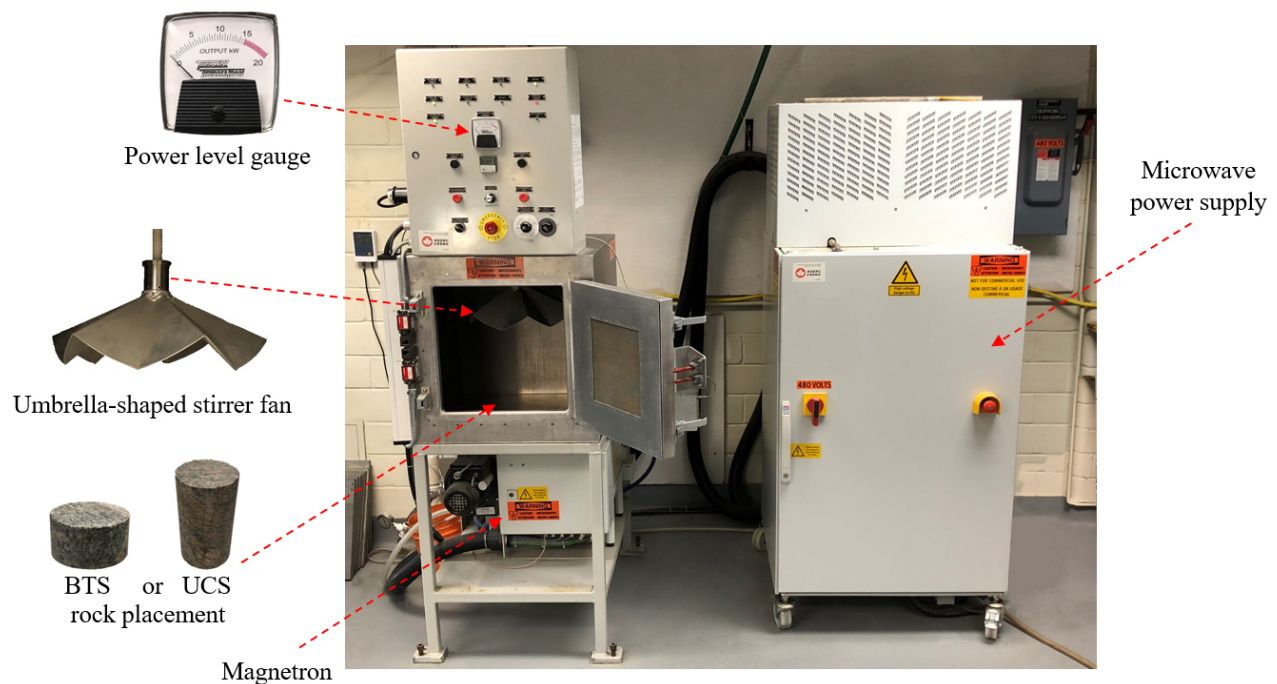


Figure 6.2: Industrial multi-mode, variable high-power (up to 15 kW) microwave cavity system in the Geomechanics Laboratory at McGill University

As discussed earlier in Chapter 4, two different sample sizes, standard BTS and UCS, were prepared from the selected rock types for multi-mode microwave irradiation experiments (see section 4.1 for more details). The height and diameter of each sample were measured by a digital Vernier caliper. Since the samples were selected from different rock types, the weight of each sample was measured using a digital balance with an accuracy of  $10^{-2}$  g. Mean height, diameter,

and weight from triplicate measurements were calculated for each sample and were used as inputs to the numerical models. The samples were then placed inside the cavity and subsequently irradiated according to the respective experimental conditions listed in Table 6.1.

Table 6.1: The experimental conditions for multi-mode microwave irradiation tests

Rock type	Sample size	Microwave power level, P (kW)	Microwave exposure time, t (s)
<b>Basalt</b>	UCS	5	40, 45, 60
		15	6, 7, 10, 11
	BTS	5	10, 16, 20
		12	8, 10, 12
<b>Granite</b>	UCS	5	45, 60, 65
		12	8, 10, 14
	BTS	5	30, 37, 50
		7	16, 25, 29
<b>Kimberlite #1</b>	UCS	5	10, 20
		12	6, 12
	BTS	5	6, 12
		7	6, 12
<b>Kimberlite #2*</b>	BTS	10	10

\*Note that because of the limitation of the number of samples available for this rock type, only one experimental setting was assigned and the result of this rock type was used for numerical model validation only.

After irradiating the samples with different microwave operating parameters and experimental configurations, thermal images were captured by a thermal camera from the surface of the irradiated samples for thermal analysis. Immediately after this step, calorimetric studies were conducted to measure the heat (energy) absorbed by the samples for further analyses on the energy effectiveness of multi-mode microwave cavities in the heating and pre-conditioning of rocks.

## 6.2.2 Calculation of microwave ramp-up time

One of the main advantages of employing the calorimetric test approach is its ability to measure the delay time of a microwave system. When microwave generators start to operate, a delay time occurs from when the microwave energy is generated and transmitted from the magnetron through the waveguide into the cavity until the microwave system is working at its full loading power (the desired power level). For instance, if a high-power microwave system needs to

be working at a 15 kW power level, there is a delay time from when the generator produces the

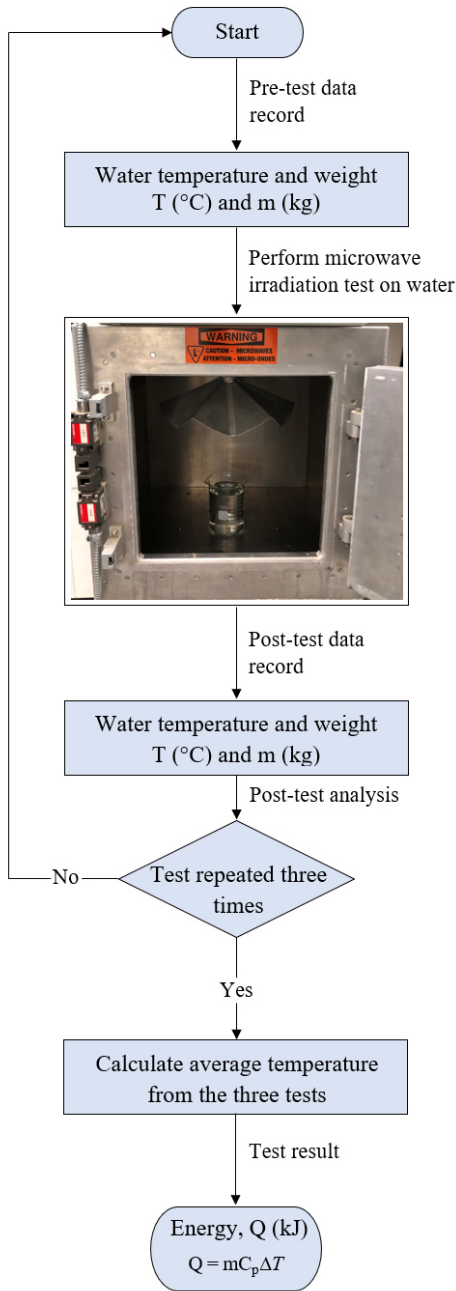


Figure 6.3: Experimental procedures for calorimetric studies

required microwave energy at 0 kW until full loading condition, that is, until the power level of 15 kW is reached. Because of this delay time, the absorption of microwave energy by the material under irradiation will be affected. This means that during the time up to full 15 kW power is achieved, the material under irradiation will still absorb part of the induced microwave energy until full absorption. Thus, it is very important to calculate the time it takes for the material to absorb the incoming energy on the basis of the absolute exposure time of irradiation. This delay time for energy absorption of the material corresponding to the desired microwave power is usually referred to as the microwave “ramp-up time”. Although this ramp-up time might not affect the analyses of the results for high exposure times of microwaves, it has to be accurately calculated and taken into account in the numerical models corresponding to microwave irradiation experiments with low exposure times (< 10s), as the effect of ramp-up time is considerable. This important parameter has been commonly neglected in most research studies. Therefore, in the present section, the microwave ramp-up time is defined precisely, and its calculation process by the method of calorimetry is described. Figure 6.3 shows the experimental procedures for calorimetric studies conducted with water to define microwave ramp-up time.

The corresponding results of the calorimetric measurements on water are given in the plots of Figure 6.4(a), which represent the amount of heat (energy) absorbed by water after microwave irradiation with three power levels of 5, 7, and 10 kW and exposure times ranging from 3s to 10s. It can be seen that almost half of the irradiated microwave energy is absorbed as sensible heat within the sample/water while the remainder is rejected into the cooling loop of the microwave

system in order to protect the microwave generator from heat damage. By evaluating the results of the calorimetric measurements, another plot which represents a formula for the calculation of ramp-up time with respect to the input microwave power level is provided in Figure 6.4(b). The ramp-up times can then be calculated for different microwave power levels by substituting the value of the power, P (kW), into ( $y = 0.2027 \times P$ ).

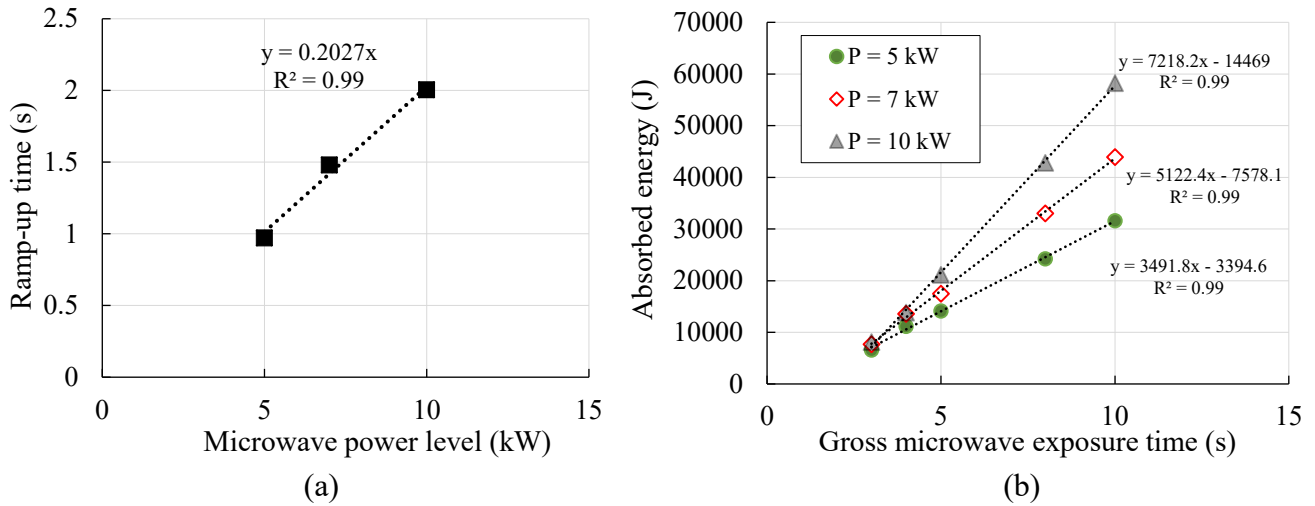


Figure 6.4: The results of calorimetric tests conducted with water to define microwave ramp-up time: (a) the absorbed energy in water with respect to the gross exposure times of microwaves and (b) the calculated ramp-up time as a function of microwave power level

As the calorimetric study of microwave-irradiated rock samples enhances the accuracy of the energy analyses, by taking all of the losses into account, data from the calorimetric measurements were used to validate the numerical models with respect to the heat (energy) absorbed by the samples. In addition, by accurately calculating the ramp-up time of the microwave system for different power levels, an absolute microwave exposure duration of an experiment can be obtained; therefore, the results of its corresponding numerical model can be validated at that absolute exposure duration to arrive at a valid and trustworthy numerical model. Hence, the calculated ramp-up times were considered in all numerical models in such a way that they were subtracted from the overall time of the experiments for validation of the models with absolute microwave exposure times.

### 6.2.3 Results and discussion

In this section, the experimental results of multi-mode microwave irradiation tests of the selected rock samples are provided as follows. First, in section 6.2.3.1, the results of thermal

images captured from the surface of the irradiated rock samples are analyzed by plotting the maximum temperature changes (difference of maximum surface temperature obtained and initial temperature of the rock) with respect to microwave exposure time for all irradiated rock samples. Then, in section 6.2.3.2, the measured values of heat (energy) absorbed by the irradiated rock samples, after microwave tests, are provided and compared for various experimental conditions. This section further demonstrates how multi-mode microwave irradiation with different microwave operating parameters influences the selected rocks in terms of the amount of heat (energy) absorbed by the samples. (Later, these results of calorimetric measurements are used to validate corresponding numerical models of each practical test in section 6.3.4.1) Finally, a parametric study was carried out to examine the influence of microwave operating parameters on the overall heat (energy) absorption by the selected rock types.

### **6.2.3.1 Thermal analysis from surface temperature measurements**

Although by multi-mode microwave irradiation, the inside of a rock sample heats more than its outside (surface)—because of the volumetric impact of the multi-mode microwave irradiation—the obtained value of maximum surface temperature of an irradiated rock from the thermal camera can still be a good indicator for initial comparisons between the results of the microwave tests. However, to compare this value for different rock types under microwave exposures at various experimental conditions, since the initial temperature of the rock samples before microwave irradiation tests might vary from one test condition to another, the difference between the initial temperature of the rock and its maximum surface temperature after irradiation (simply called “maximum surface temperature change” in the present study) gives a better evaluation for later parametric studies. It is important to note that the difference between the outside (surface) temperature and the inside (volumetric) temperature mainly causes thermal stresses within the rock particles and subsequent breakage of the rock. Moreover, the higher the difference between the outside and inside temperature of an irradiated rock samples, the more the chance of the rock being completely shattered. In addition, there exist some special cases in which a rock type needs to be heated at a limited maximum temperature. For instance, in the treatments of the kimberlite samples, the intent was to find the most efficient microwave operating parameter setting to irradiate the samples not reaching 500 °C—the maximum temperature above which diamond crystals embedded in the rock could be damaged.



In the present study, first, cylindrical samples of BTS and UCS sizes were exposed to multi-mode microwave irradiation with the experimental conditions listed in Table 6.1. After microwave irradiation tests, the temperature distributions were captured using a Fluke TIS65-30Hz thermal image camera with IR-Fusion technology and a resolution of  $260 \times 195$  pixels. The emissivity values specific to each rock type, as outlined in section 4.3.1, were set in the thermal camera before thermal imaging (see Table 4.6 for emissivity values of the selected rock types). Post processing of the thermal images was done using FLIR software provided by FLUKE Connect™ (FLUKE, 2020). Figure 6.5 depicts the process of capturing thermal images from the surface of the irradiate rock samples.

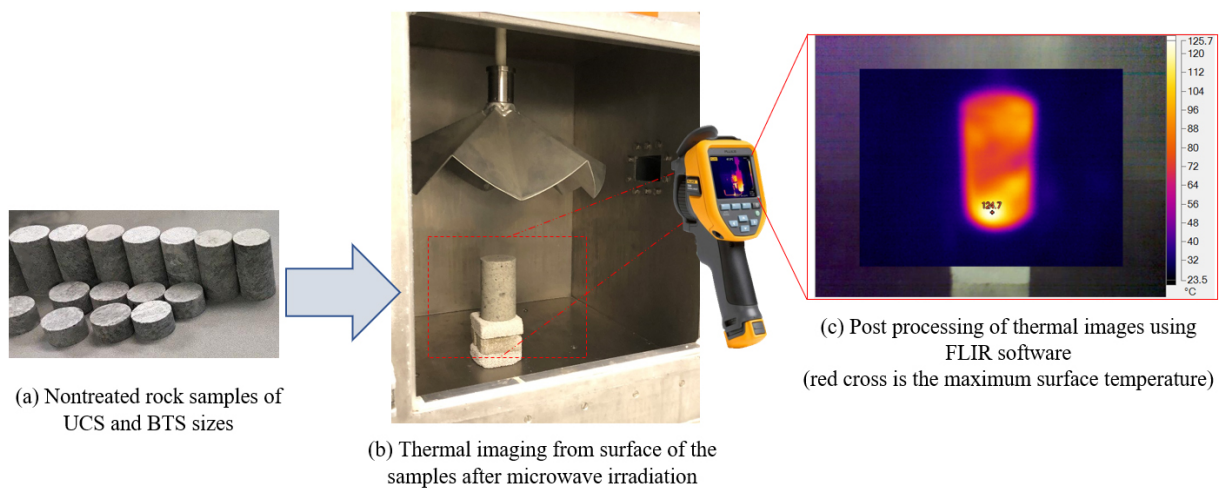


Figure 6.5: The process of thermal imaging by a thermal camera from rock samples after multi-mode microwave irradiation tests: (a) nontreated rock samples of UCS and BTS sizes ready for irradiation, (b) thermal imaging from surface of the irradiated samples, and (c) post processing of thermal images using FLIR software

As shown in Figure 6.5(c), the maximum surface temperatures were read from thermal images for all the irradiated rock samples. Then, for better evaluating the effects of microwave operating parameters, i.e. exposure time and power level, on the heating of the selected rock samples, the mean of maximum surface temperature changes,  $\Delta T$  ( $^{\circ}\text{C}$ ), were calculated from the differences between the samples' maximum surface temperatures and initial temperatures. The obtained mean values were plotted with respect to the input microwave operating parameters for all irradiated rock samples at their BTS and UCS sizes as follows. First, the results of multi-mode microwave irradiation tests for cylindrical samples of basalt at BTS and UCS sizes are shown in Figures 6.6 and 6.7.



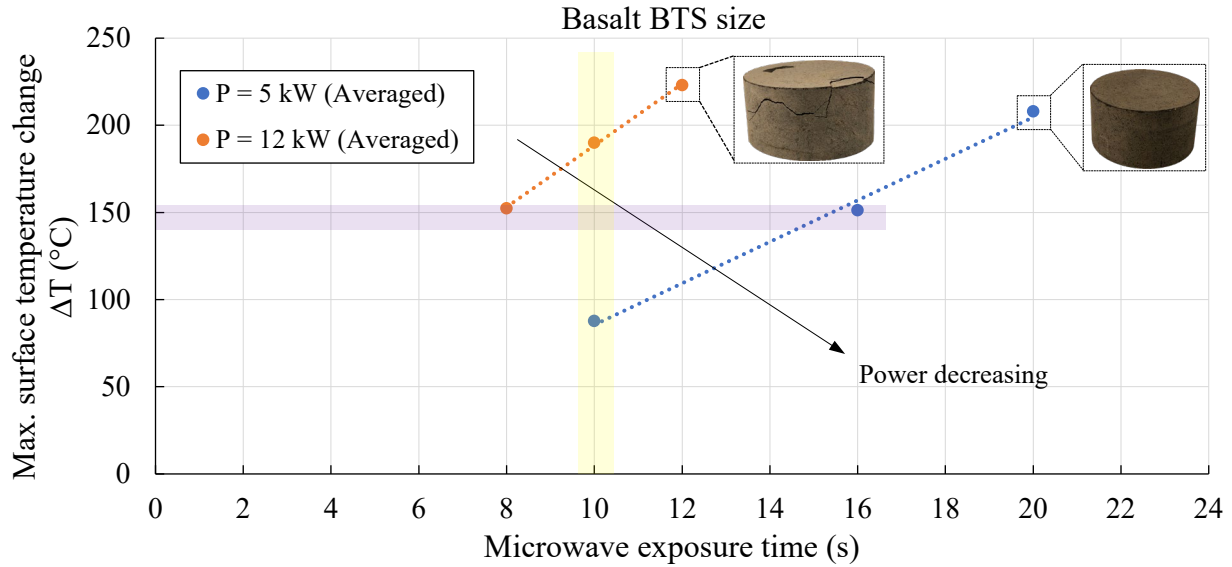


Figure 6.6: The plots of maximum surface temperature change with respect to various microwave exposure times for BTS size samples of basalt exposed to multi-mode microwave irradiation at the two power levels of 5 kW and 12 kW

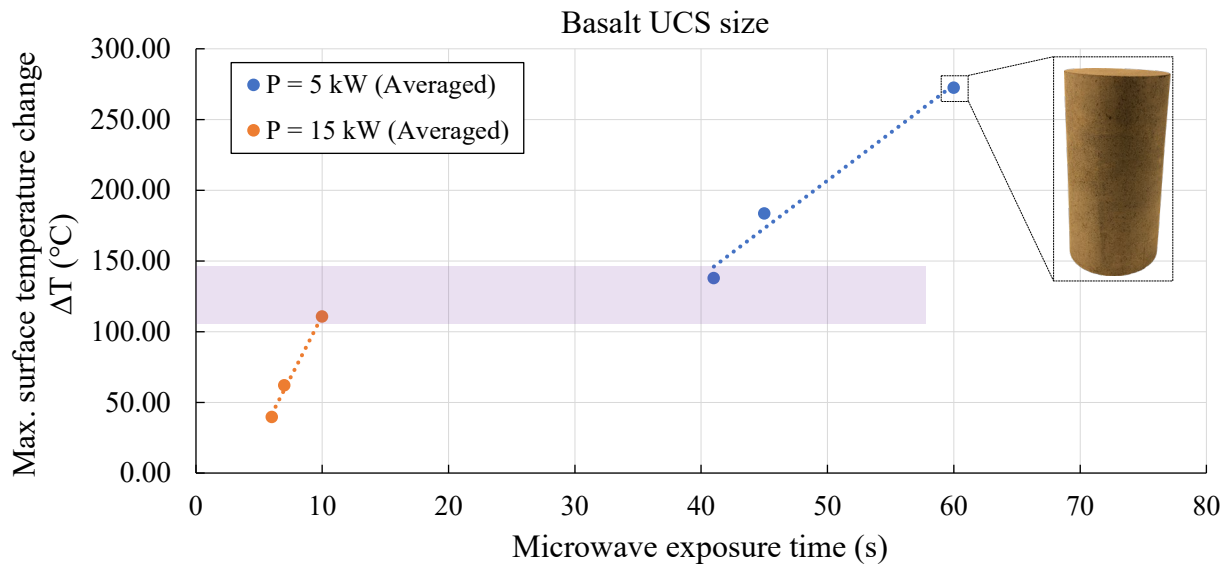


Figure 6.7: The plots of maximum surface temperature change with respect to different microwave exposure times for UCS size samples of basalt exposed to multi-mode microwave irradiation at the two power levels of 5 kW and 12 kW

The plots given in above figures demonstrate the effects of multi-mode microwave irradiation with different power levels and exposure times on surface heating of the samples of basalt. First, by looking at the results of the irradiated BTS size samples of basalt in Figure 6.6, it

can be seen that regardless of the input power level, the higher the microwave exposure time, the more maximum surface temperature change is achieved. At 5 kW irradiation and 16s microwave exposure, the obtained maximum surface temperature in the BTS samples is almost equivalent to when the BTS samples were irradiated at 12 kW and a lower microwave exposure, 8s (see the shaded purple area in Figure 6.6). This shows that in terms of energy consumption, the BTS samples irradiated at 5 kW consumed 80 kJ energy to achieve the same maximum surface temperature ( $\sim 150\text{ }^{\circ}\text{C}$ ) compared to when the samples were irradiated at 12 kW, which consumed 96 kJ. Therefore, the irradiation of the BTS size samples at 5 kW was 16.6% more economical than its irradiation at 12 kW. In addition, in the irradiation of the BTS size samples at the constant microwave exposure of 10s, the samples irradiated at a higher microwave power, 12 kW, achieved two times (50%) more maximum surface temperature ( $2\times\Delta T$ ) in comparison to the samples irradiated at 5 kW; but instead, 120 kJ energy was applied, that is  $3\times$  more energy consumption than with 5 kW (50 kJ) (see the yellow shaded area in Figure 6.6). This, therefore, verifies that while less power at higher exposure times induced more energy into the BTS size samples of basalt, it was more beneficial than higher power at lower exposures.

To better evaluate the results in terms of pre-conditioning by multi-mode microwave irradiation in addition to surface heating of the BTS size samples of basalt after microwave treatments, images of the irradiated samples at their highest heated conditions are shown in Figure 6.6. Experimentally, no visual cracking was observed on the irradiated samples of basalt until 12 kW power was applied at 12s. Again, by comparing this case with the samples irradiated at 5 kW and 20s microwave exposure, it can be inferred that inducing higher microwave energy inputs, 144 kJ, rather than the lower one, 100 kJ, caused severe cracking that might be due to a thermal shock—when there is a huge difference between the temperature of surface (outside) and inside a rock sample, a thermal shock occurs, which results in severe cracking and shattering. In conclusion, more microwave exposure at lower power levels is considered more economical than less exposure at higher microwave power levels for the BTS size samples.

Now, it is time to evaluate the results obtained for UCS size samples of basalt. In Figure 6.7, one can observe that there is a significant difference between the results obtained for the UCS size samples of basalt irradiated at 15 kW power level and shorter exposure times ( $< 10\text{s}$ ) and those irradiated at 5 kW power level and longer exposure times ( $> 40\text{s}$ ). Similar to the results obtained for the BTS size samples of basalt, a moderated slope in the change trend of the maximum surface

temperatures was obtained for the lower microwave power level, 5 kW. At 5 kW power and 41s exposure of the UCS samples in comparison to 15 kW power and 10s, although 26.82% more energy was induced in the rock, the same maximum surface temperature change was achieved (see the purple shaded area in Figure 6.6). Thus, the behavior of the UCS size samples of basalt after their irradiation at 5 kW and 12 kW can be assumed to be the same as that of the BTS size samples. The only difference was that no visible cracking was observed in the UCS size samples after their irradiation even at 15 kW, which means that more energy was needed to pre-condition the UCS size samples of basalt for visible cracking. The results of multi-mode microwave irradiation tests for cylindrical samples of the BTS size granite are shown in Figures 6.8.

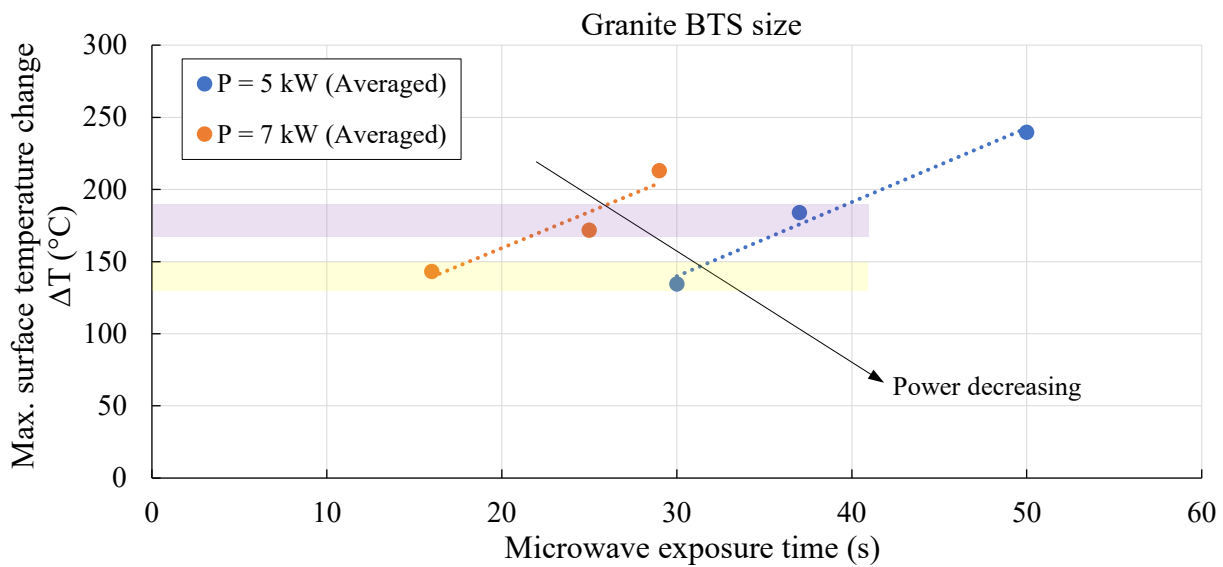


Figure 6.8: The plots of maximum surface temperature change with respect to various microwave exposure times for BTS size samples of granite exposed to multi-mode microwave irradiation at the two power levels of 5 kW and 7 kW

By comparing the plots given in Figure 6.8 with the plots given Figure 6.6, it can be seen that the response of the BTS size samples of granite was almost similar to that of the BTS size samples of basalt. However, the only difference that can be observed in Figure 6.8 is that because granite samples were irradiated at two power levels close to each other, 5 kW and 7 kW, no significant maximum surface temperature change was observed in the samples irradiated at 16s exposure in comparison to the irradiated samples at 30s microwave exposure time (see the yellow shaded area in Figure 6.8). The same phenomenon occurred for the samples exposed to 25s and 37s (see the purple shaded area in Figure 6.8).

The results of multi-mode microwave irradiation tests for cylindrical samples of the UCS size granite are shown in Figures 6.9.

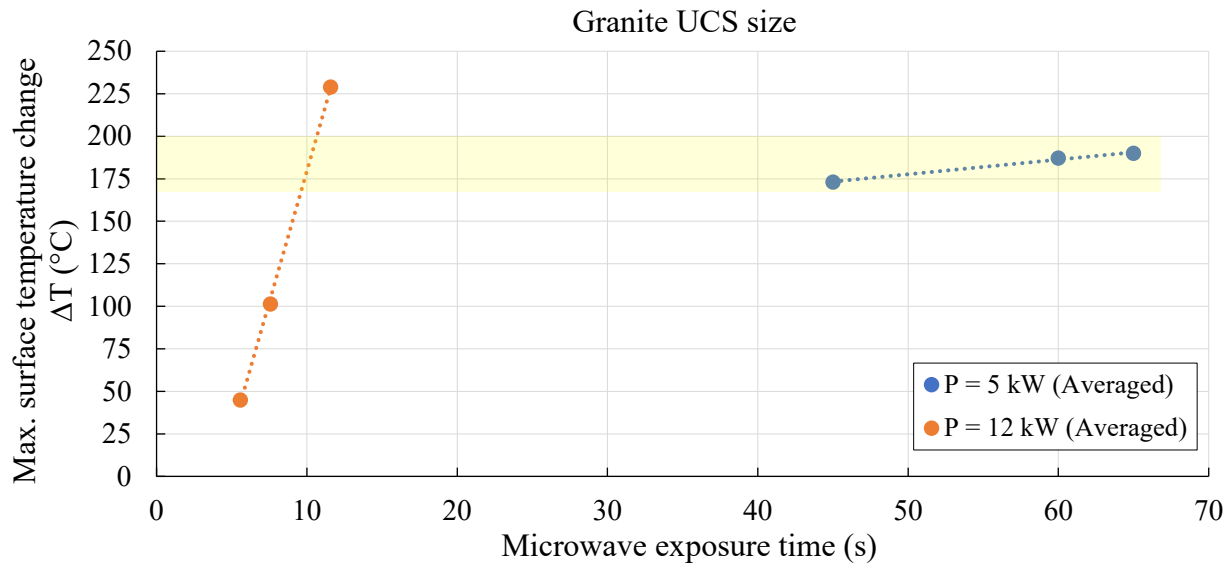


Figure 6.9: The plots of maximum surface temperature change with respect to various microwave exposure times for UCS size samples of granite exposed to multi-mode microwave irradiation at the two power levels of 5 kW and 12 kW

Contrary to the BTS size samples of granite, the USC size samples when irradiated at two power levels of 5 kW and 12 kW showed a very different response in comparison to the UCS size samples of basalt. For the granite samples, no significant maximum surface temperature change was observed when the samples were irradiated at 45s, 60s, and 65s microwave exposures. But, instead, at 12 kW microwave power, an exposure time of 12s resulted in 55.3% more maximum surface temperature change than an exposure time of 5.57s. This means that by doubling the microwave exposure, the maximum surface temperature on the UCS size samples of granite doubled. It can be concluded that at high power levels of microwaves and larger samples (UCS size in the case of this discussion) in comparison to smaller samples (BTS size in the case of this discussion), the effect of microwave exposure duration is significantly high for the heating of granite.

The final analysis of the present section is related to the thermal response of the BTS and UCS sizes of kimberlite #1. First, the results of the maximum surface temperature change with respect to the input microwave exposure are plotted in Figure 6.10. However, it should be noted here that because of the limitation in the number of samples available for the microwave irradiation tests, only two microwave exposures were tested for each power level.

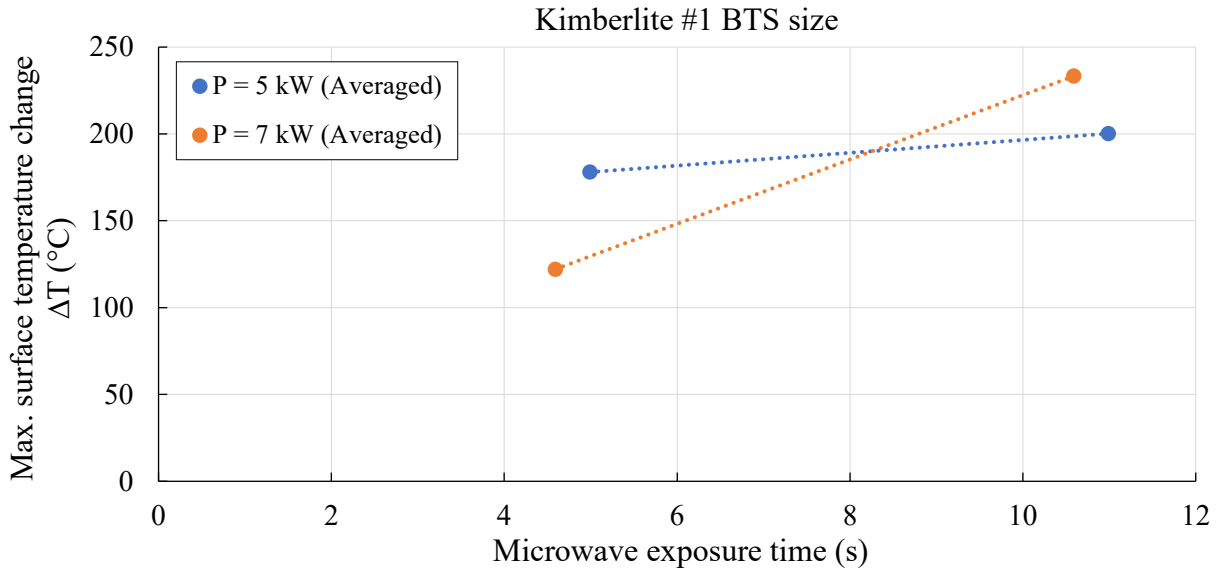


Figure 6.10: The plots of maximum surface temperature change with respect to various microwave exposure times for BTS size samples of kimberlite #1 exposed to multi-mode microwave irradiation at the two power levels of 5 kW and 7 kW

By comparing the plots shown in Figure 6.10 for the BTS size kimberlite # 1 samples and the plots shown in Figure 6.8, it can be seen that although the same microwave input parameters were applied on these two rock types, the response of the kimberlite #1 samples at 5 kW were completely different than the granite samples. The maximum surface temperature change obtained for the samples irradiated under 5s microwave exposure was higher at 5 kW power level, but an inversion occurred for the exposure at 11s. However, it can be concluded from the results that regardless of the input microwave power, higher microwave exposures achieve higher maximum surface temperatures on the BTS size kimberlite samples.

In the cases where UCS size samples of kimberlite #1 were exposed to multi-mode microwave treatments at the two power levels of 5 kW and 12 kW, similar to the other two UCS size rock samples, basalt and granite, higher microwave exposure caused more maximum surface temperature changes on the samples (see Figure 6.11). However, as shown by the yellow shaded area in Figure 6.11, the result of surface temperature changes on the samples irradiated at the 12 kW input microwave power level under 3.5s microwave exposure was the same as the samples irradiated at 5 kW power under 9s microwave exposure. Thus, in terms of an economical point of view, the higher input power level of microwave at shorter exposure time (42 kJ) is more

economical than the treatment of the UCS size kimberlite #1 samples at the lower input microwave power and higher exposure: 5 kW and 9s.

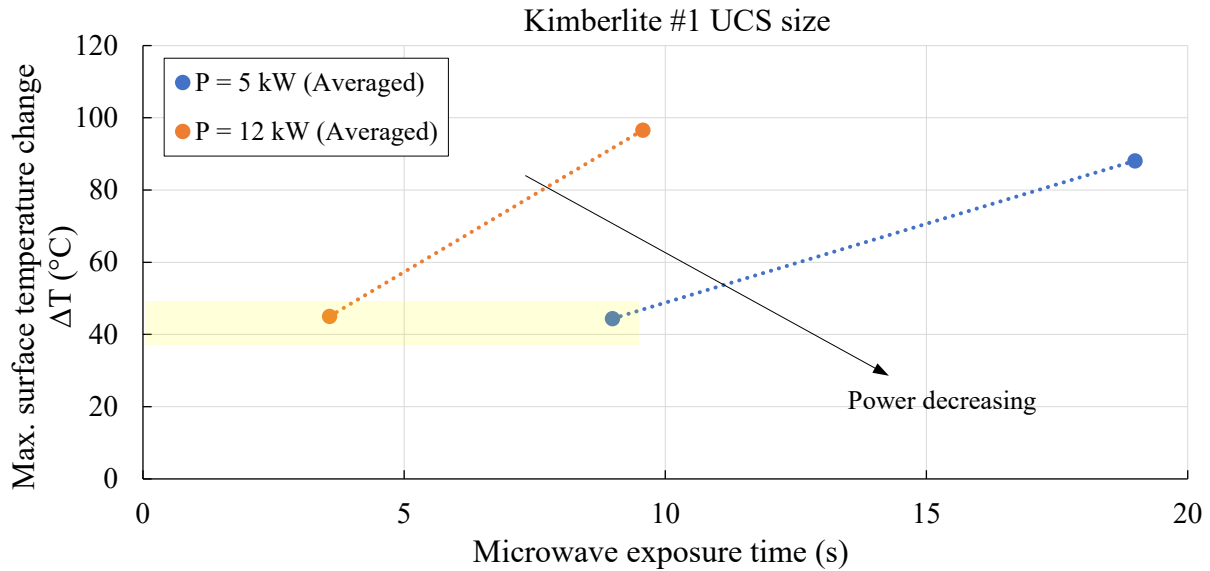


Figure 6.11: The plots of maximum surface temperature change with respect to various microwave exposure times for UCS size samples of kimberlite #1 exposed to multi-mode microwave irradiation at two power levels of 5 kW and 12 kW

In the following section, the experimental results of the heat (energy) absorbed by the BTS and UCS sizes of the selected rock samples from calorimetric measurements are provided. An energy effectiveness analysis of multi-mode microwave irradiation of the selected rock samples based on the results will be given, which produces a better conclusion about multi-mode microwave irradiation effects on rocks.

### 6.2.3.2 Heat (energy) analysis from calorimetric measurements

Having developed an appropriate measurement technique (calorimetric testing), it is time to evaluate the total heat (energy) absorbed,  $Q_{total}$ , by the irradiated BTS and UCS sizes rock samples for all microwave test conditions. Thus, the present section provides all the findings from the calorimetric measurements and discusses the results obtained for basalt, granite, and kimberlite #1. The process of calculating the corresponding values of  $Q_{total}$  for each multi-mode microwave experiment is as follows. After irradiating a selected rock sample, the amount of heat (energy) absorbed by the rock,  $Q_R$ , was calculated from the final balanced temperature of the water and the irradiated rock in the calorimeter using the sample's initial temperature, mass, and specific heat

capacity. Subsequently, the same calculation was made for the calculation of the heat (energy) absorbed by the water in the calorimeter,  $Q_w$ . By adding the two values,  $Q_R$  and  $Q_w$ , the values of the total heat (energy) absorption from the calorimetric tests were obtained. Figures 6.12 to 6.13 illustrate the plots of the total heat (energy) absorption from the calorimetric tests with respect to the input microwave energy after irradiation of BTS and UCS size samples of basalt and granite.

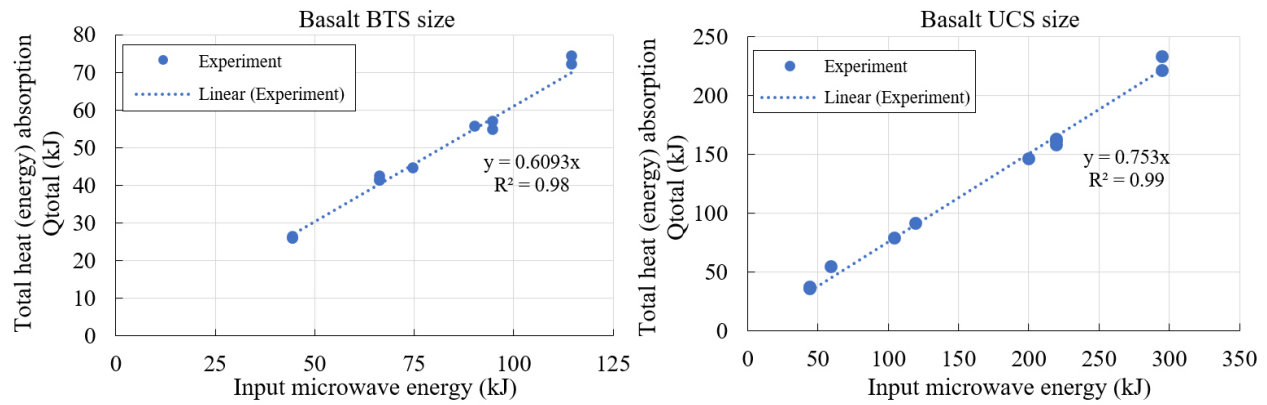


Figure 6.12: Effect of input microwave energy on the total heat (energy) absorption after irradiating BTS (left) and UCS (right) size samples of basalt in the multi-mode microwave cavity

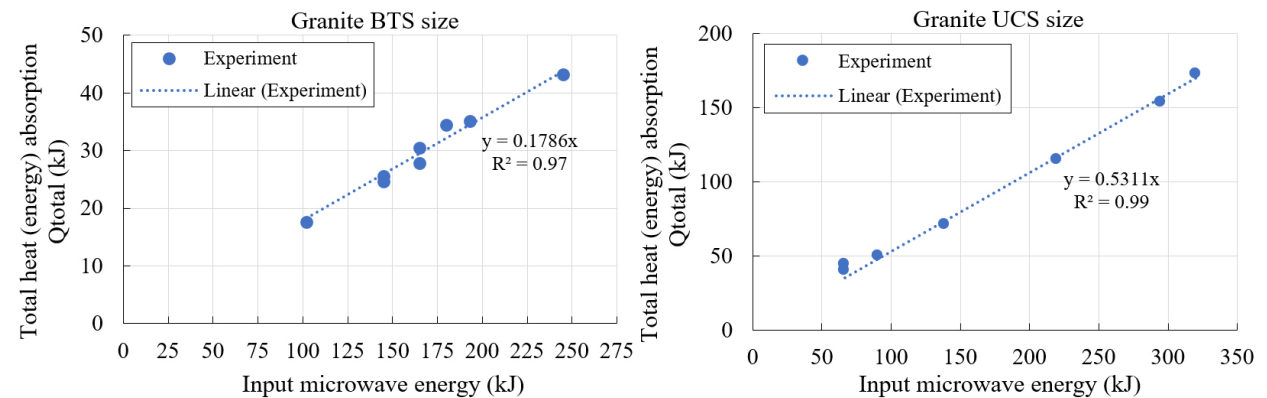


Figure 6.13: Effect of input microwave energy on the total heat (energy) absorption after irradiating BTS (left) and UCS (right) size samples of granite in the multi-mode microwave cavity

The above figures show that the distribution of data obtained from the experiments linearly change with the input microwave energy; the slopes of each trendline in the plots are indicators of the efficiency of microwave irradiation. In this section, HOME—which is defined as the ratio of heat absorbed to the microwave energy—is a proper metric that is adopted from Hassani et al.’s (2020) study for measuring the efficiency in converting microwave energy to heat. Using this newly introduced parameter and revisiting the results given in Figure 6.13 for granite BTS size samples, it can be inferred that the multi-mode cavity setup does not provide suitable conditions

for irradiation of the small samples of granite as the resulting HOME yielded low values for the irradiated granite BTS size samples (in high input microwave energy). However, an overall conclusion can be drawn from the results shown in Figures 6.12 and 6.13. They indicate that for both basalt and granite, the obtained values of HOME were higher for the UCS size samples than the BTS. This means that the larger the samples of basalt and granite, the more effective their heating in the multi-mode microwave cavity. The same conclusion can be stated for the irradiated samples of kimberlite #1 (see Figure 6.14).

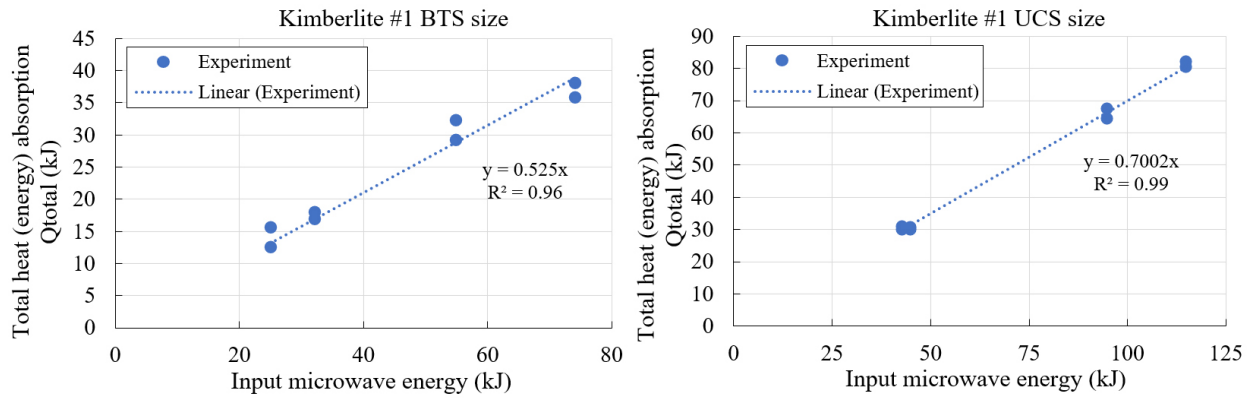


Figure 6.14: Effect of input microwave energy on the total heat (energy) absorption after irradiating BTS (left) and UCS (right) size kimberlite #1 samples in multi-mode microwave cavity

In addition, by comparing the plots shown in Figures 6.12 to 6.14, it can be seen that regardless of the type of the rock exposed to a specific multi-mode microwave irradiation, the higher input microwave energy increases the total heat (energy) absorbed by the rock samples. This makes sense because the heat absorption by rocks is directly related to the dissipation of the microwave energy inputs. Thus, an overall conclusion that can be drawn based on the results of the calorimetric tests presented in this section is as follows: by increasing the input microwave energy and with larger rock samples, more heat (energy) absorption in the rock can be achieved for multi-mode microwave irradiation application. The results of the experimental calorimetric tests presented in this section in Figures 6.12 to 6.14 are used to validate the corresponding numerical models developed for each microwave test condition and rock type (see section 6.3.4.1).

### 6.2.3.3 Effect of microwave ramp-up time

In this section, the effects of calculated microwave ramp-up time on the results of the calorimetric tests obtained for the selected rock samples after their irradiation in the multi-mode microwave cavity system at different power levels and exposure times are studied.



Referring to the calculated microwave ramp-up times presented in section 6.2.2, it can be seen that the obtained microwave ramp-up time was according to the input power level of the specific microwave irradiation experiment (see Figure 6.4(a)). Thus, the input microwave energy, which is the product of the microwave exposure time (s) and the input microwave power level (kW), changes for different microwave conditions applied to the experiments. To better demonstrate how the variations of the input microwave energy influence the results of the experiments, the HOME values were calculated for the microwave energy inputs with and without taking into account the calculated ramp-up times. Figure 6.15 shows the results obtained for the BTS and UCS size samples of basalt; similar plots for the BTS and UCS size samples of granite and kimberlite #1 are given in Appendix A.1.

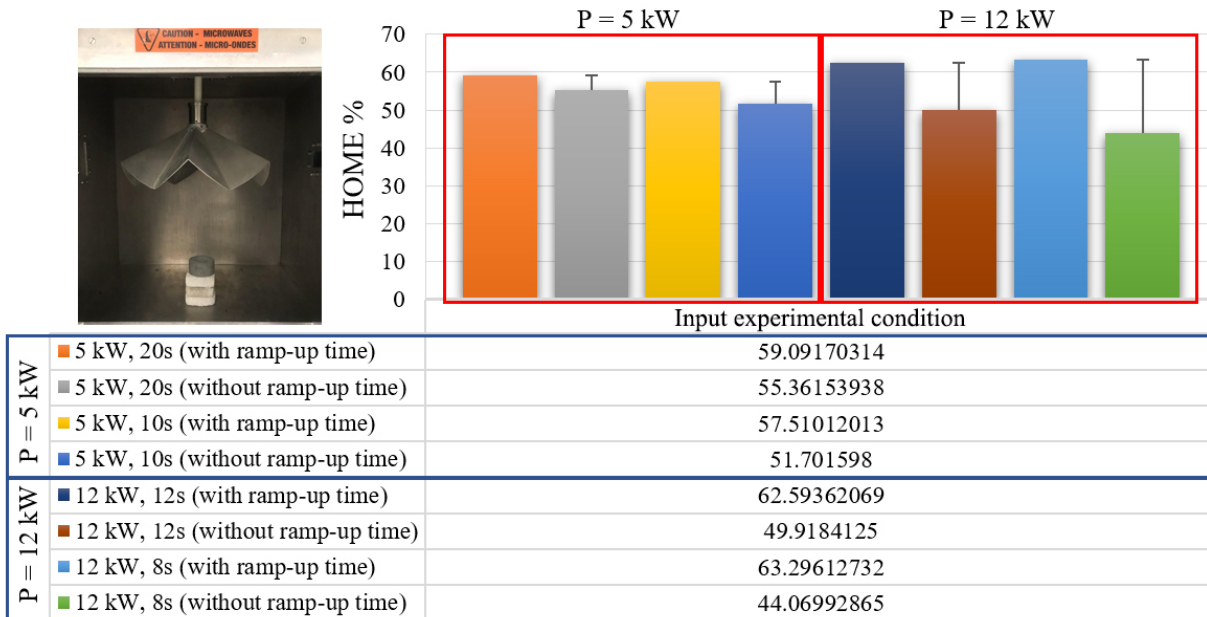


Figure 6.15: Effect of microwave ramp-up time on the amount of heat (energy) absorption of BTS size samples of basalt after their irradiation in the multi-mode microwave cavity

By comparing the results of experimental calorimetric measurements considering the effect of ramp-up time as opposed to not considering ramp-up time, a better picture of the effect of microwave ramp-up times can be achieved. The results when taking into account the microwave ramp-up time were significant at high levels of microwave power ( $> 10$  kW), whereas at low microwave power levels the differences between the results were very small. Moreover, at short microwave exposures (i.e. less than 10s), the effect of the ramp-up time was high. Hence, for the numerical model validation, only the results of the microwave tests with ramp-up times were used.

### 6.3 Numerical modeling of multi-mode microwave irradiation

In this part of the chapter, the development of a fully-coupled electromagnetic and heat transfer multiphysics model of microwave-assisted rock heating process is presented. The present numerical study employs the Finite Element Method (FEM) based numerical solver COMSOL Multiphysics v5.5a to simulate the microwave heating of cylindrical rock samples in a multi-mode microwave cavity. A solution of coupled electromagnetic and heat transfer multiphysics models in 3D space requires a great many computational resources; hence, it is a time-consuming process. Thus far, researchers have made several simplifications in their numerical model development approach that prevent their models from being considered trustworthy. For example, in order to reduce the number of mesh elements required to solve the electromagnetic wave and heat transfer equations in a coupled way, many researchers have assumed a simple geometry in their multi-mode microwave cavity model without taking into account some of the features of the actual multi-mode microwave system design, such as the stirrer fan and its rotation in the cavity. Therefore, one of the main objectives is to develop a comprehensive and integrated model of a multi-mode microwave cavity to enable the study of microwave heating of rocks by numerically simulating the actual experimental conditions applied in the microwave irradiation of various rock types. A validated numerical model enhances the study of rock heating and pre-conditioning by multi-mode microwave irradiation. With the known properties of a rock type, not only the simulation of microwave heating process of the rock is valid, but also the energy effectiveness evaluation of the process is possible. The specific objectives of the present numerical study are to:

- i. Develop a fully-coupled electromagnetic and heat transfer model of a multi-mode microwave cavity system with a rotating stirrer fan designed to numerically simulate the heat (energy) absorption of rocks after microwave irradiation with different operating parameters using a novel approach,
- ii. Validate the numerical model with the experimental data from calorimetric tests in terms of the amount of the sensible heat (energy) absorbed by the samples of rocks,
- iii. Conduct parametric studies from the validated models to examine the effectiveness and energy saving potential of multi-mode microwave cavities in rock heating and pre-conditioning.

### 6.3.1 Novel model of multi-mode microwave system with rotating stirrer fan

The geometry of the multi-mode microwave cavity, including the dimension of the microwave oven and the novel design of an umbrella-shaped stirrer fan, was constructed in AutoCAD and SolidWorks and exported to COMSOL Multiphysics, as shown in Figure 6.16. The microwave model geometry includes a block-shaped cavity with a size of  $60\text{ cm} \times 60\text{ cm} \times 60\text{ cm}$ , a rectangular port functioning as a microwave waveguide operated at 2.45 GHz (TE<sub>10</sub> mode), and an umbrella-shaped stirrer fan for the propagation of the incoming electromagnetic waves from the port into the cavity. As shown in Figure 6.16, the geometric model was developed in line with the high power 15 kW multi-mode microwave cavity system located at McGill University. As a result, the dimensions of the constituent parts of the multi-mode microwave model exactly match the practical microwave cavity system used in the experiments.

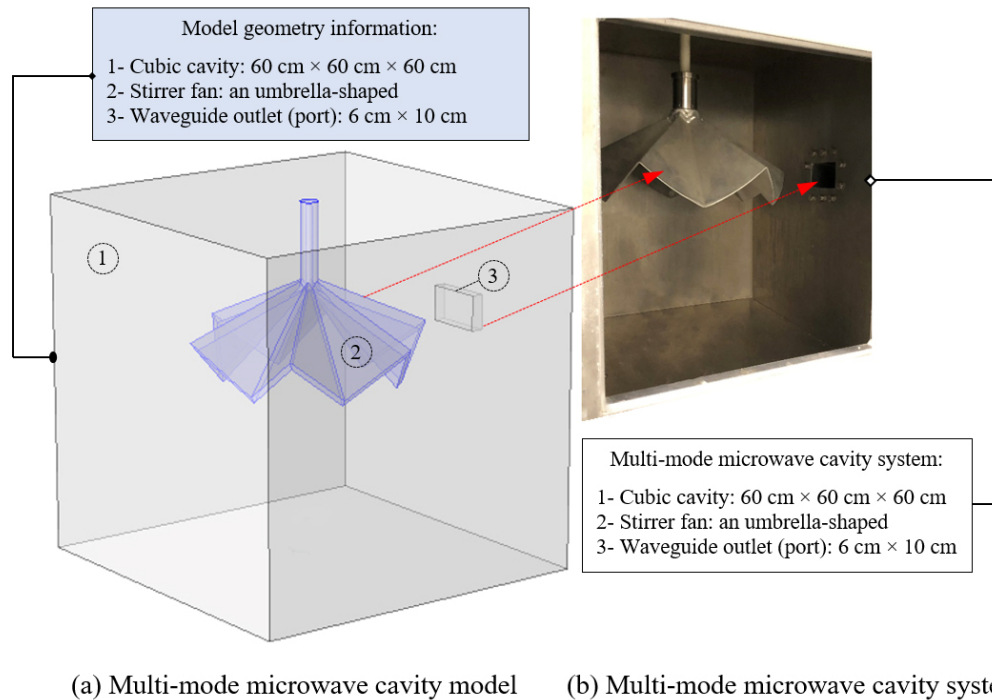


Figure 6.16: Schematic of (a) the multi-mode microwave cavity model comprising a waveguide port and an umbrella-shaped stirrer fan and (b) the actual multi-mode microwave cavity system used for the practical microwave irradiation tests

For the following reasons, (1) the COMSOL Multiphysics software in its electromagnetic physics mode/module was not compatible with the software's inherent moving mesh which enables the rotation of a stirrer fan (or an object in general) in the computation domain of the study,

and (2) the simulation of a moving part in a numerical model with an extra fine mesh size requires a huge amount of computational resources, e.g. a computer with high Random Access Memory (RAM) and graphics card, the present study introduces a novel approach to overcome the problem of not being able to rotate the stirrer fan—which is an essential part of the multi-mode microwave cavity in the actual experiment—during electromagnetic simulation in COMSOL Multiphysics software. This novel approach uses the MATLAB-COMSOL interface algorithm to manually rotate the geometry of the stirrer fan in the 3D computational domain, which gives the practical rotation of the stirrer fan in the multi-mode microwave irradiation experiments. All the steps designed in the simulation of the manual rotation and the computation of the heat (energy) absorption by the samples are given in a flowchart in Figure 6.17.

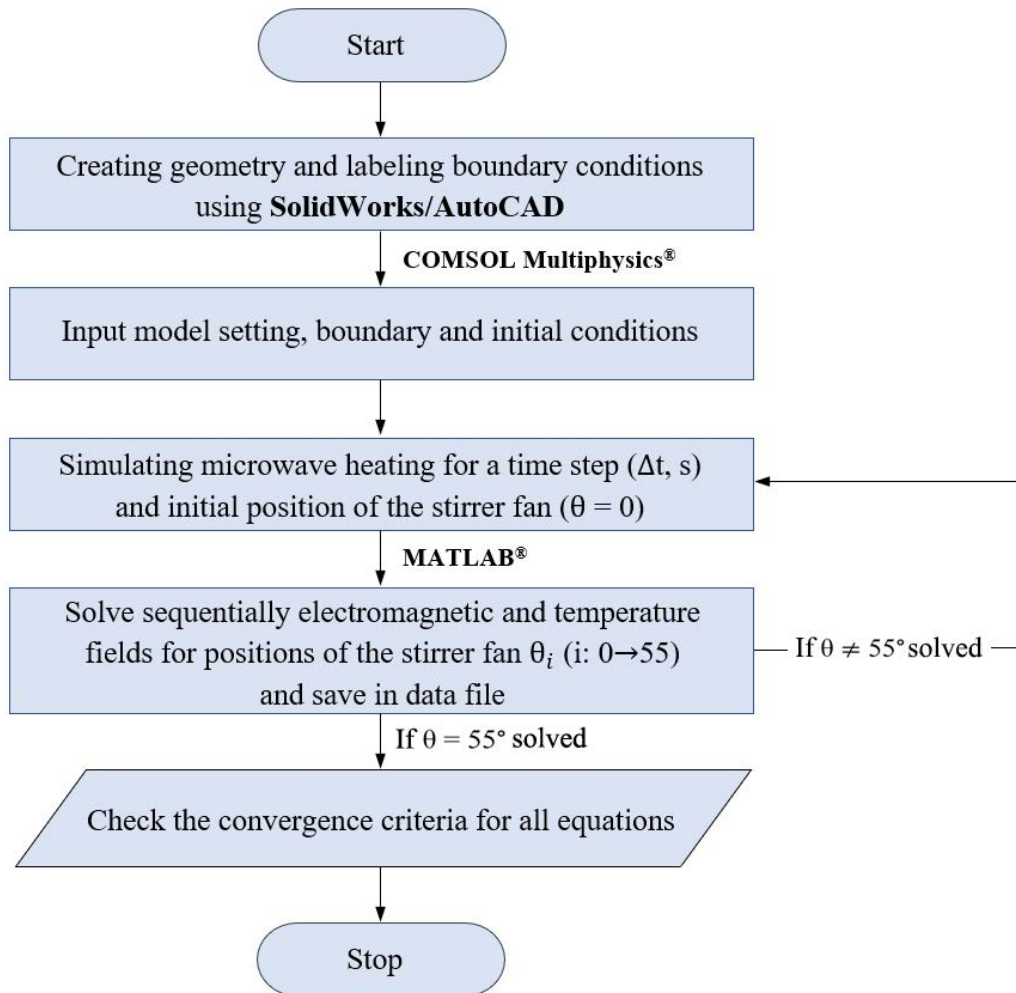


Figure 6.17: Flowchart of the solver algorithm for modeling processes of multi-mode microwave irradiation using COMSOL-MATLAB interface depicting a novel simulation approach for rotational stirrer fan

### 6.3.2 Mathematical modeling

Calculating microwave-induced heat (energy) absorption of rocks using a 3D modeling approach requires an in-depth numerical simulation technique that connects the following multiphysics: electromagnetic physics (Maxwell's theory) and thermal physics (heat transfer theory). The present study develops a fully coupled modeling approach that can comprehensively address the electromagnetic and thermal multiphysics interactions and their coupling behaviors in rocks when subjected to microwaves. Several numerical models are developed to address the effects of variations in the dielectric properties of the rocks and to be validated against experimental data from calorimetric tests. The mathematical formulation of the present study for development of the proposed modeling approach involves two components: the electromagnetic physics (from Maxwell's theory) and the thermal physics (from heat transfer theory). An analytical flowchart of the fully coupled numerical modeling approach for simulation of the microwave heating process is presented in Figure 6.18.

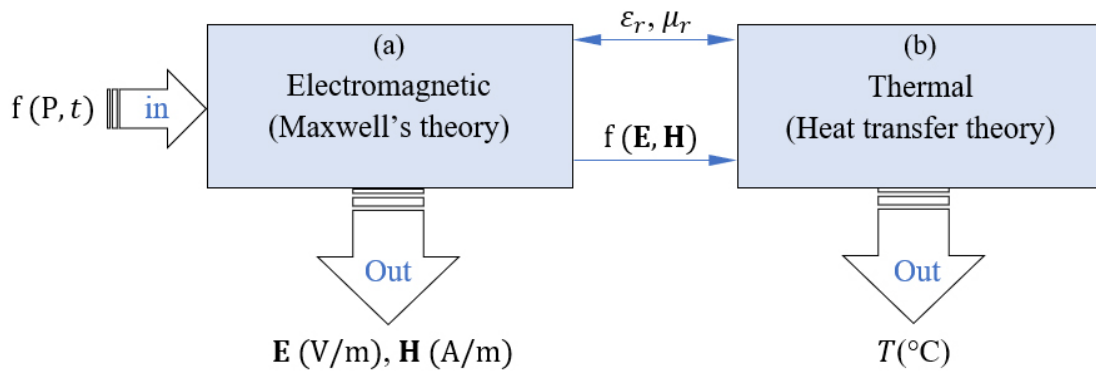


Figure 6.18: Analytical flowchart of the fully coupled numerical modeling approach representing the interaction between electromagnetic and thermal multiphysics where (a)→(b) is the input from electromagnetic to thermal multiphysics and (a)↔(b) represents the interactions between the two multiphysics

As shown in the flowchart, the electromagnetic and thermal multiphysics are simulated and solved by a fully coupled numerical modeling approach in such a way that they can mutually interact with each other to solve for electromagnetic fields and temperature distribution. More specifically, a function  $f(P, t)$  comprising microwave power level,  $P$  (kW), and exposure time,  $t$  (s), is applied as an initial input operating parameter of the microwave into the electromagnetic part of the model. The solution of the model from mutual interaction between the two multiphysics

gives the results of electric field distribution,  $\mathbf{E}$  (V/m), magnetic field distribution,  $\mathbf{H}$  (A/m), and the resulting temperature,  $T$  ( $^{\circ}\text{C}$ ), in the irradiated rock sample. The full set of governing equations and initial and boundary conditions is provided in the following sections.

### 6.3.2.1 Electromagnetic physics (Maxwell's theory)

Maxwell's equations are a set of partial differential equations (PDEs), in either differential or integral form, stating the relationships between the fundamental electromagnetic quantities (Fawzi et al., 1978). Solving these equations subject to certain boundary conditions is the problem of electromagnetic analysis on a macroscopic level. The governing equation for the problem of the electromagnetic physics is given as (Huang et al., 2018):

$$\nabla \times \mu_r^{-1} (\nabla \times \mathbf{E}) - k_0^2 \left( \epsilon_r - \frac{j\sigma_e}{\omega\epsilon_0} \right) \mathbf{E} = 0 \quad (6.1)$$

where  $\mu_r$  is the relative permeability and assumed to be ( $\mu_r = 1$ ) for the linear material model,  $\epsilon_0$  is the permittivity of free space ( $\epsilon_0 = 8.86 \times 10^{-12}$  F/m) (Hong et al., 2016),  $\omega$  (rad/s) is the angular frequency, and  $\sigma_e$  (S/m) is given as the electrical conductivity. The wave number of free space  $k_0$  (rad/m) is defined in equation (6.2) as

$$k_0 = \frac{\omega}{c_0} \quad (6.2)$$

where  $c_0$  is the speed of light in a vacuum ( $c_0 = 2.998 \times 10^8$  m/s). From the formula presented in equation (6.1), it can be seen that an electromagnetic wave (microwave) loses its energy while traveling through a lossy dielectric medium such as rock; and subsequently, part of the electromagnetic power is converted into thermal energy within the rock. This conversion of microwave energy into thermal energy is proportional to the dielectric loss factor,  $\epsilon''$ , and square of the electric field strength (see section 3.2.6 for more details).

### 6.3.2.2 Thermal physics (heat transfer theory)

The coupling interactions of electromagnetic and thermal multiphysics are used to model microwave heating in the rock models under microwave treatments with the same conditions as practical tests. As shown in Figure 6.18, in the electromagnetic physics of the presented modeling approach a function of  $f(\mathbf{E}, \mathbf{H})$  is applied as an input to the thermal physics (see (a)→(b) in Figure (6.18)). This multiphysics interface adds an electromagnetic wave in the frequency domain

interface and a heat transfer in the solid interface, which is the rock sample under irradiation. Then, the multiphysics couplings add the electromagnetic losses from the electromagnetic wave part as a heat source. The heat transfer in a rock sample under irradiation can then be expressed by the heat balance relation given in equation (6.3) (Hong et al., 2016):

$$\rho C_p \frac{\partial T}{\partial t} + \rho C_p \mathbf{u} \cdot \nabla T + \nabla \cdot (\mathbf{q}) = Q_e + Q_{ted} \quad (6.3)$$

where  $T$  ( $^{\circ}\text{C}$ ) is the temperature,  $\rho$  ( $\text{kg/m}^3$ ) is the rock density,  $C_p$  ( $\text{J/kg } ^{\circ}\text{C}$ ) is the rock specific heat capacity at constant pressure, and  $k$  ( $\text{W/m } ^{\circ}\text{C}$ ) is the thermal conductivity of the rock. With zero velocity fields,  $\mathbf{u}$  ( $\text{m/s}$ ), at all coordinates, the second term on the left side of equation (6.3), the advective term, is equal to zero. Heat flux,  $\mathbf{q} = -k\nabla T$ , generated from the interior to the exterior of the rock under microwave irradiation can be expressed by the internal temperature changes using Fourier's law. Thus, by substituting the heat flux into equation (6.3), the following relation obtains:

$$\rho C_p \frac{\partial T}{\partial t} = k\nabla^2 T + Q_e + Q_{ted} \quad (6.4)$$

The heat sources on the right side of the equation are  $Q_e$  ( $\text{W/m}^3$ ), which denotes electromagnetic heat sources, and  $Q_{ted}$  ( $\text{W/m}^3$ ), which represents the thermoelastic damping effects in solids and is assumed to be zero since no thermoelastic damping effect was considered in the numerical models of the present study.

To couple the electromagnetic and thermal multiphysics in the modeling of microwave-rock interaction, the electromagnetic loss in equation (6.3),  $Q_e$  ( $\text{W/m}^3$ ), should be separated into two parts: (i) the resistive heating losses,  $Q_{rh}$  ( $\text{W/m}^3$ ), which are assigned as ohmic/heating losses due to electric current, and (ii) the magnetic losses,  $Q_{ml}$  ( $\text{W/m}^3$ ). These heat sources can then be calculated from the following relations,

$$Q_e = Q_{rh} + Q_{ml} \quad (6.5)$$

$$Q_{rh} = \frac{1}{2} \cdot (\mathbf{J}_e \cdot \mathbf{E}) \quad (6.6)$$

$$Q_{ml} = \frac{1}{2} \cdot \text{Real} (i\omega \mathbf{B} \cdot \mathbf{E}) \quad (6.7)$$

where  $\mathbf{B}$  (Tesla) is the magnetic flux density.

### 6.3.2.3 Initial and boundary conditions

In this section, the applied initial and boundary conditions in the microwave-rock models are defined as follows. For the electromagnetic physics, an impedance boundary condition is applied to the metallic/copper walls of the microwave cavity model and the waveguide to ensure that the electromagnetic waves remain inside the microwave system and are solved in the frequency domain. A mathematical expression of this boundary condition is given in equation (6.8),

$$\sqrt{\frac{\mu_0\mu_r}{\varepsilon_0\varepsilon_r - j\sigma_e/\omega}} \mathbf{n} \times \mathbf{H} + \mathbf{E} - (\mathbf{n} \cdot \mathbf{E}) \mathbf{n} = (\mathbf{n} \cdot \mathbf{E}_s) \mathbf{n} - \mathbf{E}_s \quad (6.8)$$

where  $\mu_0$  is the permeability of free space ( $\mu_0 = 4\pi \times 10^{-7}$  H/m) and  $\mathbf{E}_s$  (V/m) is the source electric field, which is 0. For simplicity, the metallic waveguide and cavity walls can also be considered as perfect electric conductors where the following boundary condition applies (as this boundary condition was assigned to the metallic boundaries of the stirrer fan):

$$\mathbf{n} \times \mathbf{E} = 0 \quad (6.9)$$

The rectangular waveguide outlet (port) boundary of the microwave horn antenna is assigned as rectangular and excited by a transverse electric wave form ( $TE_{m,n}$ ), where  $m$  and  $n$  are the mode numbers of the electromagnetic waves. In this case,  $TE_{10}$  mode ( $m = 1, n = 0$ ) is the only propagating mode for the frequencies between 1.95 GHz and 3.70 GHz; the numerical models of the present study are simulated at 2.45 GHz (COMSOL Multiphysics, 2018).

For the thermal physics, assuming minimal heat loss to the surroundings, the Neumann boundary condition (specified for perfectly insulated boundaries) is applied at the outer surface of the rock sample. A mathematical expression of this boundary condition is given in equation (6.10) (Chen et al., 1999).

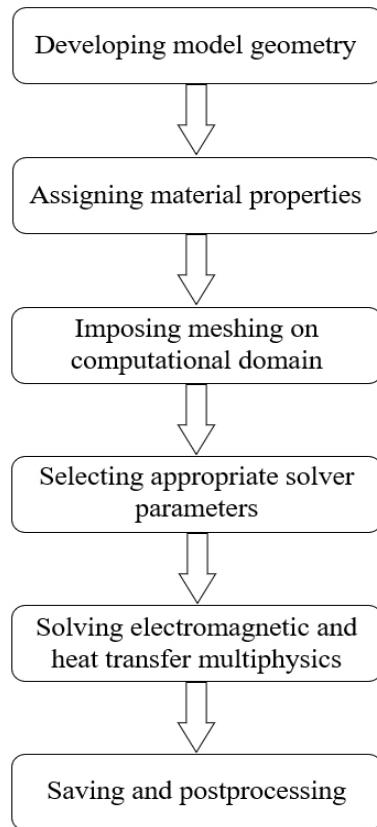
$$-\mathbf{n} \times \mathbf{q} = 0 \quad (6.10)$$

Finally, after the boundary conditions were defined, the following assumptions were made as initial conditions and applied in the numerical models. The initial temperature of air was set at approximately room temperature (22 °C). However, for the initial temperature of the rock samples,  $T_0$  (°C), in their corresponding numerical models, the initial temperature values measured experimentally for the rock samples, specific to each practical test condition, before microwave irradiation tests were used as inputs to the numerical models.



### 6.3.3 Numerical methodology

The corresponding heat transfer and electromagnetic wave equations together with associated initial and boundary conditions were solved with finite element solver COMSOL Multiphysics 5.5a (COMSOL Multiphysics, 2018). Quadratic Lagrange elements were



implemented for all variables of the electromagnetics and heat transfer modules. For time discretization, the Backward Differentiation Formula (BDF) solver was employed as an implicit solver that uses backward differentiation formulas with a second order of accuracy. The MULTifrontal Massively Parallel Sparse (MUMPS) direct solver was also employed as a sparse solver that is optimized for solving the system of equations in parallel, with a relative convergence tolerance of  $10^{-6}$  for all variables, as this solver offers additional options for customization of parallel computing. Furthermore, it was very important to carry out a mesh independent study to find the optimal mesh size for the given model. Meshing of the microwave cavity and waveguide domains was performed using the rule of ten linear elements per wavelength (COMSOL Multiphysics, 2018). Detailed information about meshing the geometry of microwave-rock models is given in the mesh independence study section (see section 6.3.3.3).

Figure 6.19: Steps for model development

Finally, all computations were carried out on a computer with Intel Xeon dual processors @ 3.40 GHz frequency and 128 GB Random Access Memory (RAM). In addition, the programming language and numerical computing environment, Matlab 2020a (see [(MathWorks, 2020)] for detail), was also employed as an interface with COMSOL for parameter adaption and to assign steps for automatic solutions and post processing of the results obtained from the models. All the steps needed for model development are shown in Figure 6.19.

#### 6.3.3.1 COMSOL Multiphysics

Comsol multiphysics is a modeling software based on the Finite Element Method (FEM). The software itself can handle any physical process that can be described with partial differential equations (PDEs) or through various predefined multiphysics modeling templates, which are

usually called modes/modules in the software manual (COMSOL Multiphysics, 2018). It offers a fast and versatile environment for multiphysics modeling of a system with various phenomena and facilitates all the required steps in a numerical modeling process, including drawing the geometry of a computational domain, meshing, solving, and, finally, post processing of the results.

COMSOL offers various predefined modeling templates, referred to as physics modes, which allow users to conveniently simulate/model various processes, e.g. electromagnetic wave propagation, dielectric heating by microwaves, heat transfer in solids, structural deformation of solids, etc. In this study, two multiphysics modeling modes/modules, comprising both electromagnetic waves mode in a frequency domain and heat transfer in solids mode, are utilized to carry out computational simulations of the interactions between electromagnetic waves (microwaves) and a solid dielectric material (rock sample). To deal with this coupled process, COMSOL allows users to easily extend their models for one type of physics into multiphysics models and solve coupled physics phenomena, simultaneously. With all these features, the users are independent to establish their own equations for a particular process, couple it with the built-in physics mode, and define and assign appropriate material properties, boundary conditions, and source terms with any function of the dependent variables and then solve the multiphysics in a fully coupled way. Even if users are not satisfied with the available Graphic User Interface (GUI) in COMSOL Multiphysics, the software allows accessing the model as a script for any modification, manipulation, run, and control either directly from the COMSOL script or by MATLAB command line.

### **6.3.3.2 Finite element method**

Finite element simulations were carried out to simulate the process of microwave heating of the selected rock types—i.e. basalt, granite, and two types of kimberlite, kimberlite #1 and kimberlite #2—in the multi-mode microwave cavity system to determine the thermal heat (energy) absorption by the rock samples and to evaluate the internal temperature changes in the rock models irradiated at different microwave operating parameters, including various exposure times and power levels. Several numerical models were developed with the same conditions in the practical tests, and their results are compared and validated with the experimental data from the calorimetric tests. The final mode, given by equations (6.1) to (6.10), together with the appropriate initial and boundary conditions for all multimode microwave models, constitute a highly coupled nonlinear

differential algebraic system for the dependent variables  $\mathbf{E}$ ,  $\mathbf{H}$ , and  $T$ . The FE solver, COMSOL Multiphysics, was chosen to implement the derived models because of its versatility in handling general coupled nonlinear partial differential equations for the fully coupled electromagnetic and thermal multiphysics interaction.

### 6.3.3.3 Mesh independence study

In order to ensure mesh independent solutions, a mesh independence study was carried out for the numerical models presented in this thesis, one of which is shown in Figure 6.20. Convergence tests were carried out by decreasing both minimum and maximum mesh sizes in the desired computation domain, which increased the number of elements uniformly in the rock models' geometry, re-computing the solution of the finer mesh, and comparing the solution of different mesh sizes. When the true solution is unknown, one classical technique is to use a numerical solution on a finer mesh as a reference solution. By plotting the results of a numerical model with respect to various implemented mesh sizes within the desired solution region—which is the rock sample in the microwave cavity in this case study—the trend of solutions must converge to a specific value. When the plotted solutions with respect to different mesh sizes become steady (the trend line converges to a specific value), a mesh independence model is obtained. Thus, its associated mesh size is used for modeling of the other numerical models with different experimental conditions. Figure 6.20 shows the results of the average dissipated power obtained in the BTS size kimberlite #2 simulated at 10 kW input microwave power under 10s exposure.

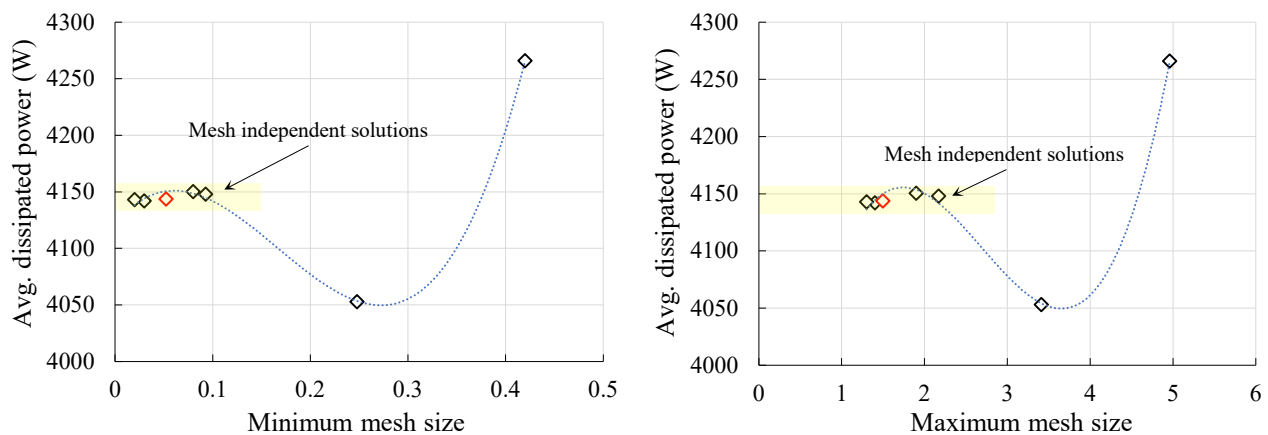


Figure 6.20: An example of the results of the mesh independence study, showing the averaged dissipated power in the BTS size kimberlite #2 rock model after its irradiation at 10 kW power with respect to minimum mesh size (left) and maximum mesh size (right)

As shown in Figure 6.20 by the yellow shaded area, mesh independent solutions were achieved after several mesh adaptations were performed in the microwave model. A mesh-independent solution was ensured by comparing the results obtained using a normal mesh consisting of 5,158 boundary elements, followed by several mesh adaptations until the difference in the accumulated/computed dissipated power in the solid rock samples was below 1% (an extremely fine mesh). Thus, as shown in Figure 6.20 by the red diamonds, the extra fine mesh size was chosen for meshing the models' geometry. The geometries for all the numerical models were resolved for this mesh size after ensuring that it gives mesh independent solutions.

#### **6.3.3.4 Novel simulation strategy for rotation of the stirrer fan**

The rotation of the stirrer fan in a multi-mode microwave model is a continuous and complex process that needs an accurate simulation strategy in order to correctly mimic the same electromagnetic wave propagation within the cavity as in the practical multi-mode microwave irradiation experiment. Because, typically, the electromagnetic waves and heat transfer multiphysics are solved in two different study steps—frequency domain and time dependent—it is very complicated to add another movable part (a moving mesh) in the model's domain and solve all three parts in a coupled way, which results in a heavy simulation. Therefore, in the present study, the continuous rotation of the stirrer fan in the microwave-assisted rock heating process was not achieved using the COMSOL Multiphysics<sup>®</sup> software; but instead, the continuous process of rotating the stirrer fan was approximated by manually moving the stirrer at discrete angles in which its location changes over time. As a result, the stirrer fan was at a different orientation at each rotational step within one complete rotation of the stirrer. However, finding the appropriate rotation angle steps for the stirrer fan is a critical factor, as it significantly influences the absorption of heat (energy) by the rock sample inside the multi-mode microwave cavity; larger discrete angles may miss some of the hot or cold spots of the standing wave pattern and the dissipated power density calculated may not be accurate. The rotation steps of the stirrer fan should be assigned so that by reflecting the true electromagnetic wave propagation in the same cavity as in a practical test, true heat absorption by the sample is predicted. As shown the Figure 6.21(a), the stirrer fan in the actual multi-mode microwave cavity system has six edges, which means that in every 60° rotation of the stirrer, the same electromagnetic wave patterns are repeated. Therefore, in the

simulation of the angle steps, manual rotations up to less than  $60^\circ$  were needed for the present study in order to capture the true heat (energy) absorbed by the rock models.

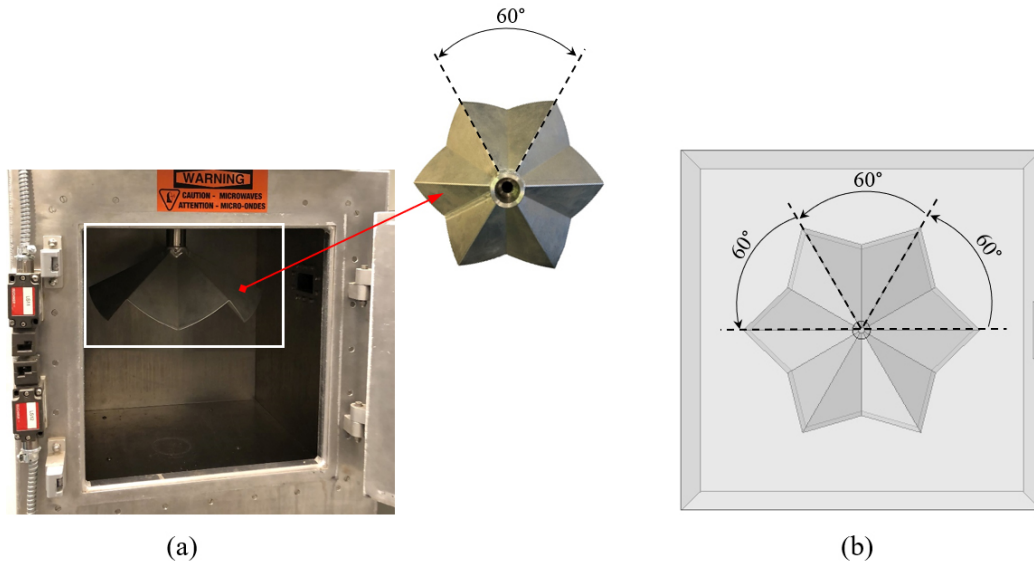


Figure 6.21: The novel strategy applied for the simulation of rotating stirrer fan in the multi-mode microwave cavity model where (a) shows the geometry of the multi-mode microwave cavity system and (b) shows the modeling of stirrer fan in the multi-mode microwave model

The smaller the discrete angle used for rotating the stirrer fan, the longer the simulation time and vice versa. Larger discrete angles may also miss the correct standing wave pattern. Hence, to find an optimized rotation angle of the stirrer fan, the effect of various angle steps of the stirrer on the heat (energy) absorption of a rock sample inside the multi-mode microwave cavity model was studied. Similar to the approach used in the mesh independence study, several numerical models were developed for the BTS size kimberlite #2 sample. Then, the models were simulated by manually rotating the stirrer fan at different angle step sizes,  $0.5^\circ$ ,  $1^\circ$ ,  $1.5^\circ$ ,  $2^\circ$ , ...,  $10^\circ$  within a  $60^\circ$  cycle of the stirrer fan, and solving the model for each angle step size was defined sequentially. (It should be noted here that because the positions of the stirrer fan at  $0^\circ$  and  $60^\circ$  are the same, only one of them was solved; for example, if the angle step of  $10^\circ$  was assigned, the model solved only for  $0^\circ$ ,  $10^\circ$ ,  $20^\circ$ ,  $30^\circ$ ,  $40^\circ$ , and  $50^\circ$ .) Subsequently, the averaged values of the heat (energy) absorption by the rock sample for different angle step sizes were calculated and compared. As a result of this investigation, it was found that an angle step size of  $5^\circ$  for the rotation of the stirrer fan can predict a valid, trustworthy result with a reasonable computation time. Therefore, the rotation of the stirrer fan at  $5^\circ$ , within a  $60^\circ$  cycle, was chosen from among the other angle steps to be set in all the numerical models of the present study. For a better understanding of how the

above-introduced novel strategy was employed in the present study for the numerical modeling of microwave-assisted heating of rocks, an empty multi-mode microwave cavity model (assuming there was only air in the cavity space) was subjected to an input power level of 3 kW. Then 3D propagation of the induced electric field norm inside the microwave cavity in which its stirrer fan rotates every time  $5^\circ$  from its initial position ( $\theta = 0^\circ$ ) up to  $55^\circ$  within a  $60^\circ$  cycle was obtained from the simulation. The results of this numerical trial are shown in both 2D and 3D plots in Figure 6.22. The figure provides 2D plots of electric field distribution at xy and xz cut planes (2D slices from the 3D distribution) and the averaged plots from all the rotation angles of the stirrer fan.

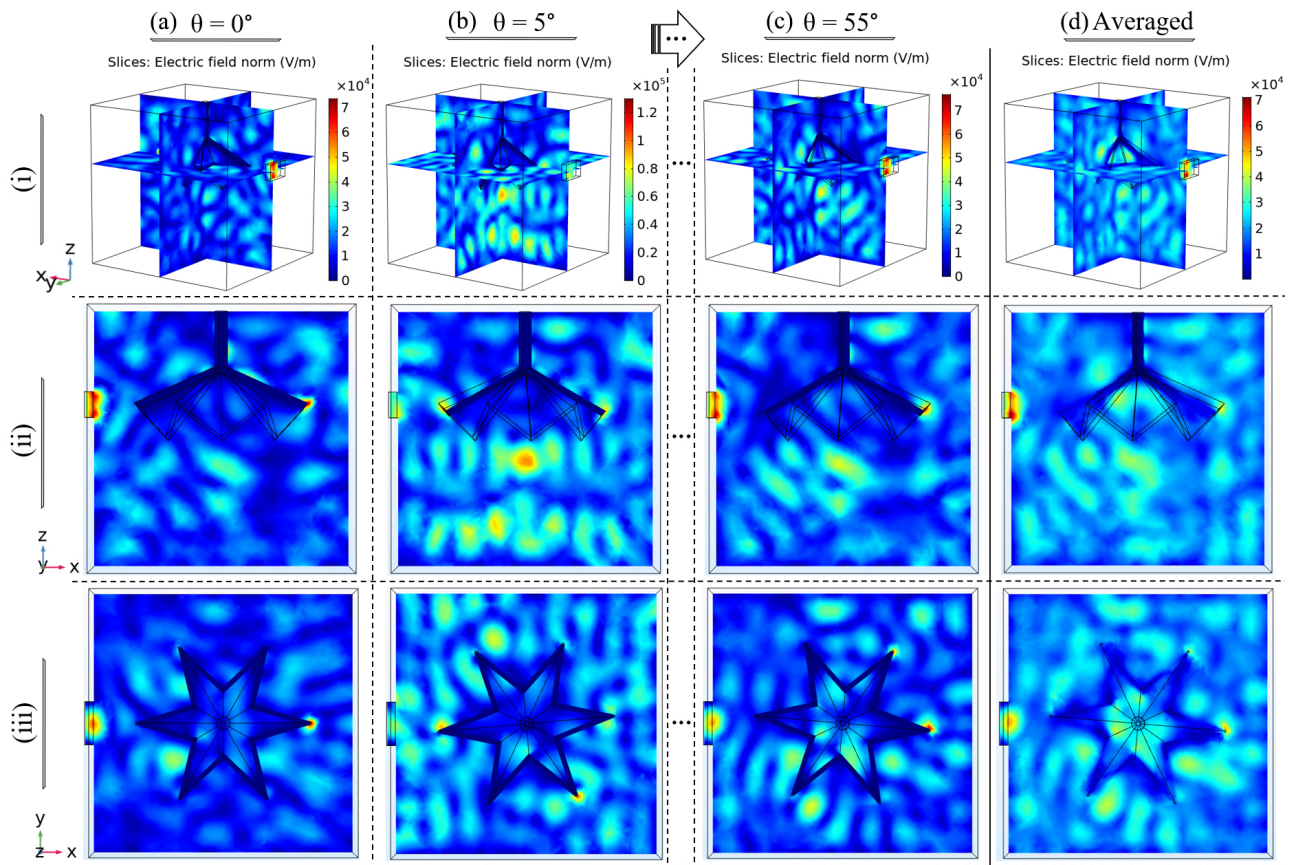


Figure 6.22: Illustration of the electric field distribution obtained for different positions of the stirrer fan inside an empty multi-mode microwave cavity model with an input power level of 3 kW from to initial rotation angle of (a)  $\theta = 0^\circ$  to (b)  $\theta = 5^\circ$  until when (c)  $\theta = 55^\circ$ ; and finally, (d) the obtained averaged electric field distribution, which is the overall electric field distribution in the cavity from averaging of all the obtained electric field distribution. Both (i) 3D and 2D plots: (ii) xz cut plane and (iii) xy cut plane, are shown in the figure.

As shown above, the resulting electric field distribution was obtained from averaging all the obtained electric field distributions at different (manual) rotation angles of the stirrer fan in the multi-mode microwave cavity model. The overall distribution of the electric field represents the actual propagation of the incoming electromagnetic waves inside the practical microwave system. Thus, the simulation of the heat (energy) absorption by any type of rock sample in the presented multi-mode microwave cavity model was expected to be very close to the results of the practical tests. This evaluation is presented in the following section.

### **6.3.4 Results and discussion**

In this section, the results of the numerical modeling of multi-mode microwave irradiation on the selected rock types are presented and discussed as follows. First, the results of model validation against experimental data from calorimetric tests are provided and discussed. Then, the effects of the calculated microwave ramp-up times on the results of the numerical models of the same practical tests' conditions are investigated. Finally, because the selected rock types of the present study, granite, kimberlite #1 and kimberlite #2, showed variations in their dielectric properties after measurements from one sample of each rock type to another, the effect of dielectric properties' variation for each rock type on its heat (energy) absorption were scrutinized by using the validated numerical models.

#### **6.3.4.1 Model validation**

The numerical models were validated against experimental data from the calorimetric tests. The following process was done for calorimetric measurements of the irradiated rock samples, processing the obtained data, and validating the numerical models. First, cylindrical BTS and UCS size samples of basalt, granite, and two types of kimberlite, kimberlite #1 and kimberlite #2, were exposed to microwave irradiation tests under various microwave exposure times and power levels, depending upon the microwave condition applied to the specific experimental test. The total heat (energy) absorbed by the rock samples was then measured using the method of calorimetry for all multi-mode microwave tests. Afterwards, the same practical tests were numerically modeled for all multi-mode microwave irradiation experiments with their specific experimental conditions. A very good agreement between the models and the experimental data was observed, which can be discerned from the plots given in Figures 6.23 to 6.25 for the BTS and UCS size samples of basalt, granite, kimberlite #1, and kimberlite #2.

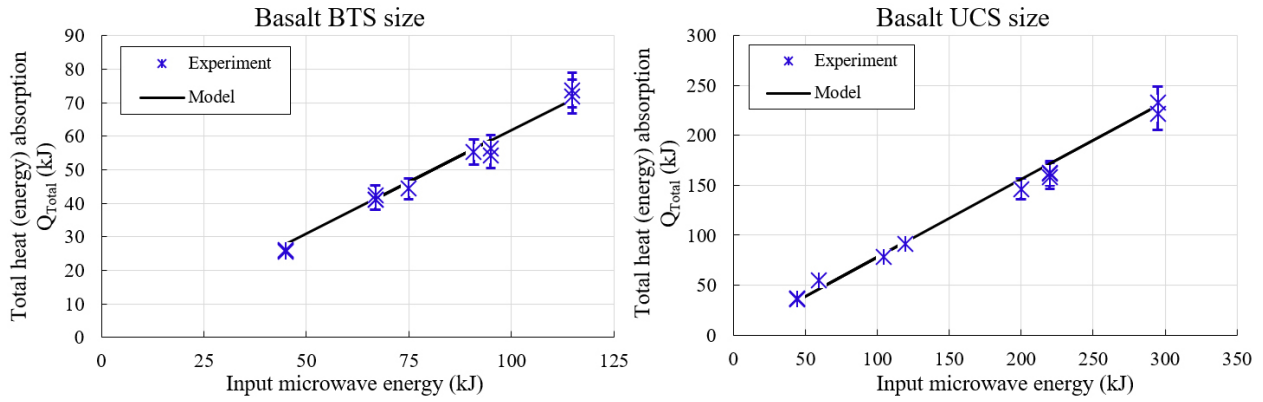


Figure 6.23: Numerical model validation against experimental data from calorimetric measurements for BTS (left) and UCS (right) size samples of basalt

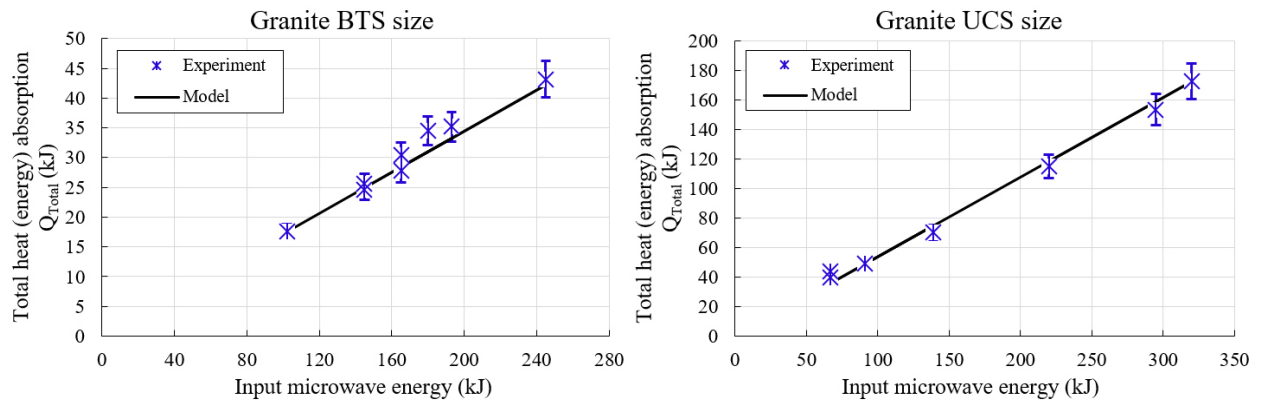


Figure 6.24: Numerical model validation against experimental data from calorimetric measurements for BTS (left) and UCS (right) size samples of granite

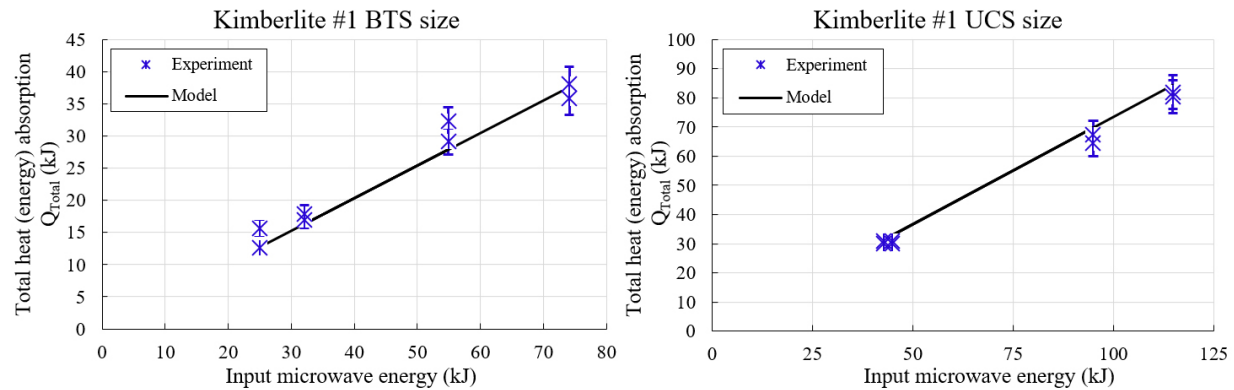


Figure 6.25: Numerical model validation against experimental data from calorimetric measurements for BTS (left) and UCS (right) size samples of kimberlite #1

As mentioned earlier in Table 6.1, because of the limitation of the number of samples available for the kimberlite #2, only one experimental setting was assigned to the microwave



irradiation of this rock type. It should also be noted that only BTS size samples from kimberlite #2 were prepared and tested in the multi-mode microwave cavity. Similar to the other rock samples, the amount of the heat (energy) absorbed by the BTS size samples of kimberlite #2 after irradiating them in the multi-mode microwave cavity at 10 kW input power and 10s of microwave exposure time was compared to its corresponding numerical model result. Good agreement between the model and the experimental data was observed as in the case of other rock models.

The numerical results of the total heat absorbed by the samples show small deviations from the experimental results for the selected rock samples. However, the small errors that are shown by error bars in Figures 6.23 to 6.25 are all within 5%; for some experimental data, less than 1% error was observed in comparison to their corresponding numerical model data. The reason behind these small deviations is that there were variations in the measured dielectric properties of the selected rock samples at 2.45 GHz; therefore, since there was only one dielectric property input ( $\epsilon' - j\epsilon''$ ) needed for the numerical modeling of each rock sample, this small variation between the numerical model result and the experimental data was expected. Another point here is that the measured dielectric properties of the selected rock samples were all at room temperature. Thus, with a proper temperature-dependent dielectric property input to the numerical models, a very small to no error should be expected. The following section analyzes the effect of various input dielectric properties in the numerical models of the selected rock samples.

#### **6.3.4.2 Analysis of dielectric property variations**

From recent literature about microwave applications in heating and pre-conditioning of rocks, it can be inferred that the thermal and structural responses of rocks to microwaves vary significantly from one rock type to another or even different rock samples within one rock type because of the differences in dielectric properties—dielectric constant ( $\epsilon'$ ) and dielectric loss factor ( $\epsilon''$ )—of their constituent minerals. Therefore, one of the main purposes of having a validated numerical model of a multi-mode microwave cavity system is to use it as a powerful tool to find the exact dielectric properties of a rock sample from the experimentally measured values of its dielectric properties, which are usually within a specific range. To better understand this statement, the variations of the measured dielectric properties at the frequency of 2.45 GHz for the two rock types, kimberlite #1 and granite, are depicted in Figures 6.26 and 6.27 where the averaged values of the measured properties are shown by the dashed lines.

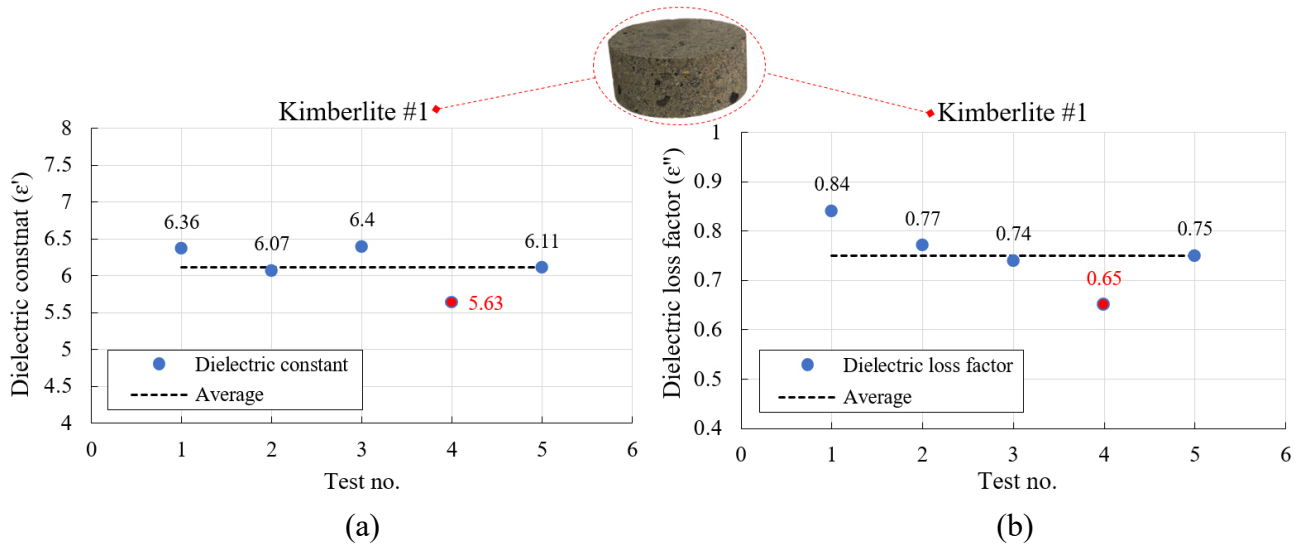


Figure 6.26: Variation of the measured (a) dielectric constant ( $\epsilon'$ ) and (b) dielectric loss factor ( $\epsilon''$ ) for kimberlite #1 at the frequency of 2.45 GHz with respect to five different tests for one sample. Note that the numerical models of both BTS and UCS size samples with the values shown in red were found to give the minimum errors when compared with the experimental data

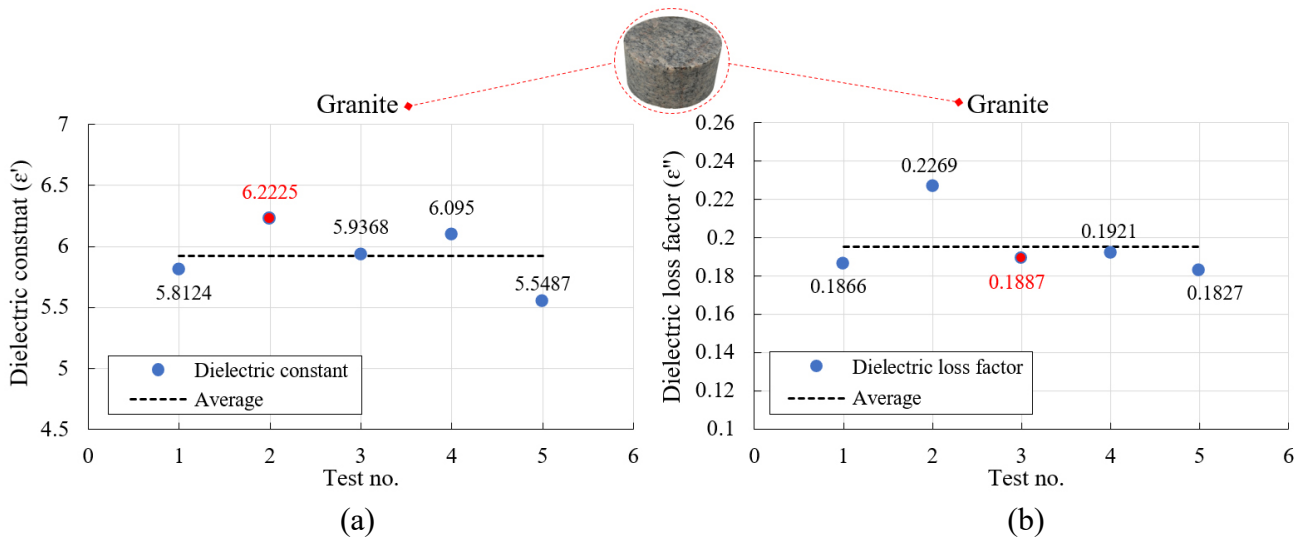


Figure 6.27: Variation of the measured (a) dielectric constant ( $\epsilon'$ ) and (b) dielectric loss factor ( $\epsilon''$ ) for granite at the frequency of 2.45 GHz with respect to five different tests for one sample. Note that the numerical models of both BTS and UCS size samples with the values shown in red were found to give the minimum errors when compared with the experimental data

As shown in above figures, no major difference between the measured values were observed. However, in the numerical models, even a small difference was found to have a major influence on the result of the numerical model. Therefore, to check which one of the measured values should

be used in the numerical models of granite and kimberlite #1, several numerical models were simulated with all the measured dielectric properties given in Figures 6.26 and 6.27. For the kimberlite #1 samples, when  $\epsilon' = 5.63$  and  $\epsilon'' = 0.65$  were assigned to the models, the minimum error between the model and the experiment was achieved; therefore, in the validation of the BTS and UCS sizes of kimberlite #1 models, the dielectric property input of  $(5.63-j\cdot0.65)$  was used for all microwave conditions. Similarly, for the granite samples, when  $\epsilon' = 5.2225$  and  $\epsilon'' = 0.1887$  were assigned to the models, the minimum error between the model and the experiment was achieved; therefore, in the validation of the BTS and UCS sizes of granite models, the dielectric property input of  $(5.222-j\cdot0.1887)$  was used for all microwave conditions. As a result of this investigation, a good agreement was achieved in the validation of the numerical results of the two rock types (see Figures 6.24 and 6.25).

Thus far, the variations in the dielectric properties of granite and kimberlite #1 have been discussed. Now, it is time to discuss the other two rock types: basalt and kimberlite #2. The samples of basalt were the most homogeneous rock type in the present project. Therefore, no significant variation was observed for basalt; as a result, the dielectric property input of  $(8.1-j\cdot0.7)$  was used for all numerical models of basalt. The validation of the models was accomplished with a very good agreement with the input of dielectric properties for both BTS and UCS size samples of basalt irradiated at different microwave conditions. For the numerical modeling of the BTS size kimberlite #2 samples in the multi-mode microwave cavity model, a similar approach was utilized for choosing the best dielectric property input to the numerical model of this rock type. However, since only one condition was defined and applied in the experimental test of kimberlite #2, a more in-depth analysis of the effect of variations in dielectric properties of rocks (a parametric study) was conducted by using the numerical model of kimberlite #2 samples. In this respect, several numerical models with different values of dielectric constant ( $\epsilon' = 3$  to  $8$ ) and dielectric loss factor ( $\epsilon'' = 0.1$  to  $0.9$ ) were performed with the same conditions applied to the practical tests of kimberlite #2 ( $P = 10$  kW,  $t = 10$ s). The average dissipated power (W) in the rock samples after their simulations in the multi-mode microwave cavity model with various input dielectric properties was then obtained and plotted. The results of this investigation are shown in Figures 6.28 to 6.30. The plots given in these figures demonstrate how the variation in the dielectric properties of rocks after their irradiation in a multi-mode microwave cavity affect the average dissipated power in rocks. Figure 6.28 shows how various inputs of dielectric constant ( $\epsilon'$ ) affect the amount of average

dissipated power after microwave exposure. The trend changes in the plots of this figure show that the higher the input dielectric constant and loss factor, the higher the average dissipated power in the sample is. Similarly, Figures 6.29 and 6.30 depict the effects of dielectric loss factor ( $\epsilon''$ ) and loss tangent ( $\tan \delta$ ), respectively. Loss tangent ( $\tan \delta$ ) is another property that can be used to determine the effect of variation in the input dielectric properties of rocks.

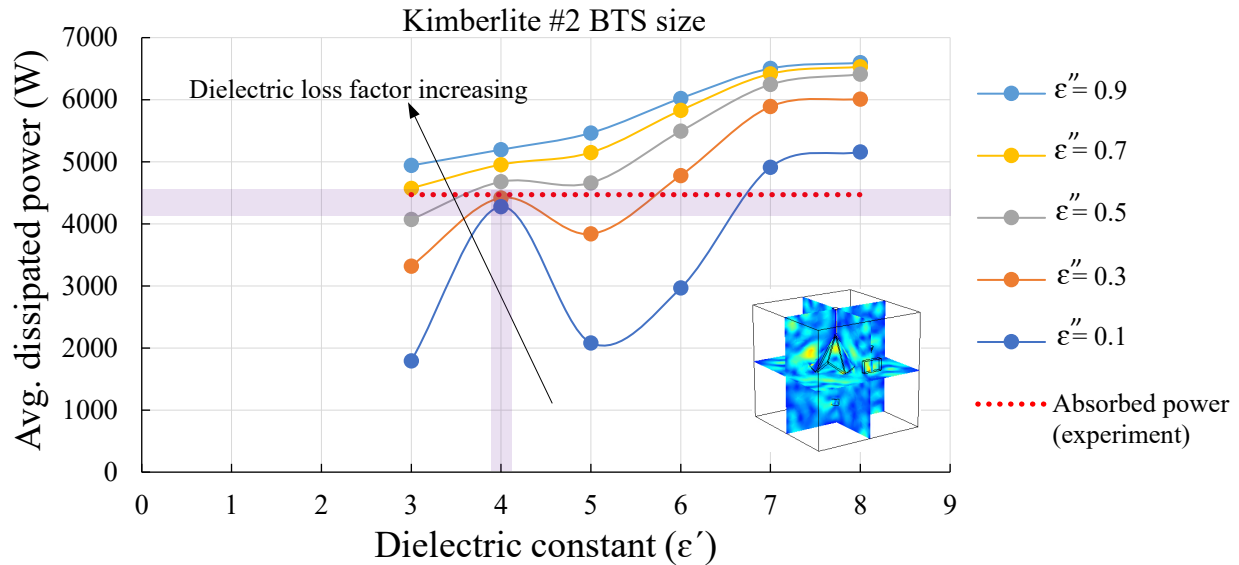


Figure 6.28: The effect of variations of dielectric constant ( $\epsilon'$ ) on the average dissipated power by kimberlite #2 BTS size after its irradiation at 10 kW and 10s microwave exposure

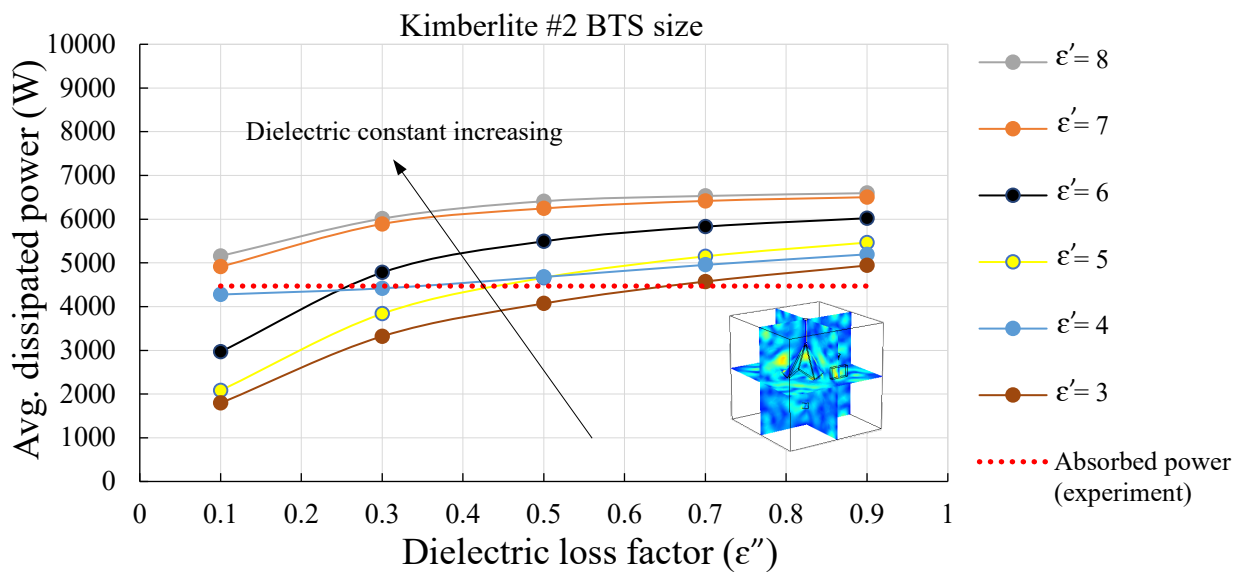


Figure 6.29: The effect of variations of dielectric loss factor ( $\epsilon''$ ) on the average dissipated power by kimberlite #2 BTS size sample after its irradiation at 10 kW and 10s microwave exposure

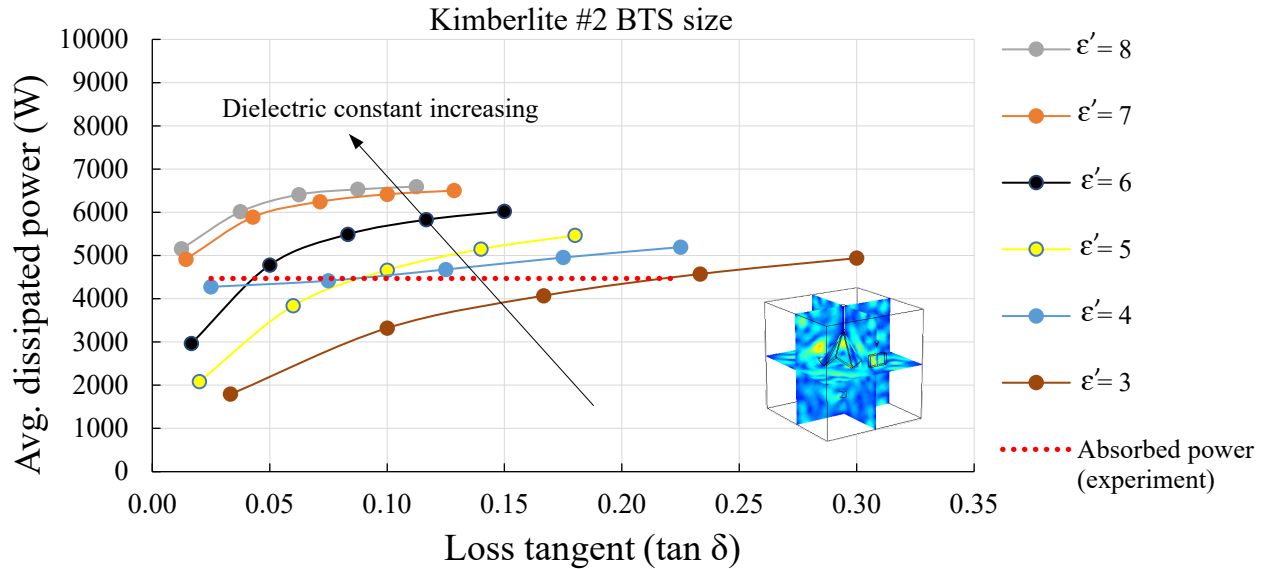


Figure 6.30: The effect of variations of loss tangent ( $\tan \delta$ ) on the average dissipated power by kimberlite #2 BTS size sample after its irradiation at 10 kW and 10s microwave exposure

The plots in above figures indicate that, in general, the higher the input dielectric constant and loss factor, the higher the average dissipated power in a rock sample is. The last step of the present parametric study was to find appropriate input dielectric properties for the numerical models of the kimberlite #2 samples and their validation against experimental data from calorimetric measurements. To this end, the measured values of absorbed power by the method of calorimetric on the microwave treated samples is shown by a red dashed line in Figures 6.28 to 6.30. However, the plots given in Figure 6.28 represents the effect of variation of both  $\epsilon'$  and  $\epsilon''$  on the rock's power absorption; there is a clear indication of higher and shorter wavelengths of the applied electromagnetic waves in the cavity from maximum and minimum points in the plots. Thus, the two regions closest to the red dashed line, which is the absorbed power in the sample from the experiment, are shaded purple in Figure 6.28. The intersection of these two purple areas gives the corresponding dielectric properties that should be used as input to the numerical model. Although two data points coincided in the region assigned, only one data point ( $4 - j0.7$ ) was the value within the range of dielectric properties of kimberlite #2 that was measured by the coaxial probe technique. With this input dielectric property, the numerical model of kimberlite #2 sample was validated against its experimental data with  $R^2 = 0.98$ . The end conclusion of the above results is that, with a validated numerical model not only further investigation on the effects of experimental tests was possible, but also the measured values of dielectric properties which are

usually within a specific range can be scrutinized to find the exact value of the rocks under consideration.

## 6.4 Conclusions

Based on the overall findings of this chapter from the results of both the experiments and the models, it can be deduced that the irradiation of basalt, granite, kimberlite #1, and kimberlite #2 in the multi-mode microwave cavity was very effective. However, the intensity of the rock surface temperature increase and the amount of heat (energy) absorption by the rock samples were mainly dependent on (1) the input microwave operating parameters, (2) size of the samples, and (3) dielectric properties of the rock. Among these three influencing parameters, the size of the samples, however, had a great impact on the absorption of the heat (energy) in all three rock types.

From the results of surface temperature measurements and by comparison of these measurements with respect to the different conditions applied, the following conclusions were drawn. For BTS size samples of basalt, the results indicated that low microwave power levels at high exposure times were considered more beneficial—more energy (heat) absorbed by the samples—than higher power levels at shorter exposure times. A similar observation was made for the UCS size samples of basalt. In the heating of the samples of granite, the effect of microwave exposure duration was found to be significantly higher for the UCS size samples of granite at high microwave power levels as opposed to the BTS size samples in which no significant impact was observed. Finally, for the UCS size samples of kimberlite #1, the higher input microwave power levels at shorter exposure times were more economical than the treatments of samples at the lower input power level and higher exposures.

An overall conclusion that can be drawn from the results of the experimental calorimetric measurements on the irradiated rock samples is that the resulting energy absorption by the BTS size samples of all the selected rocks was less than that of the UCS size samples. In terms of efficiency, irradiation of small rock samples was found to be less effective than for the larger samples; HOME values were lower for the BTS size samples than those of the UCS size samples. Finally, from the results of the numerical models for investigating the effect of variations in the dielectric properties of rocks, it was found that the higher the input dielectric constant and loss factor, the greater the average dissipated power in the rock sample.

# Chapter 7

## Concluding remarks

### 7.1 Summary and conclusions

In this thesis, the two types of microwave cavity systems, single-mode and multi-mode, along with their technical and systematic microwave irradiation mechanisms for pre-conditioning and breakage of rocks, are comprehensively defined and introduced. A commercial high power (up to 15 kW) microwave system—capable of being converted from a single-mode cavity with horn antenna to a multi-mode cavity with rotational stirrer fan—was used for (a) irradiating several rectangular specimens of basalt in the single-mode microwave cavity at different power levels, exposure times, and distances from the horn antenna, and (b) irradiating several cylindrical BTS and UCS size samples of four different rock types: basalt, granite, kimberlite #1, and kimberlite #2, at different microwave power levels and exposure times. In addition to the experimental approach, a numerical model of the multi-mode microwave cavity system with a novel strategy for simulation of the rotational stirrer fan (mode stirrer) is developed, analyzed, and validated against the experimental data from calorimetric tests. The validated numerical model is used to accurately predict the same effects (energy/absorption by the rock samples) obtained from the experiments and to evaluate the efficiency of multi-mode microwave irradiation on the selected rock types by numerically analyzing the amount of heat absorbed by the samples. With the validated numerical model, the efficiency of multi-mode microwave irradiation on other rock types with known electrical and thermal properties can be predicted with a high level of confidence. The numerical modeling approach is the initial step to gain more in-depth information on phenomena occurring inside rocks and/or minerals under microwave irradiation. A numerical model that is validated with experimental data is a novel contribution that can be employed for future investigations without costly experiments.

The results and analyses of the present work show that significant improvements in reducing the rocks' overall strength can be achieved by exposures to microwave irradiation at certain experimental conditions. However, because of the systematic differences between the single-mode and multi-mode microwave cavities in terms of their irradiation mechanisms, different conditions

have to be defined and applied, depending upon the specific effects a project seeks. A brief summary and overview of the two research stages presented in the current thesis follow.

For the concept and scope of the first stage of the present thesis, the single-mode microwave system with electromagnetic waves irradiated from a horn antenna into a metallic cavity facing the specimens of basalt was considered a good exemplary model for an actual in-field replica for future industrial implementation. The results of single-mode microwave irradiation tests on basalt indicate that microwaves have the potential to reduce the strength of rocks and pre-condition them prior to their breakage by mechanical tools; therefore, this procedure reduces the time and effort required for excavation and/or downstream processes. Thus, there is now a potential hope for continuous hard rock breakage operations with the application of single-mode microwave irradiation of rocks prior to their breakage by mechanical tools. For instance, it was assumed that in future field applications, by installing several microwave antennas at the front of a disc cutter, the electromagnetic waves applied to the surface of the rock can pre-condition it by thermally inducing several microcracks. Induction of microcracks on the surface of hard rocks results in enhanced and faster breakage operations, a greater depth of penetration from one cycle of a cutting machine, and especially a longer lifetime for disc cutters. All these benefits are expected to save millions of dollars in costs.

For the concept and scope of the second stage of the present thesis, the multi-mode microwave cavity system with microwaves irradiated from a waveguide port into a metallic cavity facing a rotational stirrer fan for propagation of the electromagnetic waves in the cavity was used to irradiate cylindrical BTS and UCS size samples of four different rock types under various experimental conditions. From calorimetric analysis on irradiated rocks in the multi-mode microwave system, the exact amount of the energy absorbed by the samples was determined. Appropriate sensitivity analyses as well as parametric studies were then conducted. Furthermore, all practical tests of the multi-mode microwave irradiation of the selected rock samples were numerically simulated for validation of the multi-mode microwave cavity model with various rock types and microwave conditions to arrive at a trustworthy numerical model. The models agreed very well with the experimental data. Hence, the validated numerical model was used to predict the effect of variations in the dielectric properties of rocks when exposed to multi-mode microwave irradiation tests, and the corresponding effects of different input dielectric properties on the dissipation of power by the rocks were assessed. By developing a novel numerical model of the



multi-mode microwave irradiation system with a rotational stirrer fan, numerically simulating the multi-mode microwave treatment of selected rock types with the same conditions of the practical tests, validating the numerical models with the experimental data, and establishing more efficient cavity setups by parametric studies, microwave energy effectiveness values were achieved. This is a novel contribution of this thesis which is a promising tool for future design, optimization (improving heating and pre-conditioning capacity), and even innovation in the implementation of large-scale microwave-assisted rock breakage systems.

The findings of the present thesis can be summarized in the following concluding remarks:

- The distribution and intensity of temperature at the surface of a rock sample after its exposure to single-mode microwave irradiation were highly dependent on the rock's position in the microwave cavity and the distance of the rock from the microwave horn antenna. Shorter distances from the horn antenna ( $< 10$  cm) result in greater damage.
- Higher microwave power levels were required for the single-mode microwave system in order to have the same damage at longer distances of a rock's surface from the horn antenna and vice versa.
- In the application of multi-mode microwave irradiation for the heating and pre-conditioning of rocks, the ratio of the size of the cavity with respect to the rock plays an important role; smaller samples usually absorb less microwave energy than larger samples in a multi-mode microwave system.
- The effect of microwave ramp-up time on the amount of sensible heat (energy) absorption of rocks is significant at high microwave power levels ( $> 10$  kW) and short exposure times ( $t < 15$  s).
- The electrical properties of rocks, i.e. dielectric constant and loss factor, are the most important parameters specifying the absorption of microwave energy. With the increasing dielectric constant of a rock sample, the average dissipated power in the sample increases.
- Despite the relatively high (more than 50%) efficiency of the irradiation of UCS size samples of granite and both BTS and UCS size samples of basalt and kimberlite in the multi-mode microwave cavity system, the total heat (energy) absorption by the BTS size samples of granite after their exposure to multi-mode microwave irradiation was very low. Thus, the irradiation of small samples of granite was found to be inefficient after a low efficiency value (less than 20%) was achieved.

## 7.2 Outlook and recommendations for future research

The concept of microwave-assisted rock heating and pre-conditioning appears to be feasible. The current research demonstrates the practical applications of single-mode and multi-mode microwave irradiation on the heating and pre-conditioning of rocks prior to their breakage by mechanical means, such as disc cutters, and/or for the purpose of their processing. Another significant contribution for future applications of microwaves in the mining industry is the concept of mine-to-mill operation for continuous mining operations; microwave-assisted rock breakage appears to be economically viable.

The following are recommendations for future research:

- Conduct single-mode and multi-mode microwave irradiation tests at very high power levels ( $> 50$  kW) on various rock types and minerals at short microwave exposure times ( $< 5$  s).
- Test the pulsed waveform (rather than the continuous form) of microwaves at different frequencies with both single-mode and multi-mode microwave cavity systems.
- Enhance the numerical model of multi-mode microwave irradiation by coupling all three electromagnetic, thermal, and mechanical multiphysics in the simulation of the microwave-assisted rock pre-conditioning process to predict the amount of mechanical stresses and the breakpoints of a rock type.
- Implement a small-scale field test based on the results of the present research for future large-scale implementations and practical applications.

## Bibliography

- World Health Organization (WHO). (2005). Electromagnetic fields and public health: microwave ovens. Information sheet Available on <http://www.who.int>
- Abdulagatov, I. M., Emirov, S. N., Abdulagatova, Z. Z., & Askerov, S. Y. (2006). Effect of pressure and temperature on the thermal conductivity of rocks. *Journal of Chemical & Engineering Data*, 51(1), 22–33.
- Abdulagatova, Z., Abdulagatov, I. M., & Emirov, V. N. (2009). Effect of temperature and pressure on the thermal conductivity of sandstone. *International Journal of Rock Mechanics and Mining Sciences*, 46(6), 1055–1071. <https://doi.org/10.1016/j.ijrmms.2009.04.011>
- Abramoff, M. D., Magalhães, P. J., & Ram, S. J. (2004). Biophotonics international. *Biophotonics International*, 11(7), 36–42. <https://dspace.library.uu.nl/handle/1874/204900>
- Agilent, Note. (2006). Agilent basics of measuring the dielectric properties of materials. Agilent literature number.
- Ali, A. Y., & Bradshaw, S. M. (2009). Quantifying damage around grain boundaries in microwave treated ores. *Chemical Engineering and Processing: Process Intensification*, 48(11-12), 1566-1573. <https://doi.org/10.1016/j.cep.2009.09.001>
- Ali, A. Y., & Bradshaw, S. M. (2010). Bonded-particle modelling of microwave-induced damage in ore particles. *Minerals Engineering*, 23(10), 780–790. <https://doi.org/10.1016/j.mineng.2010.05.019>
- Ali, A. Y. (2010). Understanding the effects of mineralogy, ore texture and microwave power delivery on microwave treatment of ores (Doctoral dissertation, University of Stellenbosch).
- Amankwah, R. K., Khan, A. U., Pickles, C. A., & Yen, W. T. (2005). Improved grindability and gold liberation by microwave pretreatment of a free-milling gold ore. *Transactions of the Institutions of Mining and Metallurgy, Section C: Mineral Processing and Extractive Metallurgy*, 114(1), 30–36. <https://doi.org/10.1179/037195505X28447>
- Amankwah, R. K., & Ofori-Sarpong, G. (2011). Microwave heating of gold ores for enhanced grindability and cyanide amenability. *Minerals Engineering*, 24(6), 541–544. <https://doi.org/10.1016/j.mineng.2010.12.002>
- Andrade, O. M., Iskander, M. F., & Bringham, S. (1992). High temperature broadband dielectric properties measurement techniques. *MRS Online Proceedings Library Archive*, 269.
- Antunes, E., Schumann, J., Brodie, G., Jacob, M. V., & Schneider, P. A. (2017). Biochar produced from biosolids using a single-mode microwave: Characterisation and its potential for phosphorus removal. *Journal of Environmental Management*, 196, 119–126. <https://doi.org/10.1016/j.jenvman.2017.02.080>
- Arfken, G. B., Weber, H. J., & Harris, F. E. (2013). Chapter 14-Bessel Functions. *Mathematical Methods for Physicists*, 643-713.
- Avanthi Isaka, B. L., Ranjith, P. G., Rathnaweera, T. D., Perera, M. S. A., & De Silva, V. R. S. (2019). Quantification of thermally-induced microcracks in granite using X-ray CT imaging and analysis. *Geothermics*. <https://doi.org/10.1016/j.geothermics.2019.04.007>

- Balanis, C. A. (1999). *Advanced engineering electromagnetics*. John Wiley & Sons.
- Balbastre, J. V., De Los Reyes, E., Nuño, M. C., & Plaza, P. (2006). Design guidelines for applicators used in the microwave heating of high losses materials. In *Advances in Microwave and Radio Frequency Processing - Report from the 8th International Conference on Microwave and High Frequency Heating* (pp. 31–38). [https://doi.org/10.1007/978-3-540-32944-2\\_4](https://doi.org/10.1007/978-3-540-32944-2_4)
- Batchelor, A. R., Jones, D. A., Plint, S., & Kingman, S. W. (2016). Increasing the grind size for effective liberation and flotation of a porphyry copper ore by microwave treatment. *Minerals Engineering*, *94*, 61–75. <https://doi.org/10.1016/j.mineng.2016.05.011>
- Begley, S. (2010). Electromagnetic properties of materials: Characterization at microwave frequencies and beyond. In *Agilent Webinar*.
- Bobicki, E. R., Liu, Q., & Xu, Z. (2018). Microwave treatment of ultramafic nickel ores: Heating behavior, mineralogy, and comminution effects. *Minerals*, *8*(11), 1–19. <https://doi.org/10.3390/min8110524>
- Bradshaw, S., Louw, W., Merwe, C. van der, Reader, H., Kingman, S., Celuch, M. M., Kijewska, W., van der Merwe, C., Reader, H., Kingman, S., Celuch, M. M., & Kijewska, W. (2007). Techno-economic considerations in the commercial microwave processing of mineral ores. *Journal of Microwave Power and Electromagnetic Energy*, *40*(4), 228–240. <https://doi.org/10.1080/08327823.2005.11688544>
- Bradshaw, S. M., Ali, A. Y., Marchand, R., & Barnard, A. (2011). Performance quantification of applicators for microwave treatment of crushed mineral ore. *Journal of Microwave Power and Electromagnetic Energy*. <https://doi.org/10.1080/08327823.2011.11689796>
- Brodie, G., Jacob, M. V., & Farrell, P. (2016). *Microwave and Radio-Frequency Technologies in Agriculture: an introduction for agriculturalists and engineers*. Walter de Gruyter GmbH & Co KG.
- Brodusch, N., Demers, H., & Gauvin, R. (2018). Imaging with a commercial Electron Backscatter Diffraction (EBSD) camera in a scanning electron microscope: a review. *Journal of Imaging*, *4*(7), 88. <https://doi.org/10.3390/jimaging4070088>
- Bruland, A. (1999). Hard rock tunnel boring advance rate and cutter wear. *Trondheim: Norwegian Institute of Technology*.
- Buttress, A. J., Binner, E., Yi, C., Palade, P., Robinson, J. P., & Kingman, S. W. (2016). Development and evaluation of a continuous microwave processing system for hydrocarbon removal from solids. *Chemical Engineering Journal*, *283*, 215–222. <https://doi.org/10.1016/j.cej.2015.07.030>
- Buttress, A. J., Katrib, J., Jones, D. A., Batchelor, A. R., Craig, D. A., Royal, T. A., Dodds, C., & Kingman, S. W. (2017). Towards large scale microwave treatment of ores: Part 1 – Basis of design, construction and commissioning. *Minerals Engineering*, *109*, 169–183. <https://doi.org/10.1016/j.mineng.2017.03.006>
- Can, N. M., & Bayraktar, I. (2007). Effect of microwave treatment on the flotation and magnetic separation properties of pyrite, chalcopyrite, galena and sphalerite. *Mining, Metallurgy & Exploration*, *24*(3), 185–192. <https://doi.org/10.1007/BF03403214>

- Čermák, V., & Rybach, L. (1982). Thermal conductivity and specific heat of minerals and rocks. *Landolt-Börnstein: Numerical Data and Functional Relationships in Science and Technology, New Series, Group V (Geophysics and Space Research), Volume Ia, (Physical Properties of Rocks)*, Edited by G. Angenheister, Springer, Berlin-Heidelberg, 305–343.
- Charikinya, E. (2015). *Characterising the effect of microwave treatment on bio-leaching of coarse, massive sulphide ore particles* (Doctoral dissertation, Stellenbosch: Stellenbosch University).
- Chen, G., Chen, J., Guo, S., Li, J., Srinivasakannan, C., & Peng, J. (2012). Dissociation behavior and structural of ilmenite ore by microwave irradiation. *Applied Surface Science*, 258(10), 4826–4829. <https://doi.org/10.1016/j.apsusc.2011.12.121>
- Chen, H., Marks, B. P., & Murphy, R. Y. (1999). Modeling coupled heat and mass transfer for convection cooking of chicken patties. *Journal of Food Engineering*. [https://doi.org/10.1016/S0260-8774\(99\)00111-9](https://doi.org/10.1016/S0260-8774(99)00111-9)
- Chen, L. F., Ong, C. K., Neo, C. P., Varadan, V. V., & Varadan, V. K. (2004). *Microwave electronics: measurement and materials characterization*. John Wiley & Sons.
- Chen, T. T., Dutrizac, J. E., Haque, K. E., Wyslouzil, W., & Kashyap, S. (1984). The relative transparency of minerals to microwave radiation. *Canadian Metallurgical Quarterly*, 23(3), 349–351. <https://doi.org/10.1179/cmqr.1984.23.3.349>
- Cheng, D. K. (1989). *Field and wave electromagnetics*. Pearson Education India.
- Cigla, M., Yagiz, S., & Ozdemir, L. (2001). Application of tunnel boring machines in underground mine development. *Proceedings of 17th International Mining Congress and Exhibition of Turkey, 155–164*, 155–164.
- Civelek, C., & Bechteler, T. F. (2008). Lagrangian formulation of electromagnetic fields in nondispersive medium by means of the extended Euler-Lagrange differential equation. *International Journal of Engineering Science*, 46(12), 1218–1227. <https://doi.org/10.1016/j.ijengsci.2008.06.007>
- COMSOL Multiphysics. (2018). COMSOL Multiphysics User's Guide. Version 5.4. In *COMSOL AB (5.4)*. COMSOL AB. <https://www.comsol.com/>
- Constant, E. W. (2002). Why evolution is a theory about stability: Constraint, causation, and ecology in technological change. *Research Policy*, 31(8–9), 1241–1256. [https://doi.org/10.1016/S0048-7333\(02\)00061-6](https://doi.org/10.1016/S0048-7333(02)00061-6)
- Coster, H. P., & FRS, E. C. B. D. (1948). The electrical conductivity of rocks at high temperatures. *Geophysical Journal International*, 5, 193–199.
- Da Silva, G. R., Espiritu, E. R. L., Mohammadi-Jam, S., & Waters, K. E. (2018). Surface characterization of microwave-treated chalcopyrite. *Colloids and Surfaces A: Physicochemical and Engineering Aspects*, 555(April), 407–417. <https://doi.org/10.1016/j.colsurfa.2018.06.078>
- Dehkhoda, S., & Fairhurst, C. (2017). Rapid excavation and tunneling techniques. *Hydraul Fract J*, 4(1), 101-108.
- Dentith, M., & Mudge, S. T. (2014). *Geophysics for the mineral exploration geoscientist*. Cambridge University Press.

- Didenko, A. N., Zverev, B. V., & Prokopenko, A. V. (2005). Microwave fracturing and grinding of solid rocks by example of kimberlite. *Doklady Physics*, 50(7), 349–350. <https://doi.org/10.1134/1.2005358>
- Dutta, T., Kim, K. H., Uchimiya, M., Kwon, E. E., Jeon, B. H., Deep, A., & Yun, S. T. (2016). Global demand for rare earth resources and strategies for green mining. *Environmental Research*, 150, 182–190. <https://doi.org/10.1016/j.envres.2016.05.052>
- Eastlund, B. J., & Jenkins, L. M. (2008). Atmospheric heating as a research tool: Link to space-based solar power. *The 17th Joint Conference on Planned and Inadvertent Weather Modification/Weather Modification Association Annual Meeting*. <https://doi.org/10.1109/AERO.2008.4526526>
- Fawzi, T. H., Fabriano-Alves, M., & Burke, P. E. (1978). The linear travelling-wave induction problem. *International Journal of Engineering Science*, 16(3), 203–213. [https://doi.org/10.1016/0020-7225\(78\)90048-4](https://doi.org/10.1016/0020-7225(78)90048-4)
- Feng, X., Lu, G., Li, Y., Zhang, X., Wen, J., Tong, T., & Gong, Y. (2020). High-power microwave borehole fracturing device for engineering rock mass. U.S. Patent No. 16/317,738.
- Ferrari-John, R. S., Batchelor, A. R., Katrib, J., Dodds, C., & Kingman, S. W. (2016). Understanding selectivity in radio frequency and microwave sorting of porphyry copper ores. *International Journal of Mineral Processing*. <https://doi.org/10.1016/j.minpro.2016.08.011>
- Fitzgibbon, K., & Veasey, T. (1990). Thermally assisted liberation—a review. *Minerals Engineering*, 3(1), 181–185. [https://doi.org/10.1016/0892-6875\(90\)90090-X](https://doi.org/10.1016/0892-6875(90)90090-X)
- FLUKE. (2020). *FLUKE Connect*. <https://www.fluke.com/>
- Forster, J., Maham, Y., & Bobicki, E. R. (2018). Microwave heating of magnesium silicate minerals. *Powder Technology*, 339, 1–7. <https://doi.org/10.1016/j.powtec.2018.07.069>
- Gabriel, C., Gabriel, S., Grant, E. H., Halstead, B. S. J., & Michael P Mingos, D. (1998). Dielectric parameters relevant to microwave dielectric heating. *Chemical Society Reviews*, 27(3), 213–223. <https://doi.org/10.1039/a827213z>
- Ghodgaonkar, D. K., Varadan, V. V., & Varadan, V. K. (1989). A free-space method for measurement of dielectric constants and loss tangents at microwave frequencies. *IEEE Transactions on Instrumentation and Measurement*, 38(3), 789–793.
- Griffiths, D. J. (2017). *Introduction to Electrodynamics*. Cambridge University Press. <https://doi.org/10.1017/9781108333511>
- Groslik, U., Dikhtyar, V., & Jerby, E. (2002). Coupled Thermal-Electromagnetic Model For Microwave Drilling. *European Symposium on Numerical Methods in Electromagnetics, JEE'02 Proc., March 6-8, 2002, Toulouse, France*, 146–151.
- Haase, R. G. B. (1991). Non-explosive mining: An untapped potential for the South African gold-mining industry. *Journal of the Southern African Institute of Mining and Metallurgy*, 91(11), 381–388.
- Haque, K. E. (1999). Microwave energy for mineral treatment processes—a brief review. *International Journal of Mineral Processing*, 57(1), 1–24. [https://doi.org/10.1016/S0301-7516\(99\)00009-5](https://doi.org/10.1016/S0301-7516(99)00009-5)

- Harrison, P. C. (1997). *A fundamental study of the heating effect of 2.45 GHz microwave radiation on minerals* (Doctoral dissertation, University of Birmingham).
- Hartlieb, P., Kuchar, F., Moser, P., Kargl, H., & Restner, U. (2018). Reaction of different rock types to low-power (3.2 kW) microwave irradiation in a multimode cavity. *Minerals Engineering*, *118*(December 2017), 37–51. <https://doi.org/10.1016/j.mineng.2018.01.003>
- Hartlieb, P., Leindl, M., Kuchar, F., Antretter, T., & Moser, P. (2012). Damage of basalt induced by microwave irradiation. *Minerals Engineering*. <https://doi.org/10.1016/j.mineng.2012.01.011>
- Hartlieb, P., Toifl, M., Kuchar, F., Meisels, R., & Antretter, T. (2016). Thermo-physical properties of selected hard rocks and their relation to microwave-assisted comminution. *Minerals Engineering*, *91*, 34–41. <https://doi.org/10.1016/j.mineng.2015.11.008>
- Hartlieb, P., & Grafe, B. (2017). Experimental study on microwave assisted hard rock cutting of granite. *BHM Berg-und Hüttenmännische Monatshefte*, *162*(2), 77-81. <https://doi.org/10.1007/s00501-016-0569-0>
- Hartlieb, Philipp, Grafe, B., Shepel, T., Malovyk, A., & Akbari, B. (2017). Experimental study on artificially induced crack patterns and their consequences on mechanical excavation processes. *International Journal of Rock Mechanics and Mining Sciences*. <https://doi.org/10.1016/j.ijrmmms.2017.10.024>
- Hartlieb, Philipp, & Rostami, J. (2018). Rock mechanics implications of microwave treatment of rock as part of a hybrid system for mechanical excavation of rock for civil and mining applications. *Geomechanics and Geodynamics of Rock Masses-Volume 2: Proceedings of the 2018 European Rock Mechanics Symposium*, 1017.
- Hartman, H. L., Britton, S. G., Mutmansky, J. M., Gentry, D. W., Schlitt, W. J., Karmis, M., & Singh, M. M. (1994). *SME mining engineering handbook* (Vol. 2). Society for Mining, Metallurgy, and Exploration Denver.
- Hartman, H. L., & Mutmansky, J. M. (2002). *Introductory mining engineering*. John Wiley & Sons.
- Hassani, F., & Nekoovaght, P. (2011). The development of microwave assisted machineries to break hard rocks. *28th International Symposium on Automation and Robotics in Construction, ISARC 2011*, 678–684.
- Hassani, F., Nekoovaght, P. M., & Gharib, N. (2016). The influence of microwave irradiation on rocks for microwave-assisted underground excavation. *Journal of Rock Mechanics and Geotechnical Engineering*, *8*(1), 1–15. <https://doi.org/10.1016/j.jrmge.2015.10.004>
- Hassani, Ferri, Shadi, A., Rafezi, H., Sasmito, A., & Ghoreishi-Madiseh, S. A. (2020). Energy analysis of the effectiveness of microwave-assisted fragmentation. *Minerals Engineering*.
- Havens, K. J., & Sharp, E. J. (2015). *Thermal imaging techniques to survey and monitor animals in the wild: A methodology*. Academic Press.
- Hidayat, M. I. P., Felicia, D. M., Rafandi, F. I., & Machmudah, A. (2020). Effects of sample shapes and thickness on distribution of temperature inside the mineral ilmenite due to microwave heating. *Minerals*, *10*(4). <https://doi.org/10.3390/min10040382>

- Hong, Y. Du, Lin, B. Q., Li, H., Dai, H. M., Zhu, C. J., & Yao, H. (2016). Three-dimensional simulation of microwave heating coal sample with varying parameters. *Applied Thermal Engineering*. <https://doi.org/10.1016/j.applthermaleng.2015.10.041>
- Huang, J., Xu, G., Chen, Y., & Chen, Z. (2019). Simulation of microwave's heating effect on coal seam permeability enhancement. *International Journal of Mining Science and Technology*, 29(5), 785–789. <https://doi.org/10.1016/j.ijmst.2018.04.017>
- Huang, J., Xu, G., Hu, G., Kizil, M., & Chen, Z. (2018). A coupled electromagnetic irradiation, heat and mass transfer model for microwave heating and its numerical simulation on coal. *Fuel Processing Technology*, 177(April), 237–245. <https://doi.org/10.1016/j.fuproc.2018.04.034>
- Huang, J., Xu, G., Liang, Y., Hu, G., & Chang, P. (2020). Improving coal permeability using microwave heating technology—A review. *Fuel*, 266(January), 117022. <https://doi.org/10.1016/j.fuel.2020.117022>
- Incropera, F. P., DeWitt, D. P., Bergman, T. L., & Lavine, A. S. (2007). *Fundamentals of Heat and Mass Transfer*. <https://doi.org/10.1073/pnas.0703993104>
- Irannajad, M., Mehdilo, A., & Salmani Nuri, O. (2014). Influence of microwave irradiation on ilmenite flotation behavior in the presence of different gangue minerals. *Separation and Purification Technology*, 132(3), 401–412. <https://doi.org/10.1016/j.seppur.2014.05.046>
- Jerby, E., Meir, Y., & Faran, M. (2013). Basalt melting by localized-microwave thermal-runaway instability. *14th International Conference on Microwave and High Frequency Heating, AMPERE 2013, September*, 254–257.
- Jerby, Eli, & Dikhtiar, V. (2000). *Method and device for drilling, cutting, nailing and joining solid non-conductive materials using microwave radiation* (Patent No. 6114676). U.S. Patent and Trademark Office. <https://doi.org/https://patents.google.com/patent/US6114676A/en>
- Jerby, Eli, & Dikhtyar, V. (2003). The microwave drill. In *Water Well Journal* (Vol. 57, Issue 7).
- Jerby, Eli, Nerovny, Y., Meir, Y., Korin, O., Peleg, R., & Shamir, Y. (2018). A silent microwave drill for deep holes in concrete. *IEEE Transactions on Microwave Theory and Techniques*, 66(1), 522–529. <https://doi.org/10.1109/TMTT.2017.2729509>
- John, R. S., Batchelor, A. R., Ivanov, D., Udoudo, O. B., Jones, D. A., Dodds, C., & Kingman, S. W. (2015). Understanding microwave induced sorting of porphyry copper ores. *Minerals Engineering*, 84, 77–87. <https://doi.org/10.1016/j.mineng.2015.10.006>
- Jokovic, V. (2012). *Microwave Processing of Minerals* (Issue February).
- Jokovic, V., Antonio, C., & Morrison, R. (2019). MW heating of rock particles and their cross-dependencies. *Minerals Engineering*, 141(June), 105834. <https://doi.org/10.1016/j.mineng.2019.105834>
- Jones, D. A., Kingman, S. W., Whittles, D. N., & Lowndes, I. S. (2005). Understanding microwave assisted breakage. *Minerals Engineering*, 18(7), 659–669. <https://doi.org/10.1016/j.mineng.2004.10.011>



- Jones, D. A., Kingman, S. W., Whittles, D. N., & Lowndes, I. S. (2007). The influence of microwave energy delivery method on strength reduction in ore samples. *Chemical Engineering and Processing: Process Intensification*, 46(4), 291–299. <https://doi.org/10.1016/j.cep.2006.06.009>
- Jones, D. A., Lelyveld, T. P., Mavrofidis, S. D., Kingman, S. W., & Miles, N. J. (2002). Microwave heating applications in environmental engineering—A review. *Resources, Conservation and Recycling*, 34(2), 75–90. [https://doi.org/10.1016/S0921-3449\(01\)00088-X](https://doi.org/10.1016/S0921-3449(01)00088-X)
- Kahraman, S., & Gunaydin, O. (2009). The effect of rock classes on the relation between uniaxial compressive strength and point load index. *Bulletin of Engineering Geology and the Environment*, 68(3), 345–353. <https://doi.org/10.1007/s10064-009-0195-0>
- Kahraman, Sair, Canpolat, A. N., & Fener, M. (2020). The influence of microwave treatment on the compressive and tensile strength of igneous rocks. *International Journal of Rock Mechanics and Mining Sciences*, 129(March 2019), 104303. <https://doi.org/10.1016/j.ijrmms.2020.104303>
- Khan, M. T., & Ali, S. M. (2012). A brief review of measuring techniques for characterization of dielectric materials. *International Journal of Information Technology and Electrical Engineering*, 1(1).
- Kingman, S. (1996). Microwave processing of materials. In *Annual Review of Materials Science* (Vol. 26, Issue 1). <https://doi.org/10.1146/annurev.ms.26.080196.001503>
- Kingman, S. W. (2006). Recent developments in microwave processing of minerals. *International Materials Reviews*, 51(1), 1–12. <https://doi.org/10.1179/174328006X79472>
- Kingman, S. W., Jackson, K., Bradshaw, S. M., Rowson, N. A., & Greenwood, R. (2004). An investigation into the influence of microwave treatment on mineral ore comminution. *Powder Technology*, 146(3), 176–184. <https://doi.org/10.1016/j.powtec.2004.08.006>
- Kingman, S. W., Jackson, K., Cumbane, A., Bradshaw, S. M., Rowson, N. A., & Greenwood, R. (2004). Recent developments in microwave-assisted comminution. *International Journal of Mineral Processing*, 74(1–4), 71–83. <https://doi.org/10.1016/j.minpro.2003.09.006>
- Kingman, S. W., & Rowson, N. A. (1998). Microwave treatment of minerals—a review. *Minerals Engineering*, 11(11), 1081–1087. [https://doi.org/10.1016/S0892-6875\(98\)00094-6](https://doi.org/10.1016/S0892-6875(98)00094-6)
- Kingman, Samuel William. (2009). *Pre treatment of multi-phase materials using high field strength electromagnetic waves*. Google Patents.
- Kingman, Vorster, W., & Rowson, N. A. (2000). The Influence of mineralogy on microwave assisted grinding. *Minerals Engineering*. [https://doi.org/10.1016/S0892-6875\(00\)00010-8](https://doi.org/10.1016/S0892-6875(00)00010-8)
- Kobusheshe, J. (2010). *Microwave enhanced processing of ores*.
- Kothari, C. (2004). Research methodology: methods and techniques. *New Age International*.
- Kumar, P., Sahoo, B. K., De, S., Kar, D. D., Chakraborty, S., & Meikap, B. C. (2010). Iron ore grindability improvement by microwave pre-treatment. *Journal of Industrial and Engineering Chemistry*, 16(5), 805–812. <https://doi.org/10.1016/j.jiec.2010.05.008>

- Li, H., Lin, B., Chen, Z., Hong, Y., & Zheng, C. (2017). Evolution of coal petrophysical properties under microwave irradiation stimulation for different water saturation conditions. *Energy and Fuels*, 31(9), 8852–8864. <https://doi.org/10.1021/acs.energyfuels.7b00553>
- Li, H., Shi, S., Lin, B., Lu, J., Lu, Y., Ye, Q., Wang, Z., Hong, Y., & Zhu, X. (2019). A fully coupled electromagnetic, heat transfer and multiphase porous media model for microwave heating of coal. *Fuel Processing Technology*, 189(October 2018), 49–61. <https://doi.org/10.1016/j.fuproc.2019.03.002>
- Li, H., Shi, S., Lu, J., Ye, Q., Lu, Y., & Zhu, X. (2019). Pore structure and multifractal analysis of coal subjected to microwave heating. *Powder Technology*, 346, 97–108. <https://doi.org/10.1016/j.powtec.2019.02.009>
- Li, J., Kaunda, R. B., Arora, S., Hartlieb, P., & Nelson, P. P. (2019). Fully-coupled simulations of thermally-induced cracking in pegmatite due to microwave irradiation. *Journal of Rock Mechanics and Geotechnical Engineering*, 11(2), 242–250. <https://doi.org/10.1016/j.jrmge.2018.12.007>
- Li, K., Chen, J., Chen, G., Peng, J., Ruan, R., & Srinivasakannan, C. (2019). Microwave dielectric properties and thermochemical characteristics of the mixtures of walnut shell and manganese ore. *Bioresource Technology*, 286(April), 121381. <https://doi.org/10.1016/j.biortech.2019.121381>
- Li, X., Wang, S., Xu, Y., Yao, W., Xia, K., & Lu, G. (2019). Effect of microwave irradiation on dynamic mode-I fracture parameters of Barre granite. *Engineering Fracture Mechanics*, 224(October 2019), 106748. <https://doi.org/10.1016/j.engfracmech.2019.106748>
- Li, Z., Haigh, A., Soutis, C., & Gibson, A. (2018). Principles and applications of microwave testing for woven and non-woven carbon fibre-reinforced polymer composites: a topical review. *Applied Composite Materials*, 25(4), 965–982. <https://doi.org/10.1007/s10443-018-9733-x>
- Li, Zhao, Z., Xiouras, C., Stefanidis, G. D., Li, X., & Gao, X. (2019). Fundamentals and applications of microwave heating to chemicals separation processes. *Renewable and Sustainable Energy Reviews*, 114(March), 109316. <https://doi.org/10.1016/j.rser.2019.109316>
- Like, Q., Jun, D., & Pengfei, T. (2015). Study on the effect of microwave irradiation on rock strength. *Journal of Engineering Science and Technology Review*, 8(4), 91-96.
- Lin, B., Li, H., Chen, Z., Zheng, C., Hong, Y., & Wang, Z. (2017). Sensitivity analysis on the microwave heating of coal: A coupled electromagnetic and heat transfer model. *Applied Thermal Engineering*, 126, 949–962. <https://doi.org/10.1016/j.applthermaleng.2017.08.012>
- Lindroth, D. P., Morrell, R. J., & Blair, J. R. (1991a). *Microwave assisted hard rock cutting* (Patent No. US5003144A). U.S. Patent and Trademark Office. <https://www.osti.gov/servlets/purl/867753>
- Liu, F. (2014). *Exploration of microwave-assisted breakage of rocks: The effect of size, shape, and internal discontinuity of rock on microwave distribution* (Doctoral dissertation, McGill University Libraries).

- Lovás, M., Kováčová, M., Dimitrakis, G., Čuvanová, S., Znamenáčková, I., & Jakabský, Š. (2010). Modeling of microwave heating of andesite and minerals. *International Journal of Heat and Mass Transfer*, 53(17–18), 3387–3393. <https://doi.org/10.1016/j.ijheatmasstransfer.2010.03.012>
- Lovas, M., Znamenackova, I., Zubrik, M., Kovacova, M., & Dolinska, S. (2011). The application of microwave energy in mineral processing—a review. *Acta Montanistica Slovaca*, 16(2), 137–148.
- Lu, G. M., Feng, X. T., Li, Y. H., & Zhang, X. (2019). The microwave-induced fracturing of hard rock. *Rock Mechanics and Rock Engineering*, 52(9), 3017–3032. <https://doi.org/10.1007/s00603-019-01790-z>
- Lu, G. M., Feng, X. T., Li, Y. H., Hassani, F., & Zhang, X. (2019). Experimental investigation on the effects of microwave treatment on basalt heating, mechanical strength, and fragmentation. *Rock Mechanics and Rock Engineering*, 52(8), 2535–2549. <https://doi.org/10.1007/s00603-019-1743-y>
- Lu, Gao ming, Li, Y. hui, Hassani, F., & Zhang, X. (2017). The influence of microwave irradiation on thermal properties of main rock-forming minerals. *Applied Thermal Engineering*, 112, 1523–1532. <https://doi.org/10.1016/j.applthermaleng.2016.11.015>
- Lu, Gaoming, Feng, X., Li, Y., & Zhang, X. (2020). Influence of microwave treatment on mechanical behaviour of compact basalts under different confining pressures. *Journal of Rock Mechanics and Geotechnical Engineering*, 12(2), 213–222. <https://doi.org/10.1016/j.jrmge.2019.06.009>
- Lu, G. M., Li, Y. H., Hassani, F., & Zhang, X. (2016). Review of theoretical and experimental studies on mechanical rock fragmentation using microwave-assisted approach. *Chin J Geotech Eng*, 38(8), 1497–1506. <https://doi.org/10.11779/CJGE201608018>
- Madding, R. P. (1999, March). Emissivity measurement and temperature correction accuracy considerations. In *Thermosense XXI* (Vol. 3700, pp. 393–401). International Society for Optics and Photonics.
- Maidl, B., Schmid, L., Ritz, W., & Herrenknecht, M. (2008). *Hardrock tunnel boring machines*. John Wiley & Sons.
- Makul, N., Rattanadecho, P., & Agrawal, D. K. (2014). Applications of microwave energy in cement and concrete—a review. *Renewable and Sustainable Energy Reviews*, 37, 715–733. <https://doi.org/10.1016/j.rser.2014.05.054>
- Marland, S., Merchant, A., & Rowson, N. (2001). Dielectric properties of coal. *Fuel*, 80(13), 1839–1849.
- Mathews, J. P., Pone, J. D. N., Mitchell, G. D., & Halleck, P. (2011). High-resolution X-ray computed tomography observations of the thermal drying of lump-sized subbituminous coal. *Fuel Processing Technology*. <https://doi.org/10.1016/j.fuproc.2010.08.020>
- MathWorks. (2020). *Matlab R2020a*. <http://www.mathworks.com>
- Maurer, W. (1968). *Novel drilling techniques*.
- Maurer, W. C. (1979). *Novel derilling techniques*.

- Meisels, R., Toifl, M., Hartlieb, P., Kuchar, F., & Antretter, T. (2015). Microwave propagation and absorption and its thermo-mechanical consequences in heterogeneous rocks. *International Journal of Mineral Processing*, 135, 40–51. <https://doi.org/10.1016/j.minpro.2015.01.003>
- Meng, Y., Tang, L., Yan, Y., Oladejo, J., Jiang, P., Wu, T., & Pang, C. (2019). Effects of microwave-enhanced pretreatment on oil shale milling performance. *Energy Procedia*, 158, 1712–1717. <https://doi.org/10.1016/j.egypro.2019.01.398>
- Meredith, R. J. (1998). *Engineers' handbook of industrial microwave heating* (Issue 25). Institution of Electrical Engineers. <https://trove.nla.gov.au/version/208145305>
- Metaxas, A. C. and, & Meredith, R. J. (1983). *Industrial microwave heating* (Issue 4). IET.
- Metaxas, A. C., & Meredith, R. J. (2011). Dielectric loss. *Industrial Microwave Heating*, 5–25. [https://doi.org/10.1049/pbpo004e\\_ch2](https://doi.org/10.1049/pbpo004e_ch2)
- Mitchell, R. H. (2013). *Kimberlites: mineralogy, geochemistry, and petrology*. Springer Science & Business Media.
- Monti, T., Tselev, A., Udoudo, O., Ivanov, I. N., Dodds, C., & Kingman, S. W. (2016). High-resolution dielectric characterization of minerals: A step towards understanding the basic interactions between microwaves and rocks. *International Journal of Mineral Processing*, 151, 8–21. <https://doi.org/10.1016/j.minpro.2016.04.003>
- Morrison, R. D. (2013). *Rock analysis apparatus and method* (Patent No. US 8,446,156 B2).
- Nekoovaght Motlagh, P. (2009). An investigation on the influence of microwave energy on basic mechanical properties of hard rocks (Doctoral dissertation, Concordia University).
- Motlagh, P. N. (2015). Physical and mechanical properties of rocks exposed to microwave irradiation: potential application to tunnel boring. *McGill University, Montreal*.
- Murray, C., Courtley, S., & Howlett, P. F. (1994). Developments in rock-breaking techniques. *Tunnelling and Underground Space Technology Incorporating Trenchless*, 9(2), 225–231. [https://doi.org/10.1016/0886-7798\(94\)90034-5](https://doi.org/10.1016/0886-7798(94)90034-5)
- Napier-Munn, T. J., Morrell, S., Morrison, R. D., & Kojovic, T. (1996). Mineral comminution circuits: their operation and optimisation. *JKMRC Monograph Series in Mining and Mineral Processing*, 2.
- Nasseri, M. H. B., Young, R. P., Rezanezhad, F., & Cho, S. H. (2009). Application of 3D X-ray CT scanning techniques to evaluate fracture damage zone in anisotropic granitic rock. *ROCKENG09: Proceedings of the 3rd CANUS Rock Mechanics Symposium*, (May), 1–12.
- Natanzi, A. S., & Laefer, D. F. (2014). Using chemicals as demolition agents near historic structures. In *9<sup>th</sup> International Conference on Structural Analysis of Historical Constructions*, Mexico City, Mexico, 14-17 October, 2014. <http://researchrepository.ucd.ie/handle/10197/6798>
- National Research Council. (1994). Drilling and excavation technologies for the future. *The National Academies Press*. <https://doi.org/10.17226/2349>
- Ndeda, R., Sebusang, E., Marumo, R., & Ogur, E. (2015). Review of thermal surface drilling technologies. *Proceedings of Sustainable Research and Innovation Conference*, 61–69.

- Nekoovaght, P. M. (2015). Physical and mechanical properties of rocks exposed to microwave irradiation: potential application to tunnel boring. *McGill University, Montreal*.
- Nicco, M., Holley, E. A., Hartlieb, P., Kaunda, R., & Nelson, P. P. (2018). Methods for characterizing cracks induced in rock. *Rock Mechanics and Rock Engineering*. <https://doi.org/10.1007/s00603-018-1445-x>
- Nienhaus, K., Kuchinke, C., & Röllinger, D. (2013). Emission analysis of the cutting tools used for hard rock cutting with regard to status monitoring. *ISRM International Symposium-EUROCK 2013*.
- Ong, K. C. G., & Akbarnezhad, A. (2018). *Microwave-assisted concrete technology*. CRC Press. <https://doi.org/https://doi.org/10.1201/b17917>
- Ouellet, J., Radziszewski, P., Raghavan, V., Satish, H., & Hassani, F. (2013). *Electromagnetic energy assisted drilling system and method* (Patent No. Patent No. 8,550,182). Google Patents. <https://patents.google.com/patent/US8550182B2/en>
- Palacky, G. J. (1988). Resistivity characteristics of geologic targets. *Electromagnetic Methods in Applied Geophysics, 1*, 53–129.
- Panofsky, W. K. H., & Phillips, M. (2005). *Classical electricity and magnetism*. Courier Corporation.
- Pederick, S., & Lever, P. J. A. (2004). Increased flexibility using waterjet assisted blasthole drilling. *EXPLO2004*.
- Peinsitt, T., Kuchar, F., Hartlieb, P., Moser, P., Kargl, H., Restner, U., & Sifferlinger, N. a. (2010). Microwave heating of dry and water saturated basalt, granite and sandstone. *International Journal of Mining and Mineral Engineering*. <https://doi.org/10.1504/IJMME.2010.031810>
- Peng, Z., Hwang, J. Y., Park, C. L., Kim, B. G., & Onyedika, G. (2011). Numerical analysis of heat transfer characteristics in microwave heating of magnetic dielectrics. *Metallurgical and Materials Transactions A: Physical Metallurgy and Materials Science, 43(3)*, 1070–1078. <https://doi.org/10.1007/s11661-011-1014-3>
- Persson, P., Holmberg, R., & Lee, J. (1994). *Rock blasting and explosives engineering*. CPC press. <https://doi.org/10.1201/9780203740514>
- Pozar, D. (2012). Microwave Engineering Fourth Edition. In *Wiley*. <https://doi.org/TK7876.P69> 2011
- Rakrueangdet, K., Nunak, N., Suesut, T., & Sritham, E. (2016). Emissivity measurements of reflective materials using infrared thermography. *International MultiConference of Engineers and Computer Scientists (IMECS)*.
- Ramezanzadeh, A., & Hood, M. (2010). *A state-of-the-art review of mechanical rock excavation technologies*.
- Ramo, S., Whinnery, J. R., & Van Duzer, T. (1994). *Fields and waves in communication electronics*. John Wiley & Sons.
- Reddy, M. V., Hemanth, K. S., & Mohan, C. V. (2013). Microwave power transmission—a next generation power transmission system. *IOSR Journal of Electrical and Electronics Engineering (IOSR-JEEE), 4(5)*, 24-28. <https://doi.org/10.9790/1676-0452428>

- Res, J., Wladzielczyk, K., & Ghose, A. K. (2003). *Environment-friendly techniques of rock breaking*. CRC Press.
- Rizmanoski, V. (2011). The effect of microwave pretreatment on impact breakage of copper ore. *Minerals Engineering*, 24(14), 1609–1618. <https://doi.org/10.1016/j.mineng.2011.08.017>
- Rizmanoski, V., & Jokovic, V. (2016). Synthetic ore samples to test microwave/RF applicators and processes. *Journal of Materials Processing Technology*, 230, 50–61. <https://doi.org/10.1016/j.jmatprotec.2015.04.032>
- Rodriguez, R., Crandall, D. M., Song, X., Verba, C. A., & Soeder, D. J. (2014). *Imaging Techniques for Analyzing Shale Pores and Minerals* (Dec 2014) (No. NETL-TRS-6-2014). NETL.
- Rostami, J. (2011). Mechanical rock breaking. In *SME Mining Engineering Handbook, Third Edition* (Issue 2011, p. 388). <https://books.google.ru/books?id=5uq-kdfHLWUC>
- Sahoo, B. K., De, S., & Meikap, B. C. (2011). Improvement of grinding characteristics of Indian coal by microwave pre-treatment. *Fuel Processing Technology*, 92(10), 1920–1928. <https://doi.org/10.1016/j.fuproc.2011.05.012>
- Sahyoun, C., Rowson, N. A., Kingman, S. W., Groves, L., & Bradshaw, S. M. (2005). The influence of microwave pretreatment on copper flotation. *Journal of The South African Institute of Mining and Metallurgy*, 105(1), 7–13.
- Saif, T., Lin, Q., Singh, K., Bijeljic, B., & Blunt, M. J. (2016). Dynamic imaging of oil shale pyrolysis using synchrotron X-ray microtomography. *Geophysical Research Letters*. <https://doi.org/10.1002/2016GL069279>
- Satish, H., Quellet, J., Raghavan, V., & Radziszewski, P. (2006). Investigating microwave assisted rock breakage for possible space mining applications. *Transactions of the Institutions of Mining and Metallurgy, Section A: Mining Technology*, 115(1), 34–40. <https://doi.org/10.1179/174328606X101902>
- Satish, H. (2005). Exploring microwave assisted rock breakage for possible space mining applications. *McGill University, Montreal*.
- Schön, J. H. (2015). *Physical properties of rocks: Fundamentals and principles of petrophysics*. Elsevier.
- Scott, G., Bradshaw, S. M., & Eksteen, J. J. (2008). The effect of microwave pretreatment on the liberation of a copper carbonatite ore after milling. *International Journal of Mineral Processing*, 85(4), 121–128. <https://doi.org/10.1016/j.minpro.2007.08.005>
- Seipold, U. (1990). Pressure and temperature dependence of thermal transport properties of granites. *High Temp. High Pressures*, 22, 541–548.
- Sengupta, D. L., & Sarka, T. K. (2003). Maxwell, Hertz, the Maxwellians, and the early history of electromagnetic waves. *IEEE Antennas and Propagation Magazine*, 45(2), 13–19. <https://ieeexplore.ieee.org/abstract/document/1203114>
- Sheen, J. (2005). Study of microwave dielectric properties measurements by various resonance techniques. *Measurement: Journal of the International Measurement Confederation*, 37(2), 123–130. <https://doi.org/10.1016/j.measurement.2004.11.006>

- Shepel, T., Grafe, B., Hartlieb, P., Drebenstedt, C., & Malovyk, A. (2018). Evaluation of cutting forces in granite treated with microwaves on the basis of multiple linear regression analysis. *International Journal of Rock Mechanics and Mining Sciences*. <https://doi.org/10.1016/j.ijrmms.2018.04.043>
- Sikong, L., & Bunsin, T. (2009). Mechanical property and cutting rate of microwave treated granite rock. *Songklanakarinn Journal of Science and Technology*, 31(4), 447–452.
- Singh. (1998). Non-Explosive Applications of the PCF Concept for Underground Excavation. *Tunnelling and Underground Space Technology*, 13(3), 305–311. [https://doi.org/10.1016/s0886-7798\(98\)00062-5](https://doi.org/10.1016/s0886-7798(98)00062-5)
- Singh, S., Gupta, D., Jain, V., & Sharma, A. K. (2014). Microwave processing of materials and applications in manufacturing industries: a review. *Materials and Manufacturing Processes*, 30(1), 1–29.
- Singh, V., Venugopal, R., Tripathy, S. K., & Saxena, V. K. (2017). Comparative analysis of the effect of microwave pretreatment on the milling and liberation characteristics of mineral matters of different morphologies. *Minerals and Metallurgical Processing*, 34(2), 65–75. <https://doi.org/10.19150/mmp.7506>
- Somani, A., Nandi, T. K., Pal, S. K., & Majumder, A. K. (2017). Pre-treatment of rocks prior to comminution – A critical review of present practices. *International Journal of Mining Science and Technology*, 27(2), 339–348. <https://doi.org/10.1016/j.ijmst.2017.01.013>
- Summers, D. A. (2003). *Waterjetting technology*. CRC Press.
- Summers, D. A., & Henry, R. L. (1972). Water jet cutting of sedimentary rock. *Journal of Petroleum Technology*, 24(07), 797–802.
- Swart, A. J., & Mendonidis, P. (2013). Evaluating the effect of radio-frequency pre-treatment on granite rock samples for comminution purposes. *International Journal of Mineral Processing*, 120, 1–7. <https://doi.org/10.1016/j.minpro.2013.02.002>
- Teimoori, K., Hassani, F., Sasmito, A. P., & Ghoreishi-Madiseh, S. A. (2019a). Numerical investigation on the effects of single-mode microwave treatment on rock breakage system. *17th International Conference on Microwave and High Frequency Heating* (pp. 270-278). Editorial Universitat Politècnica de València. <https://doi.org/10.4995/Ampere2019.2019.9646>
- Teimoori, K., Hassani, F., Sasmito, A., & Madiseh, A. (2019b). Experimental investigations of microwave effects on rock breakage using SEM analysis. In *AMPERE 2019. 17th International Conference on Microwave and High Frequency Heating* (pp. 1-8). Editorial Universitat Politècnica de València. <https://doi.org/10.4995/AMPERE2019.2019.9647>
- Toifl, D. M. (2016). *Numerical study of microwave induced stress and damage formation in heterogeneous rocks* (Issue May). Montanuniversitaet Leoben.
- Toifl, M., Hartlieb, P., Meisels, R., Antretter, T., & Kuchar, F. (2017). Numerical study of the influence of irradiation parameters on the microwave-induced stresses in granite. *Minerals Engineering*, 103–104, 78–92. <https://doi.org/10.1016/j.mineng.2016.09.011>

- Tungpalan, K., Wightman, E., & Manlapig, E. (2015). Relating mineralogical and textural characteristics to flotation behaviour. *Minerals Engineering*, 82, 136–140. <https://doi.org/10.1016/j.mineng.2015.02.005>
- Ulaby, F. T., Bengal, T. H., Dobson, M. C., East, J. R., Garvin, J. B., & Evans, D. L. (1990). Microwave dielectric properties of dry rocks. In *IEEE Transactions on Geoscience and Remote Sensing* (Vol. 28, Issue 3). <https://doi.org/10.1109/36.54359>
- Ulusay, R. (2015). The ISRM suggested methods for rock characterization, testing and monitoring: 2007-2014. Springer. <https://doi.org/10.1007/978-3-319-07713-0>
- Vogt, D. (2016). A review of rock cutting for underground mining: past, present, and future. *Journal of the Southern African Institute of Mining and Metallurgy*, 116(11), 1011–1026.
- Vorl ček, J., Vrbova, B., & Vrba, J. (2011). Prospective applications of microwaves in medicine. In *Advances in Cancer Therapy*. IntechOpen.
- Vorster, W., Rowson, N. A., & Kingman, S. W. (2001). The effect of microwave radiation upon the processing of Neves Corvo copper ore. *International Journal of Mineral Processing*, 63(1), 29–44. [https://doi.org/10.1016/S0301-7516\(00\)00069-7](https://doi.org/10.1016/S0301-7516(00)00069-7)
- Vosteen, H.-D., & Schellschmidt, R. (2003). Influence of temperature on thermal conductivity, thermal capacity and thermal diffusivity for different types of rock. *Physics and Chemistry of the Earth, Parts A/B/C*, 28(9–11), 499–509.
- Walkiewicz, J. W., Kazonich, G., & McGill, S. L. (1988). Microwave Heating Characteristics of Selected Minerals and Compounds. *Minerals and Metallurgical Processing*, 5(1), 39–42. <https://doi.org/10.1007/BF03449501>
- Wang, E., Shi, F., & Manlapig, E. (2011). Pre-weakening of mineral ores by high voltage pulses. *Minerals Engineering*, 24(5), 455–462. <https://doi.org/10.1016/j.mineng.2010.12.011>
- Wang, Yanmin, & Forssberg, E. (2005). Dry comminution and liberation with microwave assistance. *Scandinavian Journal of Metallurgy*, 34(1), 57–63. <https://doi.org/https://doi.org/10.1111/j.1600-0692.2005.00718.x>
- Wang, Yicai, & Djordjevic, N. (2014). Thermal stress FEM analysis of rock with microwave energy. *International Journal of Mineral Processing*, 130, 74–81. <https://doi.org/10.1016/j.minpro.2014.05.012>
- Waters, K. E., Rowson, N. A., Greenwood, R. W., & Williams, A. J. (2008). The effect of heat treatment on the magnetic properties of pyrite. *Minerals Engineering*, 21(9), 679–682. <https://doi.org/10.1016/j.mineng.2008.01.008>
- Wei, W., Shao, Z., Zhang, Y., Qiao, R., & Gao, J. (2019). Fundamentals and applications of microwave energy in rock and concrete processing—a review. *Applied Thermal Engineering*, 157, 113751. <https://doi.org/10.1016/j.applthermaleng.2019.113751>
- Whittles, D. N., Kingman, S. W., & Reddish, D. J. (2003). Application of numerical modelling for prediction of the influence of power density on microwave-assisted breakage. *International Journal of Mineral Processing*, 68(1-4), 71-91. [https://doi.org/10.1016/S0301-7516\(02\)00049-2](https://doi.org/10.1016/S0301-7516(02)00049-2)



- Wilson, J. W., Summers, D. A., & Gertsch, R. E. (1997). The development of waterjets for rock excavation. In *Proceeding of International Symposium on Mine Mechanisation and Automation*, 4, 1–10.
- Womack, J. P., & Jones, D. T. (1997). Lean thinking—banish waste and create wealth in your corporation. *Journal of the Operational Research Society*, 48(11), 1148. <https://doi.org/10.1057/palgrave.jors.2600967>
- Xu, J. (2015). Microwave Pretreatment. In *Pretreatment of Biomass: Processes and Technologies* (pp. 157–172). Elsevier. <https://doi.org/10.1016/B978-0-12-800080-9.00009-8>
- Yang, H. W., & Gunasekaran, S. (2004). Comparison of temperature distribution in model food cylinders based on Maxwell's equations and Lambert's law during pulsed microwave heating. *Journal of Food Engineering*, 64(4), 445–453. <https://doi.org/10.1016/j.jfoodeng.2003.08.016>
- Yuan, Y., & Xu, T. (2019). 3D modelling of microwave induced damage and fracturing of hard rocks. *Deep Rock Mechanics: From Research to Engineering*, 361–371. <https://doi.org/10.1201/9781351042666-36>
- Zavitsanos, P., & Bleiler, K. (1978). *Process for coal desulphurization* (Patent No. 4076607). <http://www.freepatentsonline.com/4076607.html>
- Zeng, J., Hu, Q., Chen, Y., Shu, X., Chen, S., He, L., Tang, H., & Lu, X. (2019). Experimental investigation on structural evolution of granite at high temperature induced by microwave irradiation. *Mineralogy and Petrology*, 113(6), 745–754. <https://doi.org/10.1007/s00710-019-00681-z>
- Zhang, Z.-X. (2016). Optimum Fragmentation. *Rock Fracture and Blasting*, 2, 411–423. <https://doi.org/10.1016/b978-0-12-802688-5.00021-x>
- Zhang, Z. Q., Liu, D. L., Zou, G. Q., & Chen, F. F. (2019). Influence of microwave irradiation distance on electromagnetism, temperature and stress field in rock. *53rd U.S. Rock Mechanics/Geomechanics Symposium*, 1–9.
- Zheng, Y. L., Zhang, Q. B., & Zhao, J. (2016). Challenges and opportunities of using tunnel boring machines in mining. *Tunnelling and Underground Space Technology*, 57, 287–299. <https://doi.org/10.1016/j.tust.2016.01.023>
- Zheng, Y. (2017). Fracturing of hard rocks by microwave treatment and potential applications in mechanised tunnelling (Doctoral dissertation, Monash University).
- Zheng, Yanlong, Ma, Z., Zhao, X., & He, L. (2020). Experimental investigation on the thermal, mechanical and cracking behaviours of three igneous rocks under microwave treatment. *Rock Mechanics and Rock Engineering*. <https://doi.org/10.1007/s00603-020-02135-x>
- Zheng, Y., Zhang, Q. B., & Zhao, J. (2016). Challenges and opportunities of using tunnel boring machines in mining. *Tunnelling and Underground Space Technology*, 57, 287–299. <https://doi.org/10.1016/j.tust.2016.01.023>
- Zheng, Yongchun, Wang, S., Feng, J., Ouyang, Z., & Li, X. (2005). Measurement of the complex permittivity of dry rocks and minerals: Application of polythene dilution method and Lichtenecker's mixture formulae. *Geophysical Journal International*. <https://doi.org/10.1111/j.1365-246X.2005.02718.x>

- Zheng, Zhang, Q. B., & Zhao, J. (2017). Effect of microwave treatment on thermal and ultrasonic properties of gabbro. *Applied Thermal Engineering*, 127, 359–369. <https://doi.org/10.1016/j.applthermaleng.2017.08.060>
- Zhu, J., Yang, Z., Li, X., Qi, S., Fang, Q., & Ding, Y. (2019). The experimental study of microwave heating on the microstructure of oil shale samples. *Energy Science & Engineering*. <https://doi.org/10.1002/ese3.311>
- Zhu, J., Yang, Z., Li, X., Wang, N., & Jia, M. (2018). Evaluation of different microwave heating parameters on the pore structure of oil shale samples. *Energy Science and Engineering*, 6(6), 797–809. <https://doi.org/10.1002/ese3.253>
- Znamenácková, I., Lovás, M., Hajek, M., & Jakabský, Š. (2003). Melting of andesite in a microwave oven. *Journal of Mining and Metallurgy B: Metallurgy*, 39(3–4), 549–557.

# Appendix A

## A.1 Supplementary data from Chapter 6

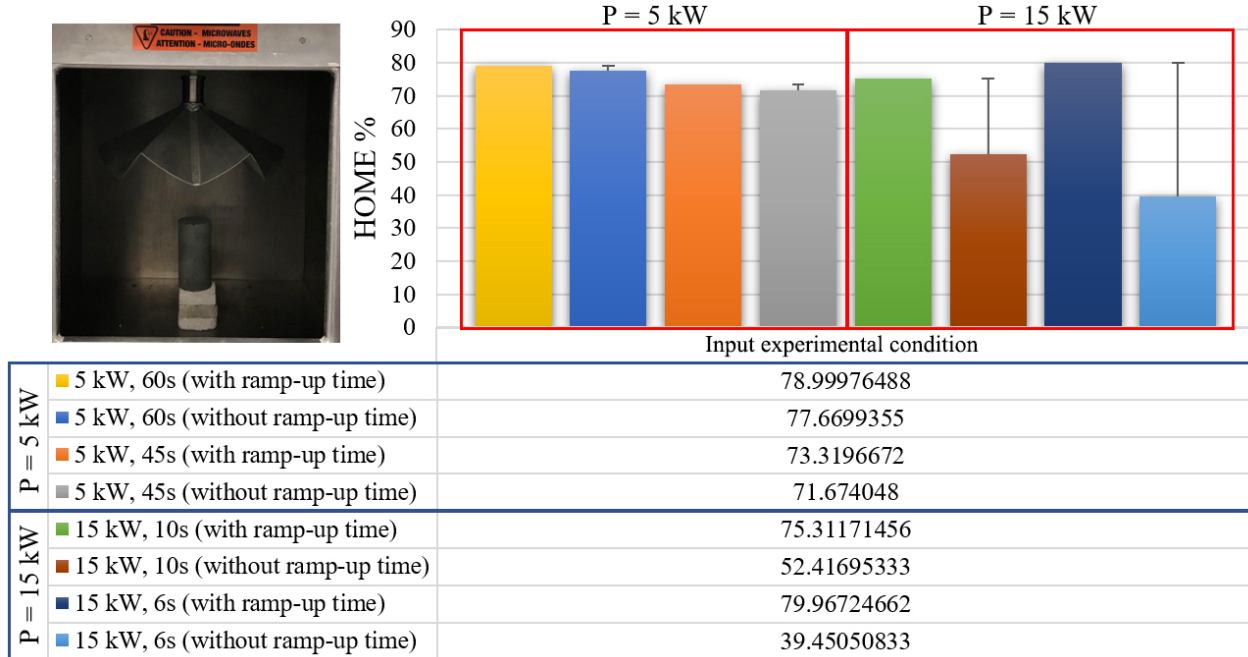


Figure A.1: Effect of microwave ramp-up time on UCS size basalt

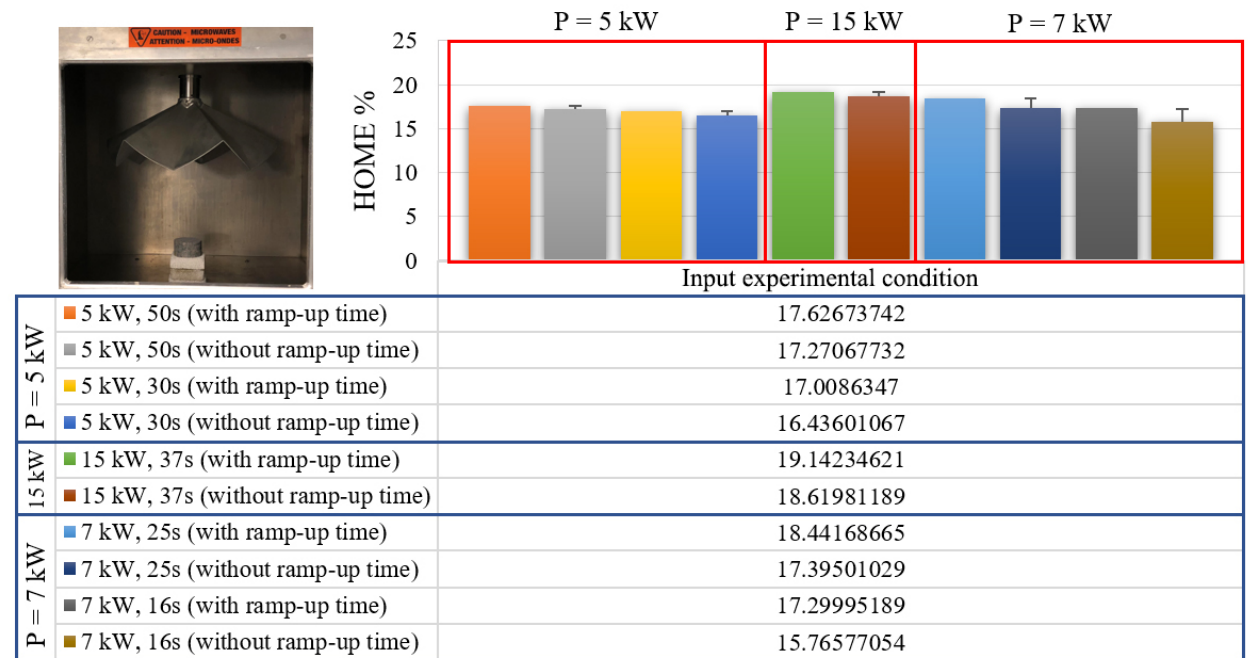


Figure A.2: Effect of microwave ramp-up time on BTS size granite

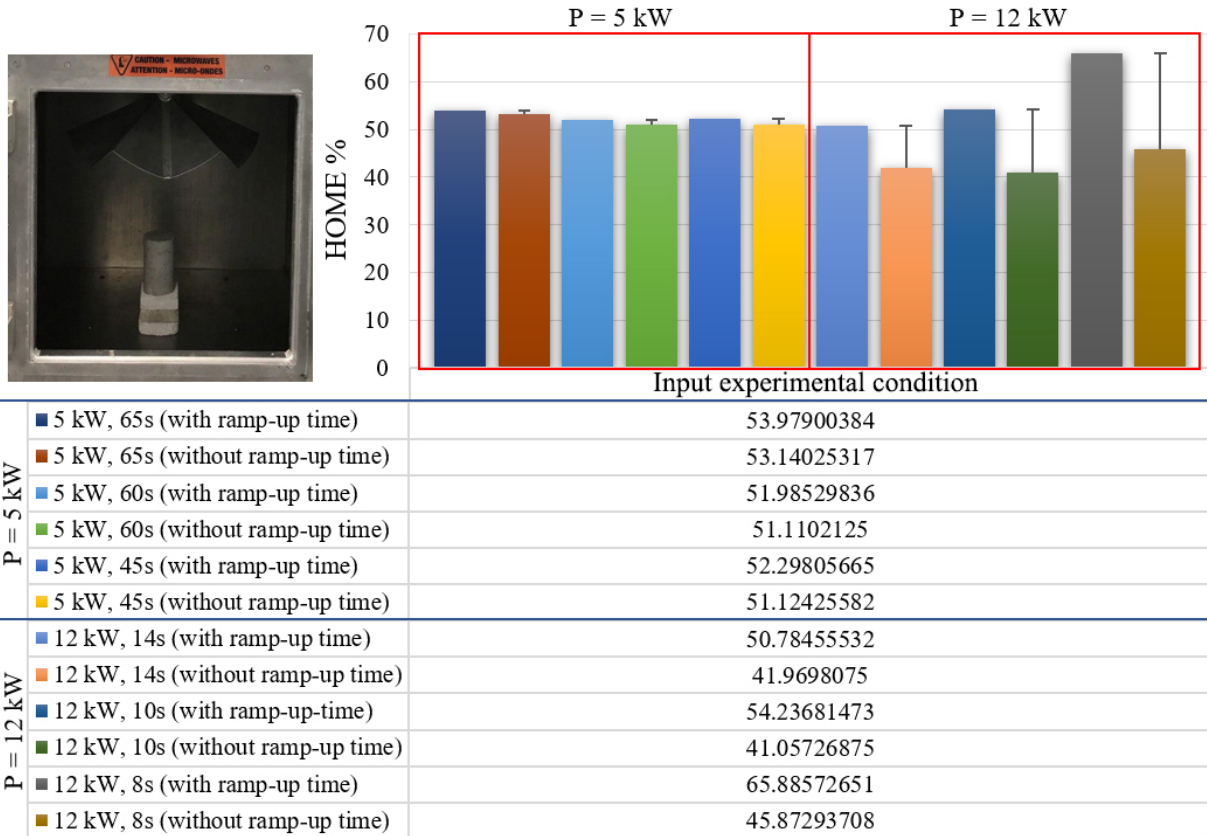


Figure A.3: Effect of microwave ramp-up time on UCS size granite

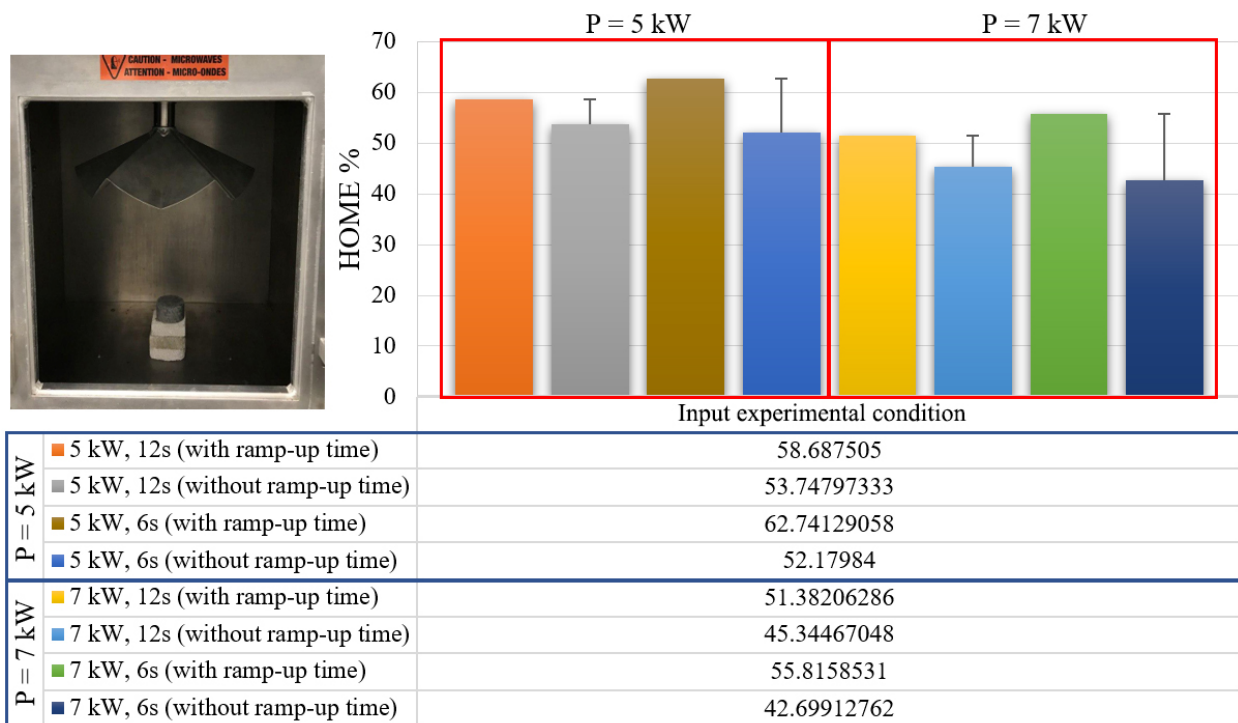


Figure A.4: Effect of microwave ramp-up time on BTS size kimberlite #1

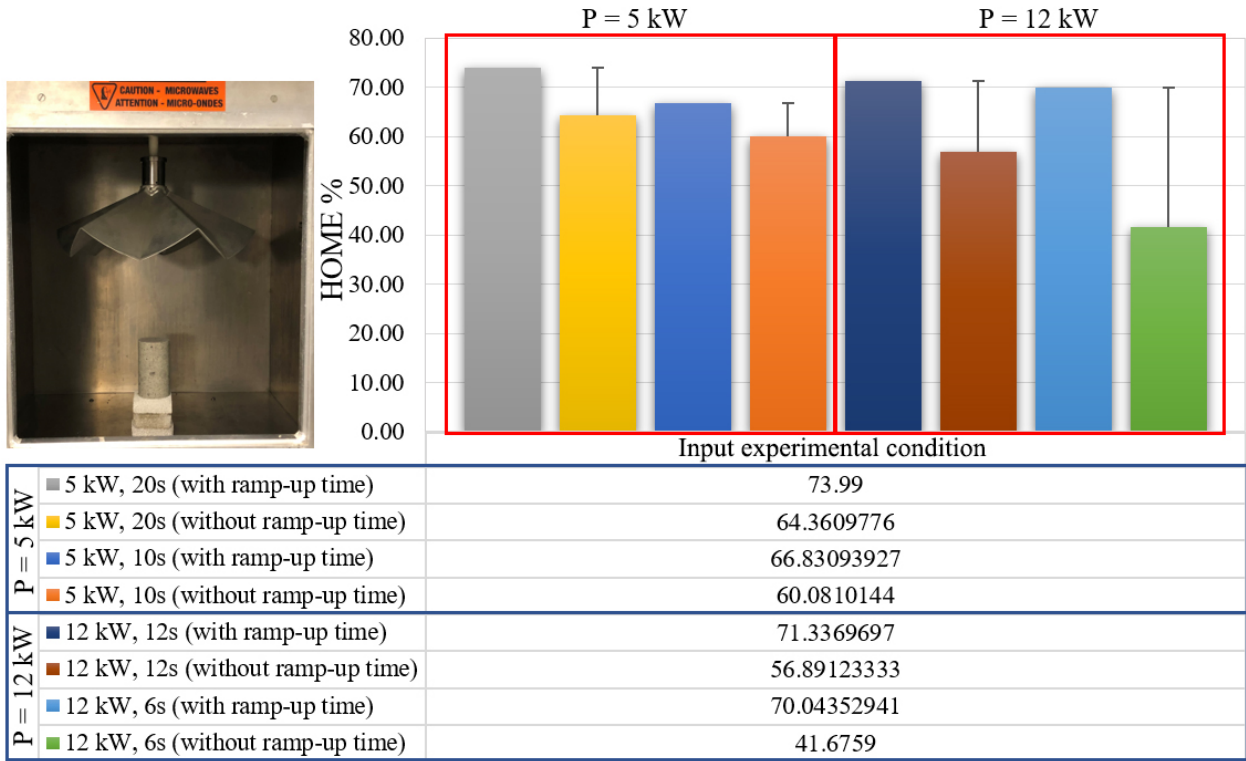


Figure A.5: Effect of microwave ramp-up time on UCS size kimberlite #1